Defense Threat Reduction Agency
8725 John J. Kingman Road, Stop 6201
Fort Belvoir, VA 22060-6201

DTRA-TR-02-5

TECHNICAL REPORT

Seismicity Characterization and Velocity Structure of Northeast Russia

May 2005

DSWA 01-98-C-0168

Kevin G. Mackey and
Kazuya Fujita

Prepared by:
Michigan State University
Dept. of Geological Sciences
East Lansing, MI 48824

DISTRIBUTION LIST UPDATE

This mailer is provided to enable DTRA to maintain current distribution lists for reports. (We would appreciate you providing the requested information.)

- ☐ Add the individual listed to your distribution list.
- ☐ Delete the cited organization/individual.
- ☐ Change of address.

NAME: ______________________________

ORGANIZATION: ______________________________

OLD ADDRESS	NEW ADDRESS
____________________	____________________
____________________	____________________
____________________	____________________

TELEPHONE NUMBER: (   ) ______________________________

DTRA PUBLICATION NUMBER/TITLE	CHANGES/DELETIONS/ADDITONS, etc. *(Attach Sheet if more Space is Required)*
____________________	____________________
____________________	____________________
____________________	____________________

DTRA or other GOVERNMENT CONTRACT NUMBER: ____________________

CERTIFICATION of NEED-TO-KNOW BY GOVERNMENT SPONSOR (if other than DTRA):

SPONSORING ORGANIZATION: ____________________

CONTRACTING OFFICER or REPRESENTATIVE: ____________________

SIGNATURE: ____________________

DEFENSE THREAT REDUCTION AGENCY
ATTN: BDLMI
8725 John J Kingman Road, MS 6201
Fort Belvoir, VA 22060-6201

DEFENSE THREAT REDUCTION AGENCY
ATTN. BDLMI
8725 John J Kingman Road, MS 6201
Fort Belvoir, VA 22060-6201

REPORT DOCUMENTATION PAGE

Form Approved
OMB No. 0704-0188

1. REPORT DATE *(DD-MM-YYYY)*	2. REPORT TYPE	3. DATES COVERED *(From - To)*
	Technical	990930 - 010930

4. TITLE AND SUBTITLE
Seismicity Characterization and Velocity Structure of Northeast Russia

5a. CONTRACT NUMBER DSWA 01-98-C-0168
5b. GRANT NUMBER N/A
5c. PROGRAM ELEMENT NUMBER RDT&E
5d. PROJECT NUMBER CD
5e. TASK NUMBER 99Q
5f. WORK UNIT NUMBER 66453

6. AUTHOR(S)
Mackey, Kevin G. and

Fujita, Kazuya

7. PERFORMING ORGANIZATION NAME(S) AND ADDRESS(ES)
Michigan State University
Dept. of Geological Sciences
East Lansing, MI 48824

8. PERFORMING ORGANIZATION REPORT NUMBER
NERSP-8

9. SPONSORING/MONITORING AGENCY NAME(S) AND ADDRESS(ES)

Defense Threat Reduction Agency
8725 John J. Kingman Road, Suite 0944
FT. Belvoir, VA 22060-6201

TDND/ Barber

10. SPONSOR/MONITOR'S ACRONYM(S)
DTRA

11. SPONSOR/MONITOR'S REPORT NUMBER(S)
DTRA TR-02-5

12. DISTRIBUTION/AVAILABILITY STATEMENT

Approved for public release; distribution is unlimited.

13. SUPPLEMENTARY NOTES

This work was sponsored by the Defense Threat reduction Agency under RDT&E RMSS Code b 4613 D CD CD 66453 5P50A

14. ABSTRACT
A seismicity catalog and associated list of phases for many events has been compiled for northeast Russia using published and unpublished data from the regional networks operating in eastern Russia (primarily Magadan, Yakutsk, and Amur), and international data files. The catalog contains about 39,000 events and 150,000 arrival times. The resultant catalog is contaminated by industrial explosions, particularly in the Amur and central Magadan districts.
A preliminary crustal velocity model was developed by obtaining best fit travel curves in conjunction with locating approximately 1300 events in eastern Russia The velocities obtained are generally in agreement with inferred tectonic regimes. These travel time curves were then used to relocate 134 larger regional events; 26 are classified as GT10. From these relocated events, consistent patterns of residuals, essentially representing Source Specific Station Corrections (SSSCs), show upper mantle velocities are elevated under the Siberian platform and slower below the Sea of Okhotsk. Seismic station parameters for the region were also compiled.
To further improve calibration capabilities in northeast Russia, a small network of digital seismic stations was deployed in the Magadan region, recording both earthquakes and ground truth mine blasts. Preliminary analysis of Lg amplitude ratios indicate that the ratio Lg(4-8Hz)Lg(0.75-1.5Hz) using peak amplitudes is not sufficient to discriminate mining explosions from earthquakes at local and near regional distances (<500km) in northeast Russia.

15. SUBJECT TERMS
Travel Time Curves, Seismic Station, Seismicity, Russia, Earthquake Location, Explosion Discrimination

16. SECURITY CLASSIFICATION OF: a. REPORT	b. ABSTRACT	c. THIS PAGE	17. LIMITATION OF ABSTRACT	18. NUMBER OF PAGES	19a. NAME OF RESPONSIBLE PERSON
U	U	U	SAR	187	

19b. TELEPHONE NUMBER *(Include area code)*

EXECUTIVE SUMMARY

Overview of Study

The primary objective of this research was to improve epicentral coordinates to better locate and identify ground truth seismic events in northeast Russia in support of Comprehensive Nuclear-Test-Ban Treaty (CTBT) monitoring. A second objective was to begin the process of explosion discrimination using digital data from stations deployed as a part of this study.

Northeastern Russia (Figure ES-1) remains one of the least researched large continental regions in the world from a seismological standpoint. This is due to geographic remoteness and lack of accessibility, as well as the absence of data available to western scientists prior to the collapse of the Soviet Union. Subsequently, access to the region's scientists and their data has allowed for the first comprehensive studies to be undertaken. Northeast Russia is a tectonically complex region formed by the amalgamation of a large number of terranes of various origins in the Mesozoic and Cenozoic (Nokleberg et al., 1994, Nokleberg et al., 2000). Thus, the crustal structure and seismic velocities are expected to vary considerably within the region.

The first step in this project was to construct computerized files of all known seismicity for the region, as well as the associated phase arrival times. Section One, The Northeastern Russia Seismicity Database, outlines the sources, data acquired, and discusses the intricacies and inconsistences involved in building this database. Assembly of this database would not have been possible without a direct knowledge of the operational procedures used in the region. The assembled seismicity data can then be used to better evaluate the region as a whole, rather than as isolated regions.

One of the problems encountered in the seismicity database was that of explosion contamination, discussed in Section Two, Explosion Contamination in the Northeast Russia Seismicity Catalog. Some regions in northeastern Russia show high levels of seismic activity, when in fact the reported events are almost entirely of anthropogenic origin. This can easily result in erroneous interpretation of seismicity distribution, seismic hazards, etc. On the other hand, known explosions are helpful for developing better travel time curves which can be used to improve epicenter locations.

Section Three, Crustal Model and Relocations of Northeast Russia Earthquakes, develops crustal velocities specifically calibrated to small regions. The calibrated travel time curves were developed in conjunction with relocating approximately 1,300 of the larger events throughout the region. Locations of events determined here are compared with the local Russian network determinations. Crustal thicknesses were determined by inverting Pg arrival times, solving for the best-fit velocities, and analyzing the Pg/P_n crossover points for 27 individual stations. The seismic velocities and crustal thickness determinations are combined into a crustal model for the Magadan region and northern Yakutia. An attempt was made to further refine the crustal model through tomography, however software problems precluded the development of a stable model.

Section Four, GT Classifications and Analysis of Teleseismic Events, carefully evaluates teleseismically recorded events to which a significant amount of previously unavailable local data were added. Results are compared to epicenters calculated by international agencies (e.g., the International Seismological Centre, ISC). Using the relocated teleseismic events, residuals essentially representing Source Specific Station Corrections (SSSCs) were mapped for arrivals at several stations.

Section Five, Digital Station Deployments, discusses operational aspects of digital stations deployed as a part of this study. Deployed stations were used to record earthquakes and obtain

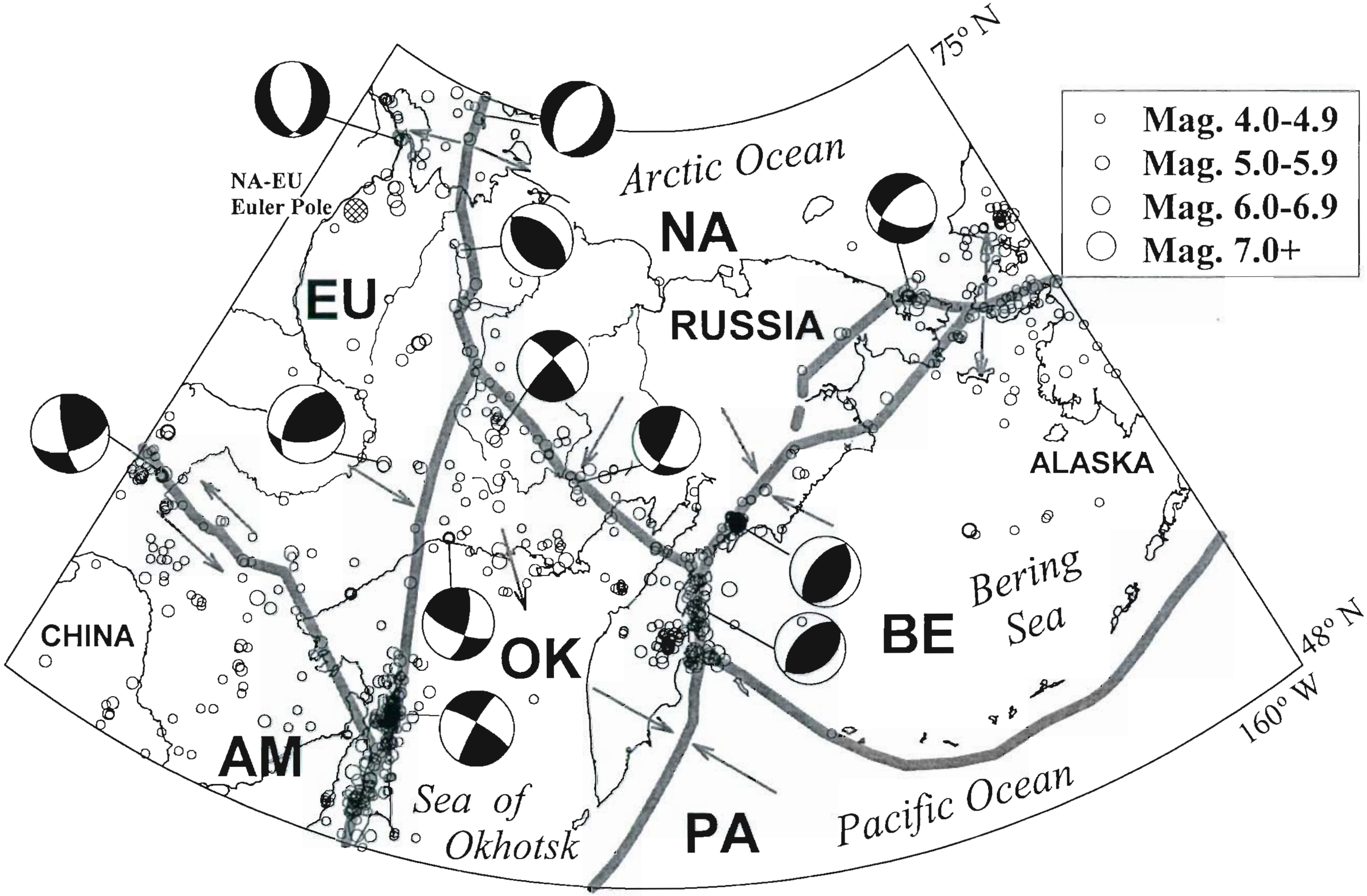

Figure ES-1. Plate tectonic map of northeast Russia with teleseismic earthquakes, representative focal mechanisms, and relative plate motions. Plates are North American (NA), Eurasian (EU), Amur (AM), Okhotsk (OK), Pacific (PA), and Bering (BE).

ground truth information on explosions in the study region. Waveforms of typical earthquakes and explosions recorded are used to investigate the possibility of discrimination between anthropogenic and tectonic sources for improved CTBT monitoring capability.

A Brief Overview of the Tectonic Regime and Geologic History

The tectonics of Northeast Russia result from complex plate interactions between the North American (NA), Eurasian (EU), and Pacific (PA) plates and a number of microplates between them, such as Okhotsk (OK), Amur (AM), and Bering (BE; Figure ES-1) that have been previously studied using teleseismic earthquakes (e.g., Chapman and Solomon, 1976; Koz'min, 1984; Fujita et al., 1990a,b; Imaev et al., 1990; Riegel et al., 1993; Seno et al., 1996; Fujita et al., 1997; Mackey et al., 1997; Imaev et al., 2000; Fujita et al., *in press*). The majority of the seismicity occurs along the Chersky Seismic Belt on the North America - Okhotsk boundary and the Stanovoi Seismic Zone on the Eurasia - Amur boundary.

The North American and Eurasian plates are presently converging in northeast Russia, resulting in the southward extrusion of the Okhotsk Block (Figure ES-1; Riegel et al., 1993; see also Seno et al., 1996). The northern portion of the study area includes the Laptev Sea rift system. The Laptev Sea rift system is the extension of the Arctic Mid-Ocean Ridge onto the Siberian continental shelf, expressed as a system of active grabens (Kim, 1986; Fujita et al., 1990a). To the south of the Siberian platform is the Stanovoi seismic zone, along which left-lateral motion is taking place between the Amur and Eurasian plates. Studies of the India-Eurasia collision have suggested extremely far-field extrusion effects, which results in the eastward extrusion of the Amur plate relative to the Eurasian plate (Tapponier et al., 1982; Peltzer and Tapponier, 1988). The Bering block, encompassing the Bering Sea, is driven by subduction of the Pacific Plate and extrusion of southwestern Alaska causing a clockwise rotation relative to the North American plate (Mackey et al., 1997).

The central portion of the study area is composed of a series of exotic terranes and associated island arcs which accreted in the Mesozoic forming the Kolyma-Omolon Superterrane and Kolyma Structural Loop (Figure ES-2; e.g., Parfenov, 1991; Nokleberg et al., 1994; Nokleberg et al., 2000; Layer et al., 2001). The western portion of the study area contains the Verkhoyansk range and eastern portions of the Siberian platform. The Verkhoyansk range is a fold and thrust belt of Mesozoic age associated with the terrane accretion occurring during that time period (Nokleberg et al., 2000). The Siberian platform generally consists of a flat lying Precambrian basement overlain by a few kilometers of Riphean, Cambrian and Jurassic sedimentary materials (Parfenov, 1991). Topographically the Siberian platform is relatively flat. The southern edge of the Siberian platform is separated from exotic terranes to the south by the Hauterivian to Aptian (131-110 Ma) Mongol-Okhotsk Suture (Nokleberg et al., 2000). In Chukotka, in the eastern portion of the study area, is the South Anyui Suture which probably represents the closure of the South Anyui Basin, coincident with the opening of the Canada Basin (Nokleberg et al., 2000). Beyond the South Anyui Suture lies the Chukotka Terrane, the Bering Strait and the terranes of Alaska. Superimposed over the southern edge of the Mesozoic accretionary terranes is the Okhotsk-Chukotka Volcanic Belt, dated at 67-89 Ma (Fujita et al., 1997). Farther east is the Kamchatka-Koryak Accretionary Zone, which consists of a number of Cenozoic accreted terranes (e.g., Stavksy et al., 1990) forming the Kamchatka Peninsula and the Koryak Highlands. The central part of the study area, the Chersky Range, participated in an extensional episode in the Pliocene which resulted in the formation of the Moma rift system (Grachev, 1973; Fujita et al., 1990a). Within the past 0.5 m.y., the pole of rotation for

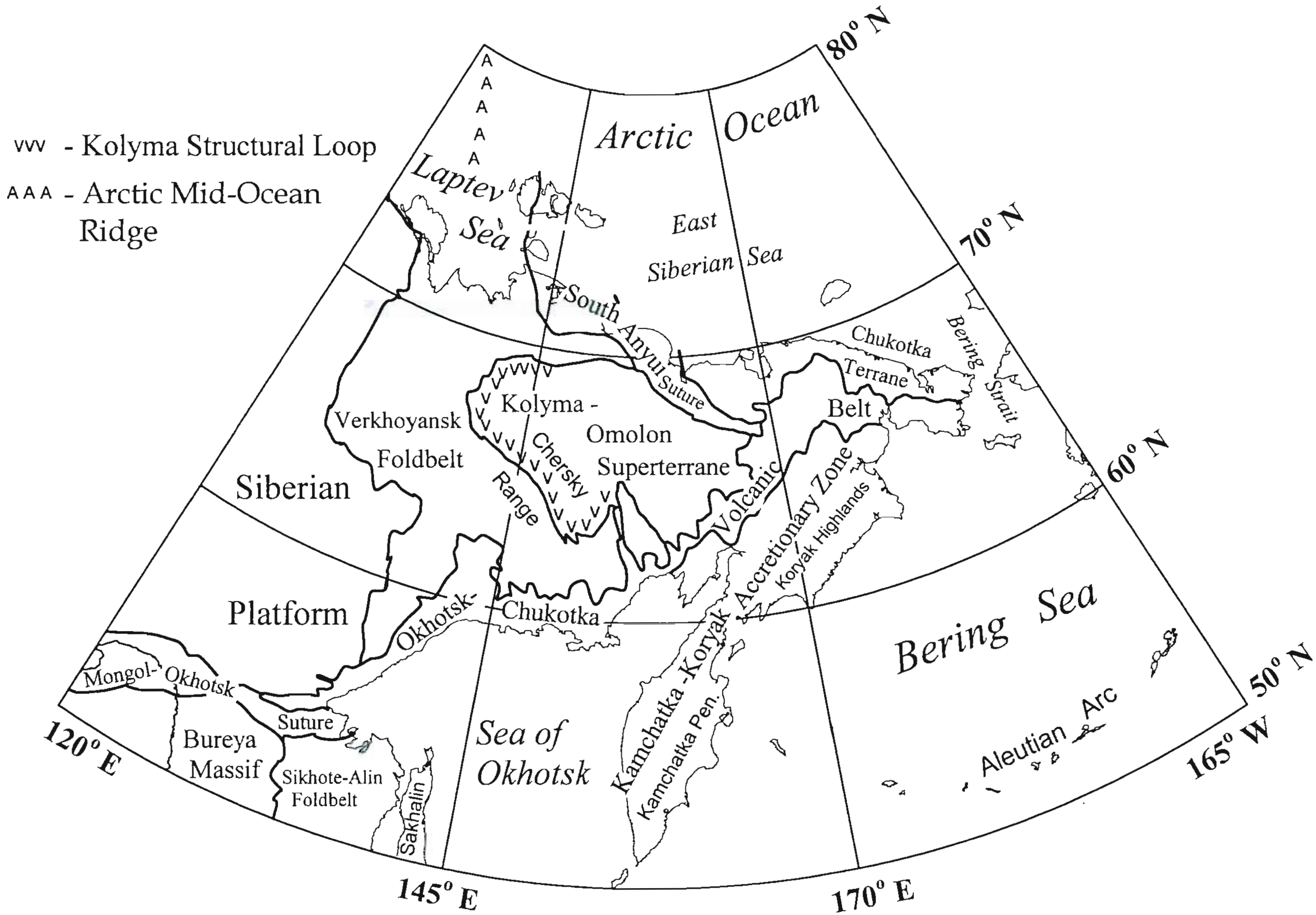

Figure ES-2. Geologic index map of northeast Russia.

the NA-EU plate (Figure ES-1) is suggested to have moved north and extensional activity along the Moma rift ceased (Cook et al., 1986). Presently, the Pacific plate is subducting along the Aleutian Arc and the eastern edge of the Kamchatka peninsula.

PREFACE

Many people were instrumental to the success of this study. Significant contributions were given for acquisition of data, data entry, logistical support and scientific discussions. We would like to thank Boris Koz'min, Larissa Gounbina, Valery Imaev, Dmirty Gounbin, Valentin Kovalev, Andrey Savchenko, Nadia Lyeshchuka, Boris Sedoff, Lerun Izmailov, Pavel Minyuk, Konstantine Chali, Evgeni Koz'min, Len Parfenov, Zina Kornilova, Alexander Larionov, Natasha Koz'mina, Evgeni Gordeev, Marina Odinyets, Alexander Evekin, Nastia Antropova, Trent Faust, Rob McCaleb, Alexandra DeJong, Allen McNamara, Dan McNamara, Roger Hansen, Paula Figura, Melissa McLean, Steve Riegel, Bob Engdahl, Hans Hartse and Michelle Mackey. Additional thanks to all station operators, Magadan EMSD personnel, Yakutsk EMSD personnel, the Susuman Mining company, OAO Tal-Yuryakh, OAO Kadakchan, ZAO Cerebro Territory, and administration of the Dukat, Galimie, Matrosova, and Kubaka mines.

Portions of this study were extensions of work supported by the National Science Foundation Office of Polar Programs grants 92-24193, 94-24139, 98-06130 and the Incorporated Research Institutions for Seismology Joint Seismic and Global Seismic Network programs.

CONVERSION TABLE

Conversion Factors for U.S. Customary to metric (SI) units of measurement.

MULTIPLY ⟶ BY ⟶ TO GET
TO GET ⟵ BY ⟵ DIVIDE

angstrom	1.000 000 x E -10	meters (m)
atmosphere (normal)	1.013 25 x E +2	kilo pascal (kPa)
bar	1.000 000 x E +2	kilo pascal (kPa)
barn	1.000 000 x E -28	meter² (m^2)
British thermal unit (thermochemical)	1.054 350 x E +3	joule (J)
calorie (thermochemical)	4.184 000	joule (J)
cal (thermochemical/cm^2)	4.184 000 x E -2	mega joule.m^2 (MJ/m^2)
curie	3.700 000 x E +1	*giga bacquerel (GBq)
degree (angle)	1.745 329 x E -2	radian (rad)
degree Fahrenheit	$t_k = (t^o f + 459.67)/1.8$	degree kelvin (K)
electron volt	1.602 19 x E -19	joule (J)
erg	1.000 000 x E -7	joule (J)
erg/second	1.000 000 x E -7	watt (W)
foot	3.048 000 x E -1	meter (m)
foot-pound-force	1.355 818	joule (J)
gallon (U.S. liquid)	3.785 412 x E -3	$meter^3$ (m^3)
inch	2.540 000 x E -2	meter (m)
jerk	1.000 000 x E +9	joule (J)
joule.kilogram (J/kg) radiation dose absorbed	1.000 000	**Gray (Gy)
kilotons	4.183	terajoules
kip (1000 lbf)	4.448 222 x E +3	newton (N)
$kip/inch^2$ (ksi)	6.894 757 x E +3	kilo pascal (kPa)
ktap	1.000 000 x E +2	newton-second/m^2 ($N\text{-}s/m^2$)
micron	1.000 000 x E -6	meter (m)
mil	2.540 000 x E -5	meter (m)
mile (international)	1.609 344 x E +3	meter (m)
ounce	2.834 952 x E -2	kilogram (kg)
pound-force (lbs avoirdupois)	4.448 222	newton (N)
pound-force inch	1.129 848 x E -1	newton-meter (N-m)
pound-force/inch	1.751 268 x E +2	newton/meter (N/m)
pound-force/$foot^2$	4.788 026 x E -2	kilo pascal (kPa)
pound-force/$inch^2$ (psi)	6.894 757	kilo pascal (kPa)
pound-mass (lbm avoirdupois)	4.535 924 x E -1	kilogram (kg)
pound-mass-$foot^2$ (moment if inertia)	4.214 011 x E -2	kilogram-$meter^2$ ($kg\text{-}m^2$)
pound-mass/$foot^3$	1.601 846 x E +1	kilogram-$meter^3$ (kg/m^3)
rad (radiation dose absorbed)	1.000 000 x E -2	**Gray (Gy)
roentgen	2.579 760 x E -4	coulomb/kilogram (C/kg)
shake	1.000 000 x E -8	second (s)
slug	1.459 390 x E +1	kilogram (kg)
torr (mm Hg, 0° C)	1.333 22 x E -1	kilo pascal (kPa)

* The bacquerel (Bq) is the SI unit of radioactivity; 1 Bq = 1 event/sec.
** The Gray (Gy) is the SI unit of absorbed radiation.

TABLE OF CONTENTS

TABLE OF CONTENTS (Continued)

Page

TABLE OF CONTENTS (Continued)

FIGURES

Page

FIGURES (Continued)

FIGURES (Continued)

Page

FIGURES (Continued)

FIGURES (Continued)

Page

TABLES

SECTION 1

THE NORTHEASTERN RUSSIA SEISMICITY DATABASE

1.1 INTRODUCTION.

Prior to the beginning of this study, there was no comprehensive database covering continental seismicity in northeastern Russia, although seismic networks have been in operation in the region for over 30 years, and significant amounts of data were collected. Areas studied here are the Magadan, Yakutsk, Amur, and Sakhalin networks, as well as minor portions of the Irkutsk and Kamchatka networks. The network boundaries are shown in Figure 1. Unfortunately, data were usually not exchanged between adjoining networks. To better understand the seismicity of northeastern Russia, it is necessary to combine as much data as possible from all sources. The combined data can be re-evaluated to improve travel time curves, hypocenter parameters, tectonic models, better understand seismicity levels, determine regions of anthropogenic sources, etc.

There are two major sections to the database developed: a complete as possible catalog of hypocenters for northeast Russia, and a database of arrival times combined from all sources and networks. In assembly of the database, several published and unpublished sources were used. A discussion of primary sources and networks follows.

This study has compiled a list of approximately 39,000 individual earthquakes throughout the region (Figure 2). Most of the events occur between 1968-2000. For about 14,000 events (Figure 3), phase data have been acquired and incorporated into computerized files; there are presently approximately 150,000 arrival times. For all networks, historic events and data recorded teleseismically are taken from standard sources such as International Seismological Summary (ISS), International Seismological Centre Bulletin (ISC), United States Geological Survey (NEIC), etc., and are not discussed with regard to specific networks.

1.2 DATA SOURCES.

1.2.1 Zemletryseniya V SSSR.

This publication (*Zemletryseniya V SSSR*:1963-1991; Earthquakes of the USSR; referred to as *Zemlet*, and *Zemletryseniya Severnoi Evrazii*: 1992-1994; Earthquakes of Northern Eurasia; also referred to as *Zemlet*) contains a yearly catalog listing event parameters for the larger earthquakes which occurred within each regional network. In general, only events of K-class 8.5 and larger are listed, although this has varied from year to year, and from network to network. In addition, the cutoff was often raised for large aftershock sequences. *Zemlet* has historically been available in the U.S.

1.2.2 Materialy po Seismichnosti Sibiri.

The bi-monthly publication (*Materialy po Seismichnosti Sibiri*; Materials on the Seismicity of Siberia; referred to as *Materialy*) contains both epicenter lists and phase data for each of the seismic networks in Siberia that investigate seismicity of continental regions for 1970-192 (Irkutsk, Magadan, Yakutsk, Amur (1979-1992), and Altai). The epicenter list provided here is generally complete, although isolated events found in the *Far East Bulletin* and in the unpublished data seem to be missing. The largest fraction of the assembled epicenter list comes from this Publication. *Materialy* also contains phase data and arrival times for events equal to or larger than a K-class of

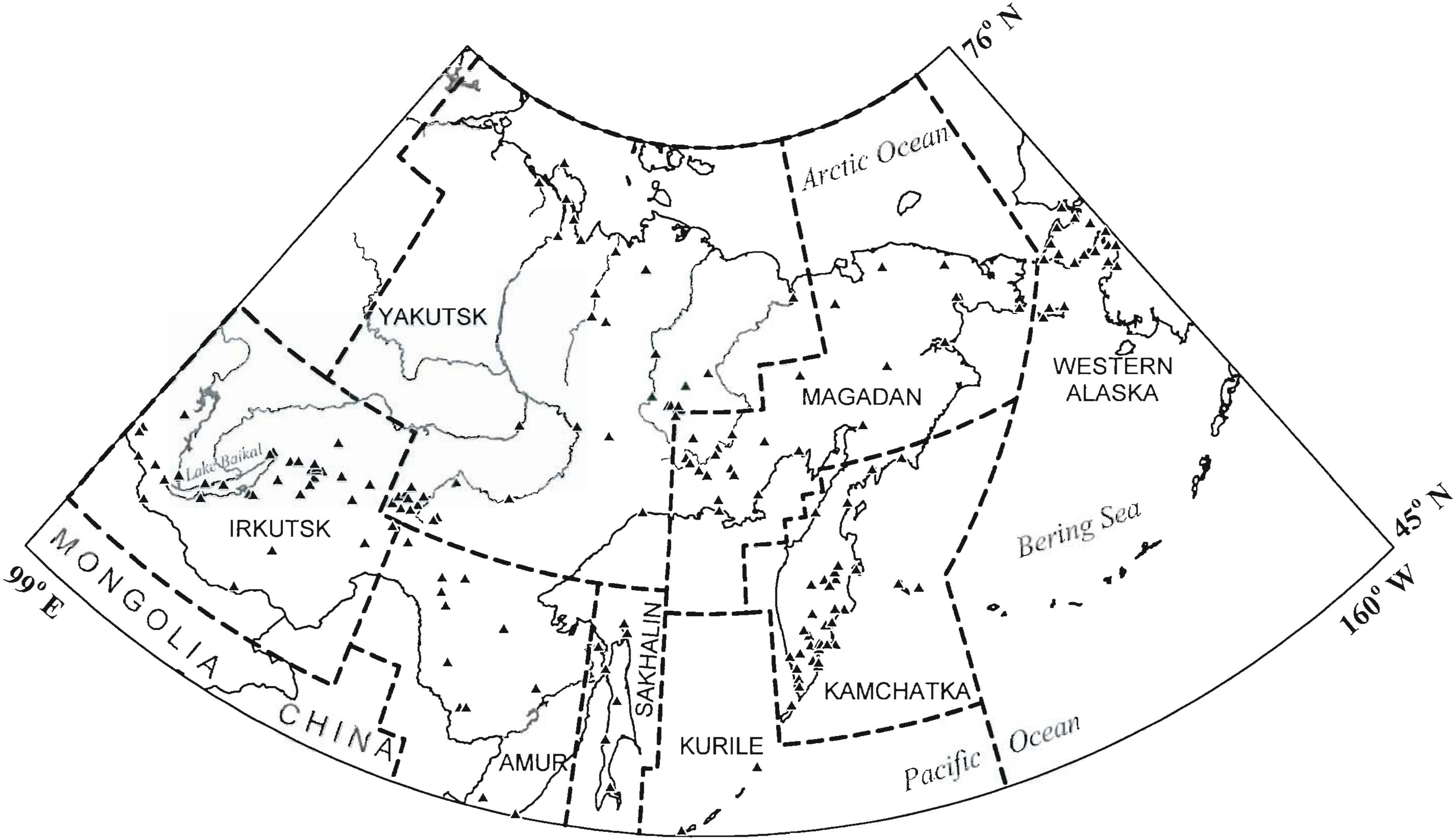

Figure 1. Seismic networks of northeast Russia. Triangles represent seismic stations that have operated at one time, most of which are now closed.

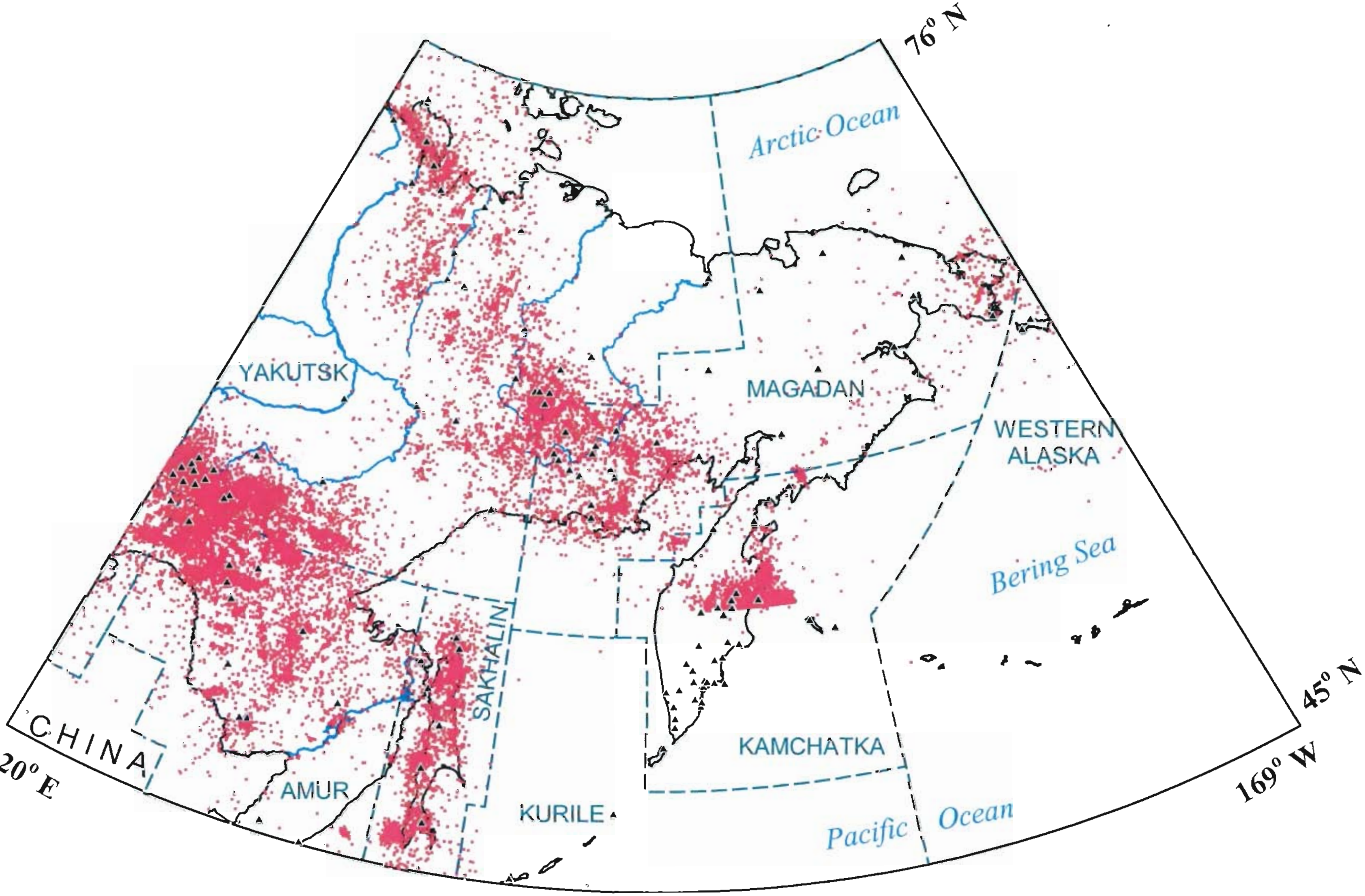

Figure 2. Seismicity of northeast Russia showing approximately 39,000 epicenters. Seismicity related to subduction of the Pacific plate under Kamchatka and the Kurile and Aleutian Islands are omitted. Seismic network boundaries and stations as in Figure 1 are shown for reference.

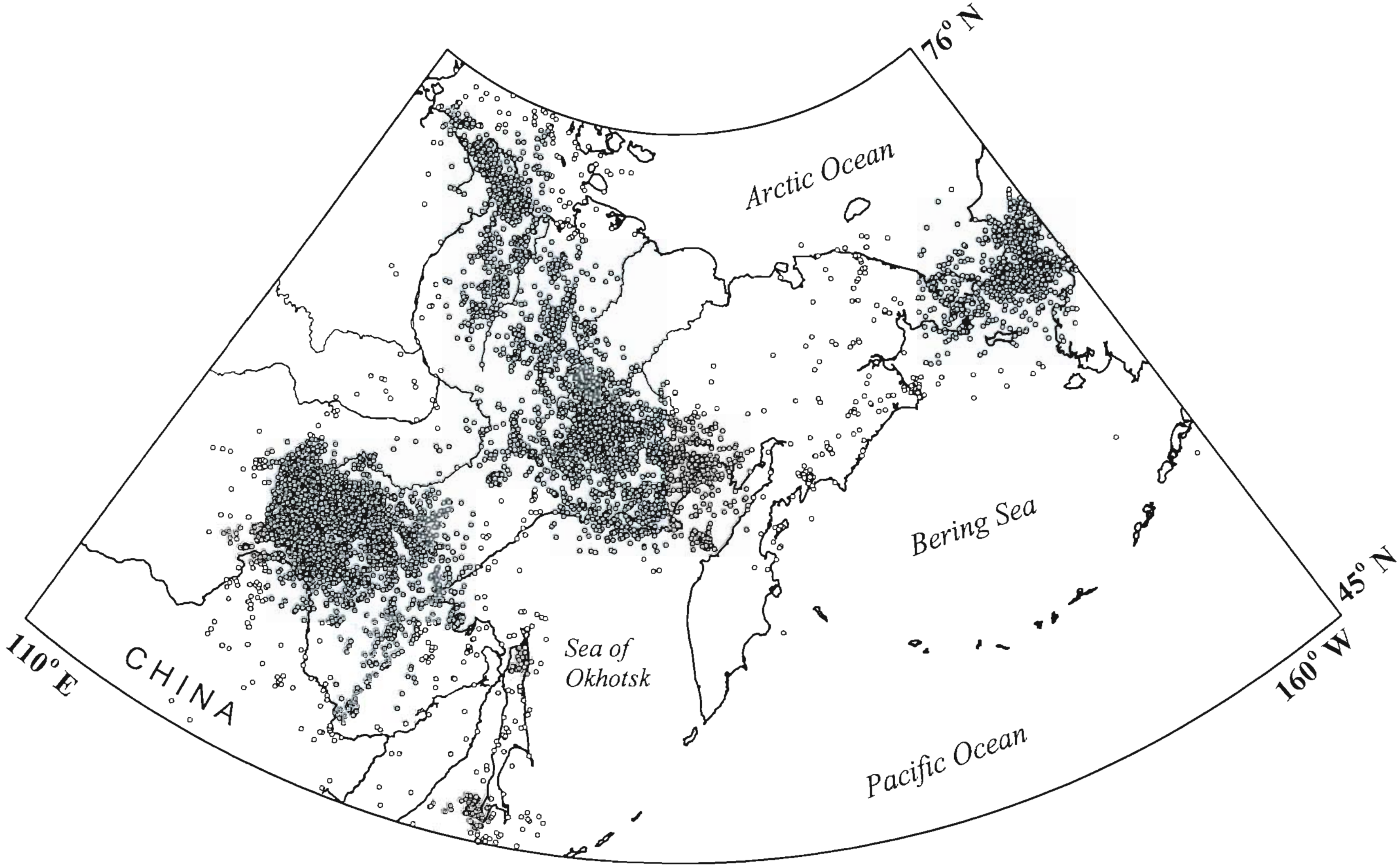

Figure 3. Events in the seismicity catalog for which phase data have been entered into the computerized database. About 14,000 events are depicted.

9.5 occurring within a network. *Materialy* was published in low print quantities with distribution generally to the seismic networks in Siberia.

1.2.3 Seismologicheskii Byulleten' - Dal'nego Vostoka.

This quarterly bulletin (*Seismologicheskii Byulleten' - Dal'nego Vostoka*; Seismological Bulletin - Far East; referred to as *Far East Bulletin*) is similar in format to *Materialy*, and contains both epicenter lists and phase data covering the time period 1972-1990. The *Far East Bulletin* covers the Magadan (listed as separate networks of "Far East" and "Chukotka"), Amur, Sakhalin, Kamchatka, and Kurile networks. The epicenter list provided here is generally complete for Magadan and Amur, although isolated events found in the unpublished data seem to be missing. For the Kamchatka network, only events of K-class larger than 9.0 are listed. Coverage of phase data varies from network to network. The *Far East Bulletin* was also published with a low print run.

1.2.4 Unpublished Magadan Network Bulletin.

The epicenter lists and phase data found in the unpublished Magadan Network Bulletin (1977-2001) for located events is identical in content and format to that found in the *Far East Bulletin*. The unpublished bulletins contain much additional material on explosions and unlocated events.

1.2.5 Unpublished Yakutsk Network Draft Material.

Unpublished data from the Yakutsk network has been acquired in varying degrees of completeness (nearly complete for 1982-1997). The material includes epicenters and phase arrival times from all earthquakes within the Yakutsk network. Also included are epicenters and phase arrival times for events that occurred in adjacent networks. Many explosions with associated arrival times are given but not always located. All of the unpublished draft material is handwritten and has had to be made machine readable. For several years of the Yakutsk draft material, a supplement of unpublished Irkutsk network data is included.

1.2.6 Unpublished Kamchatka Seismicity Catalog.

An epicenter catalog was obtained from Petropavlovsk listing all seismicity in the Kamchatka network from 1962 - 1998. The catalog contains approximately 60,000 located earthquakes. A limited amount of unpublished phase data was also obtained from Petropavlovsk.

1.2.7 Seismograms.

Supplemental arrival times were hand-picked from seismograms in Yakutsk and Magadan, as well as develicorder film in Alaska.

1.2.8 Other.

Miscellaneous data was acquired from various other publications. Earthquake data for 1920-1999 were obtained from the International Seismological Centre, the International Seismological Summary, the U.S. Geological Survey (PDE and QED listings), Alaska Earthquake Information Center (AEIC), Kondorskaya and Shebalin (1982), Andreev (1967), Avetisov (1996), Starovoit et al. (1995). Additional information on explosions was obtained from Godzikovskaya (1995).

1.3 SEISMIC NETWORKS AND DATABASE ASSEMBLY.

Assembling the seismicity database of northeast Russia required a considerable effort. A more detailed analysis of the networks can be found in Mackey (1999).

In assembly of the database, it was noted that there are some problems with data supplied to global databases, such as ISC, for events occurring in the northeast Russia. Data reported to the global databases are often preliminary time picks done by station operators, and often have high residuals. This can result from poor time picks, or a secondary Pg phase being reported as a first arriving P_n phase. The published bulletins of Russian origin (*Materialy* and *Far east Bulletin*) and unpublished data obtained from several of the networks discussed below contains a more complete, and final analysis of the seismograms, done by a professional analyst. This results in discrepancies between data reported in global databases and Russian sources. In such cases, the phase and time from the Russian sources were used, as they were not derived from preliminary seismogram analysis, and were found to contain better time and phase picks.

1.3.1 Northeast Russia Test Network.

In the mid 1960's a number of experimental seismic stations were established throughout northeast Russia to determine background seismicity levels to aid in developing permanent seismic networks (Mishin, 1967). The distribution of seismicity located using the test network (Figure 4) was instrumental in site selection for future seismic stations. Most of the temporary stations were deployed between 6 months and 1 year (Andreev, 1967). Arrival times and phase data for the recorded events are not available. Epicenters are listed in Andreev (1967).

1.3.2 Station Iul'tin and the Magadan EMSD Chukotka Network.

Small events occurring in the Chukotka region were undetected until 1966, when seismic station Iul'tin (Figure 5) opened in Chukotka. Chukotka epicenters reported in Kondorskaya and Shebalin (1982; NCSE) from 1966 to 1974 and the annual *Zemlet* from 1966 to1982 are single station locations from ILT. Statistical analysis of origin times of an epicenter cluster to the northwest of ILT has shown that this activity is likely due to blasting in gold mining operations around Polyarnyi being misidentified as tectonic events (See Section 2).

Events located to the east and south of Iul'tin define a rough northeast to southwest trend, which can not be associated with any known mining activity. Statistical analysis of origin times for these does not indicate any significant time biases, thus epicenters probably represent tectonic earthquakes. Analysis of some of these earthquakes with reread data from the western Alaska network indicates that the Iul'tin determined epicenters are of reasonable quality given the difficulties of single station locations.

The Chukotka regional network contained six seismic stations which were operated from 1982 to 1993 by the Magadan Experimental Methodological Seismological Division (Figure 6). Arrival times from station ILT supplemented data from the Chukotka network in analysis, and are included in data catalogs. Focal parameters from the Chukotka network were determined using the same procedures and seismic velocities as described below for the Magadan network. Most mining explosions were identified in the location process using time and location by local operators and excluded from earthquake catalogs and bulletins. Unfortunately, in 1993, all seismic stations in Chukotka were closed because of financial constraints. Bilibino (BILL) was reopened as an IRIS GSN station in 1995 and Anadyr (ANYS) was reopened in 1996 as an analog station with assistance from the Chukotka regional government.

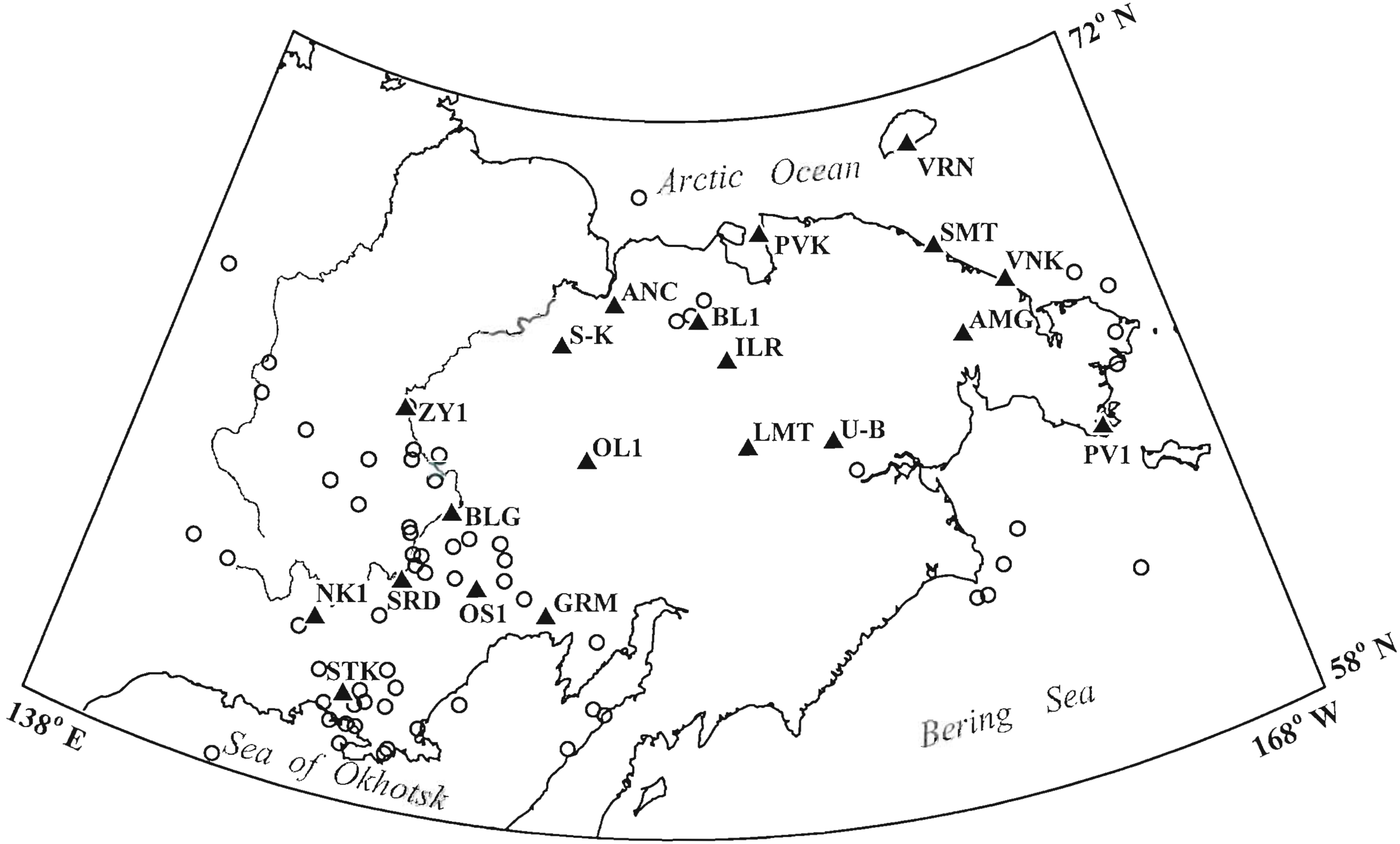

Figure 4. Seismicity and seismic stations of the northeast Russia temporary network (1962-1967).

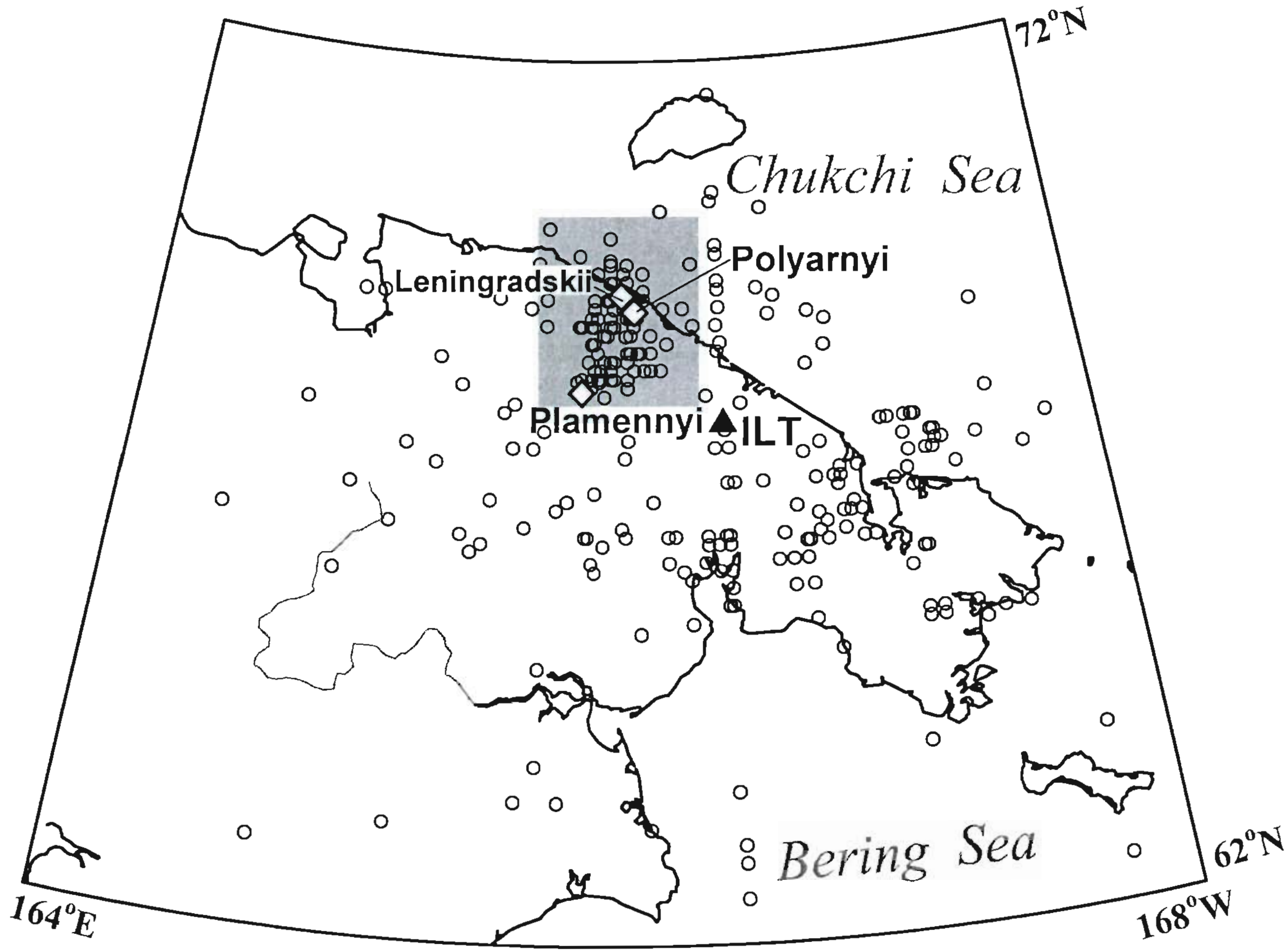

Figure 5. Seismicity located by station Iul'tin (ILT) from 1966-1982. The large cluster of seismicity to the northwest of Iul'tin (grey box) is most likely explosion contamination (see Section 2). Major mine locations are also shown as diamonds.

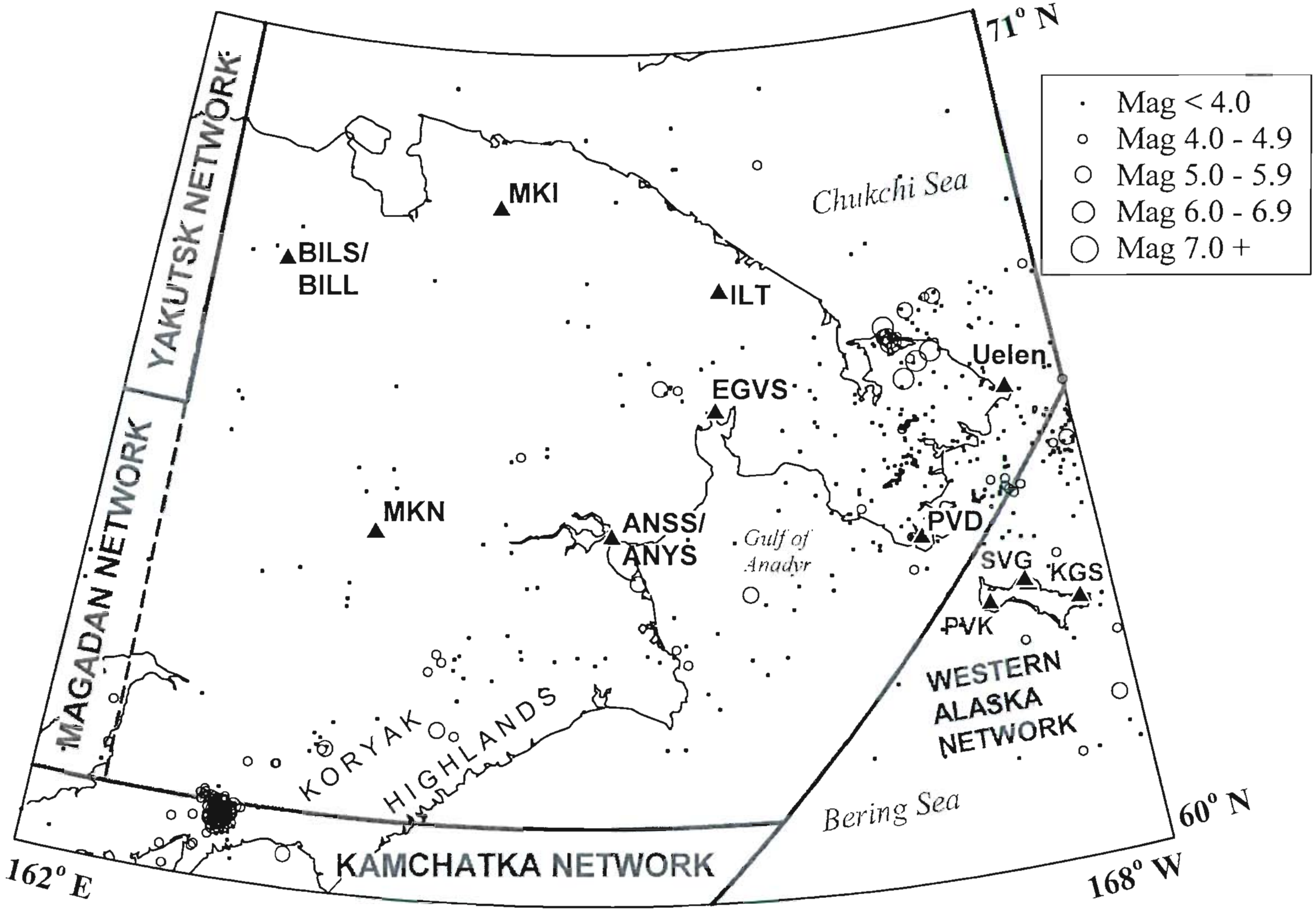

Figure 6. Seismicity and seismic stations of the Chukotka network.

Hypocenter parameters were primarily taken from *Zemlet* (1966-1982) and *Materialy* (1983-1991). Phase data and arrival times for events larger than K-class of 9.5 were taken from *Materialy* (1983-1991). Phase data and arrival time for smaller events are from the unpublished Magadan network bulletins (1983-1991). All data since 1991 is from unpublished network bulletins. For approximately 50 events, phase data and arrival times from the Chukotka network were supplemented with data reread from Alaskan stations.

1.3.3 Magadan Regional Network.

The first station opened in the region was Magadan in 1952. In the late 1960's, following the deployment of the northeast Russia test network, installation of permanent seismic stations began. These stations were initially operated in conjunction with stations in the Yakutsk network. The Magadan Experimental Methodological Seismological Division (EMSD) network was formally established in December 1979, to monitor regional seismicity. The Magadan EMSD has operated a total of 15 permanent seismic stations in the region (Figure 7), excluding those in the Chukotka network, with the largest number of stations open in the late 1980's and early 1990's. Beginning in 1992, economic problems stemming from the collapse of the Soviet Union resulted in drastic cutbacks by the network and the closure of several stations. Today, eight stations are open, with Magadan (MA2) being a Global Seismograph Network (GSN; IRIS) station. Seymchan (SEY) was established as a Geoscope station in the early 1990's. Due to equipment problems, the Geoscope station in Seymchan was essentially abandoned in the mid 1990's. In the summer of 1999, four stations were converted from analog photopaper to 24 bit resolution digital recording with assistance from MSU. This also reestablished digital recording of the abandoned Geoscope instruments in Seymchan. In 2000 and 2001, additional digital stations were opened. See Section 5 below for details on digital station deployments.

There have been three methods of determining earthquake locations in the Magadan network, each using crustal Pg and Sg wave time differences. Prior to 1982, locations were computed primarily by hand and occasionally using a "Besmas 6", an electronic calculating machine. In 1982, they began using computers for locations, which were compared to arc on map determined epicenters. The computer determined epicenters were often "adjusted" to better agree with a paper location if there was a discrepancy between the two. The adjustment procedure was dropped in the early 1990's when the network switched to computer only hypocenter calculations. In the location procedure, the travel-time curves used were derived from the 1959 Magadan-Ust' Srednikan DSS (Deep Seismic Sounding; refraction) profile (Ansimov et al., 1967; Davydova et al., 1968). In the location procedure, no station corrections are used, and station elevation is not considered (Gounbina, pers. comm.).

The unpublished Yakutsk bulletin contains a significant amount of additional data for earthquakes in the Magadan Region. However, this supplemental data is not included in any of the published bulletins containing Magadan network data, as it was not exchanged with the Magadan EMSD. The Magadan network only had access to data from the Yakutsk network station in Ust'Nera.

For the database, hypocenter parameters were primarily taken from *Zemlet* and *Materialy* (1963-1991) and unpublished network bulletins (1991- June 1999). Hypocenters from July 1999 through September 2001 were calculated as a part of this study. Phase data and arrival times for events larger than K-class of 9.5 was taken from *Materialy* (1970-1991). Phase data and arrival time for smaller events are from the *Far East Bulletin* (1972 and 1974) and unpublished Magadan network bulletins (1977-1991). All data from 1992 through June 1999 is from unpublished network bulletins. Data from July 1999 through September 2001 were acquired as a part of this study (see

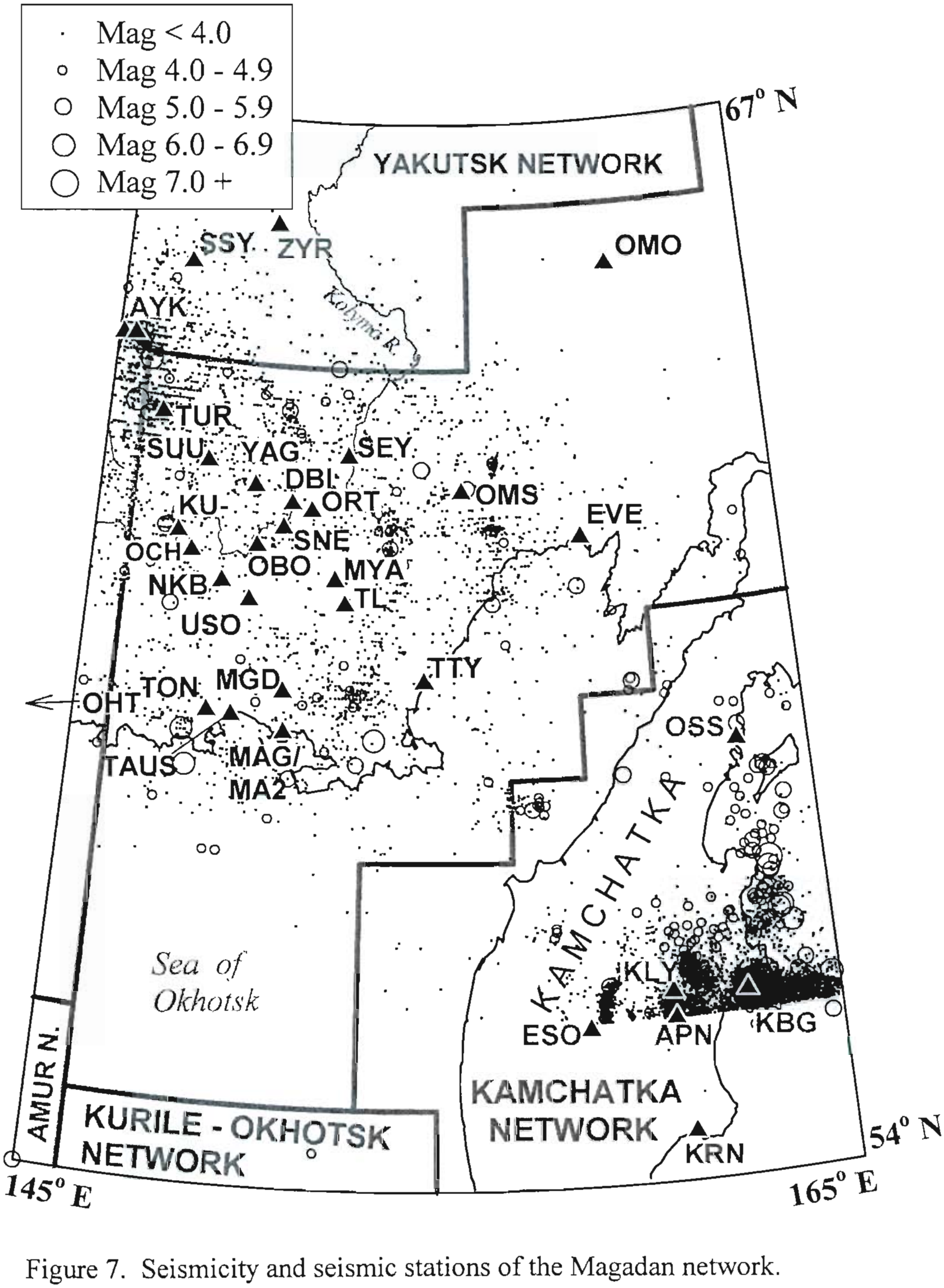

Figure 7. Seismicity and seismic stations of the Magadan network.

Section 6 of this report). All data for Magadan region events listed in the available unpublished Yakutsk bulletin were added to the data files. For several events along the boundary with the Yakutsk network, supplemental arrival times were read from Yakutsk seismograms.

1.3.4 Kamchatka Peninsula Network.

Klyuchi was the first seismic station to open on the Kamchatka peninsula in 1948, followed by Petropavlovsk in 1951. Most remaining stations in the network opened in the early 1960's (Figure 8). Because of subduction of the Pacific plate under the Kamchatka peninsula, this network monitors the most seismically active region in northeast Russia. The Kamchatka network also monitors seismic activity to the north of the subduction zone into the southern portion of the Koryak Highlands, as well as activity on many of the peninsula's active volcanoes. As this study is interested primarily in non-subduction related crustal level events, only earthquakes in the region north of 56° N (the northern edge of the subduction zone) are included. Along the boundary with the Magadan network in the Koryak Highlands and in Shelikhov Bay, many events were independently located by each network, and there seems to have been essentially no exchange of phase data for anything but the largest teleseismically recorded events. Given a choice, the Magadan network hypocenter is usually preferred over that from the Kamchatka network because the Magadan network generally had better station coverage. Hypocenter locations for the Kamchatka north of 56° N were taken from the unpublished Kamchatka seismicity catalog for 1962 to 1998. A limited amount of unpublished phase data from the Kamchatka network for events bounding the Magadan network was also obtained and used in relocations.

1.3.5 Yakutsk Regional Network.

The first station opened in Yakutsk in 1958, with the Yakutsk network being established in the late 1960's to monitor regional seismicity. The Yakutsk network has operated a large number of permanent seismic stations in the region, with the maximum number in the late 1980's and early 1990's. Beginning in 1993, economic problems stemming from the collapse of the Soviet Union resulted in drastic cutbacks by the network and the closure of several stations. In the early 1990's, IRIS stations were opened in Yakutsk and Tiksi. The station in Ust'Nera was moved in 1992, and converted to 24 bit digital acquisition in June 1999 with assistance from MSU.

All earthquake locations determined by the Yakutsk network are by the arcs on map method. For location purposes, the Yakutsk network is broken into northern (Figure 9), and southern regions (Figure 10). The northern region locates earthquakes on a 1:5,000,000 scale map, and includes stations north of 60° N, while the southern region includes stations south of 63° N. Stations used in determining locations are only those which are found within the bounds of the map on which the arcs are drawn. Data from the northern region were not used when locating earthquakes from the southern region, as the northern stations do not fit on the map. Data from the southern region were not used for northern region earthquakes for the same reason.

For the database, hypocenter parameters were primarily taken from *Zemlet* and *Materialy* (1963-1991) and unpublished network bulletins (1991-1997). Phase data and arrival times for events larger than K-class of 9.5 was taken from *Materialy* (1970-1991). Phase data and arrival time for smaller events are from unpublished Yakutsk network bulletins (1982-1997). All data since 1991 is from unpublished network bulletins. As in the case with the Magadan region, there is much data acquired by stations in other networks which was not exchanged with the Yakutsk network, and subsequently not included in any of the published bulletins. Historically, the Yakutsk network had access to data from the Magadan stations of Susuman, Seymchan, Kulu, and Debin (Figure 7), and occasionally others. However, overall, the acquired unpublished Magadan network

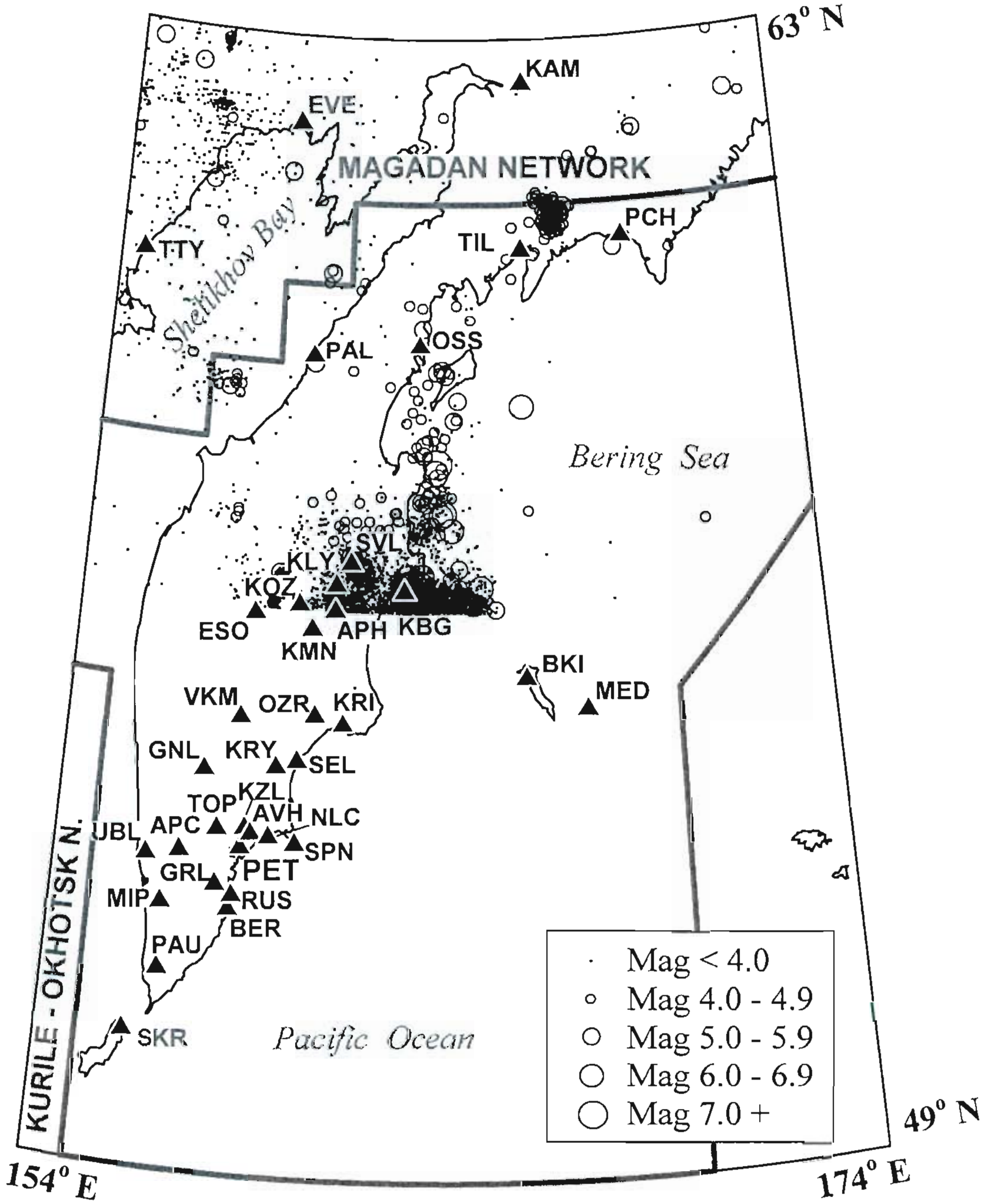

Figure 8. Seismicity and seismic stations of the Kamchatka network. Only seismicity north of 56° north are included. A few stations associated with volcano monitoring are omitted for clarity.

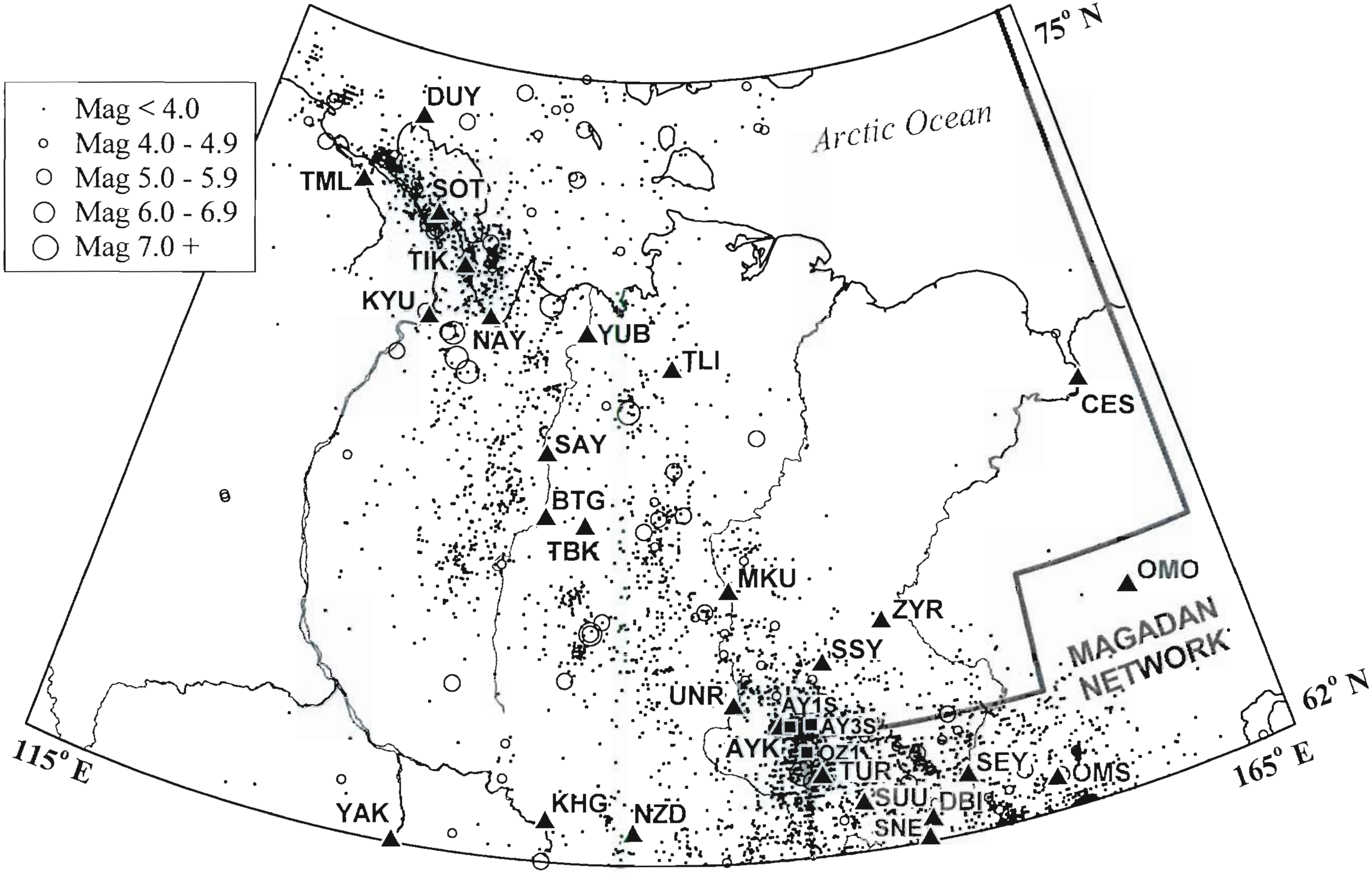

Figure 9. Seismicity and seismic stations of the northernYakutsk network. Temporary seismic stations deployed after the 1971 Aryk earthquake are shown as squares.

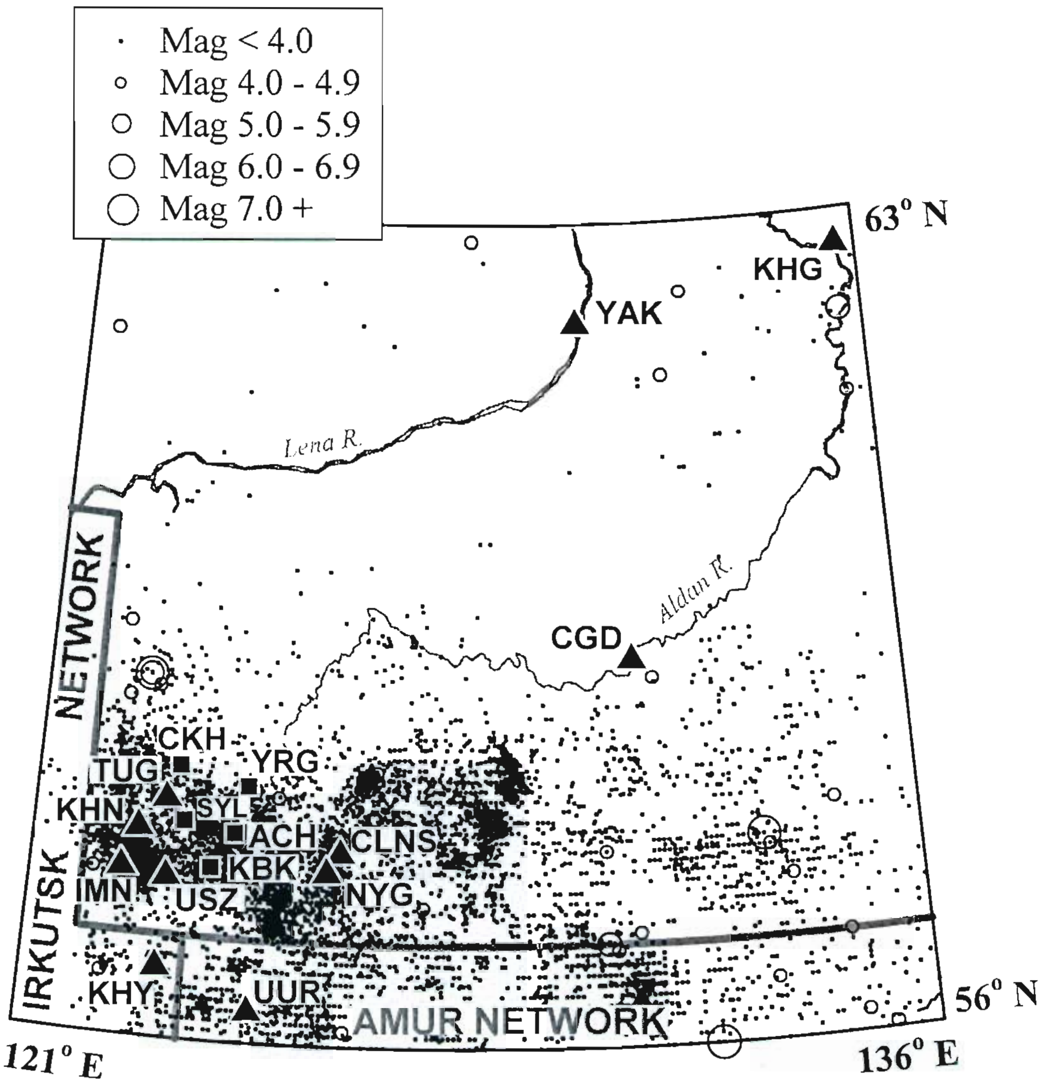

Figure 10. Seismicity and seismic stations of the southernYakutsk network. Temporary seismic stations deployed after the 1989 south Yakutia earthquake are depicted as squares.

bulletin added a significant amount of phase and arrival time data for events in the Yakutsk network. For several events along the boundary with the Magadan network, additional supplemental arrival times were read from Magadan network seismograms. Of stations in the Amur and Irkutsk regions, generally only Kirovskii (KIR), Tupik (TUP), Srednyi Kalar (SRK), and Chara (CRS) were used by the Yakutsk network.

1.3.6 Amur, Sakhalin, and Irkutsk Regional networks.

The Amur and Irkutsk networks monitor seismicity between the Eurasian plate and the Amur plate. The Sakhalin network monitors seismicity along the boundary between the Amur plate and Okhotsk block. Unfortunately, we have not worked directly with any of these networks, thus first hand knowledge of operational procedures and unpublished data are generally not available.

Permanent seismic stations in the Amur network region first opened in the early 1970's (Figure 11). Seismicity data from the Amur and Sakhalin networks comes primarily from the *Far East Bulletin* for events prior to 1979. Since 1979, event parameters are taken from *Materialy, Zemlet*, and the *Far East Bulletin*. Since 1982, many additional Amur events not found in other sources are available in the unpublished Yakutsk network bulletin.

Phase data from the Amur region is taken from the *Far East Bulletin* (1972-1978, 1985-1988), *Materialy* (1979-1990), and unpublished Yakutsk network bulletins (1982-1997). Some phase data from the Sakhalin network stations (Figure 11) are given in the published bulletins of Amur region events. Phase data from the Sakhalin network are available in the *Fat East Bulletin*, but were not included in the data files.

Seismic stations in the Irkutsk region were first established in the 1950's, with the exception of Irkutsk, which opened in 1901 (Figure 12). This study includes only a small portion of the Irkutsk network (south of 56° N between 120° and 122° E), thus only a relevant subset of the seismic stations are listed (those stations used to supplement Yakutsk and Amur network phase data). Epicenter data for the portion of the Irkutsk network of interest is taken from *Materialy*. Phase data for some of these events were included in the data files.

1.3.7 Seismic Station Parameters.

Considerable effort was devoted to compiling as complete as possible listing of seismic stations to have operated in northeastern Russia (excluding SSD military sites). The station list covers many different seismic networks (e.g. Mackey, 1999; Mackey and Fujita, 1999), and represents what is believed to be the most reliable coordinates available (Appendix A). Several of the stations given here are listed in international station compilations but with a lower level of location precision and/or accuracy. Several stations were documented to have moved slightly one or more times, but parameters for which were never updated or new station codes assigned. The majority of the information tabulated here was obtained directly from the seismic networks, personnel who actually operated stations, station site visits, and various Russian gray literature publications. However, it is not reasonable to document all sources of information used in a report of this scope. This compilation of seismic stations is continuously updated as information becomes available.

Coordinates of most stations listed were hand checked using 1:200,000 Soviet/Russian General Staff military topographic maps. In a few cases, coordinates were adjusted if the map check showed the station to be in an unreasonable place. For example, the possible location of station Bering was found to reside in the ocean, thus the coordinates of the seismic station were adjusted to place it at the meteorological station immediately onshore; a reasonable correction given knowledge of operational procedures in northeast Russia.

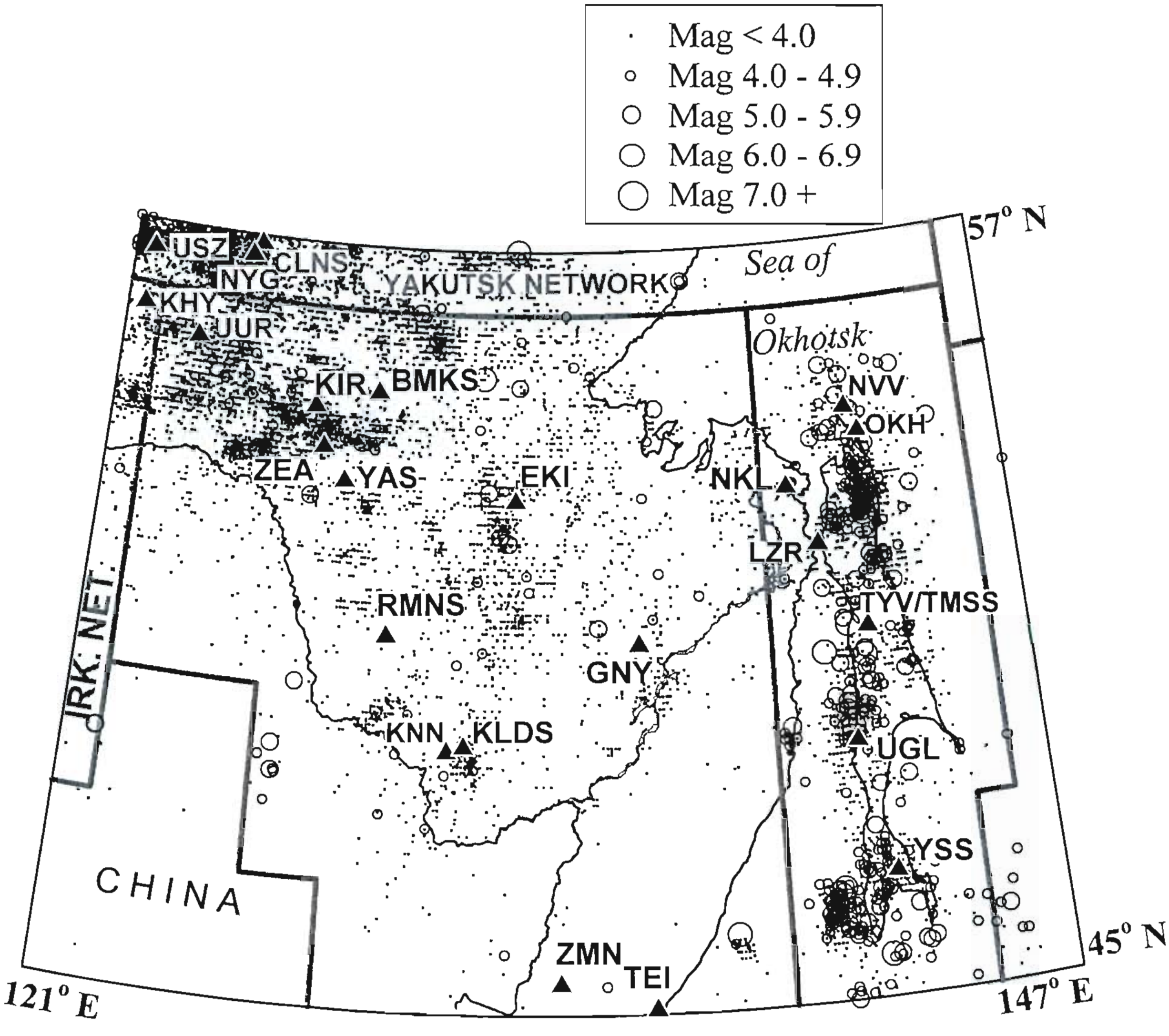

Figure 11. Seismicity and seismic stations of the Amur (left) and Sakhalin (right) networks.

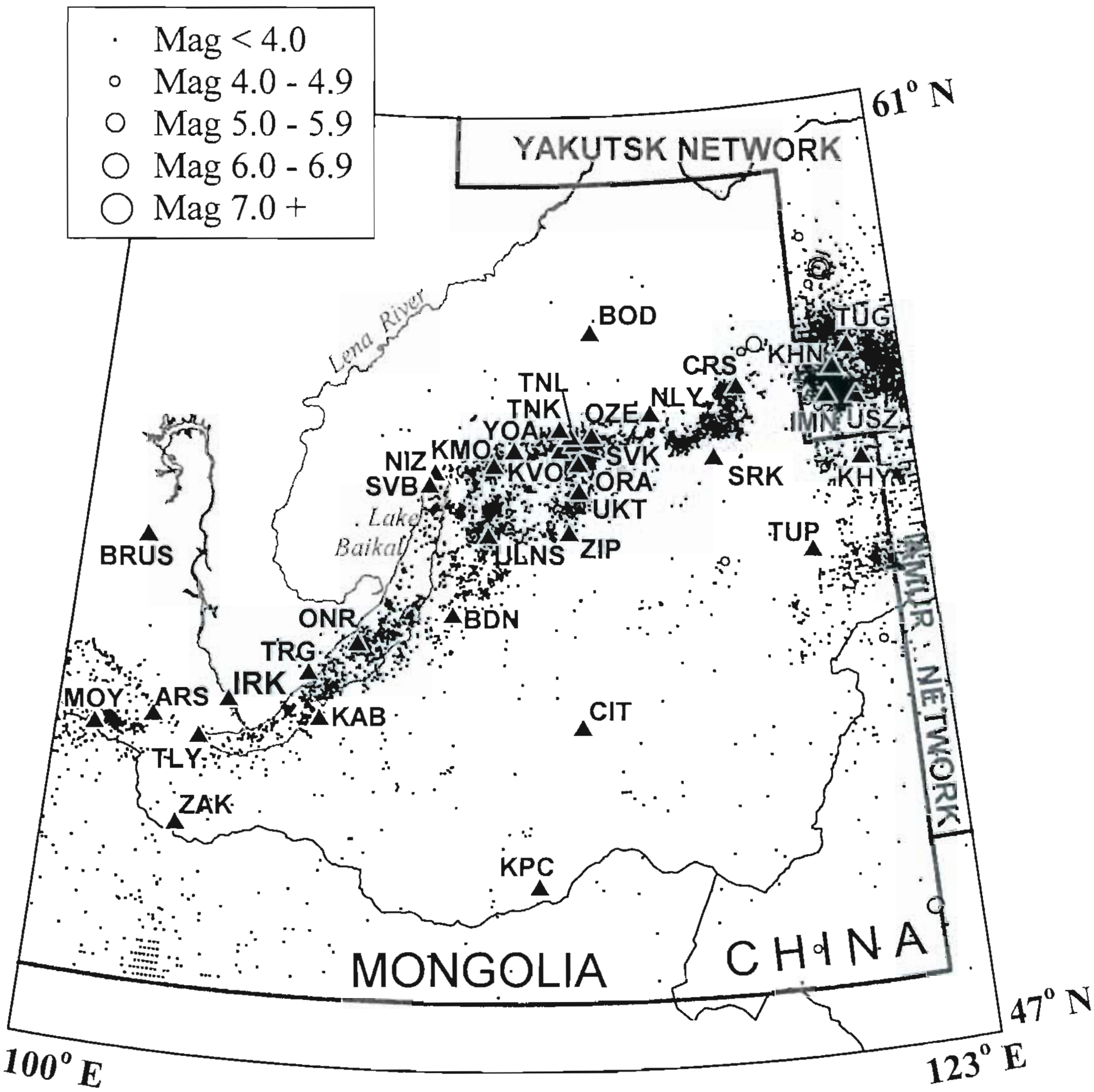

Figure 12. Seismicity and seismic stations of the Irkutsk network. Seismicity shown is primarily from 1970 through 1972.

1.3.8 Relationships between magnitude and K-class.

It is standard practice among Russian seismic networks to report magnitudes only for events of about $M_b = 4.0$ and larger. However, all events, both small and large, have sizes reported as a K-class value, which is based on the logarithm (base 10) of work release in Ergs. For determining K-class, the maximum ground motion A_{max} is determined using

$$A_{max} = (A_p + A_s)/T \qquad (1)$$

where A_p and A_s are the respective maximum amplitudes of the P and S arrivals (in microns) and T is the period (in seconds) of the wave. If no amplitude is visible for the P phase, only the S is used. The K-class value, using A_{max} from (1) and distance, is then read off a nomogram calibrated for each particular region (Solonenko, 1974; Pustovitenko and Kul'chitskii, 1974). Unfortunately, the nomograms calibrated for different regions or networks vary significantly, resulting in inconsistent event size determinations between networks. For example an earthquake having a magnitude of 3.5 may be reported to have a K-class of 9.0 in one network, and a K-class of 10.5 from the neighboring network. To better understand the sizes of events reported in the seismicity catalog, empirical linear regressions were calculated relating K-class to magnitude for each network (Figure 13). Magnitudes used are ISC reported M_b values up to 5.5. Events larger than magnitude 5.5 use ISC or NEIC reported Ms values as body wave magnitude begins to saturate (Lay and Wallace, 1995).

1.4 CONCLUSION.

The final compiled seismicity map with network boundaries and seismic stations is shown in Figure 2. In reality, the distribution of microseismicity indicates diffuse plate boundaries, probably having motion partitioned on many individual faults in a complex system, which is consistent with continental deformation (England and Jackson, 1989). Within the individual plate boundaries, there are many localized trends and clusters in the seismicity distribution which have never previously been studied in detail. However, several of these clusters and trends, particularly in the Amur region, are a result of anthropogenic sources (see Section 2). In general, the plate boundaries tend to follow the pre-existing large scale structural trends in northeast Russia, which probably represent structurally weaker, and thus easier to deform, regions. The proposed boundary between the Eurasian plate and the Okhotsk plate is somewhat problematic. There have been relatively few teleseismic events defining the location of the boundary, and there is an almost complete lack of located microseismicity in the region. The lack of located microseismicity may be entirely an artifact of the distribution of seismic networks. Note on Figure ES-1 that the region is near the intersection of the Magadan, Yakutsk, Amur, Sakhalin, and Kurile-Okhotsk networks. Furthermore, the division between the northern and southern portions of the Yakutsk networks is also in this region. There is microseismicity trending into the region from each of the Magadan, Yakutsk, and Sakhalin networks. Given the distances to individual networks stations, and the lack of data exchange between neighboring networks, small events occurring in this region are most likely simply below the detection or location threshold for any individual network. However, analysis of data from the digital station deployed in Okhotsk as a part of this study also does not show significant levels of seismicity in this region (see Section 5).

Overall, seismicity levels in northeast Russia are much higher than generally recognized in the literature. Unfortunately, economic conditions in Russia at the present time have resulted in the closure of many, if not most, of the regional seismic stations. This illustrates the importance of

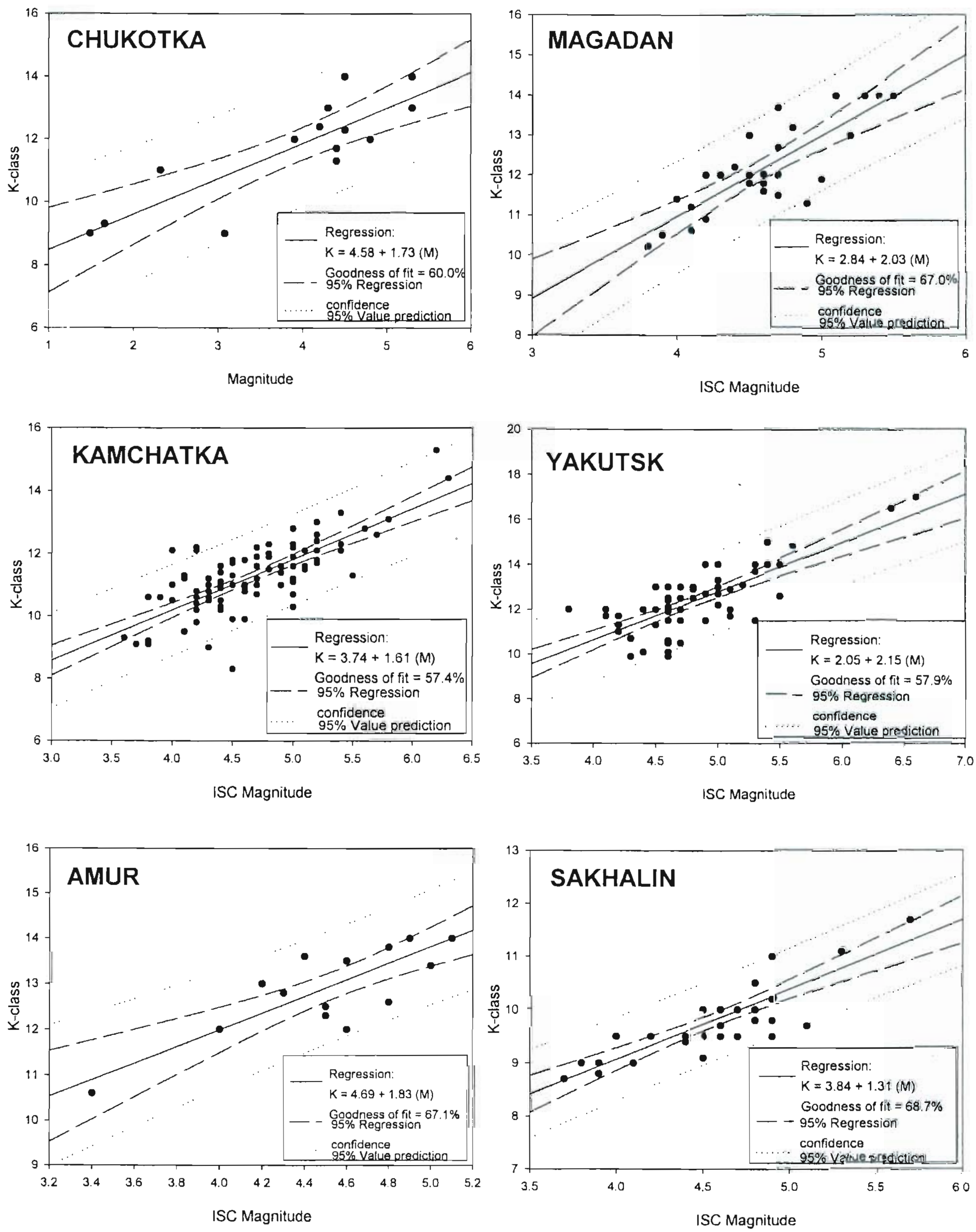

Figure 13. Linear regressions relating K-class to Magnitude for different networks in northeast Russia. Magnitudes up 5.5 are M_b and greater than 5.5 are M_s. Note that the derived regressions vary considerably between networks.

compiling the historic data, as further economic collapse in Russia could result in the permanent loss of the original data. It would take the installation of several tens of permanent digital stations and a minimum of two decades to duplicate the historic database using modern acquisition methods.

SECTION 2

EXPLOSION CONTAMINATION IN THE NORTHEAST RUSSIA SEISMICITY CATALOG

2.1 INTRODUCTION.

The newly compiled seismicity catalog for Eastern Russia (see Section 1) allows us to re-examine the regional seismicity of northeastern Russia to determine the level of explosion contamination and obtain a better idea of the level of natural seismicity in the region. In this part of Russia, explosions occur in tin, coal, and placer gold mines as well as in the construction of roads, railways, and dams. Many of the active mining regions are geographically associated with the seismically active regions, which can result in misidentification of mine blasts as earthquakes. Unfortunately, contamination of the seismicity catalog with explosions results in an erroneous perception of natural seismicity as well as seismic risk assessment.

This section summarizes explosion contamination in the study area through temporal analysis of origin times. Both time of year and time of day are considered. While analysis of waveform data for all reported earthquakes would require an unrealistic re-examination of several hundred thousand analog seismograms, a qualitative estimate of the level of explosion contamination can be obtained by examining the spatial, size, and temporal characteristics of earthquakes located by the regional networks.

2.2 DATA SOURCES.

The origin times of earthquakes used here come from the compiled seismicity database for northeastern Russia as described in Section 1. Information on known explosion locations comes from the unpublished Magadan and Yakutsk network bulletins. The unpublished Magadan bulletin lists explosions either by region (nearest town) or mine (Figure 14). Many mines or regions have hundreds of explosions identified. The unpublished Yakutsk bulletin lists explosion coordinates and origin times determined by locating the event with S-P time differences (Figure 14). The location procedure is the same as that used for earthquakes (Section 1). Only a small fraction of the explosions listed in the unpublished Yakutsk bulletin have been entered into the database. A small number of located explosions in the Amur region are given in Godzikovskaya (1995; Figure 14) for the time period 1990-1991. Mine locations from throughout the study region were taken from 1:200,000 scale Russian military topographic maps, as well as 1:500,000 TPC and 1:1,000,000 ONC scale U.S. air navigation charts (see NERSP-10, in prep.).

2.3 PREVIOUS WORK.

Early attempts at explosion filtering from the late 1960's through mid 1970's in the Magadan region simply removed all events within a particular radius of some mining regions (q.v., Riegel, 1994; Kovalev, pers. comm.). Of course, this also removes the wanted tectonic events, and results in peculiar rings of seismicity. Beginning in the late 1970's, seismic station operators attempted to discriminate close events (up to 50 - 70 km) based on waveform characteristics and information

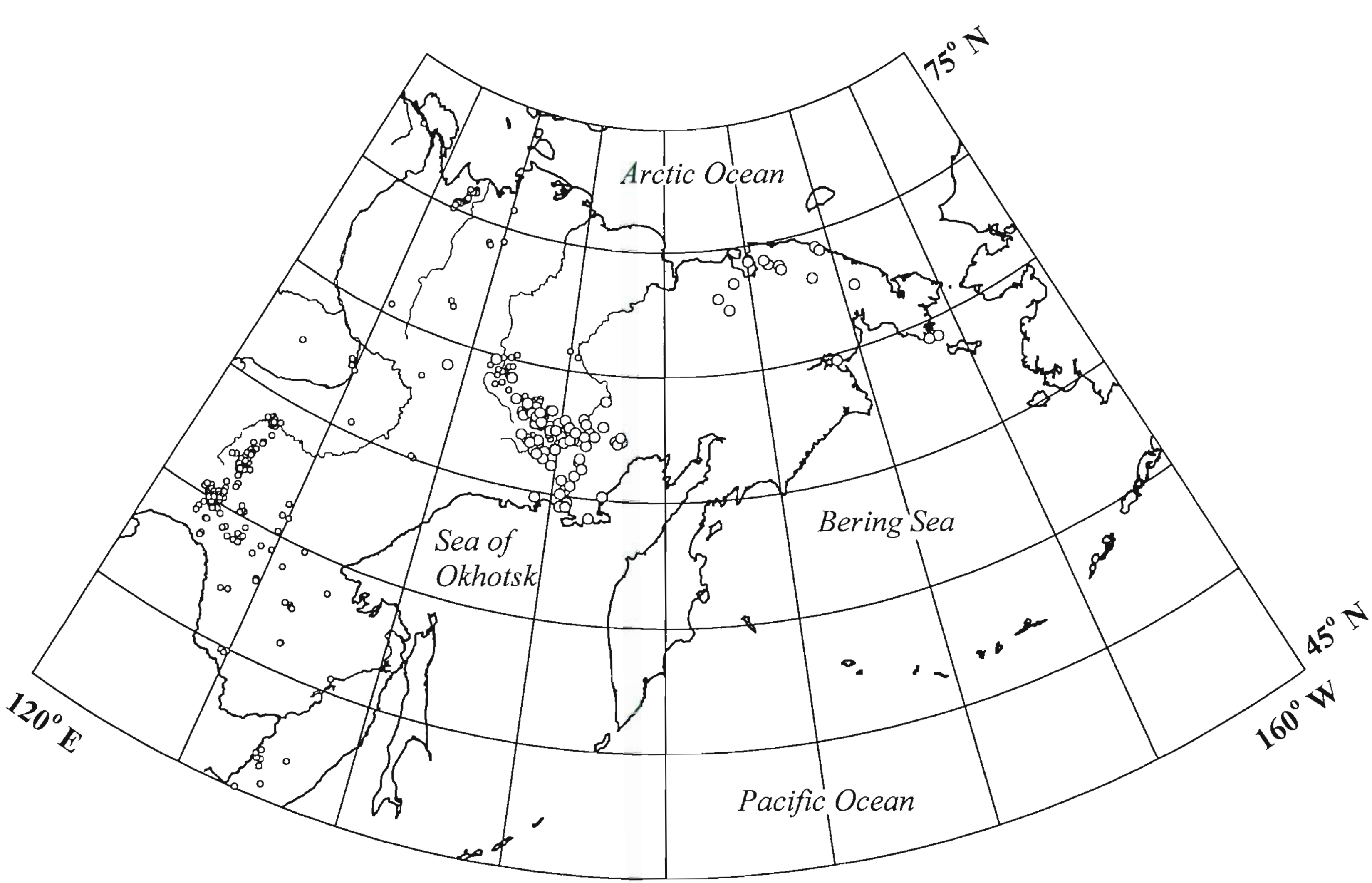

Figure 14. Explosion sources in northeast Russia listed in Russian bulletins. Small dots are individual located explosions, and large dots are towns or mines with multiple explosions. This map is not authorative for all mine explosions in the region.

from the mining companies. Unfortunately, not all mining companies provided information on their blasting activities for various reasons (Kovalev, pers. comm.).

Previous work on identifying explosion contamination in the seismicity catalog was undertaken by Godzikovskaya (1995). Godzikovskaya (1995) identified several regions of explosion contamination, particularly in the Zeya basin region of Amur, near the Kolyma and Ust' Srednekan dams on the Kolyma River, and the Polyarnyi mining district in Chukotka. However, many regions and trends of contamination were not identified because of an incomplete seismicity catalog. Odinyets (1996) identified the problem of explosion contamination in the Kolyma region. In this case, it was determined that a large fraction of earthquakes reported in the central Kolyma region are actually explosions. Industrial explosions locatable by the regional networks generally have magnitudes from about 1.5 up to a maximum of 3.5 (converted from Russian K-class) and occur during local day (Godzikovskaya, 1995; Odinyets, 1996). Placer deposit explosions are also concentrated during the late winter and early spring, when frozen ground is broken up for the summer processing season.

2.4 DISCUSSION.

Although the regional networks operating in northeastern Russia have attempted to discriminate between industrial explosions and earthquakes, all seismicity catalogs containing events of less than magnitude 3.5 from the region remain contaminated with explosions related to the break-up of placer deposits, coal, tin, and gold mining, and construction projects.

Examination of the temporal biases in the seismicity can, in a broad sense, indicate potential regions of explosion contamination (Agnew, 1990), as blasting generally occurs during the day. A small but not statistically significant number of explosions are also known to occur during the nighttime hours in many locations throughout the study area (Godzikovskaya, 1995). In Figure 15, the study area is divided into 0.5 x 1° cells in which the percentages of daytime earthquakes are calculated. North of 64°N, cell size was increased to 0.5 x 2°. Cells containing fewer than ten events were not considered to be statistically significant, thus were not analyzed. As there are five time zones spanning the region, the 12 hour local "day" period was shifted accordingly. Light blue areas represent regions where seismicity is more or less balanced between night and day, and dark blue areas are those in which seismicity is concentrated during local night. Bias of seismicity to local night is not unexpected since most seismic stations are located in populated areas and have lower cultural noise levels during the night. This is consistent with better nighttime recording, particularly for smaller events in the outlying portions of the network. Analysis of the 1989 South Yakutia aftershock sequence confirms the better conditions of nighttime recording; of 3,492 located earthquakes, 1,815 occur during local night and 1,677 during local day.

Pink areas on Figure 15 represent regions where more than 65% of the seismicity occurs during local day. Many of the regions with predominantly daytime events are associated with discrete clusters or trends of seismicity, most of which can be associated with mining or construction related blasting. Several clusters of reported seismicity in the Amur region have more than 90% of the events occurring during local day. A few cells indicate predominantly daytime seismicity, but with no apparent relation to mining. These cells are probably a result of random statistics of small numbers as they are close to the ten event cutoff. Other areas with explosion contamination are discussed in Mackey (1999).

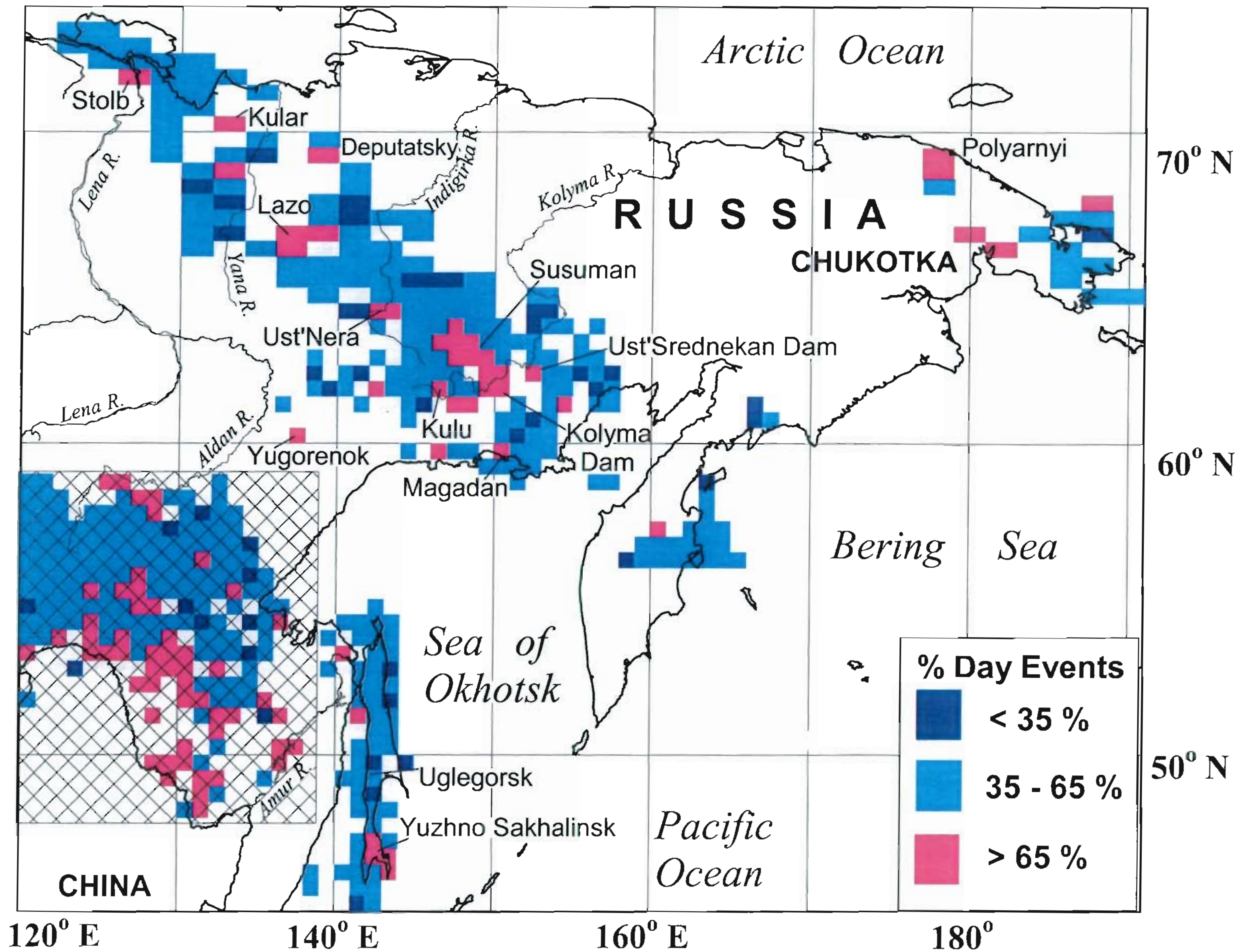

Figure 15. Percentage of seismicity occurring during local daytime. Cells containing primarily daytime events are presumed to have explosion contamination. Labeled regions are discussed in the text. Seismicity associated with subduction of the Pacific plate were not evaluated. The crosshatched area encompasses the southern Yakutia and Amur regions (Figure 16).

2.4.1 Amur and Southern Yakutsk District.

The clearest regions of explosion contamination are in the Amur District. When plotting daytime and nighttime epicenters separately (Figure 16), some distinct differences are apparent. There are several large clusters of daytime seismicity that correlate geographically with specific mining regions. For these regions, contamination levels also change with season. Clusters and trends composed primarily of daytime events have very few events of magnitude 4 or larger. Figures 17 through 21 show the number of events that occur during specific hours of specific months of the year. Figure 17 analyzes a reported cluster of seismicity in the northern part of Figure 16 (labeled 'TEST'). The seismicity in this region is believed to be tectonic, as the region is unpopulated and should not contain any contamination due to mining. The analysis of this region can therefore be used as a baseline to which other analysis can be compared. The area analyzed contains 399 located earthquakes, with 189, or 47.3%, having occurred during local daytime and 205 during local night. The number of summer and winter events occurring in this region are also similar.

Analysis of reported seismicity around the Raychikhinsk coal mining region shows activity only during winter months, and daylight hours (Figure 18). This is somewhat different than from the nearby Khingansk mining region where events occurring throughout the year but also only in the day (Figure 19). Other regions identified in the Amur region show similar distributions of origin times, and are associated with specific mining regions. See Mackey (1999) for additional discussion.

In the central portion of Figure 16A, there is a northwest-southeast trend of predominantly daytime seismicity extending several hundred kilometers. Temporal distribution of these events is shown in Figure 20 for the central segment. This trend correlates with the route of the Baikal-Amur mainline railroad (BAM). Explosions associated with its construction in the 1980's are listed as earthquakes in the seismicity catalogs. Note also that most events are located to the west of the track, indicating systematic errors in the location procedure.

The northern portion of Figure 16 includes the southern Yakutsk network, where two mining regions are of note. Aldan is a mining region with extensive deposits of gold and phlogopite mica (Shabad, 1969). The region is associated with a diffuse cluster of predominantly daytime reported seismicity. Although the seismicity occurs throughout the year, its concentration during daylight hours is more consistent with an anthropogenic source than tectonic. Explosions from the Aldan mining region are also located and listed in the unpublished Yakutsk bulletin.

To the southeast of Aldan is a dense cluster of seismicity near the settlement of Spokoynoi (Figure 15). Temporal analysis of the cluster shows a strong bias towards daytime and winter events, which would be consistent with placer mining (Figure 21). Soviet military 1:200,000 scale topographic maps (dated 1986) show extensive mine workings in the region, but list all the nearby settlements as uninhabited. This is inconsistent, as the events located here occur from the 1970's through the mid 1990's. The published literature lists no mention of any mining activity in this region, nor does the unpublished Yakutsk network bulletin identify any explosions in the region. The nature of activity at this location remains unclear, but may represent residual or exploratory mining. Temporal variation plots of other regions showing contamination on Figure 16 can be found in Mackey (1999).

Overall, the explosion contamination appears to be primarily confined to daylight hours, thus it is assumed that nighttime seismicity should better reflect the natural tectonic distribution of earthquakes (Figure 16b). A different, more northerly trend appears in the plotted nighttime earthquake epicenters, which probably delineates an active tectonic feature that was previously obscured with clusters and trends of explosions. When observing the locations of the larger

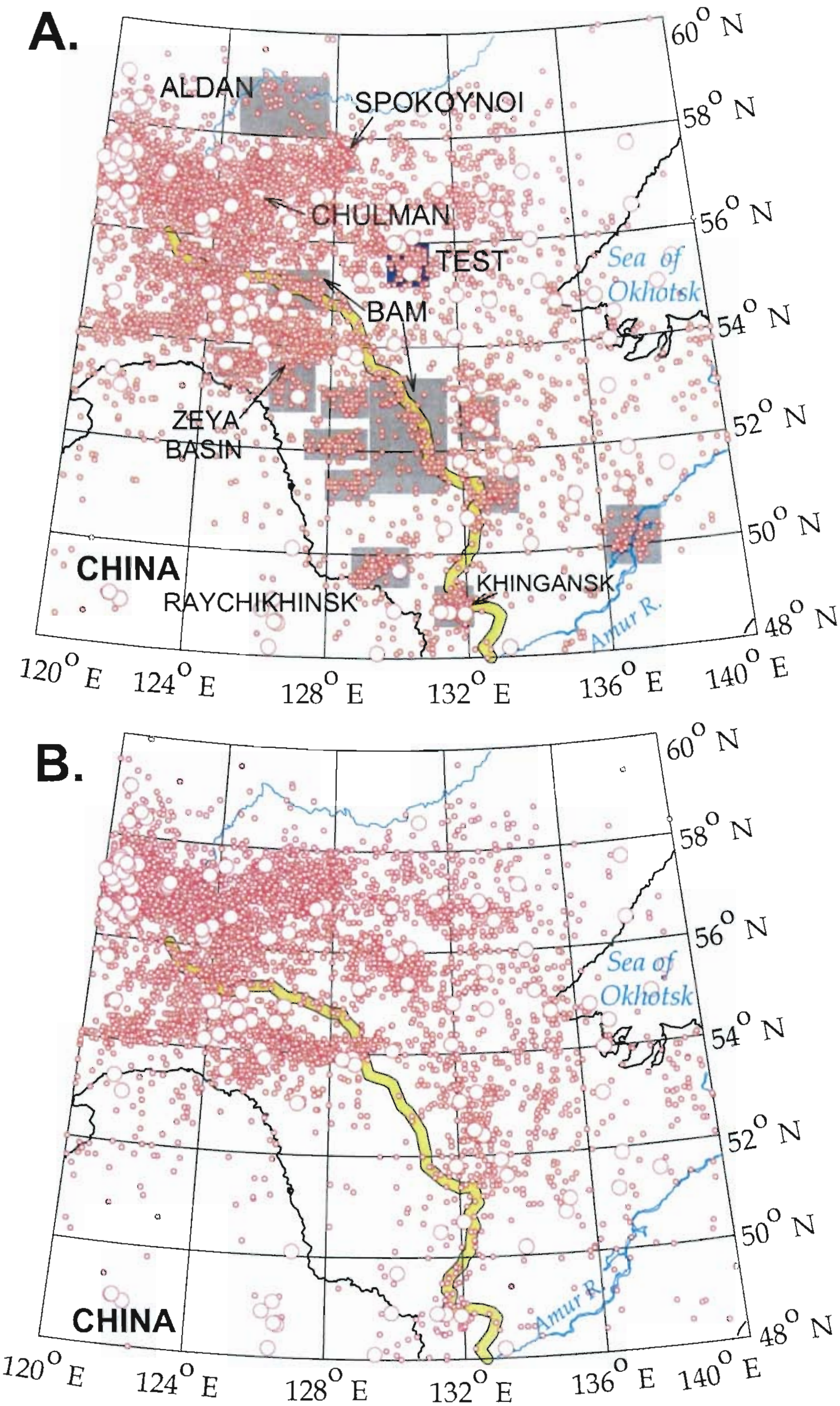

Figure 16. Day (A) and night (B) seismicity of the Amur region. Note a correlation between daytime seismicity and the Baikal-Amur (BAM) railway (yellow). Gray areas indicate clear contamination, while blue indicates the temporal variation test area (Figure 17).

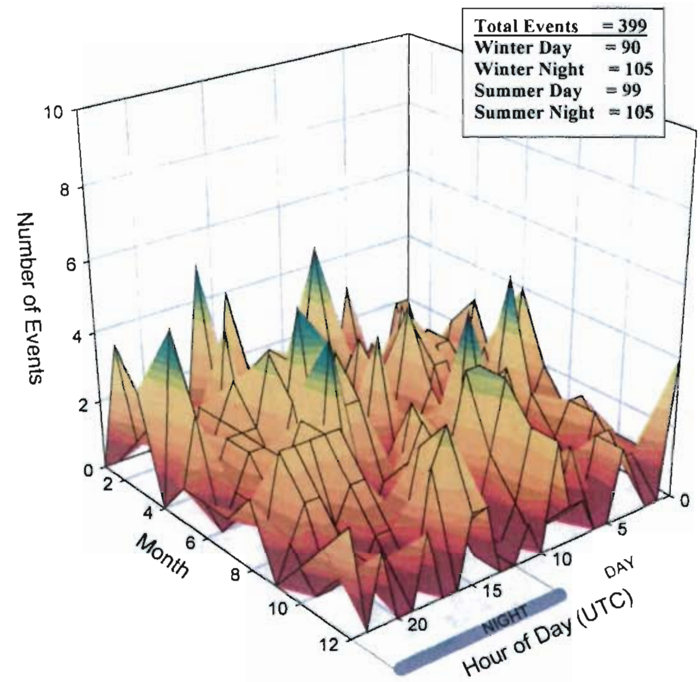

Figure 17. Temporal variation of presumed natural earthquakes from the region labeled 'TEST' on Figure 16. Note a slight bias towards nighttime events, but no seasonal bias.

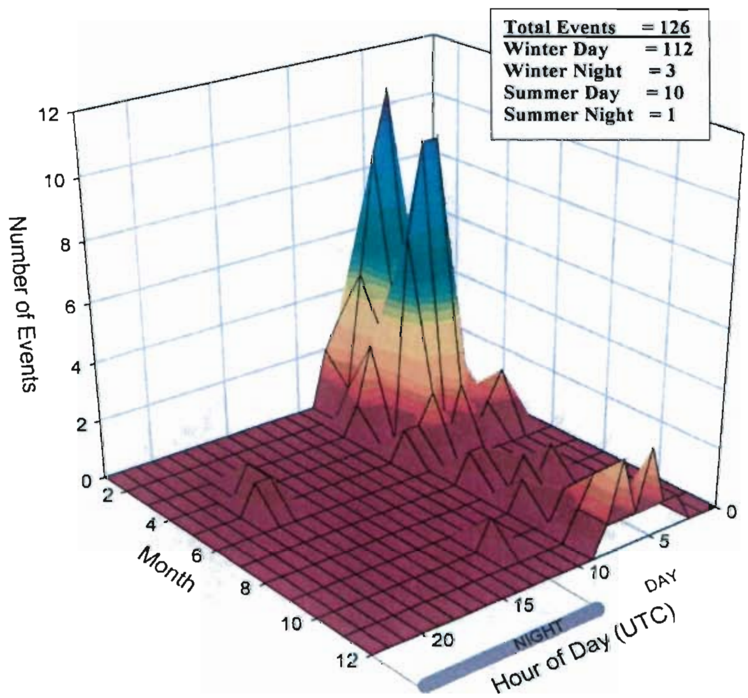

Figure 18. Temporal variation of seismicity in the region of the Raychikinsk mine. Note the strong bias towards daytime winter events.

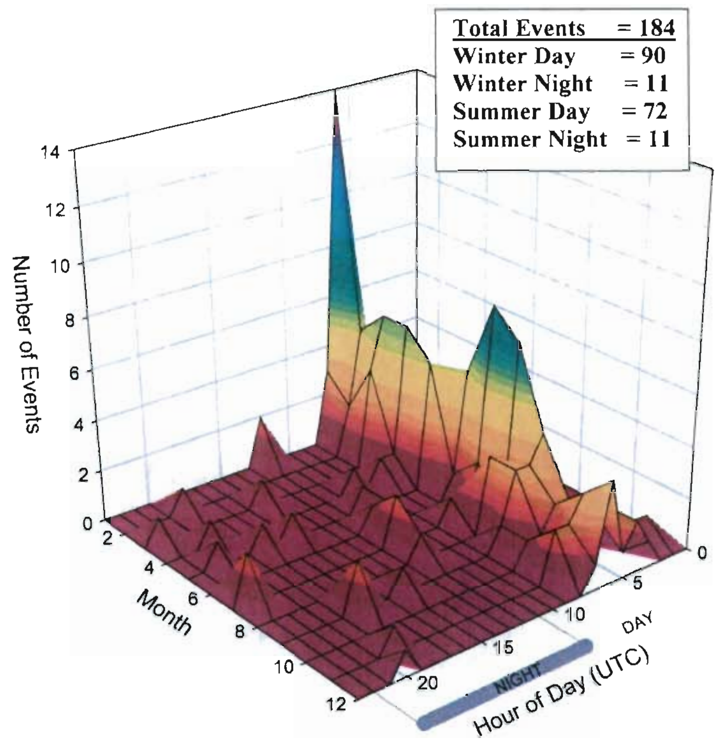

Figure 19. Temporal variation of seismicity in the region of the Khingansk mine. Note the strong bias towards daytime events.

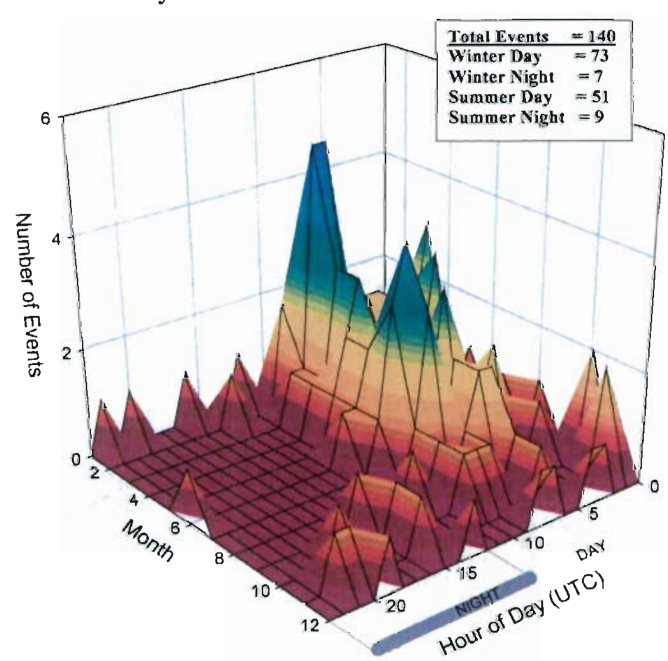

Figure 20. Temporal variation of seismicity associated with the central segment of the Baikal-Amur mainline railway. Note the bias towards daytime events. Most of these events are thought to be explosions associated with construction of the railway.

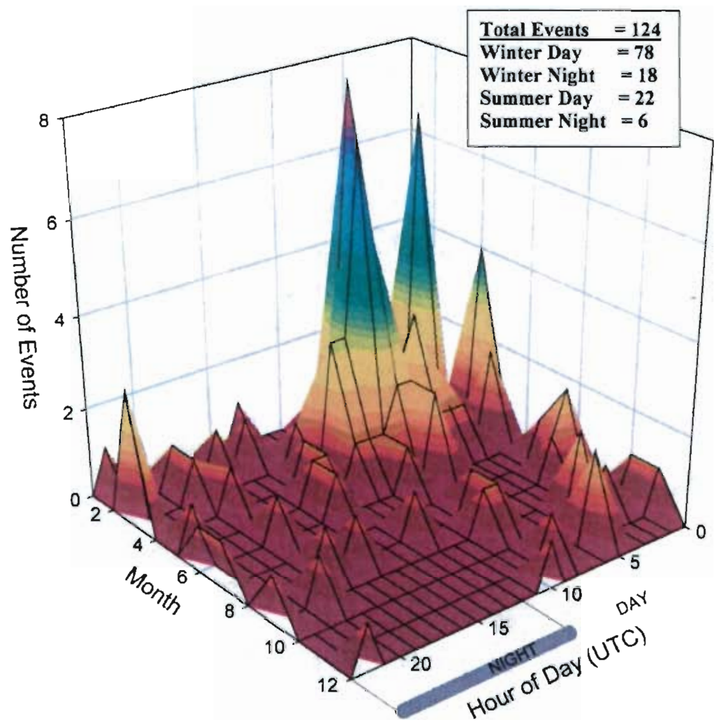

Figure 21. Temporal variation of reported seismicity in the Spokoynoi region.

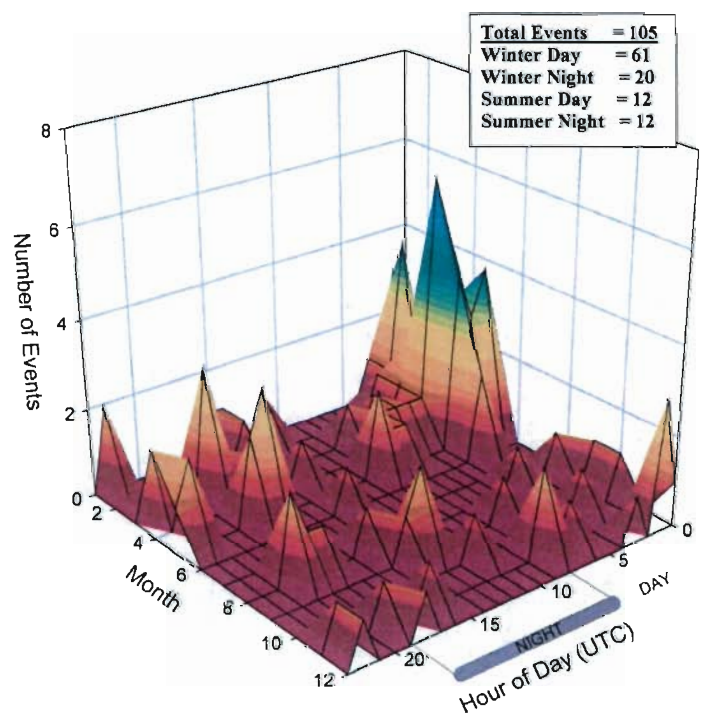

Figure 22. Temporal variation of seismicity in the Polyarnyi, Leningradskii, and Plamennyi mining region. See Figure 5.

teleseismically located events, it is found that they fall almost entirely within the regions where seismicity occurs during the night.

2.4.2 Polyarnyi-Leningradsky-Plamennyi.

Polyarnyi and Leningradsky are placer gold deposits located along the coast of the Chukchi Sea in Chukotka. Plamennyi was a mercury deposit located approximately 100 km to the south which operated from 1967 to 1972 (Pilyasov, 1993; see Figure 5). From 1966 to 1982, most of the events located in this area were single station locations obtained by the three-component seismic station at Iul'tin (ILT; see Figure 5). A clear bias towards winter and daytime is evident (Figure 22) for the cluster of events in the mining region. Comparison of origin times of ILT located events with the more recent known explosions from the same mining region yields a nearly identical temporal distribution.

2.4.3 Kolyma Gold Belt and Northern Yakutia.

A band of predominantly daytime seismicity lies along the Kolyma gold mining belt (Figure 15). Tectonically, this region is extremely complex in that it is located just south of the Ulakhan and Darpir Fault systems (Figure 23), along which motion between the Okhotsk block and the North American plate is occurring (Riegel et al., 1993; Imaev et al., 1994). As a result of the tectonic setting, easy statistical separation of anthropogenic sources from earthquakes is more troublesome. Mining in this region is primarily placer gold, but also includes coal and other minerals. Typical large blast sizes in the placer gold deposits around Susuman may range from 50 - 75 T, while explosions in the coal mines may exceed 200 T (Leith, 1994; see Section 5). Daytime and nighttime seismicity are shown on Figure 23. Temporal analysis of the large cluster of events in the area northwest of the town of Susuman indicates there is a clear bias towards local day and winter/spring (Figure 24). This bias is consistent with the distribution of known explosions from the Magadan seismic bulletin for the Susuman region (Figure 25). Based on the day/night seismicity plots in Figures 23a,b, the eastern half of the seismicity cluster is entirely explosions, while the western half probably contains some tectonic events. Note also the reduced numbers of nighttime events within a 100 kilometer radius of Susuman, which is also probably a result of mining. About 200 kilometers southeast of Susuman is the Kolyma hydroelectric station and dam. Blasting during construction of this dam resulted in contamination of the earthquake catalog (Godzikovskaya, 1995).

The level of seismic activity in northern Yakutia is lower than the Kolyma region, with much of the seismicity in isolated clusters and regions. Several of the clusters associated with mining regions and having predominantly daytime events include Lazo, Ust' Nera, and Kular with placer gold deposits, the Deputatsky tin deposit, and placer diamond exploration near Stolb (Figure 15). The placer gold deposit at Yugorenok in east-central Yakutia is also associated with a cluster of daytime events.

Explosion contamination of the seismicity catalog has clearly affected analysis of seismic hazards in the region. Vazhenin et al. (1997), citing unpublished material by T.A. Andreev, shows an increased seismic hazard level in the region north of Susuman, around Kulu, in a trend extending south from Kulu, and near the Kolyma hydroelectric station, all of which are areas of explosion contamination.

2.4.4 Sakhalin Island.

Sakhalin Island shows no clear pattern of explosion contamination except at the extreme southern tip of the island (Figure 15). The contamination here is concentrated around the city of

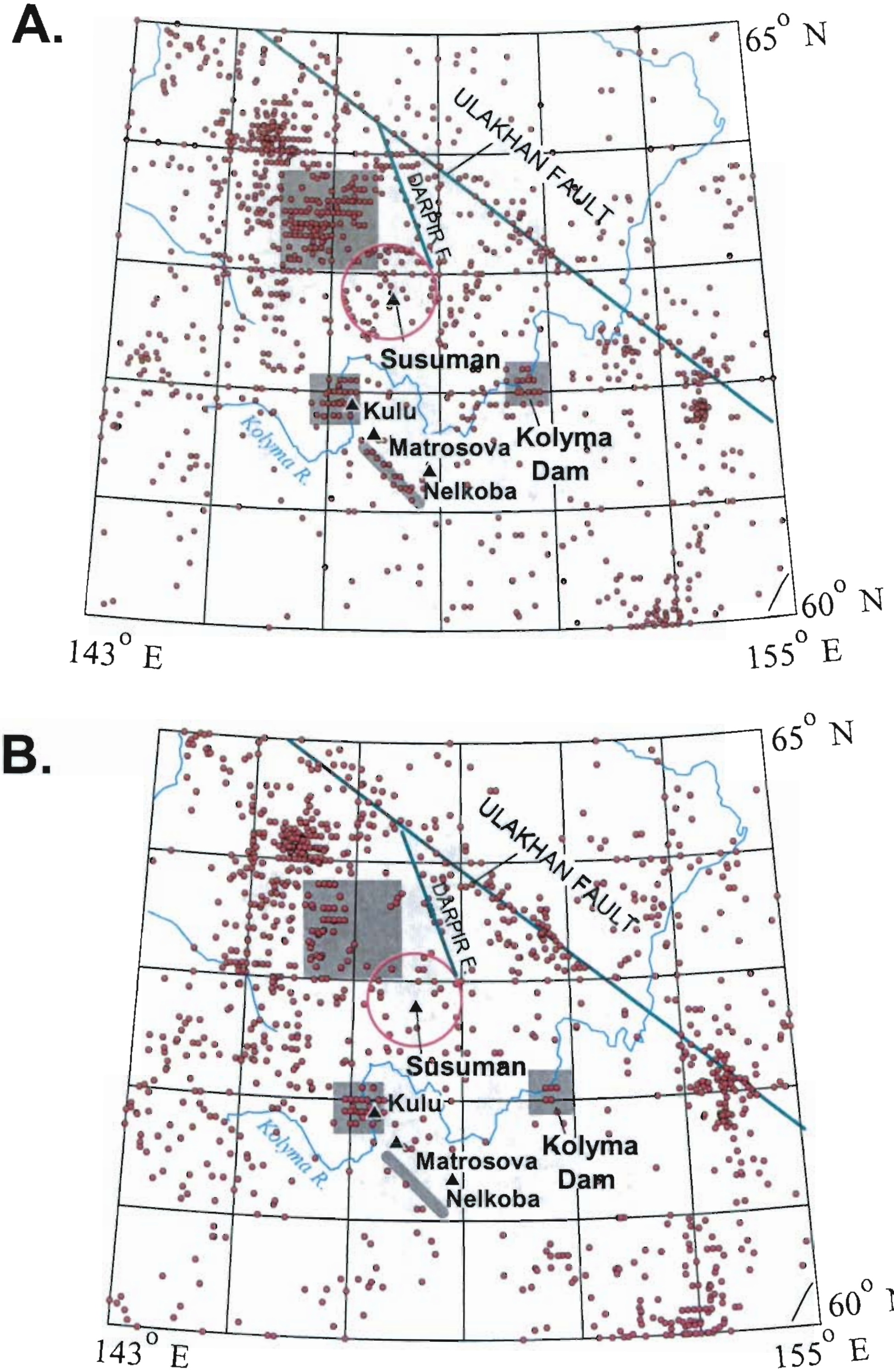

Figure 23. A. Daytime seismicity of the Kolyma gold belt. B. Nighttime seismicity of the Kolyma gold belt. Shaded areas indicate regions used in temporal analysis of event origin times and other regions of explosion contamination. Note ring of seismicity around Susuman in the daytime plot.

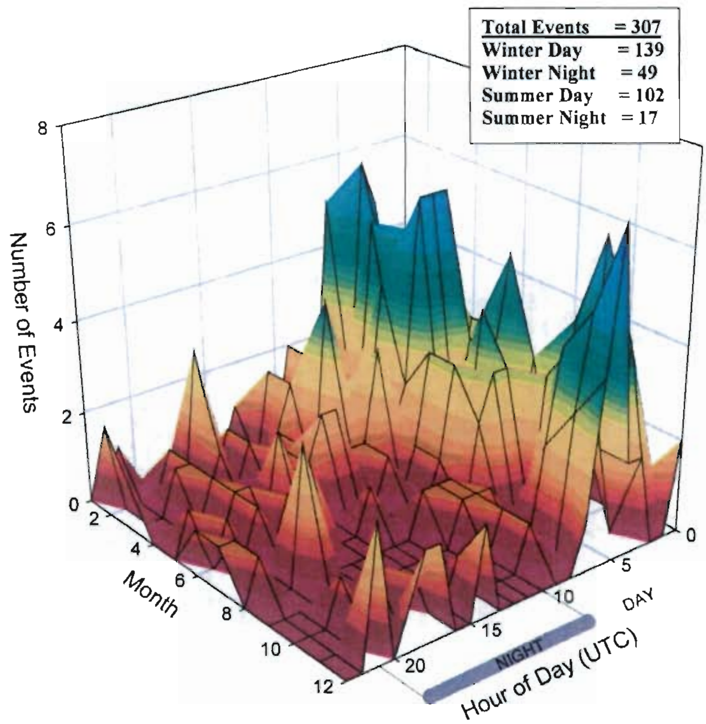

Figure 24. Temporal variation of seismicity in the region northeast of Susuman. Note the bias to winter daytime events. See also Figure 25.

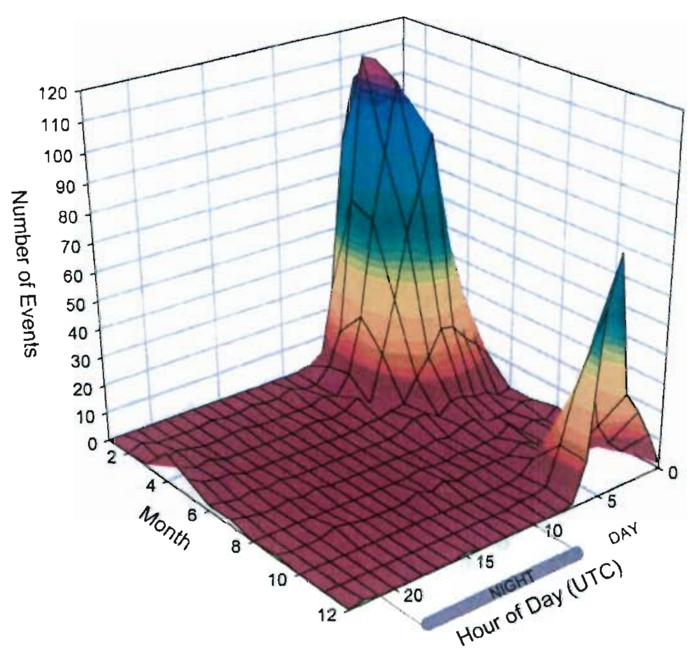

Figure 25. Temporal variation of approximately 3000 known explosions from the Susuman region. The occurrence of explosions here is consistent with the presence of explosion contamination in Figure 24.

Yuzhno Sakhalinsk where there are likely quarries for road gravel or other stone products. No bias is observed in the Uglegorsk coal mining region.

2.5 CONCLUSION.

Based on a very simplistic temporal analysis, it is evident that the seismicity catalog of northeast Siberia is heavily contaminated with industrial explosions. Identification of these explosions and their removal from the seismicity catalog is essential in studying and understanding the tectonics and associated natural seismicity of the region and the associated seismic risk. Phase data for known ground truth explosion sources can be used to develop better calibrated regional velocities and improve event location procedures for the area.

SECTION 3

CRUSTAL MODEL AND RELOCATIONS OF NORTHEAST RUSSIA EARTHQUAKES

3.1 INTRODUCTION.

The ability to accurately locate seismic events is of utmost importance for monitoring of the CTBT. Of course, high quality locations depend on using the correct velocities in the location procedure. The existing database contains several thousand events which have been located by several seismic networks, each employing different location methodology, travel time curves, and phase data (see Section 1). Hypocenter determinations throughout the study area can be improved by using a single methodology, calibrated travel time curves, and combined phase data from adjoining networks. This section summarizes the results of relocating the larger events in the study area in conjunction with developing best-fit crustal travel time curves. This section also discusses the failed attempt to develop upper mantle P_n tomography models for northeastern Russia. Of particular interest for this study was the Laptev Sea and northern Yakutia region, where the velocity model developed indicates sharp velocity contrasts.

3.2 DISCUSSION.

3.2.1 Earthquake Relocations and Crustal Velocities.

To gain a better understanding of the Russian computed locations, a composite reduced travel time curve based on the original epicenter and origin times was produced (Figure 26). Relocations computed here build on relocation work presented in Mackey (1996), and Mackey et al. (1998). The basic location routine is a standard least squares best fit routine. Originally, this program used only P phase arrivals, but was modified for this study to accept multiple phases, specifically Pg, P_n, and Sg. In keeping consistent with notation used in data sources used in this study, Lg onset is referred to here as Sg. S_n arrivals are not used as the data are very noisy.

Throughout the study area, many geologic and tectonic environments exist, which combined with the physical vastness of the region, makes it likely that no single velocity or travel time curve will reflect actual seismic velocities for any particular phase. In order to overcome this problem, the study area was broken into cells, and the best fitting velocities were determined by minimizing the sum of event RMS residuals through trial of multiple travel-time curves. Block sizes are generally 3° north-south by 5° east-west, although this was adjusted in areas with sparse activity in order to increase the number of useable events. For any given block, only events containing P_n phase arrivals (generally 2 or more) were used. This selects only the larger events, which contain more arrivals and have better azimuthal coverage of receiving stations.

Travel-time curves for Pg and Sg phases were calculated assuming a straight-ray approach. For hypocenters at depth, the travel path is assumed to be the hypotenuse of the triangle made by the depth and the surface distance. Event depths are restricted to a maximum of 33 km, as all events are assumed crustal in nature. Events for which depth tends above the surface are restricted to 0 km. This is reasonable, as the database is known to be contaminated with explosions (see Section 2).

In order to determine the best crustal velocities for locating events within a given cell, the selected events were first located with a first approximation of crustal velocities for the region. The velocities used in the first approximation were generally the best fit velocities from an adjacent cell.

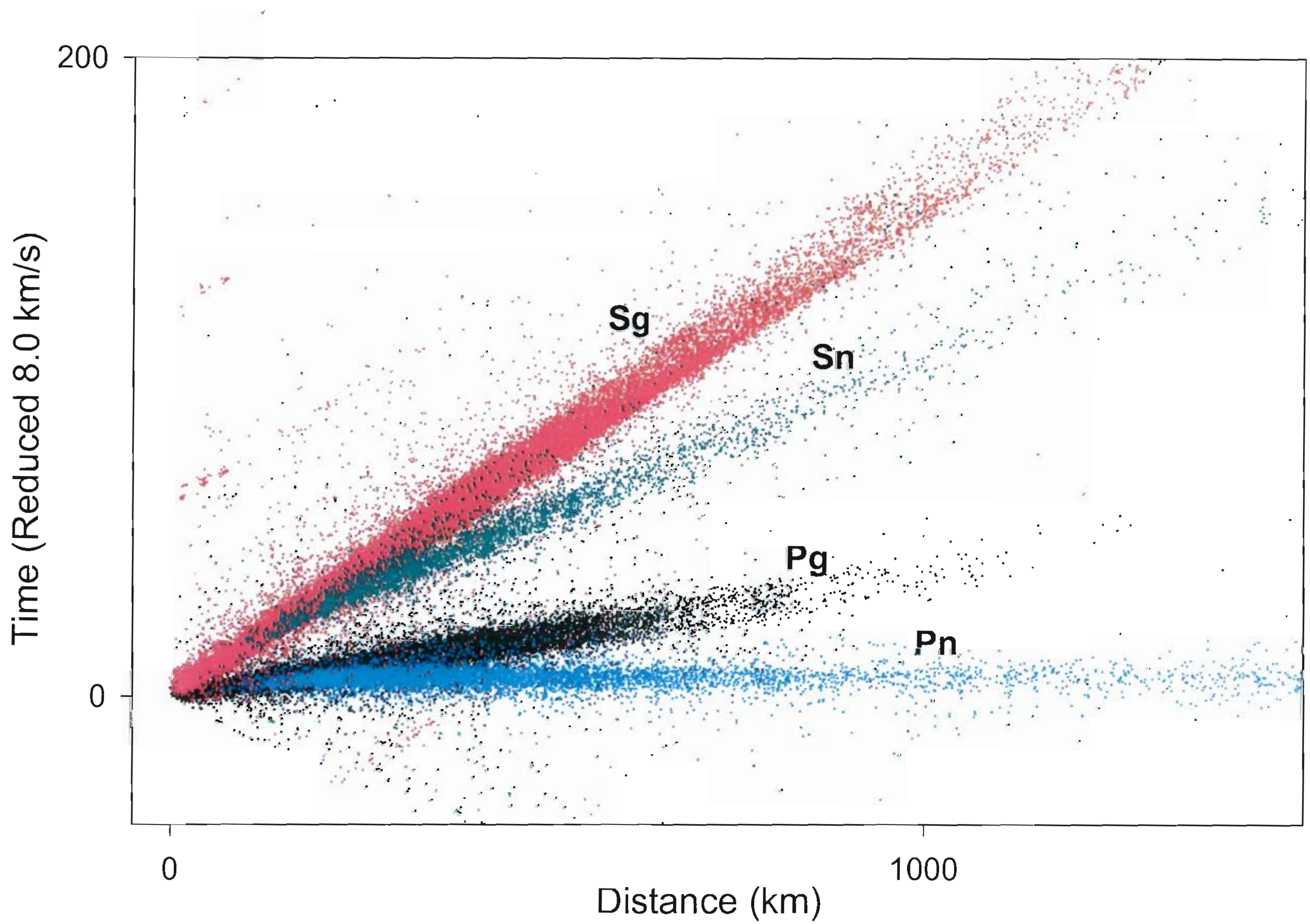

Figure 26. Composite reduced travel time curve for northeastern Russia. Only data from northeastern Russia stations are shown. Points shown use original (unrelocated) Russian locations and phase identifications.

The resulting output was analyzed for high residual arrivals, generally those greater than 3.5 seconds. High residuals are generally a result of either typographical errors, misassociated phases, or bad time picks. Typographical errors and misassociated phases were corrected, if possible, while bad time picks were flagged to be omitted from use in further locations. Events with many high residual arrivals, such that the solution is unstable, and events with four or fewer recording stations, were omitted from further analysis. Overall, less than 5% of the originally selected events were omitted due to stability problems.

In order to determine the better fitting travel time curve to use for P_n arrivals in the location procedure, the Jeffreys-Bullen (JB; Jeffreys and Bullen, 1970) P wave travel time curve was compared to the IASPEI 91 (I-91) curve (Kennett, 1991). Results for test regions in Amur, northern Yakutia, Magadan, and Chukotka indicated that the JB table did a better job of fitting the P_n arrivals in the region. Overall, when comparing RMS residuals for events located using the two travel-time curves, approximately 80% of the events have a lower RMS residual when the JB table is used as opposed to the I-91 table; the Pg and Sg velocities used in each comparison were the same. Therefore, the JB table was used in all relocations computed in this study.

Following removal of large residual time picks and correction of misassociated phases, the remaining selected events for a given block were located multiple times using different crustal velocities. Crustal velocities tested for each block range from 5.875 km/sec to 6.350 km/sec in 0.025 km/sec increments for Pg, and 3.470 km/sec to 3.650 km/sec in 0.020 km/sec increments for Sg. In this manner, the crustal velocities which best fit the events in the cell were found. The newly found best fitting velocity for each cell is then used to relocate the events a second time. After locating with the new velocity, any additional high residual arrivals (generally those over 3.0 seconds) were omitted or corrected. If any arrivals were removed or had phase associations changed, the events in the cell were again subjected to a search for the best fit crustal velocities. Three-dimensional plots of a cell's cumulative residuals for varying Pg and Sg velocities are useful to illustrate how the residuals change with differing velocities. Figures 27 and 28 illustrates how the residuals change for two cells, one in the southern Yakutsk region, the other in Magadan. Final crustal Pg velocities for each cell are shown on Figure 29 (Table 1). Sg velocities show a similar pattern (Figure 30; Table 1). In conjunction with developing the crustal velocities, a total of 1311 earthquakes were relocated in 44 geographic cells (Appendix B).

Crustal velocities in northern Yakutia are somewhat problematic, with adjacent cells alternating between high and low velocities (Figures 29 and 30). Therefore, northern Yakutia was re-evaluated using a 5° x 3° moving window, shifting the window in 1° increments. For each cell, the best fitting crustal velocities were determined by trial of multiple Pg and Sg velocities as discussed above. This resulted in a similar velocity structure as determined earlier, for both Pg and Sg arrivals, but with greatly smoothed velocity shifts and better resolution (Figures 31 and 32).

3.2.2 Results of Relocations.

Crustal velocities determined in the location process correlate well with the regional tectonic provinces. Generally the highest velocities (Pg velocities ranging from 6.225 to 6.300 km/s and Sg from 3.61 to 3.65 km/s) occur in the western portion of the study region, which is associated with the Siberian Platform. South of the Siberian platform, velocities decrease across the Mongol - Okhotsk suture (Figure ES-2). Velocities also drop sharply in the Verkhoyansk foldbelt, along the eastern edge of the Siberian platform. From the Verkhoyansk foldbelt and east through the Mesozoic terrane assembledges (Kolyma - Omolon superterrane) to the Bering Strait, crustal velocities are consistently in the 6.00 - 6.05 km/s range, and Sg velocities in the 3.51 - 3.55 km/s range, with only a few cells deviating slightly. The final analysis for velocities in northern Yakutia

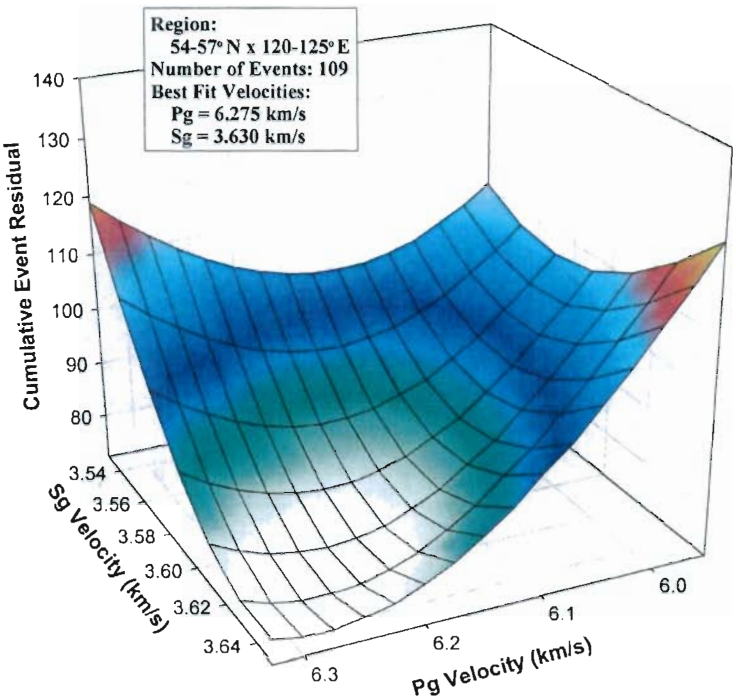

Figure 27. Pg-Sg velocity residual graph showing fast velocities for one cell in southern Yakutia.

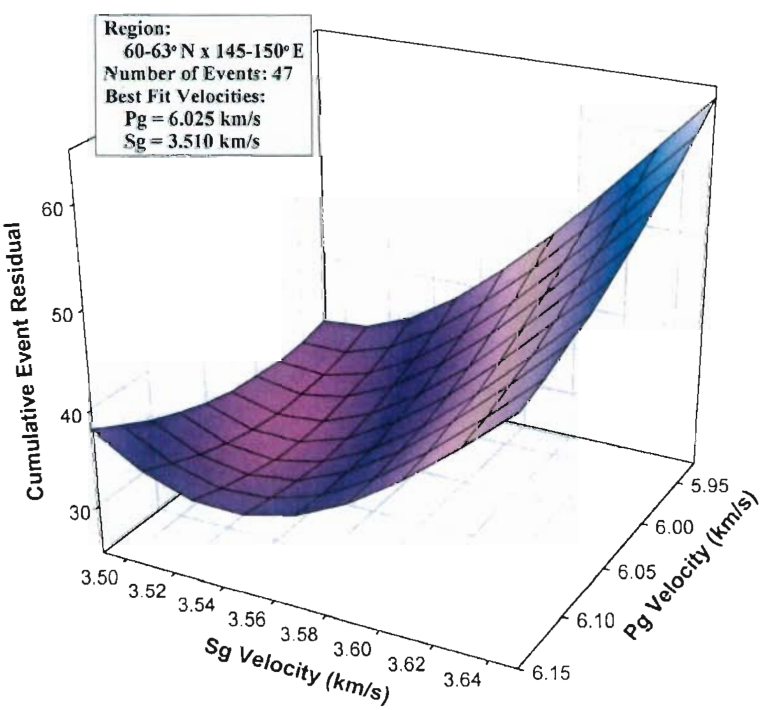

Figure 28. Pg-Sg velocity residual graph showing slow velocities for one cell in the Magadan region.

Table 1. Best fit velocities and number of events per geographic region.

Region		Best Velocities	km / sec	Number of events
48-51N	120-125E	Pg=6.040	Sg=3.530	2
48-51N	125-130E	Pg=6.025	Sg=3.530	12
48-51N	130-135E	Pg=6.100	Sg=3.550	28
48-51N	135-140E	Pg=6.100	Sg=3.550	4
51-54N	120-125E	Pg=6.100	Sg=3.570	14
51-54N	125-130E	Pg=6.125	Sg=3.570	32
51-54N	130-135E	Pg=6.125	Sg=3.570	47
51-54N	135-140E	Pg=6.075	Sg=3.550	20
54-57N	120-125E	Pg=6.275	Sg=3.630	109
54-57N	125-130E	Pg=6.175	Sg=3.590	69
54-57N	130-135E	Pg=6.150	Sg=3.590	40
54-57N	135-140E	Pg=6.100	Sg=3.570	19
57-60N	120-125E	Pg=6.275	Sg=3.630	149
57-60N	125-130E	Pg=6.300	Sg=3.650	44
57-60N	130-140E	Pg=6.275	Sg=3.630	9
57-60N	140-145E	Pg=6.075	Sg=3.570	7
57-60N	145-150E	Pg=5.950	Sg=3.510	42
57-60N	150-155E	Pg=6.040	Sg=3.510	33
57-60N	155-160E	Pg=6.025	Sg=3.510	35
60-63N	135-140E	Pg=6.050	Sg=3.570	4
60-63N	140-145E	Pg=6.050	Sg=3.530	35
60-63N	145-150E	Pg=6.025	Sg=3.530	47
60-63N	150-155E	Pg=6.025	Sg=3.510	47
60-63N	155-160E	Pg=6.06	Sg=3.51	63
60-63N	160-165E	Pg=6.05	Sg=3.51	11
60-65N	165-170E	Pg=5.975	Sg=3.470	19
60-65N	170-180E	Pg=6.000	Sg=3.470	19
60-66N	120-135E	Pg=6.225	Sg=3.610	7
63-66N	135-140E	Pg=6.050	Sg=3.550	11
63-66N	140-145E	Pg=6.050	Sg=3.530	31
63-66N	145-150E	Pg=6.025	Sg=3.510	103
63-66N	150-155E	Pg=6.025	Sg=3.530	29
63-66N	155-160E	Pg=6.025	Sg=3.510	10
63-69N	180-160W	Pg=6.050	Sg=3.530	48
65-69N	165-180E	Pg=6.060	Sg=3.530	11
66-69N	125-130E	Pg=6.275	Sg=3.610	6
66-69N	130-135E	Pg=6.075	Sg=3.570	14
66-69N	135-140E	Pg=6.200	Sg=3.550	8
66-69N	140-145E	Pg=6.175	Sg=3.570	17
66-69N	145-150E	Pg=6.040	Sg=3.53	2
69-72N	125-135E	Pg=6.050	Sg=3.550	18
69-72N	135-145E	Pg=6.200	Sg=3.590	14
72-75N	120-130E	Pg=6.225	Sg=3.570	15
72-75N	130-135E	Pg=5.900	Sg=3.510	5

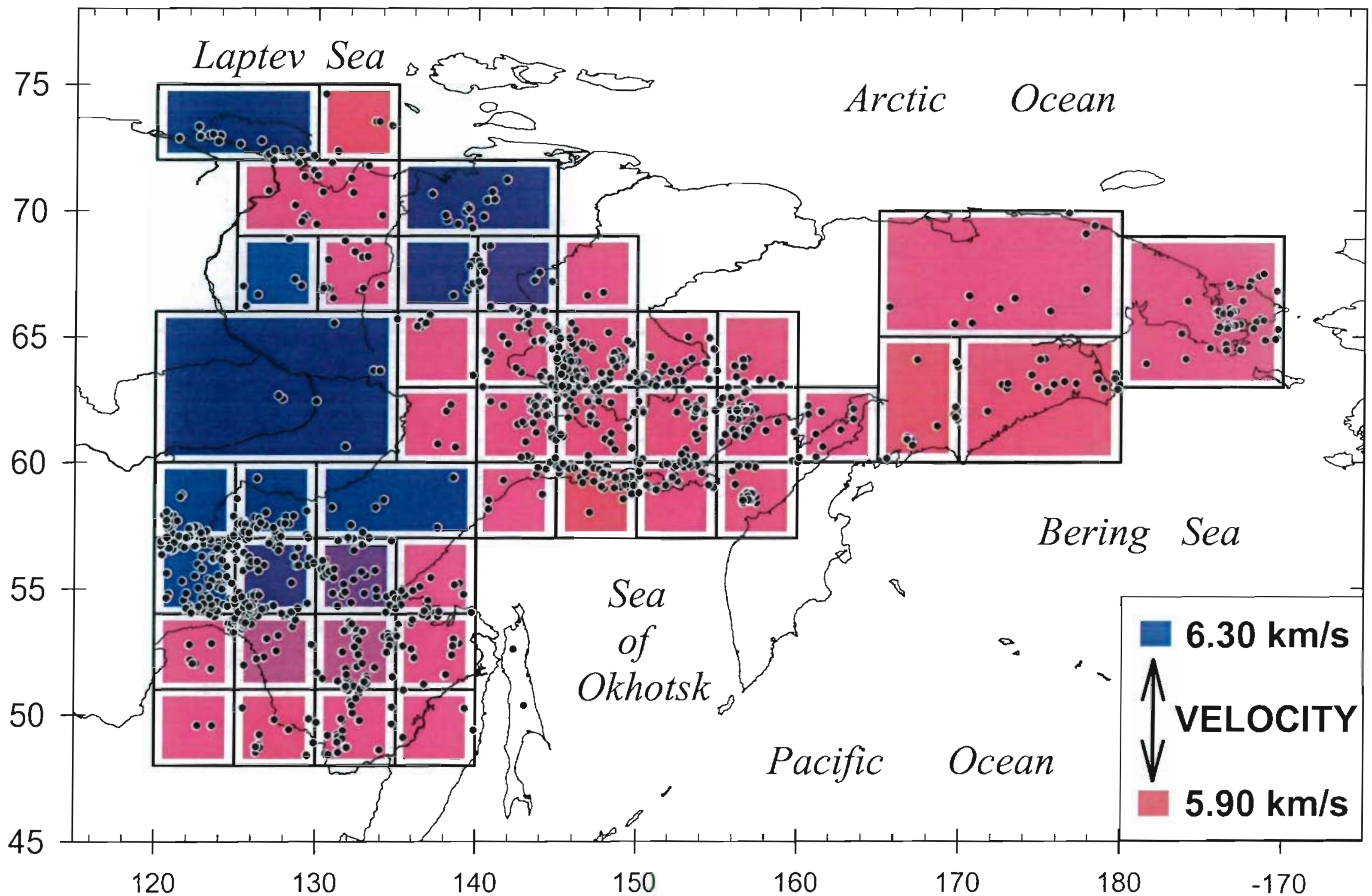

Figure 29. Grid of calibrated Pg velocities. The velocities depicted were calculated in conjunction with relocating the epicenters shown. Velocities found generally correlate with the geology, with the Precambrian Siberian Craton in the west having the highest velocities.

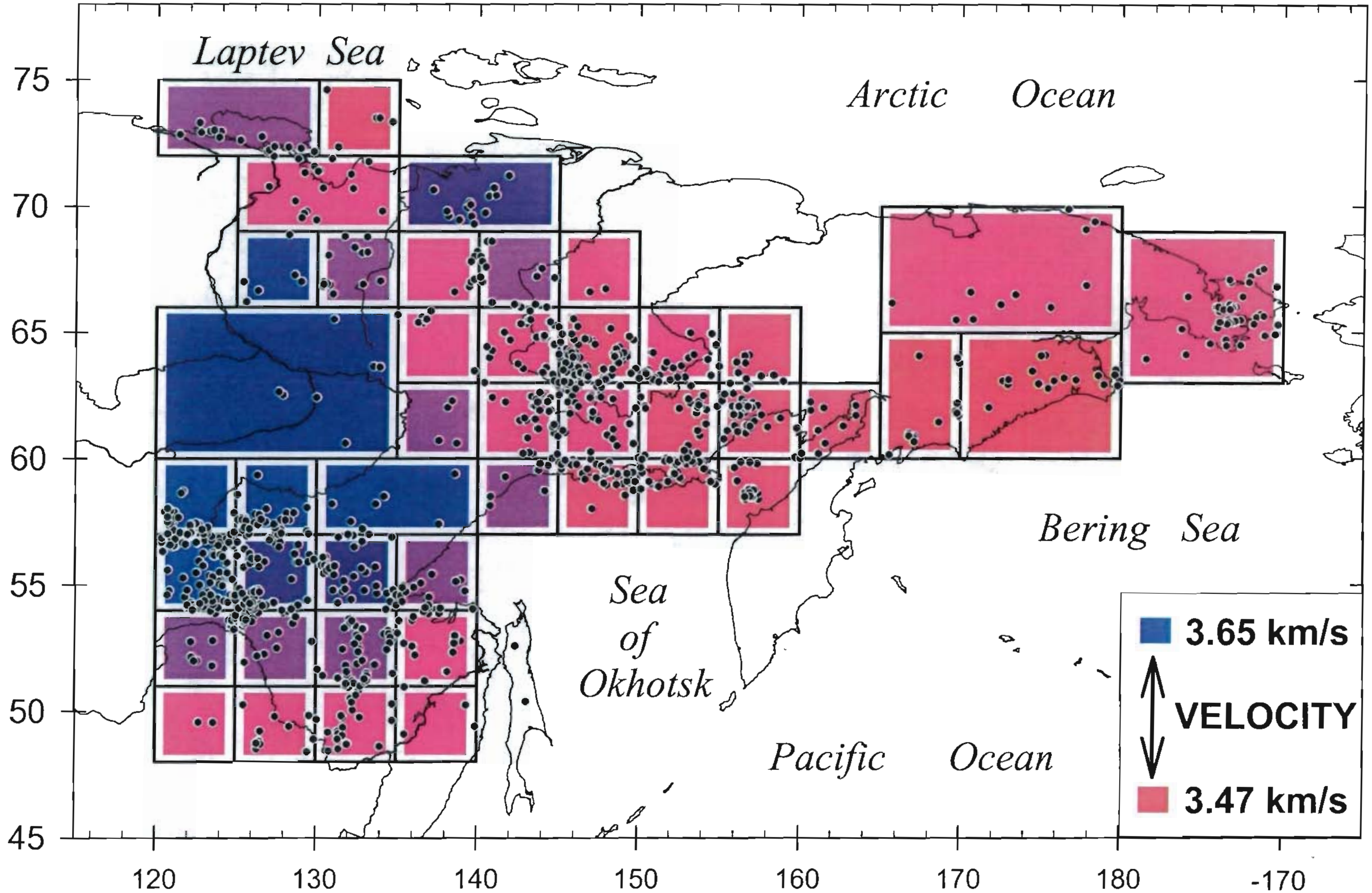

Figure 30. Grid of calibrated Sg velocities. The velocities depicted were calculated in conjunction with relocating the epicenters shown. Velocities shown generally correlate with the geology, with the Precambrian Siberian Craton in the west having the highest velocities.

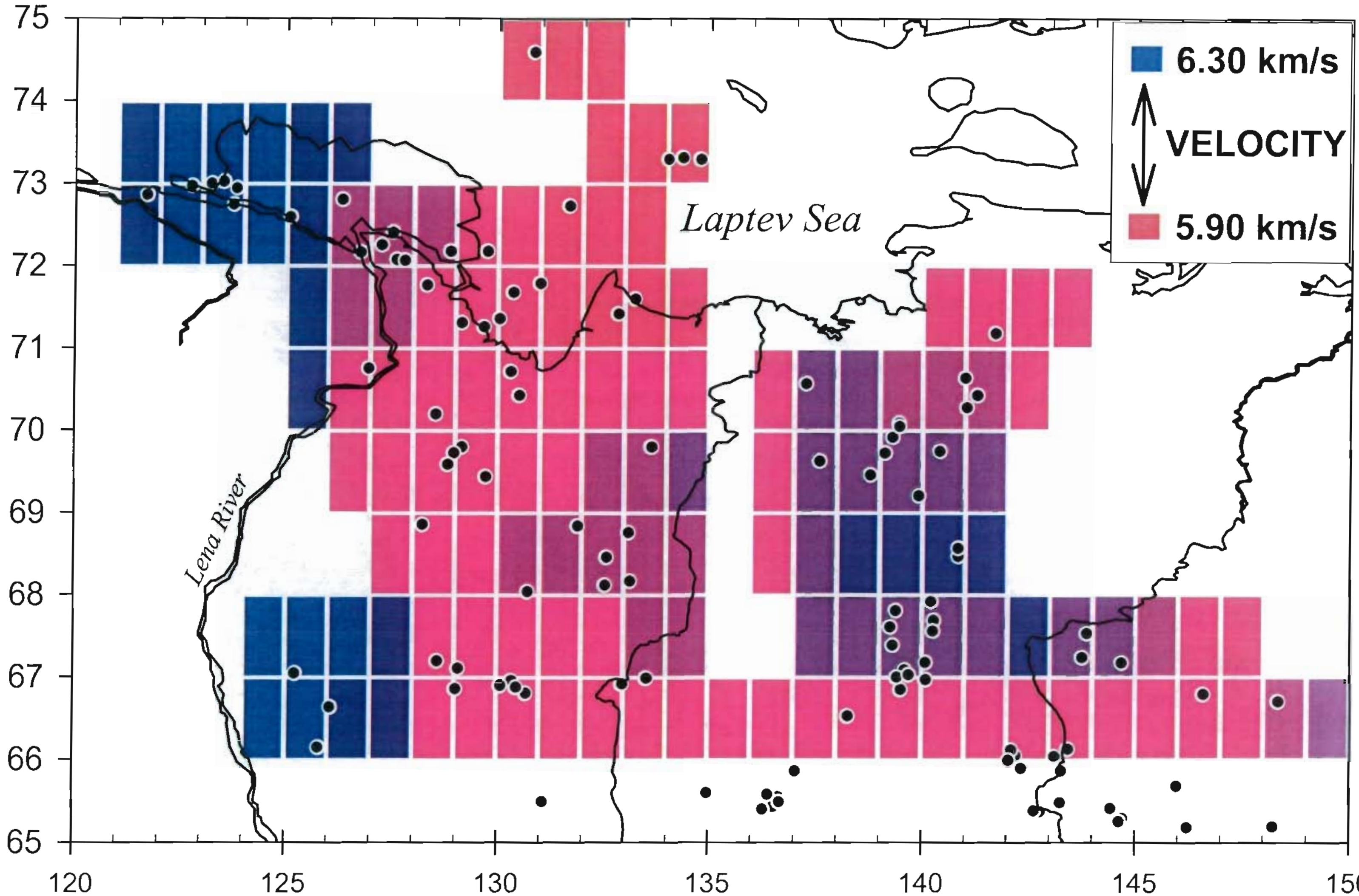

Figure 31. Pg velocities for northern Yakutia determined by using a moving window. Epicenters shown are those used in conjunction with determining velocities. Velocities found generally correlate with the geology, with the Precambrian Siberian Craton in the west having the highest velocities and the Laptev Sea Rift in the north-central portion of the figurehaving the lowest velocities.

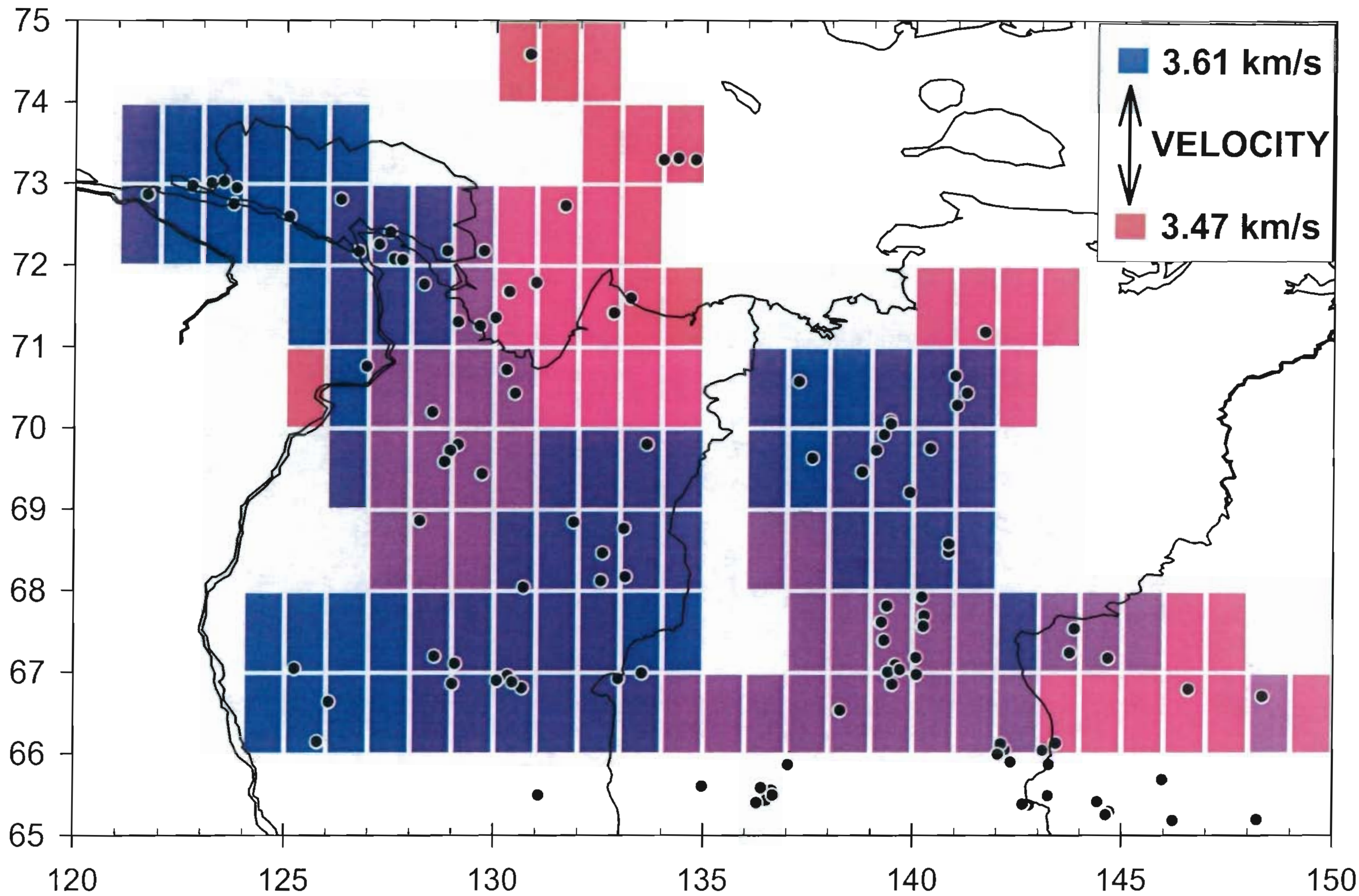

Figure 32. Sg velocities for northern Yakutia determined by using a moving window. Epicenters shown are those used in conjunction with determining velocities. Velocities found generally correlate with the geology, with the Precambrian Siberian Craton in the west having the highest velocities and the Laptev Sea Rift in the north-central portion of the figure having the lowest velocities.

indicate that the highest velocities are associated with the Siberian platform along the western edge of the region. The lowest velocities occur in the Laptev Sea and correspond to the active grabens of the continuation of the Arctic Mid-Ocean Ridge into northeast Asia (Figures 31 and 32). The velocity shifts in northern Yakutia are probably a result of rapidly changing velocity gradients associated with presently active rifting adjacent to the Siberian platform and other older tectonic structures. The low velocity region in the Laptev Sea extends into the continent, where it generally follows the strike of the grabens (Fujita et al., 1990a; Drachev, 1998; Sekretov, 1998).

Plots comparing original and relocated epicenters show clear improvement of relative locations. In the Amur region, there is improvement on a seismicity trend extending through the Zeya basin and tightening of seismicity clusters throughout the region (Figure 33). Relocated epicenters in the Magadan region show a tightening of several clusters of seismicity and a slight improvement of events along the trace of the Ulakhan fault (Figure 34). The cluster near 62° N x 157° E is due to an aftershock sequence following an event on February 11, 1987. Clusters of seismicity in the eastern portion of Chukotka are reduced to much smaller lineations (Figure 35). Unfortunately, the seismicity trend in the Koryak Highlands shows no apparent improvement, although this may be due to poor statistics resulting from a small number of events. Original and relocated epicenters for northern Yakutia are shown in Figure 36. Although epicenters clearly moved in the relocation process, the lack of clear clusters and trends makes it difficult to evaluate any improvement in relative locations. Lack of apparent improvement in northern Yakutia may be a result of apparently high lateral velocity gradients.

Travel time curves resulting from the relocated events show a distinct improvement. A composite travel time curve derived from all relocated events (Figure 37) shows a decrease in level of scatter when compared to those derived from the original Russian locations (Figure 26). Because each cell used distinct calibrated crustal velocities, the composite travel time curve (Figure 37) is somewhat smeared, as it reflects all velocities used in the relocation process. Note that arrivals identified as S_n are not plotted on Figure 37 as they were not used in the relocation process. Travel time curves from individual cells better show the improvement obtained. Figures 38 and 39 compare respective travel time curves for individual cells in the southern Yakutsk the Magadan regions (Figures 27 and 28). The level of scatter is reduced for all phases using the relocations, consistent with improved hypocenter parameters. These resulting curves for individual cells are also distinguishable from each other when compared (Figure 40).

3.2.3 Crustal Thickness.

Initial work to determine crustal structure in the region, undertaken independently of the crustal velocities and relocations addressed above, used relocations of 75 larger events that occurred throughout the Magadan and northern Yakutsk networks. Full details of this study are found in Mackey (1996) and Mackey et al. (1998). Relocations computed here were calculated using only Pg arrivals, assuming a crustal velocity of 6.00 km/s. High residual arrivals were omitted from the location routine and several misassociated phases were corrected. In order to determine the first-order crustal structure, the method of Ruff et al. (1994), is used. This method assumes that regional travel time curves for multiple earthquakes can be approximated with a regional average crustal model. Given a set of earthquakes, the Pg travel time data are simultaneously inverted, solving for the best fit velocity for the set of events, and new origin times for individual events, assuming fixed hypocenters. For a given station, any systematic variation from the regional average should be a result of local variations in crustal structure. The process of relocating the events and inverting the arrival data result in a significant reduction of scatter in the travel time curves for both Pg and P_n

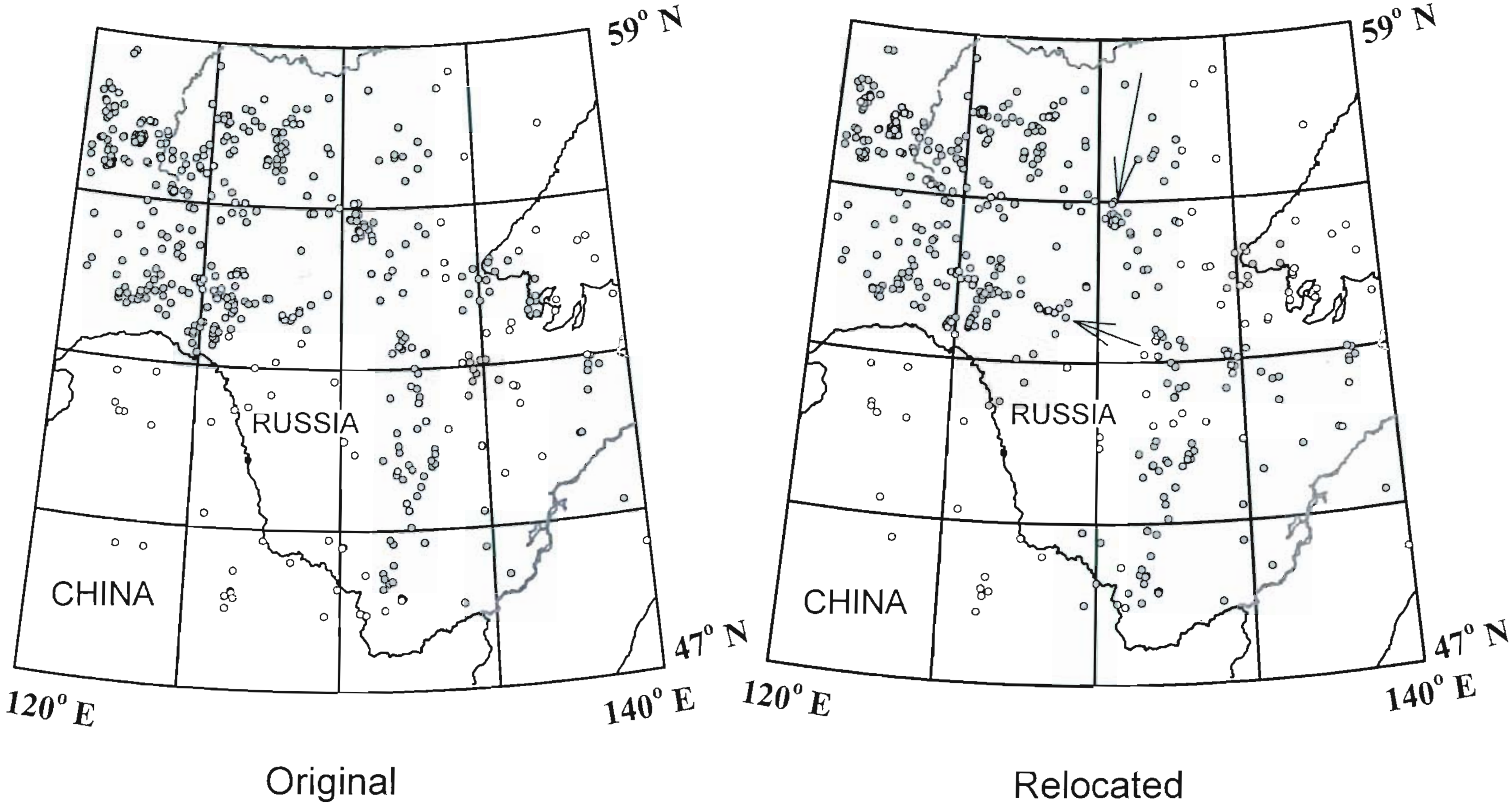

Figure 33. Original vs. relocated epicenters for the Amur region. Arrows indicate locations of improved definition of some seismicity clusters and trends.

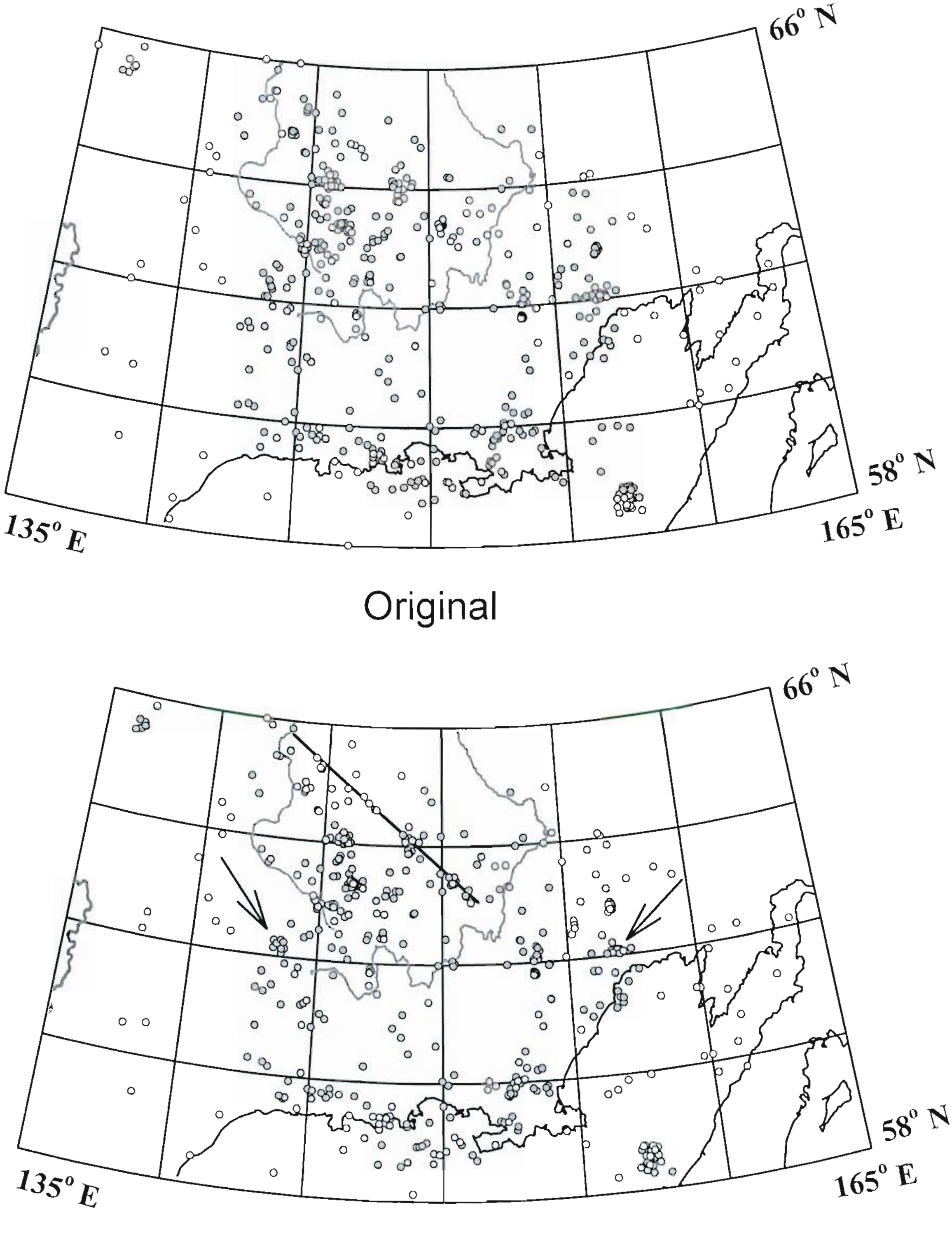

Figure 34. Original vs. relocated epicenters for the Magadan region. Ulakhan fault shown by heavy line. Note improvement in relative locations of clusters indicated with arrows, as well as many other smaller clusters.

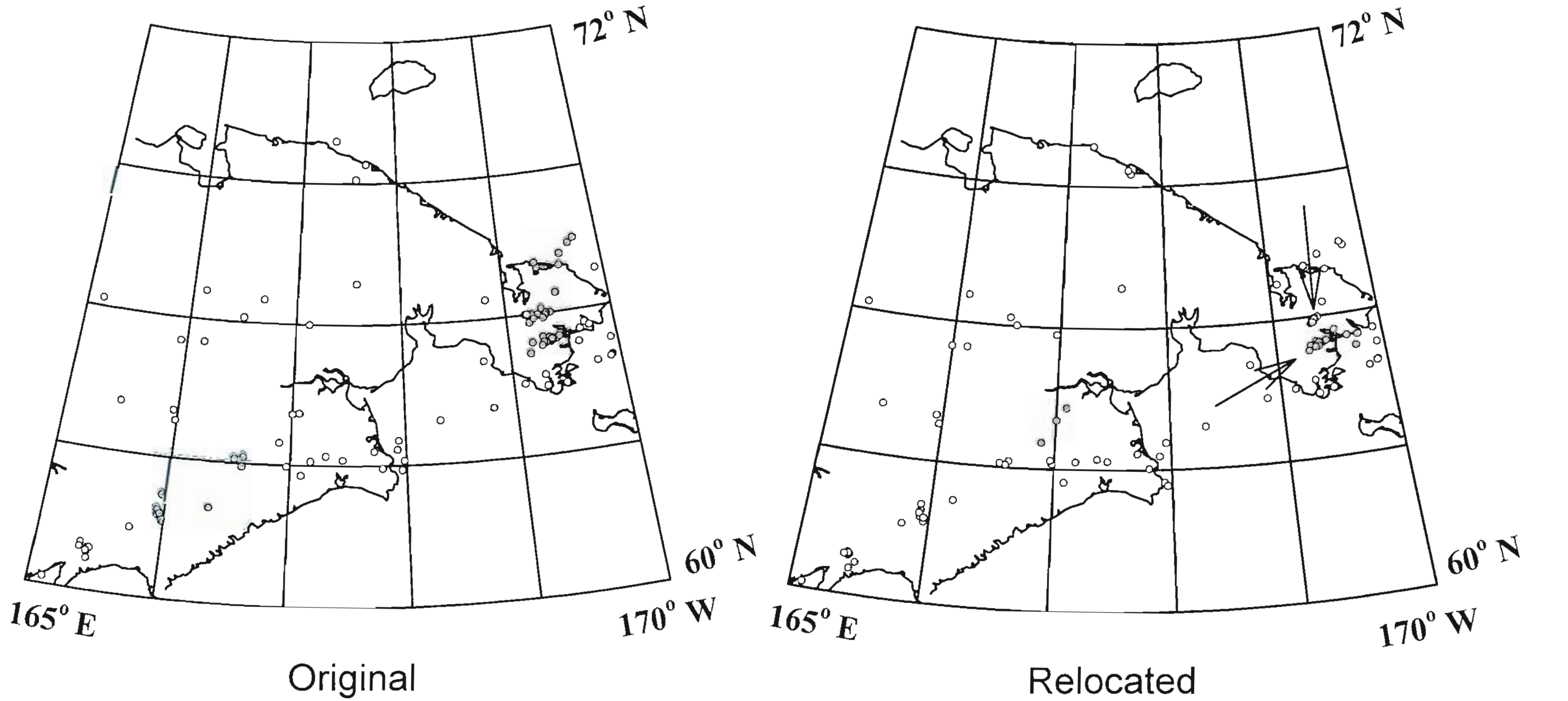

Figure 35. Original vs. relocated epicenters for Chukotka. Arrows indicate improved lineations.

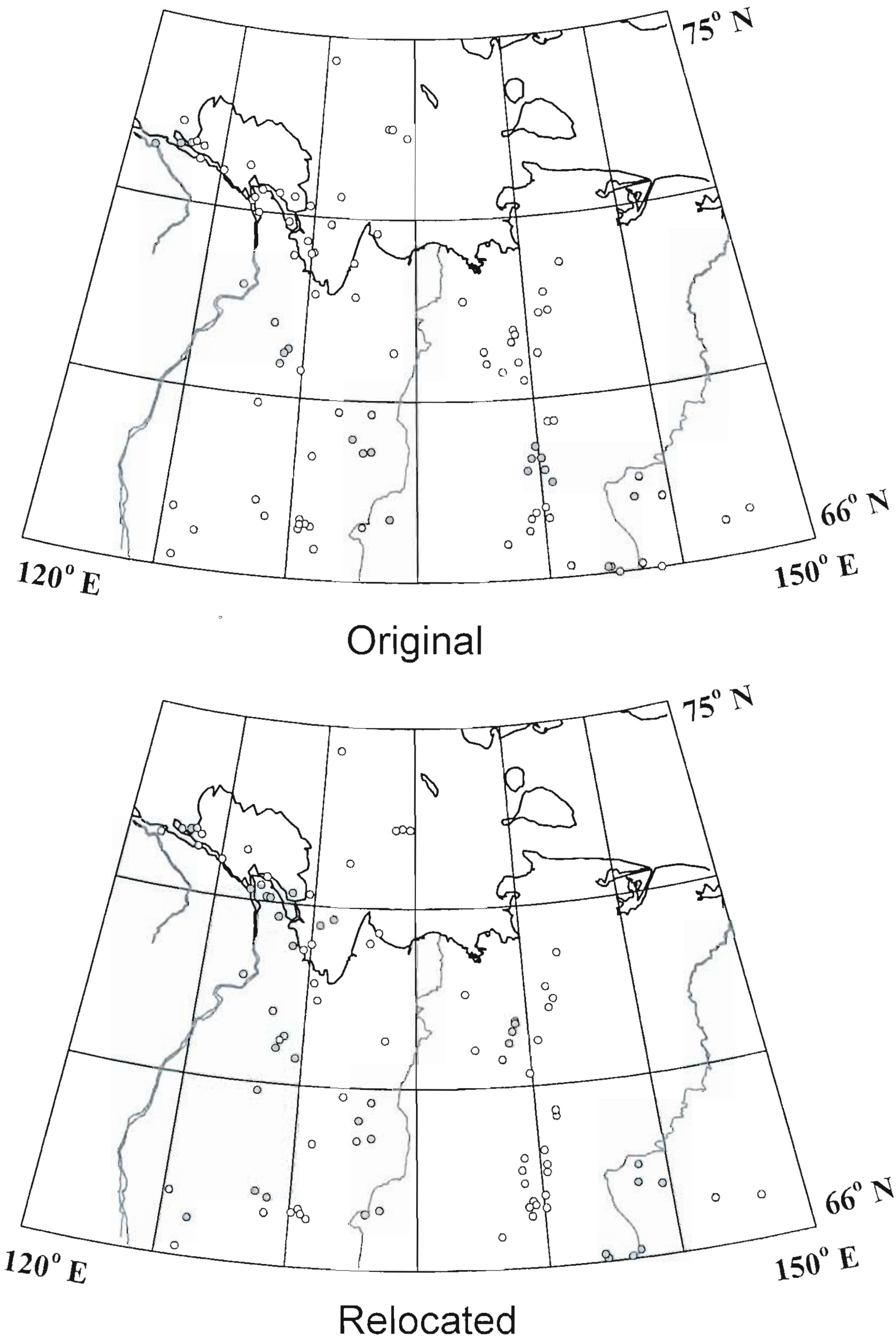

Figure 36. Original vs. relocated epicenters for northern Yakutia.

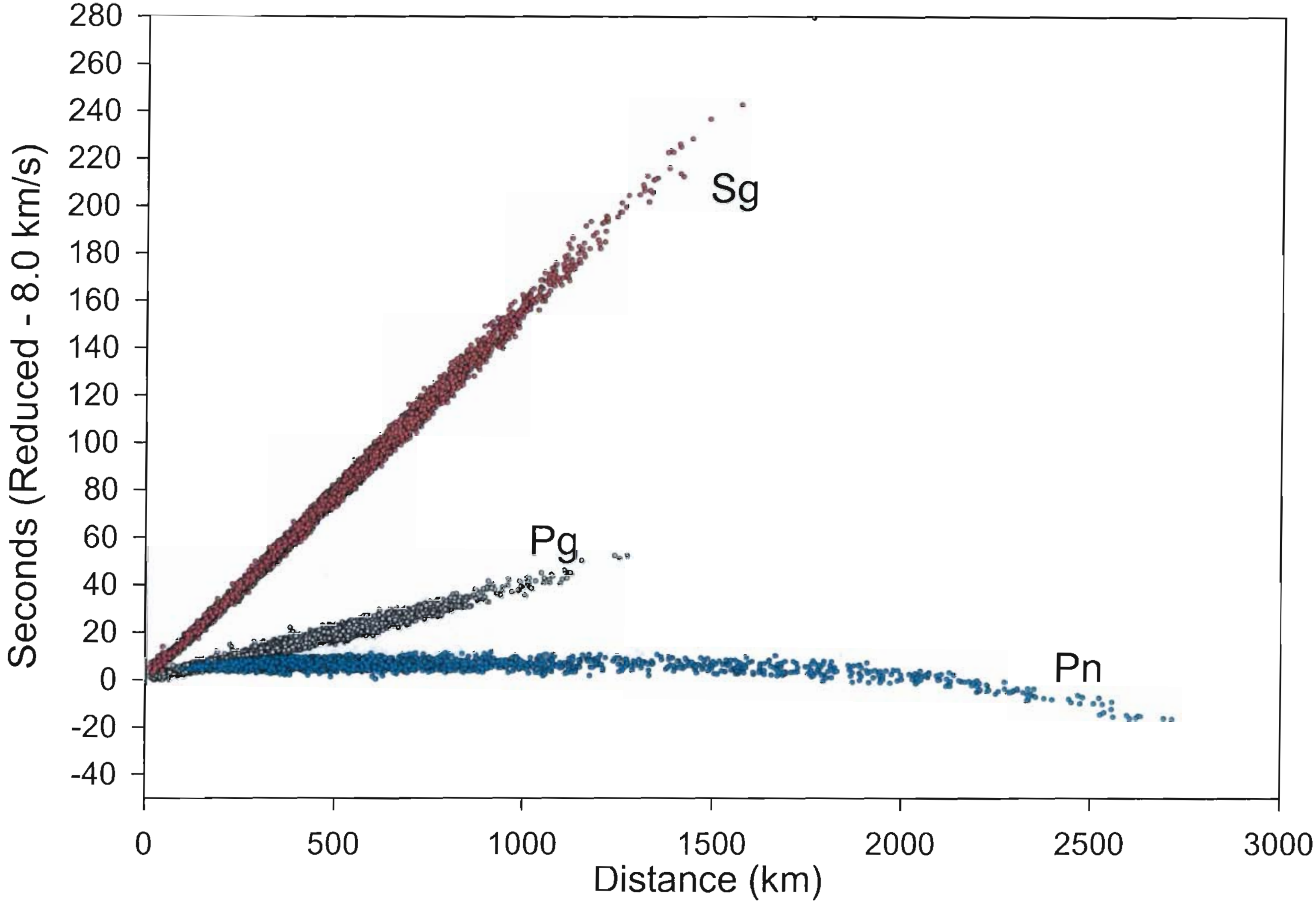

Figure 37. Composite regional reduced travel time curve for northeast Russia using hypocenter parameters from relocations. Sn data are omitted.

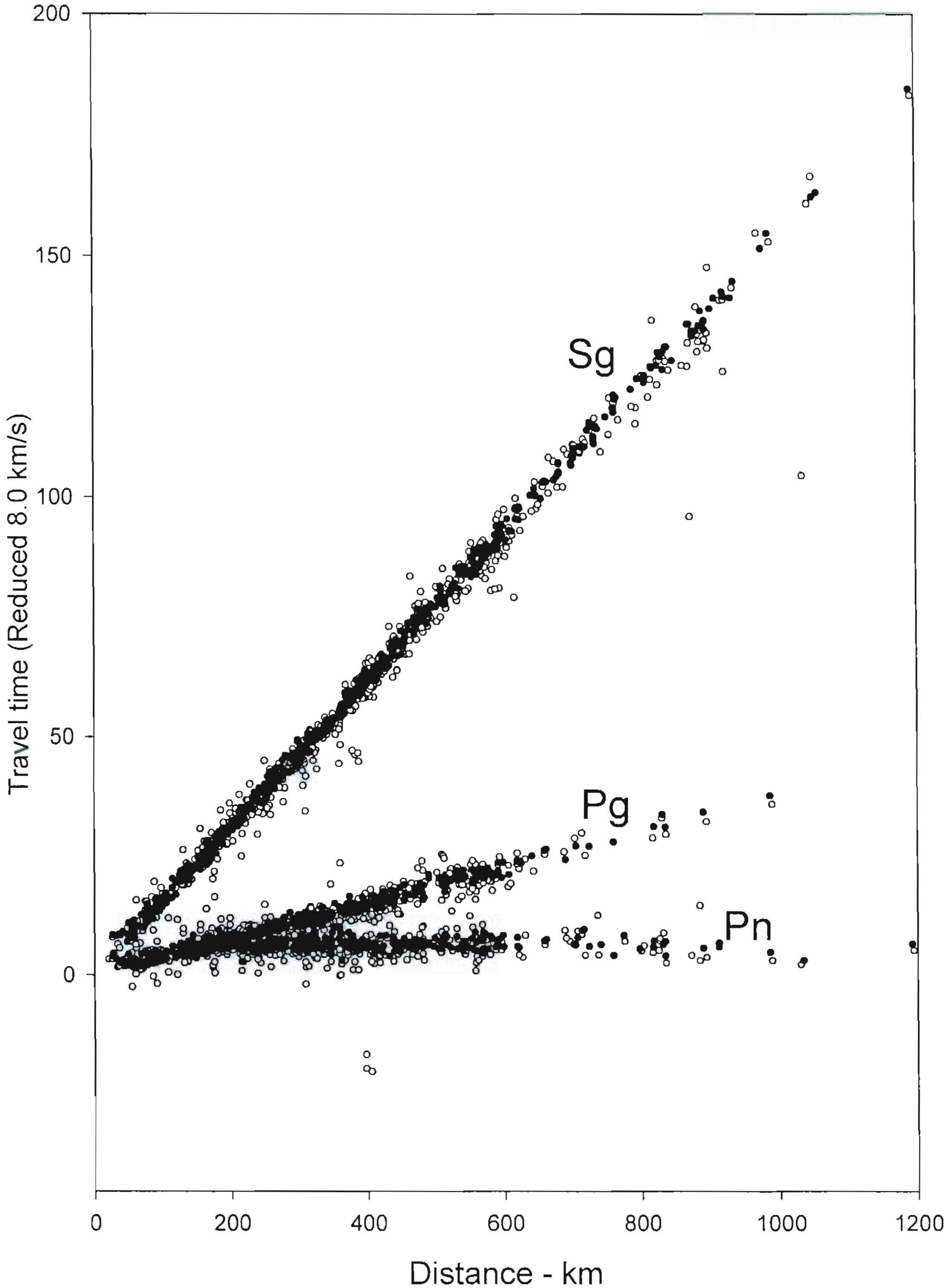

Figure 38. Travel time curve for a cell in the southern Yakutsk region (54-57°N x 120-125°E) comparing original (open circles) with relocated event parameters (closed circles). Note the significant reduction in scatter of data points. Sn data are omitted.

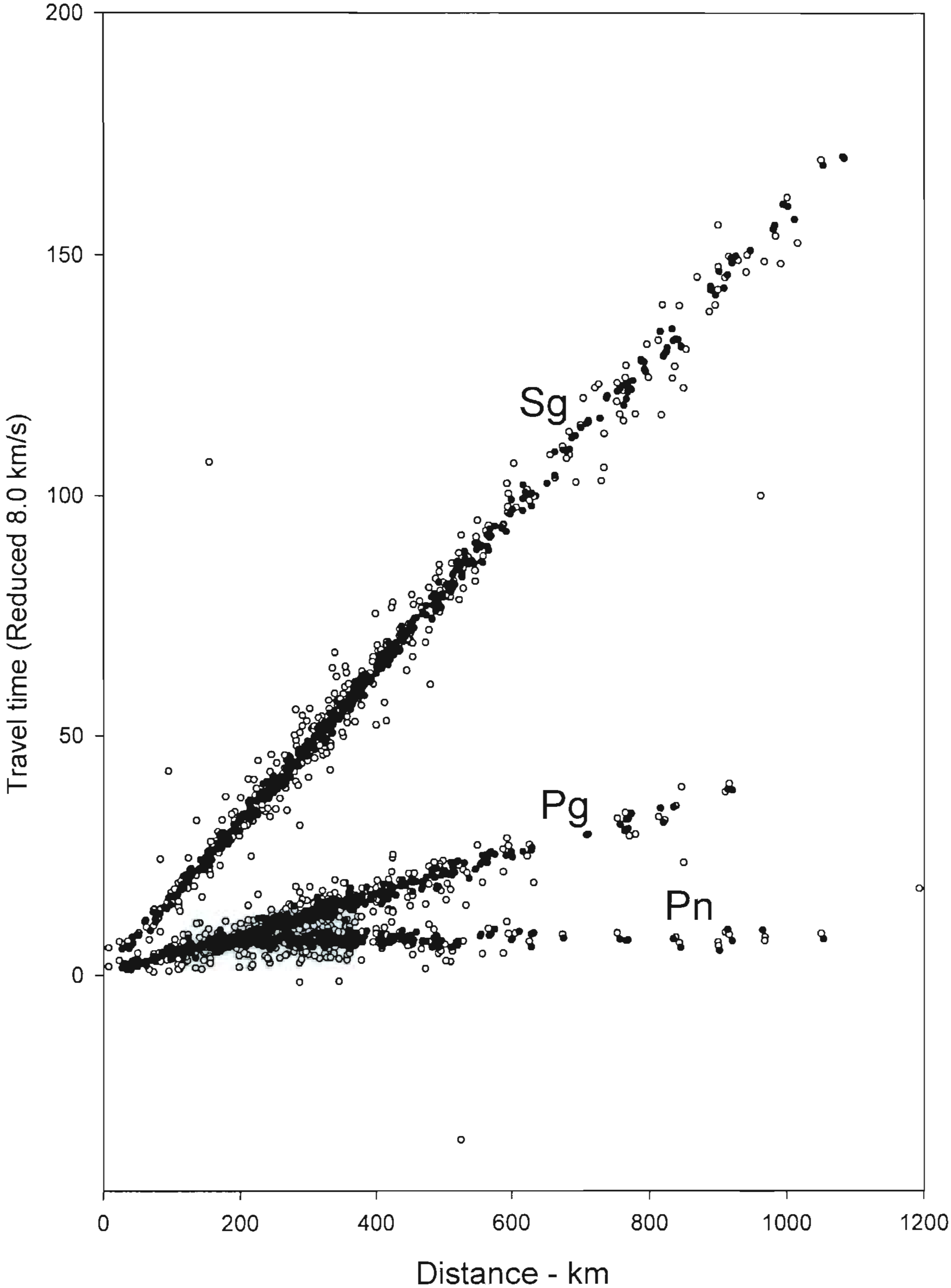

Figure 39. Travel time curve for a Magadan region cell (60-63°N x 145-150°E) comparing original (open circles) with relocated event parameters (closed circles). Note the significant reduction in scatter of data points. S_n data are omited.

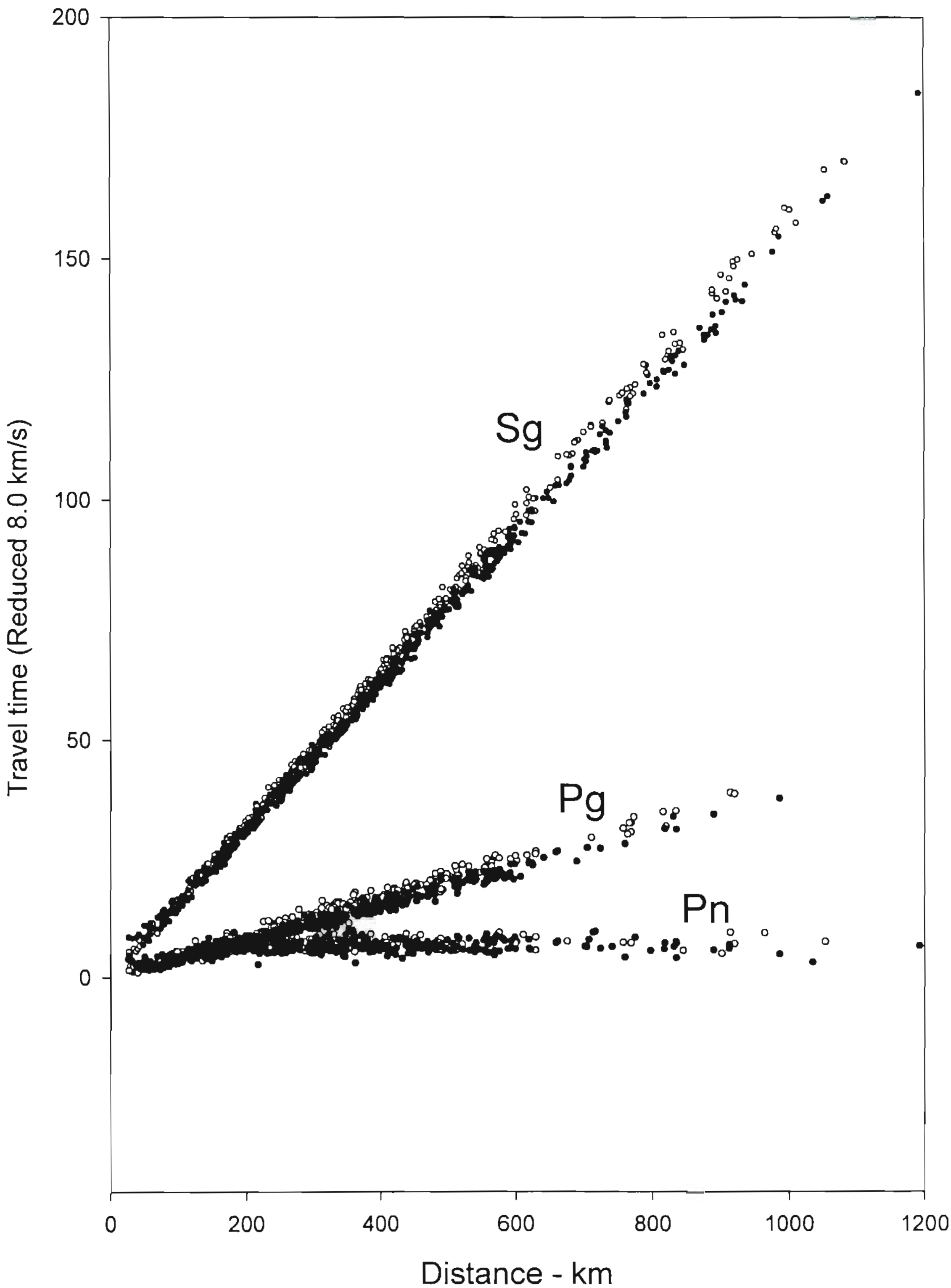

Figure 40. Travel time curve comparing the regions 60-63°N x 145-150°E (open; Magadan) and 54-57° N x 120-125° E (solid; south Yakutia). Note increased velocities for relocated events in south Yakutia. Sn data are omitted.

arrivals (Figures 41 and 42 respectively). Figure 43 depicts the Pg-P_n composite travel time curve derived from the final Pg inversion new origin times.

As a result of this inversion, the apparent velocities, crossover distance and approximate crustal thickness are obtained for the study area as a whole (Figure 43). Results of P wave velocities for the Magadan and northern Yakutsk regions indicate a generally simple structure with a 5.992 km/sec crustal layer overlying a 7.961 km/sec upper mantle. Average crustal thickness is about 37 km. Examination of individual stations extracted from the composite travel time curve allow determination of crustal structure at individual stations. Sufficient data were available for 27 stations, and present data suggest that structural variations between stations in the study area are resolvable with this method. Based on final results, errors in determining crustal thickness appear to be ± 4 km, Pg velocities ± 0.03 km/s and P_n velocities ± 0.1 km/s. Although formal errors are smaller, those cited here allow for unmodelable effects and biases such as hidden low- or high-velocity layers. Figure 44 depicts travel time curves and crustal models for 5 stations, representing the full range of thick (Khandyga) and thin (Yubileniya) crust, as well as both poorly resolved (Sasyr) and well resolved models (Omsukchan). Figure 45 contours the crustal thicknesses determined in this study. Table 2 compares crustal velocities determined here to results of several other studies. In most cases, Pg velocities determined here (Table 3) are slower than those determined independently above, although the general pattern of high and low velocities is consistent. Based on inverted data, Sg velocities appear to be 3.5 ± 0.04 km/s. For most of the area analyzed using the inversion, Sg velocities determined above by the best fitting velocities method earlier in this section are 3.51 or 3.53 km/s, consistently faster than those determined here by the inversion method, but within this error estimate.

3.2.4 Crustal Model.

The Pg and Sg velocities determined above in conjunction with relocation of earthquakes, and the P_n velocities and crustal thickness determinations from the above inversion study can be combined to establish a more complete crustal model for northeast Russia. Table 4 combines the cells in which Pg and Sg velocities are determined (Table 1) with crustal thickness and upper mantle (P_n) values interpolated from the inversion study (Figure 45).

3.3 TOMOGRAPHY

3.3.1 Previous work.

The shallow velocity structure of northeastern Russia is essentially unstudied by tomographic methods. The only previous attempt of P_n wave tomography was done by Wallace and Tinker (1998). The study investigated the portion of Siberia between 70° E and 180° E using events recorded at 11 digital broadband stations installed in the 1990's (primarily IRIS stations). The study obtained 237 arrivals from 43 earthquakes in and around Siberia. Given the geographic size of the area and the small number of raypaths, conclusive results were not obtained.

3.3.2 Tomography Code.

The tomography method used an expanded form of the Time Term Method developed by Hearn (1984) and Hearn (1991). The tomography code used was written by D. McNamara for investigating P_n tomography in the Tibetan Plateau (McNamara, 1995).

In this tomography code, assumptions are made regarding average crustal thickness, average crustal velocity and average Moho velocity. From these assumptions, the static corrections (mean P_n residual) associated with each event are determined, and new residuals are calculated. The event

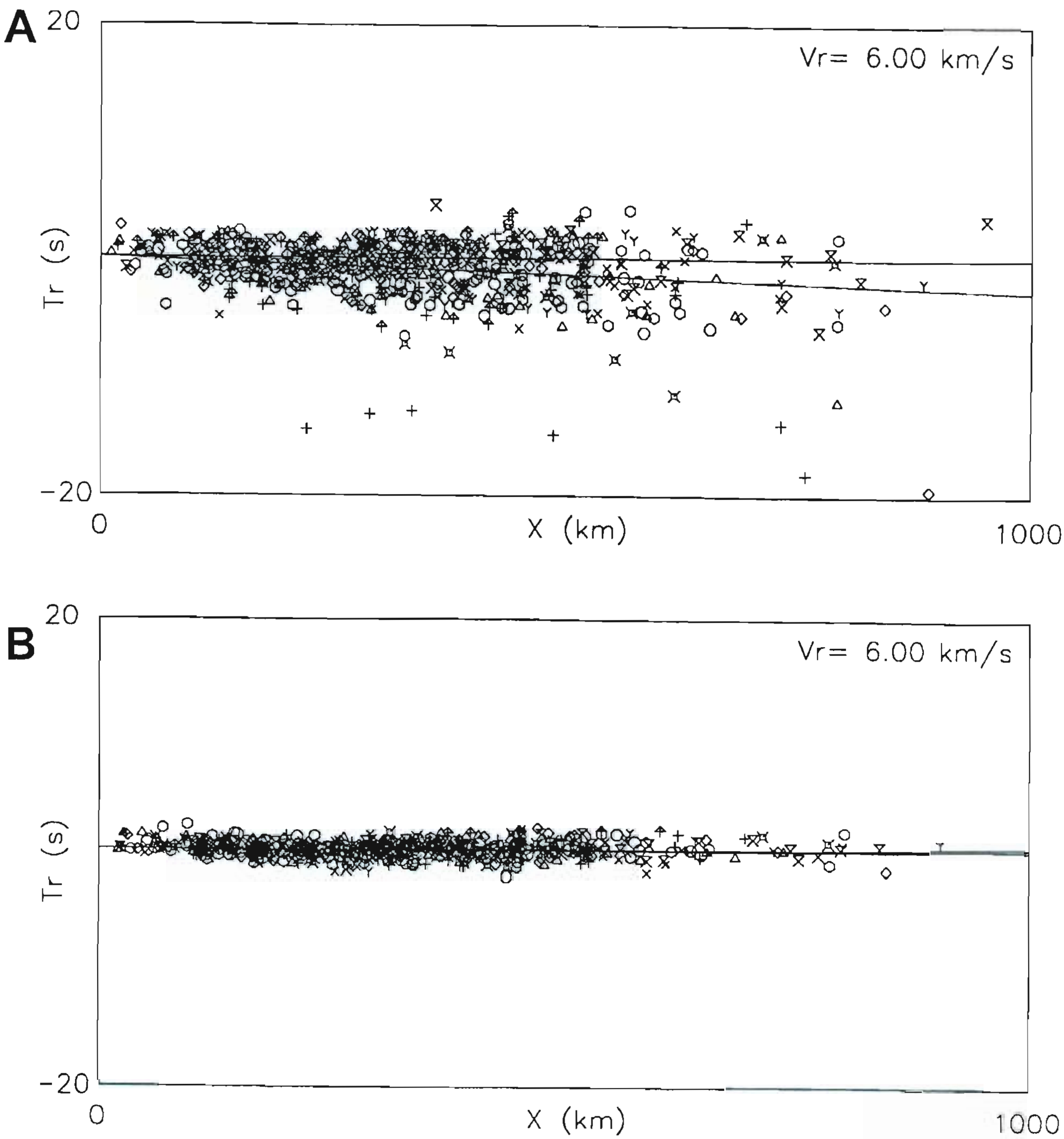

Figure 41. Reduced Pg travel time curves for determining crustal thickness. A. Using epicenters and origin times reported in *Materialy*. The best fit velocity is 6.10 km/s. B. Using relocated epicenters and new origin times from the inversion. This travel time curve indicates a Pg velocity of 5.996 km/s. Reduction velocities (*Vr*) are noted on figures. Individual events are represented by different symbols.

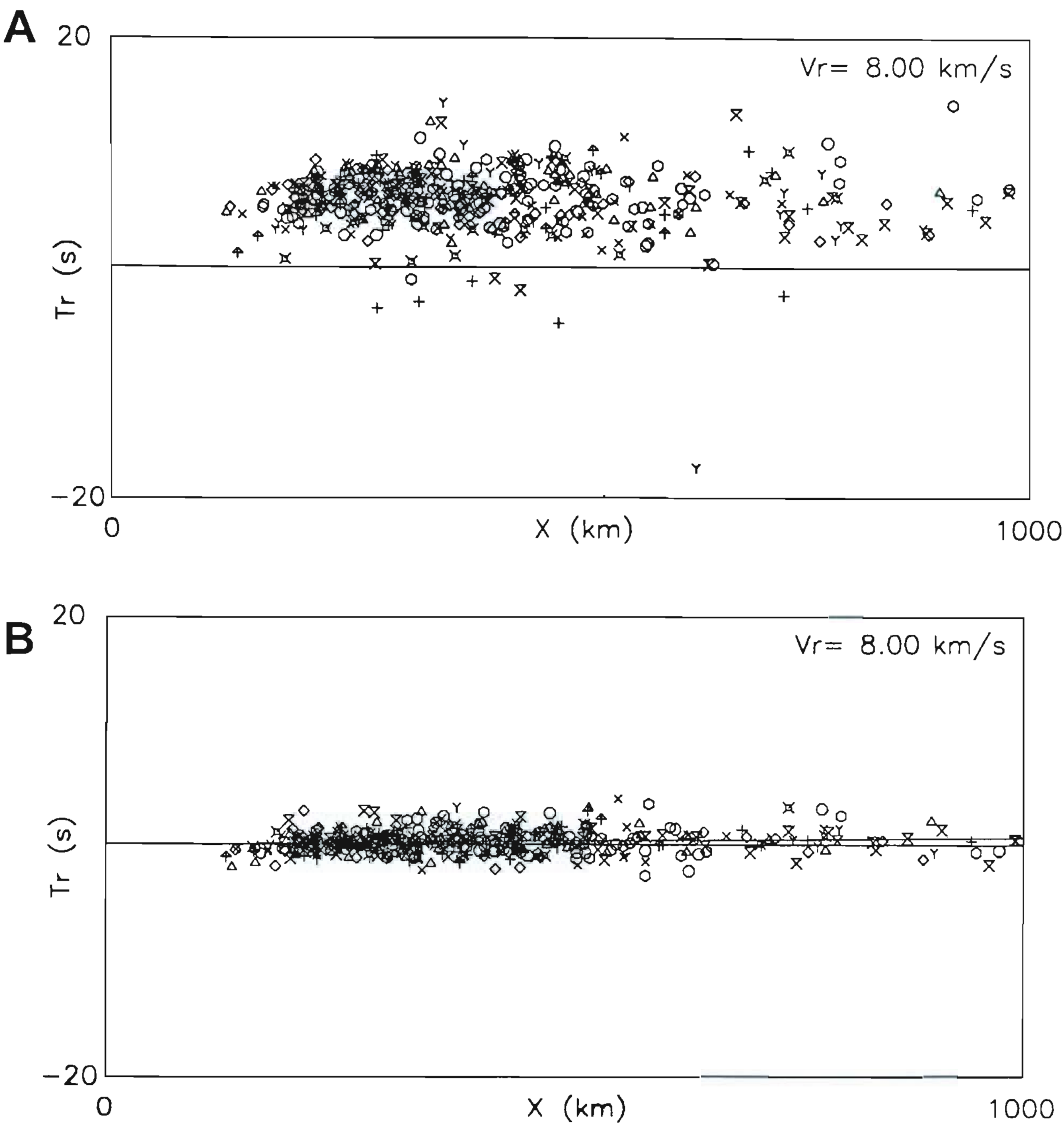

Figure 42. Reduced P_n travel time curves for determining crustal thickness. A. Using epicenters and origin times reported in *Materialy*. B. Using relocated epicenters and new origin times from the inversion. This travel time curve indicates a P_n velocity of 7.961 km/s. Reduction velocities (*Vr*) are noted on figures. Individual events are represented by different symbols.

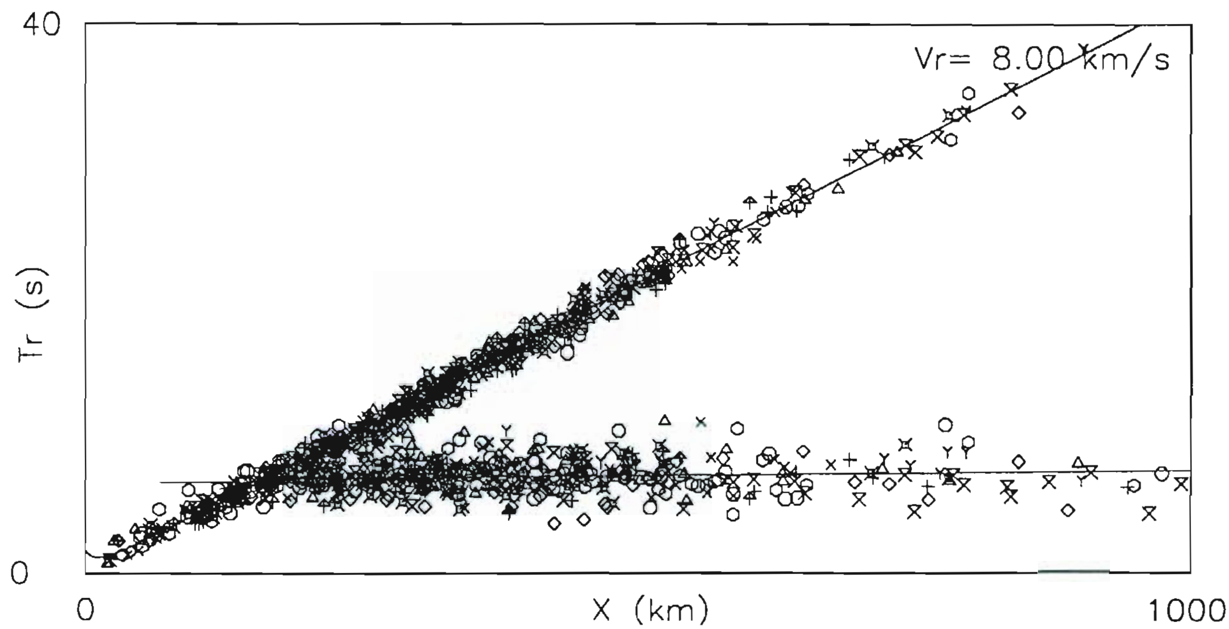

Figure 43. Reduced travel time curves for Pg and P_n data. All data plotted use the relocated epicenter and origin times from the inversion program after high residual arrivals were removed. The Pg-P_n crossover point yields a regional crustal thickness of 37 km. Pg velocity plotted is 5.996 km/s, and Pn velocity is 7.96 km/s. Reduction velocity (*Vr*) is noted on the figure. Individual events are represented by different symbols.

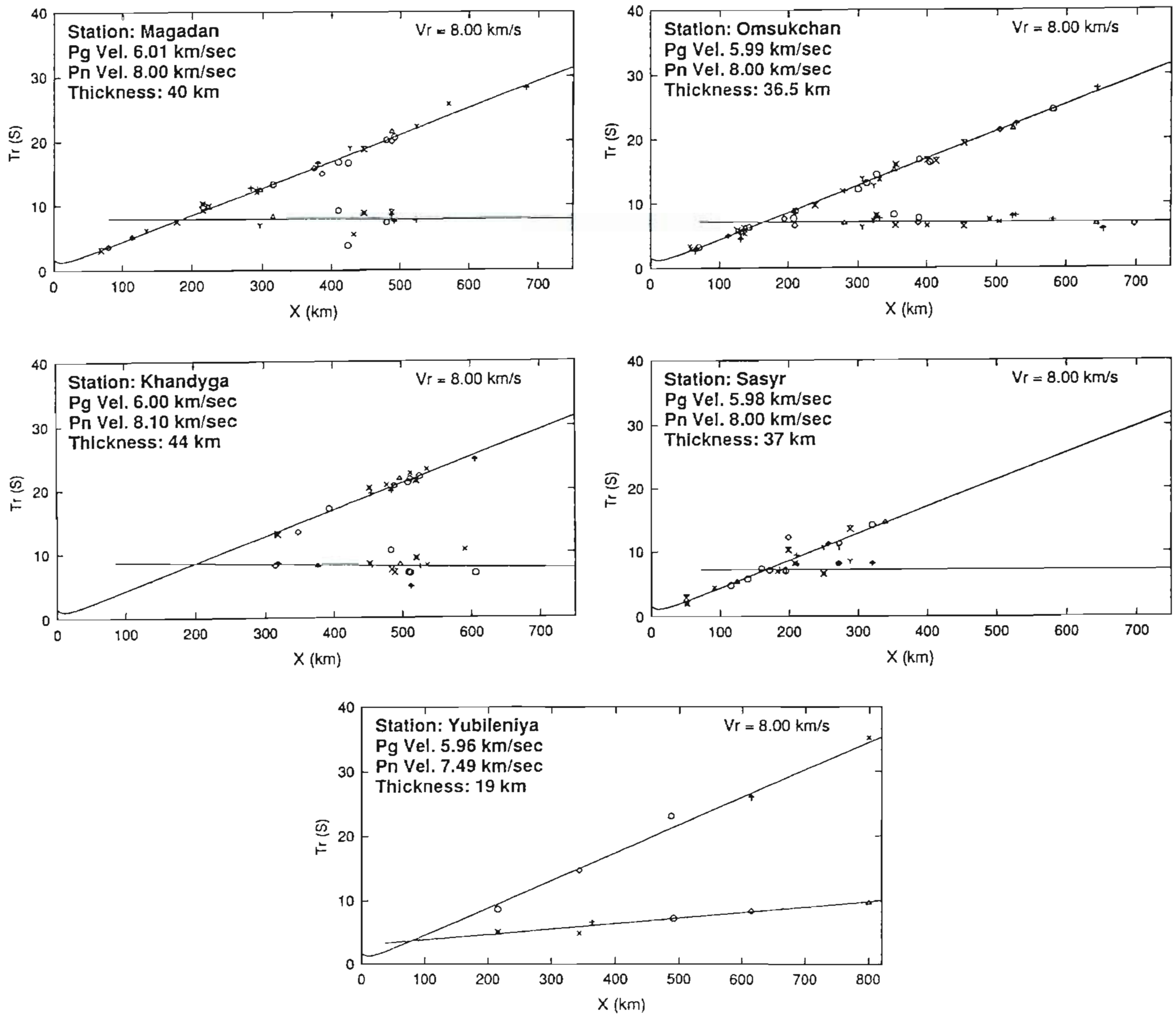

Figure 44. Travel time curves and crustal models for individual stations. For each station, Pg, Pn and reduction (Vr) velocities as well as crustal thickness are noted on figures. Individual events are represented by different symbols.

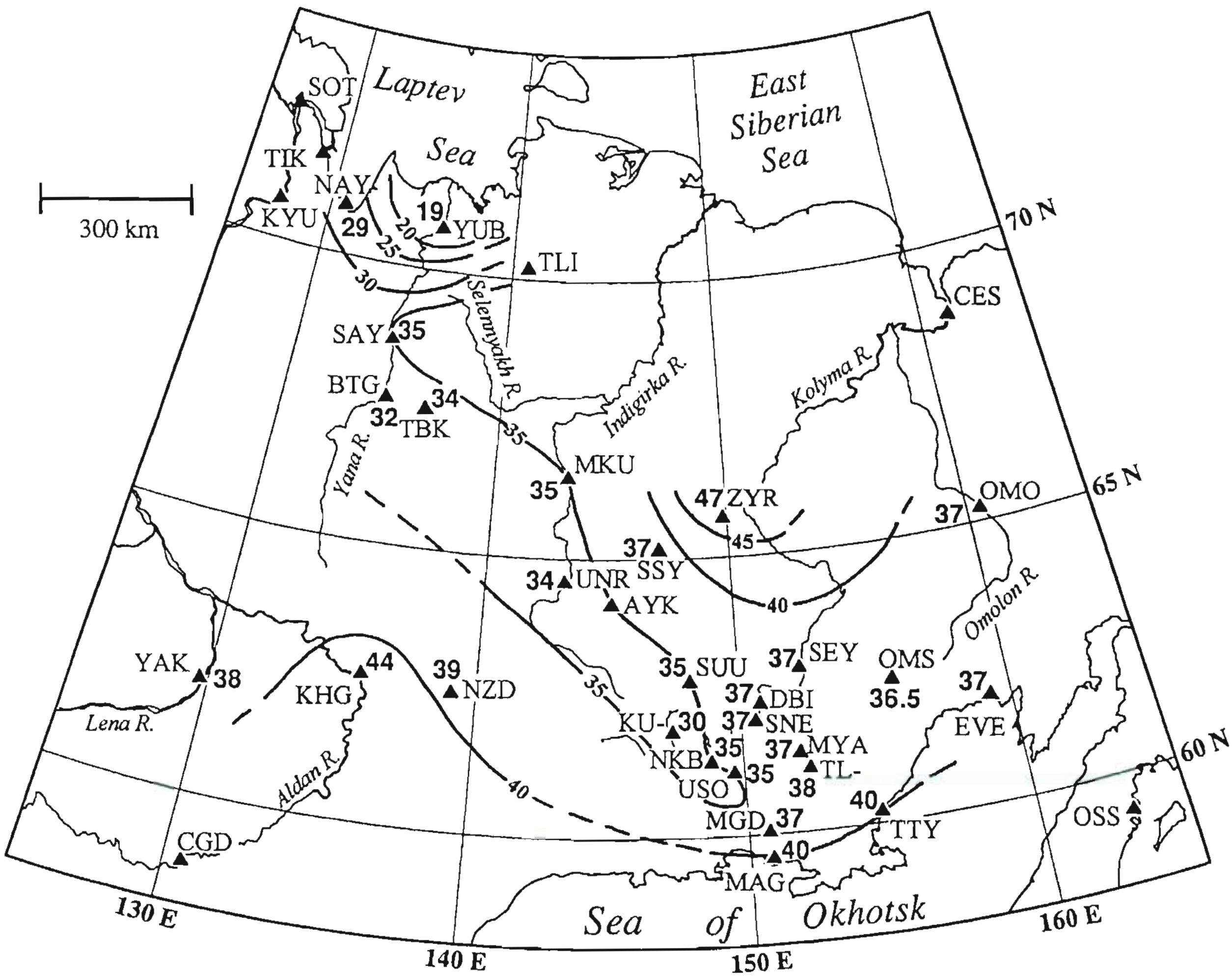

Figure 45. Summary of crustal thickness determinations for the study area contoured at 5 km intervals. Triangles denote seismic stations.

Table 2. Comparison of crustal thickness determinations for northeastern Russia

Code	Station	Belyaevsky (1974)[1]	Belyaevsky and Borisov (1974)	Bobrobnikov and Izmailov (1989)[2]	Suvorov and Kornilova (1986)	Vashchilov (1979)[5]	Mishin and Dareshkina (1966)	Bulin (1989)	Neustroev and Parfenov (1985)	This Study
BTG	Batagai				26±3					32
DBI	Debin			43.0						37
EVE	Evensk	34[3]	40[3]			33.8 (36.0)				37
KHG	Khandyga				44±8				42	44
KU-	Kulu									30
MAG	Magadan		38		30±2[4]					40
MKU	Moma				29±7					35
MYA	Myakit									37
NAY	Naiba									29
NKB	Nel'koba	39	40	38.9		38.9 (41.2) 38.9				35
NZD	Nezhdaninskoe				40±4			37	40	39
OMO	Omolon	38	38			38.9 (40.1) 38.9				37
OMS	Omsukchan	30	35	30.2	38±3	30.2 (31.8) 30.2				36.5
SAY	Saidy						40			35
SSY	Sasyr									37
SEY	Seymchan			34.0	35±13					37
SNE	Sinegor'e									37
MGD	Stekol'nyi	31	37	31.0		31.0 (32.9) 31.0				37
SUU	Susuman		45 (?)	50.0	33±3					35
TBK	Tabalakh							40		34
TTY	Takhtoyamsk									40
TL-	Talaya									38
UNR	Ust' Nera				24±3			40		34
USO	Ust' Omchug				29±3					35
YAK	Yakutsk				37±6				42	38
YUB	Yubileniya									19
ZYR	Zyryanka							41		47

[1]Attributed to work by Nikolaevsky.
[2]Values reported by Bobrobnikov and Izmailov (1989) attributed to Mishin and Dareshkina (1966). Bobrobnikov and Izmailov (1989) consider the value for Debin to be an error.
[3]Data from Belyaevsky (1974) and Belyaevsky and Borisov (1974) for Garmanda, about 20 km north of Evensk.
[4]Suvorov and Kornilova (1986) used Magadan as a calibration point based on the 1959 deep seismic sounding line.
[5]First column is attributed to Mishin and Dareshkina (1966), while values in brackets are from P-S conversions determined with a different formula.

Table 3. Pg and P_n velocities determined by inversion for specific seismic stations. P_n velocities determined by Suvorov and Kornilova (1986) are also included.

Station	Pg This Study	P_n This Study	P_n Suvorov and Kornilova (1986)
Batagai	5.97	7.94	8.1
Debin	5.99	7.97	
Evensk	6.01	8.07	
Khandyga	6.00	8.10	8.1-8.2
Kulu	5.98	7.73	
Magadan	6.01	8.00	
Moma	6.03	7.98	8.1
Myakit	5.99	7.90	
Naiba	5.96	7.70	
Nel'koba	5.97	7.87	
Nezhdaninskoe	5.98	7.98	
Omolon	5.98	7.98	
Omsukchan[1]	5.99	8.00	
Saidy	6.01	8.04	
Sasyr	5.98	8.00	
Seymchan	5.98	8.00	7.9-8.1
Sinegor'e	6.00	8.00	
Stekol'nyi	5.98	8.04	
Susuman	6.00	7.96	7.9-8.0
Tabalakh	6.01	7.94	
Takhtoyamsk	6.02	8.10	
Talaya	5.96	8.10	
Tenkeli	5.98		
Ust' Nera	5.99	7.95	8.0-8.1
Ust' Omchug	6.05	7.90	7.9-8.1
Yakutsk	6.03	8.00	
Yubileniya	5.96	7.49	
Zyryanka	5.98	8.22	
REGIONAL	5.99	8.00	

[1] Mishin and Dareshkina (1966) calculated a Pg velocity for Omsukchan of 6.02 km/sec.

Table 4. Crustal model for northeast Russia.

Lat.	Long.	Best Fit Velocities (km/s)			Crustal Thickness
48-51N	120-125E	Pg=6.040	Sg=3.530		
48-51N	125-130E	Pg=6.025	Sg=3.530		
48-51N	130-135E	Pg=6.100	Sg=3.550		
48-51N	135-140E	Pg=6.100	Sg=3.550		
51-54N	120-125E	Pg=6.100	Sg=3.570		
51-54N	125-130E	Pg=6.125	Sg=3.570		
51-54N	130-135E	Pg=6.125	Sg=3.570		
51-54N	135-140E	Pg=6.075	Sg=3.550		
54-57N	120-125E	Pg=6.275	Sg=3.630		
54-57N	125-130E	Pg=6.175	Sg=3.590		
54-57N	130-135E	Pg=6.150	Sg=3.590		
54-57N	135-140E	Pg=6.100	Sg=3.570		
57-60N	120-125E	Pg=6.275	Sg=3.630		
57-60N	125-130E	Pg=6.300	Sg=3.650		
57-60N	130-140E	Pg=6.275	Sg=3.630		
57-60N	140-145E	Pg=6.075	Sg=3.570		
57-60N	145-150E	Pg=5.950	Sg=3.510		
57-60N	150-155E	Pg=6.040	Sg=3.510	P_n =8.05	40 km
57-60N	155-160E	Pg=6.025	Sg=3.510		
60-63N	135-140E	Pg=6.050	Sg=3.570	P_n =8.04	42 km
60-63N	140-145E	Pg=6.050	Sg=3.530	P_n =7.97	38 km
60-63N	145-150E	Pg=6.025	Sg=3.530	P_n =7.92	35 km
60-63N	150-155E	Pg=6.025	Sg=3.510	P_n =7.99	37 km
60-63N	155-160E	Pg=6.06	Sg=3.51	P_n =8.06	38 km
60-63N	160-165E	Pg=6.05	Sg=3.51		
60-65N	165-170E	Pg=5.975	Sg=3.470		
60-65N	170-180E	Pg=6.000	Sg=3.470		
60-66N	120-135E	Pg=6.225	Sg=3.610	P_n =8.05	38 km
63-66N	135-140E	Pg=6.050	Sg=3.550	P_n =7.99	36 km
63-66N	140-145E	Pg=6.050	Sg=3.530	P_n =7.96	34 km
63-66N	145-150E	Pg=6.025	Sg=3.510	P_n =8.06	39 km
63-66N	150-155E	Pg=6.025	Sg=3.530	P_n =8.06	39 km
63-66N	155-160E	Pg=6.025	Sg=3.510	P_n =7.99	37 km
63-69N	180-160W	Pg=6.050	Sg=3.530		
65-69N	165-180E	Pg=6.060	Sg=3.530		
66-69N	125-130E	Pg=6.275	Sg=3.610		
66-69N	130-135E	Pg=6.075	Sg=3.570	P_n =7.99	34 km
66-69N	135-140E	Pg=6.200	Sg=3.550	P_n =7.97	34 km
66-69N	140-145E	Pg=6.175	Sg=3.570	P_n =7.98	35 km
66-69N	145-150E	Pg=6.040	Sg=3.53		
69-72N	125-135E	Pg=6.050	Sg=3.550	P_n =7.74	24 km
69-72N	135-145E	Pg=6.200	Sg=3.590	P_n =7.74	24 km
72-75N	120-130E	Pg=6.225	Sg=3.570		
72-75N	130-135E	Pg=5.900	Sg=3.510		

delays calculated are dependent on crustal thickness and velocity variations, as well as errors in hypocenter depth and origin time. The individual effects of these parameters will trade off with one another, thus the actual event statics cannot be interpreted in a meaningful way (Hearn et al., 1991).

Static corrections for receiving stations are next determined using the mean residuals for each station and new residuals are again calculated. Static corrections for the stations are primarily dependent on crustal velocity and crustal thickness. Crustal thickness can affect station statics the most (about 1 second per 10 km change in crustal thickness; Hearn et al., 1991), thus they can be interpreted as such.

Finally, cell slownesses are estimated from the weighted mean of the apparent slowness of all rays passing through each cell. The weighting for slowness in a given cell is the product of the rays traversing the cell, adjusted for the fraction of each rays total length that is included within the cell. In each iteration, the full residual remaining after the static corrections is applied to the Moho leg of the travel path. To remove any cells with extreme slowness values due to poorly sampled cells, the model is smoothed between each iteration by averaging each cell with its eight neighbors. This is, in effect, the only dampening that occurs in the process. Once the new model is determined, an updated average Moho velocity for the entire study region is calculated. New residuals are again calculated based on the updated average Moho velocity and the process beginning with event static corrections is repeated until the data converge. Iterations are usually stopped when the change in RMS residuals from one iteration to the next becomes less than 1 % (McNamara et al., 1997).

3.3.3 Results.

Considerable effort went into developing reasonable tomographic models for Northeast Russia using the code of McNamara (1995). Attempts were made to calculate models using the original Russian determined epicenters for the entire study area as well as relocated epicenters from Section 3 above for both the entire study area and a much smaller Magadan-only region, where raypath coverage was much more uniform.

For all model attempts, consistent results with converging residuals and reasonable static corrections were not achieved. Throughout the effort to develop the models, several input/output errors of the tomography code were discovered and workarounds were successfully developed. This still did not result in consistent models. Specific models developed in this process are discussed at length in Mackey (1999), but not discussed individually here due to the final determination of a negative result. The following illustrate the software variables used and changed in the attempts to develop reasonable models:

- Varying the range of acceptable velocities for data selection
- Changing the distance range for acceptable data
- Changing the number of smoothing passes between each iteration
- Changing the minimum number of P_n phases per event or station for usable data
- Varying the cell size used in the model
- Removal of some receiving stations
- Varying the assumed average crustal thickness
- Varying the assumed average Moho velocity

It was ultimately determined after looking at secondary outputs of the tomography code that there are severe indexing problems with the handling of data in the code used (McNamara, 1995). Figure 46 illustrates the apparent indexing problems with the code. The figure illustrates a mismatch between the location of raypath traces, the cells where velocity perturbations were

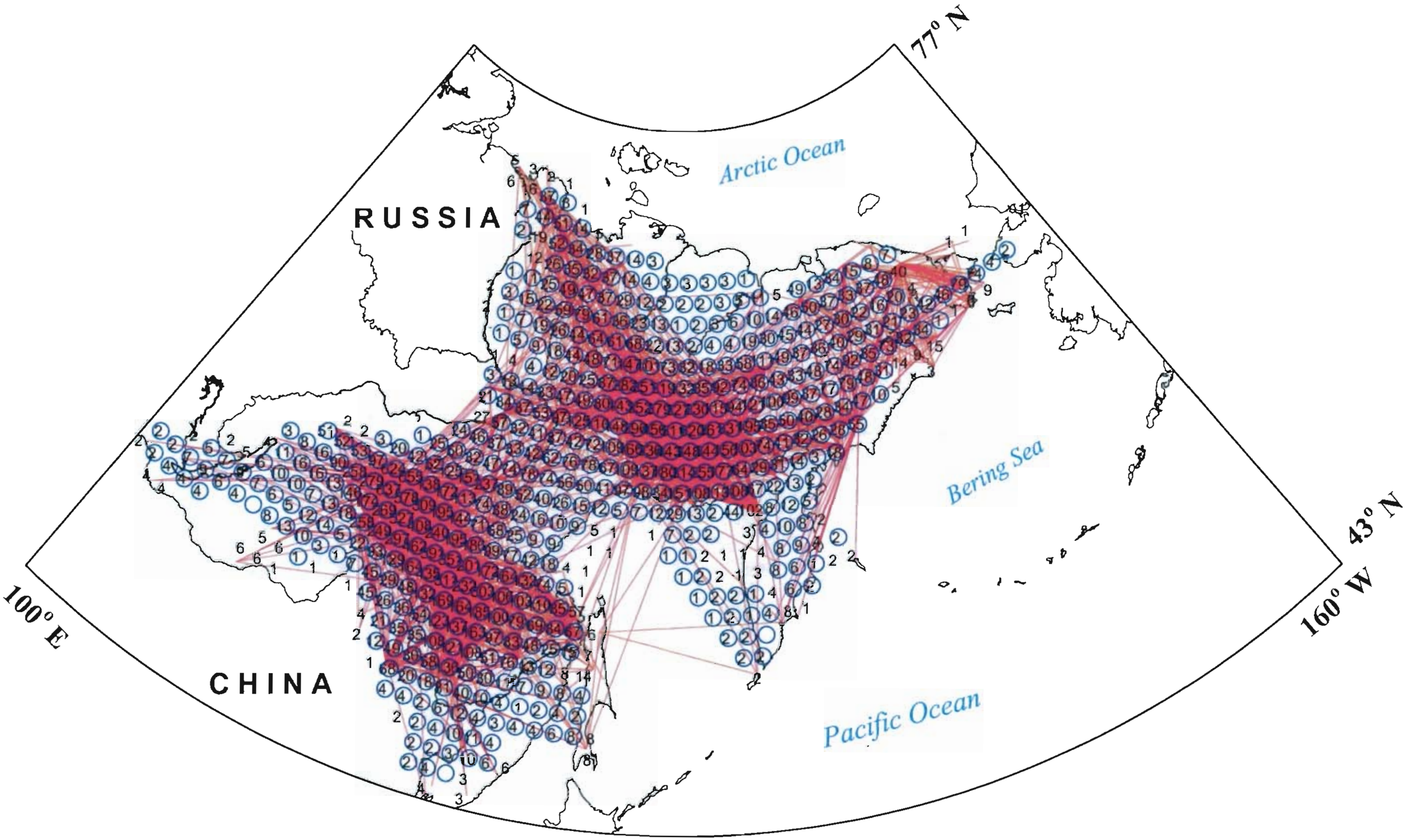

Figure 46. Raypath coverage (red lines) for the tomography study using relocated hypocenters. Black numbers indicate cells with hits and the number of hits. Blue circles indicate cells where velocity perturbations were calculated. Note that none of the three show exactly the same coverage, particularly around the edges of the raypath coverage.

calculated, and the number of raypaths recorded as hitting each cell. For example, some cells clearly have raypaths penetrating them, but record no hits, or miscount them, while other cells have no raypaths crossing them, but record hits and calculate perturbations.

It is remotely possible that some of the indexing problems may be a result of whether the code maps raypaths assuming a flat earth or as great circles. At high latitudes it is necessary to use great circle paths, but the author of the code was not certain if this was being done. Attempts to isolate the problem in the source code were not successful.

3.4 CONCLUSION.

The earthquake relocation process used here has improved the quality of hypocenter locations over the original Russian determinations, as well as developed regionally calibrated, best-fit crustal velocity models. Regional crustal velocities determined are consistent with the known geologic and tectonic setting. Improvements in epicenter locations have clarified several seismicity clusters and fault lineations in northeast Russia. Teleseismically recorded events will be further evaluated and assigned Ground Truth (GT) classifications (Section 4). Development of tomographic models for northeastern Russia was attempted, but not successful. It is believed that computer code problems contributed to this result.

SECTION 4

GT CLASSIFICATIONS AND ANALYSIS OF TELESEISMIC EVENTS

4.1 INTRODUCTION.

In effort to obtain ground truth (GT) classifications in support of CTBT monitoring for continental regions of northeastern Russia, relocations were computed 134 seismic events reported in the International Seismological Centre (ISC) or Earthquake Data Report (EDR) catalogs which occurred from 1970 through 2000 (Figure 47). ISC solutions for this region utilize data from very few local or regional stations. The patterns of arrival time residuals for several stations were plotted and found to be generally consistent with the regional geologic setting. In essence, the travel time residuals found here are mapping the upper mantle velocity structure, which compliments the crustal model as outlined in Section 3.

4.2 METHODOLOGY.

Local and regional arrivals from Russian regional seismic networks in Kamchatka, Magadan, Yakutsk, Amur, Sakhalin, and Irkutsk were used to supplement ISC and EDR data. For many of the events, selected original seismograms were inspected to obtain arrival times not otherwise recorded. Often this was for stations located in one network for an event which occurred within the area covered by another network, since data were not normally exchanged between networks.

In the process of combining local network data with ISC arrivals, it was found that for stations up to 10° distance, phases reported in ISC are sometimes incomplete or misidentified. The most common misassociation is the secondary Pg or Sg phase identified as a P_n/P or S_n/S arrival. This misidentification of phases can result in poor hypocenter determinations by ISC, particularly for events with few receiving stations or poor azimuth distribution to stations. These errors arise due to the fact that arrival times and phases reported to the ISC for many of the Russian stations are the result of preliminary data analysis. The local data bulletins contain the final analysis of arrival times and phase associations. Also, in many cases, ISC reported times are rounded to the nearest second, while local bulletins report arrivals to a tenth of second. In both cases, local bulletin data take preference over that from ISC for relocations computed in this study. The inconsistencies in local data reported by ISC are significant in that they illustrate the problem of relying on international bulletins to develop local or regional velocity models for improved monitoring of the CTBT.

Throughout the study area, many geologic and tectonic environments exist. Combined with the physical vastness of the region, this makes it likely that no single velocity or travel-time curve will reflect actual seismic velocities for any particular phase. In order to overcome this problem, the study area was broken into cells, and the best fitting velocities were determined. The best fitting velocities were then used in the relocation of ISC reported events. Full details of the methodology and procedures used in the relocation of earthquakes are discussed extensively in Mackey (1999), and Section 3 above.

Each event was relocated three times using combined local and teleseismic arrivals, only arrivals within 20° and only arrivals within 10°. To best evaluate which set of data produce the best locations, particular attention was paid to aftershock sequences, and how closely events cluster using

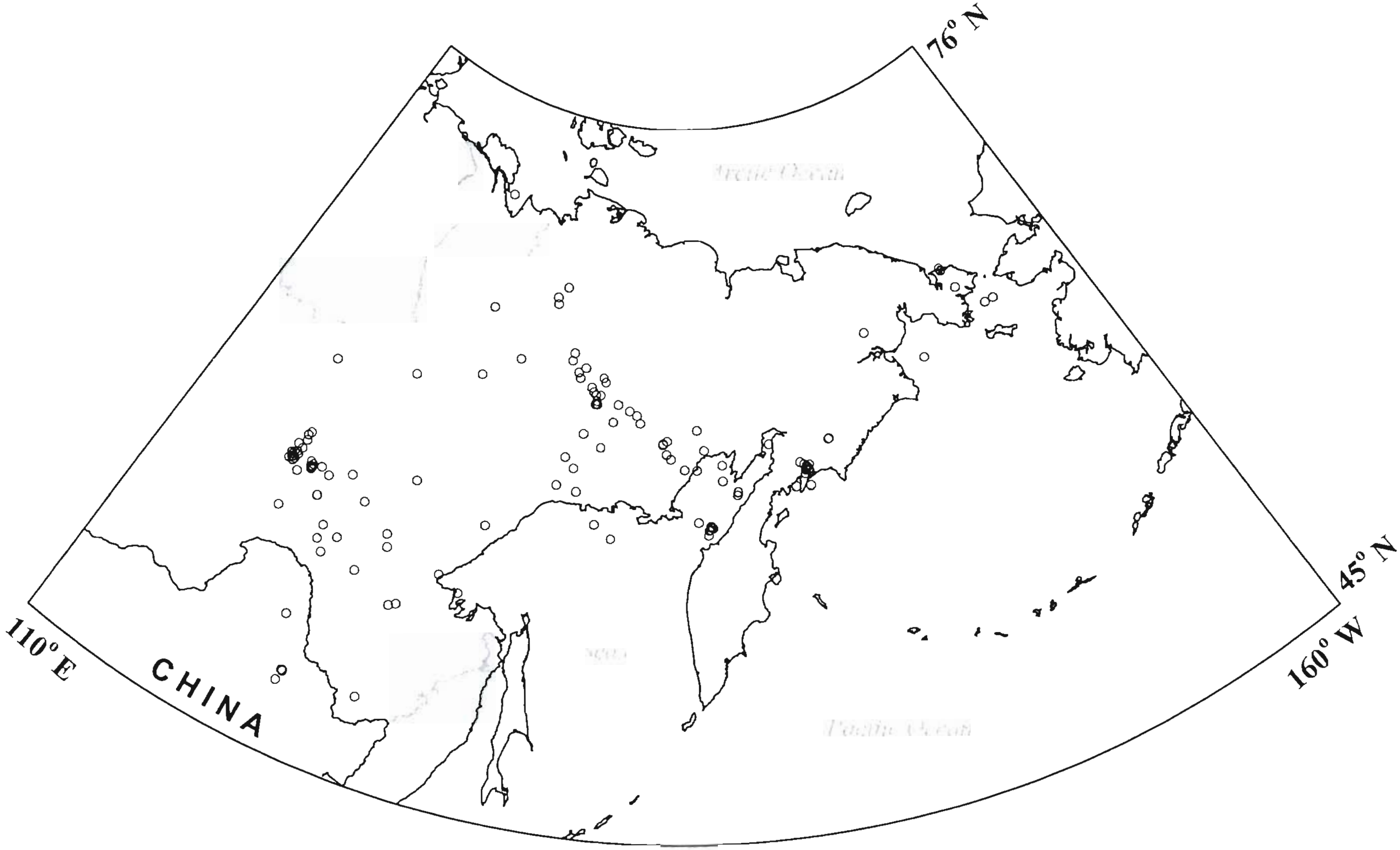

Figure 47. ISC determined for locations for teleseismic earthquakes analyzed in this study.

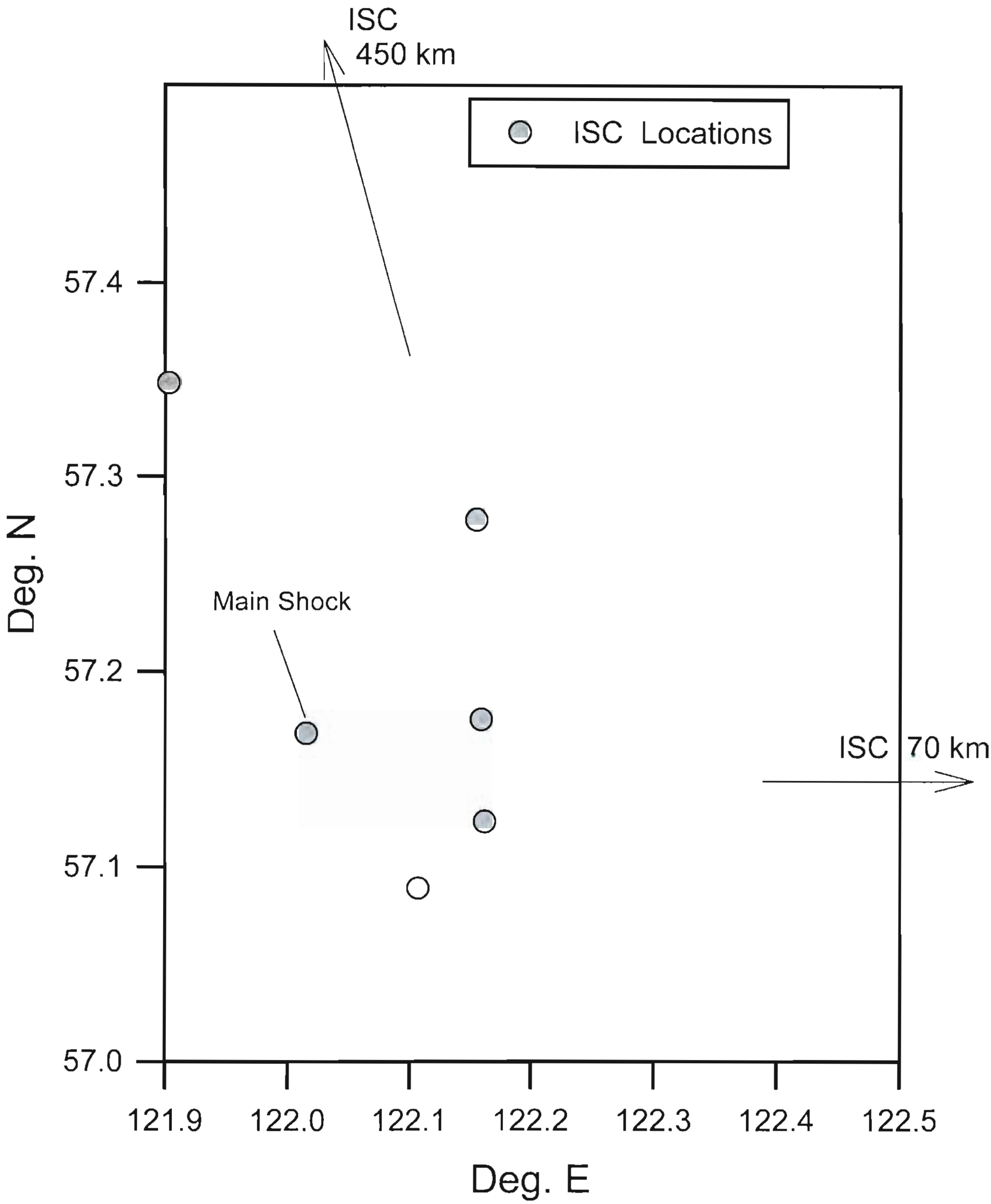

Figure 48. ISC epicenter parameters for the magnitude 6.6 south Yakutia earthquake and aftershocks. Note that 2 events are off the map.

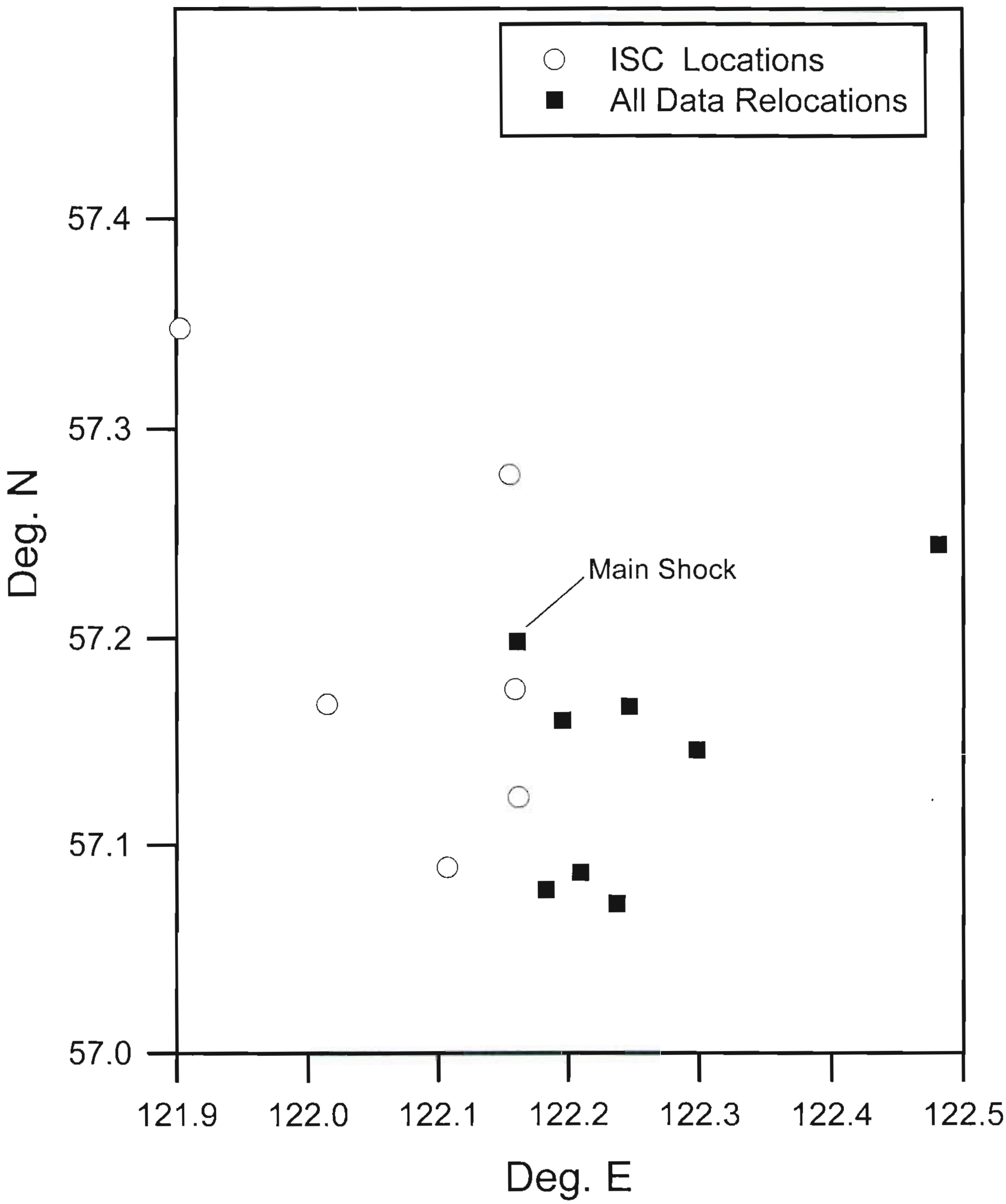

Figure 49. Relocations using data at all distances, including the addition of local and regional stations not reported in ISC. ISC locations shown for reference.

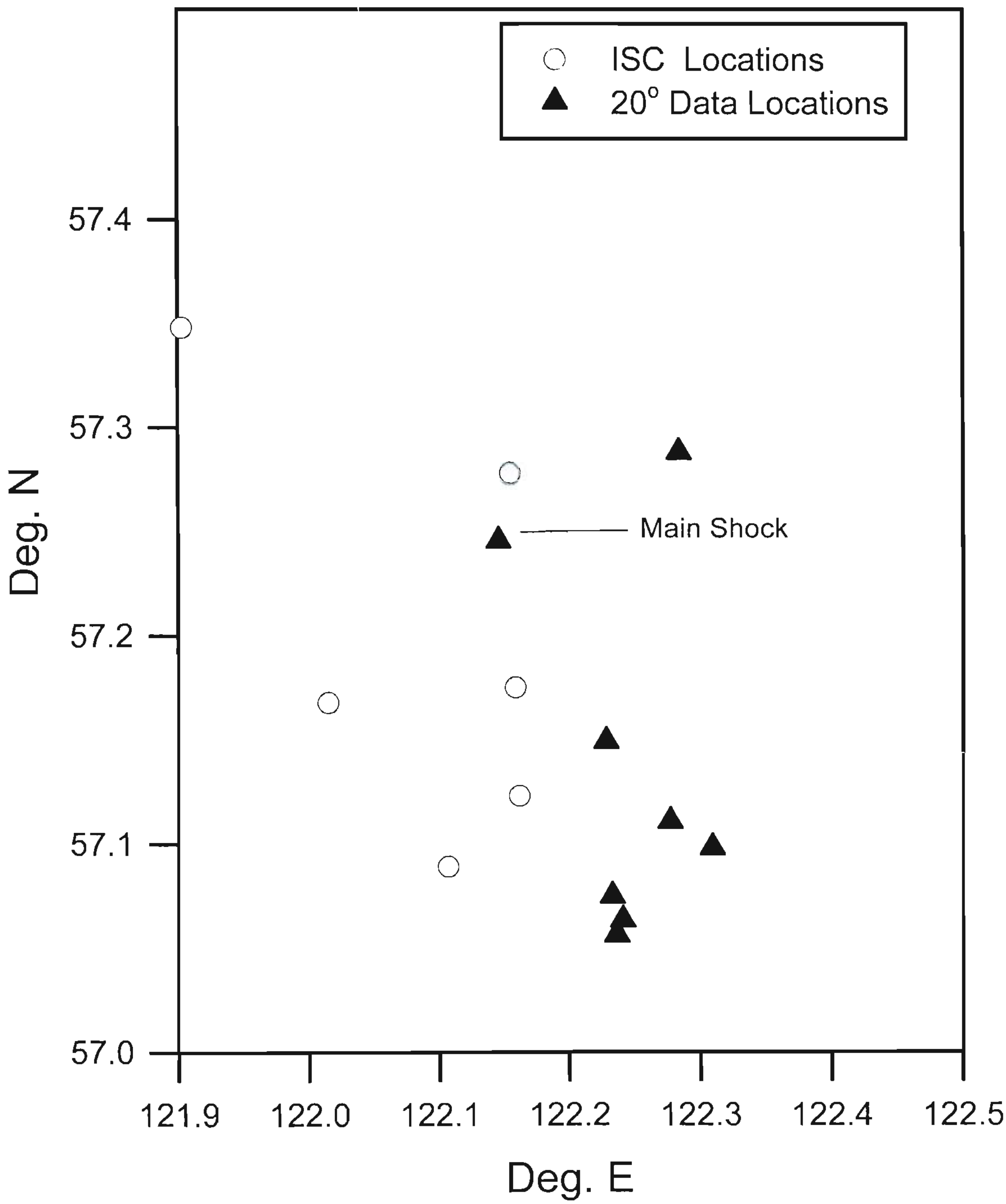

Figure 50. Relocations using data within 20° distance, including the addition of local and regional stations not reported in ISC. ISC locations shown for reference.

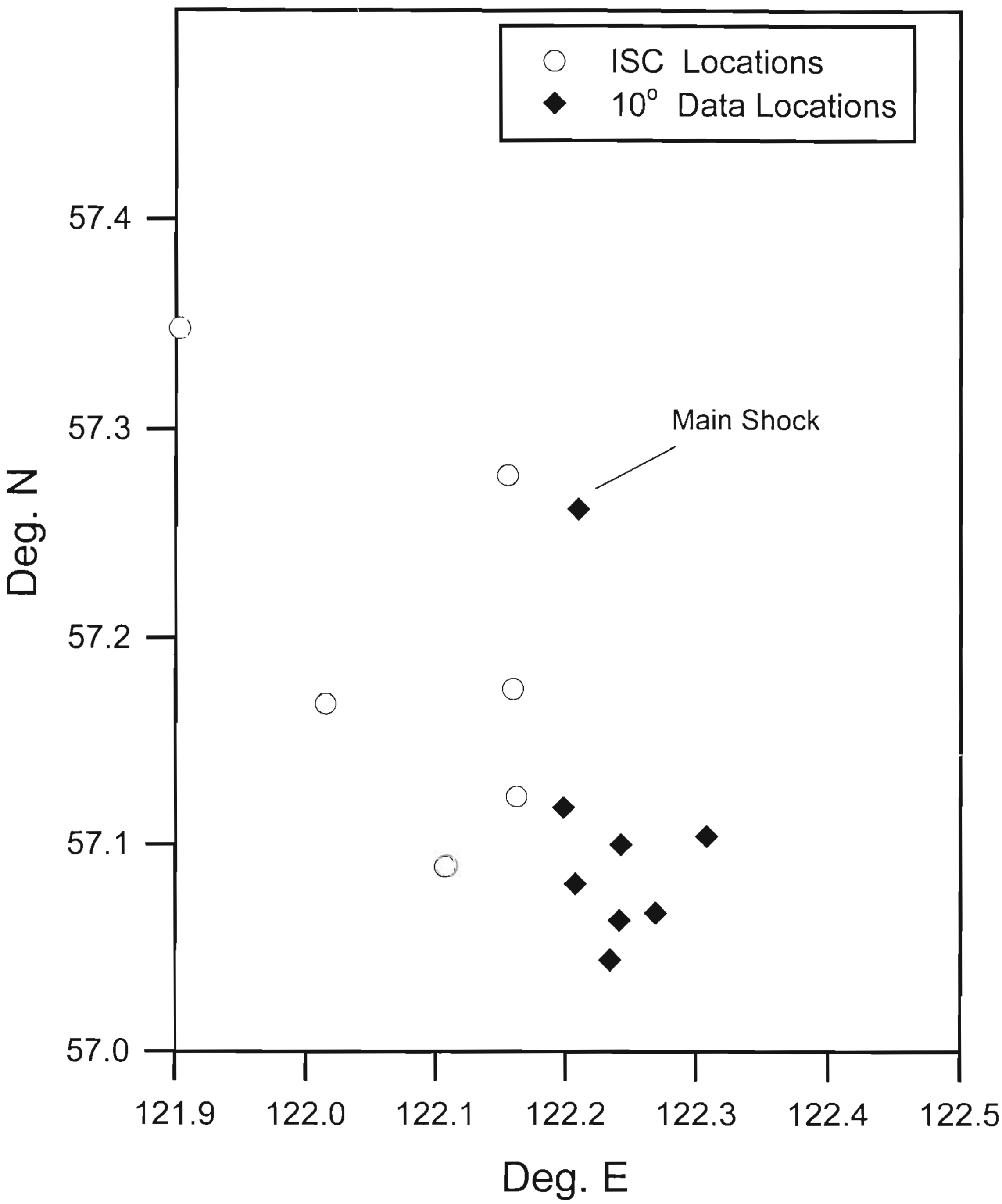

Figure 51. Relocations using data within 10° distance, including the addition of local stations not reported in ISC. ISC locations shown for reference.

the different data sets. Figures 48-51 show the differences in locations determined for an aftershock sequence from south Yakutia in 1989 (see South Yakutia Sequence section below). In this sequence, locations computed using only data either within 10° or 20° cluster best, although locations including local and teleseismic data are clearly improved over those from ISC alone. In general, for events with good azimuthal coverage of stations within 5°, the best locations are those computed with only the local (<10°) and regional (<20°) data, while events having poor azimuthal coverage of close-in stations are better located by including teleseismic data. Based on the general distribution and residuals of stations, a preferred location was selected for each event analyzed (Figures 52 and 53; Appendix C).

All relocated events are assigned GT levels, with 26 events meeting or exceeding the GT10 criteria (Figure 54). Criteria used for acceptance of GT10 events state that the event must be recorded by a minimum of five stations within 3° distance, and that for stations within 5°, the largest azimuthal gap must be 180° or less (Yang and Romney, 1999). An example of residuals and station distribution for a GT10 event is presented in Figure 55 and Table 5. A few events which formally met these criteria were excluded from GT10 classification due to high station residuals for some close in stations, or other odd station distribution problems which can result in poor epicenter control. It should also be noted that many relocated events miss the formal GT10 criteria, but it is suspected that the location determined here is within 10 km of the true epicenter based on proximity to fault traces, etc. (see discussion below). Most of the remaining relocated events meet GT25 criteria. Although no events formally qualify as GT5, many events are likely within that accuracy.

Overall, compared with ISC locations, events occurring within aftershock sequences cluster tighter, and event alignment with known active faults improves.

4.3 RESULTS.

4.3.1 Comparison with ISC Epicenters.

134 events listed in the ISC bulletin were relocated incorporating regional data. Most (90%) of the relocations differ by less than 45 km relative to the ISC parameters, with a few being significantly different (one event with poor station coverage in the ISC moved 500 km). As noted, the new locations are likely to be an improvement due to the large number of local and regional phases utilized. However, there is no large-scale spatial pattern to the azimuth or magnitude of change in epicenters calculated by ISC relative to these relocations (Figure 53).

Although there are some areas where there appears to be some consistent directional mislocation bias (e.g., the larger events in Chukotka, the Laptev Sea, and also perhaps in the north-central Verkhoyansk Range), the most consistent bias in the epicenter shift is "radial," with aftershocks and other events tending to move into tighter clusters or into lineaments (e.g., central Chersky Range). No specific areas stand out as having large differences between ISC and solutions determined here. Examination of events whose locations have the greatest differences, by more than 45 km, suggests that the relocations are much better than the ISC solutions, aside from a few exceptions at the edges of the study area.

ISC solutions are generally worse where they have no close stations or the stations fall into a narrow azimuthal range. Similarly, a few of relocations at the edges of the study area are worse because of a narrow azimuthal range without using teleseismic data; this may also have affected the travel time curve calibrations for these areas (Section 3).

An area where the relocations show clear improvement is Chukotka, where the use of both Russian and American data provides better azimuthal coverage. Throughout the remainder of the

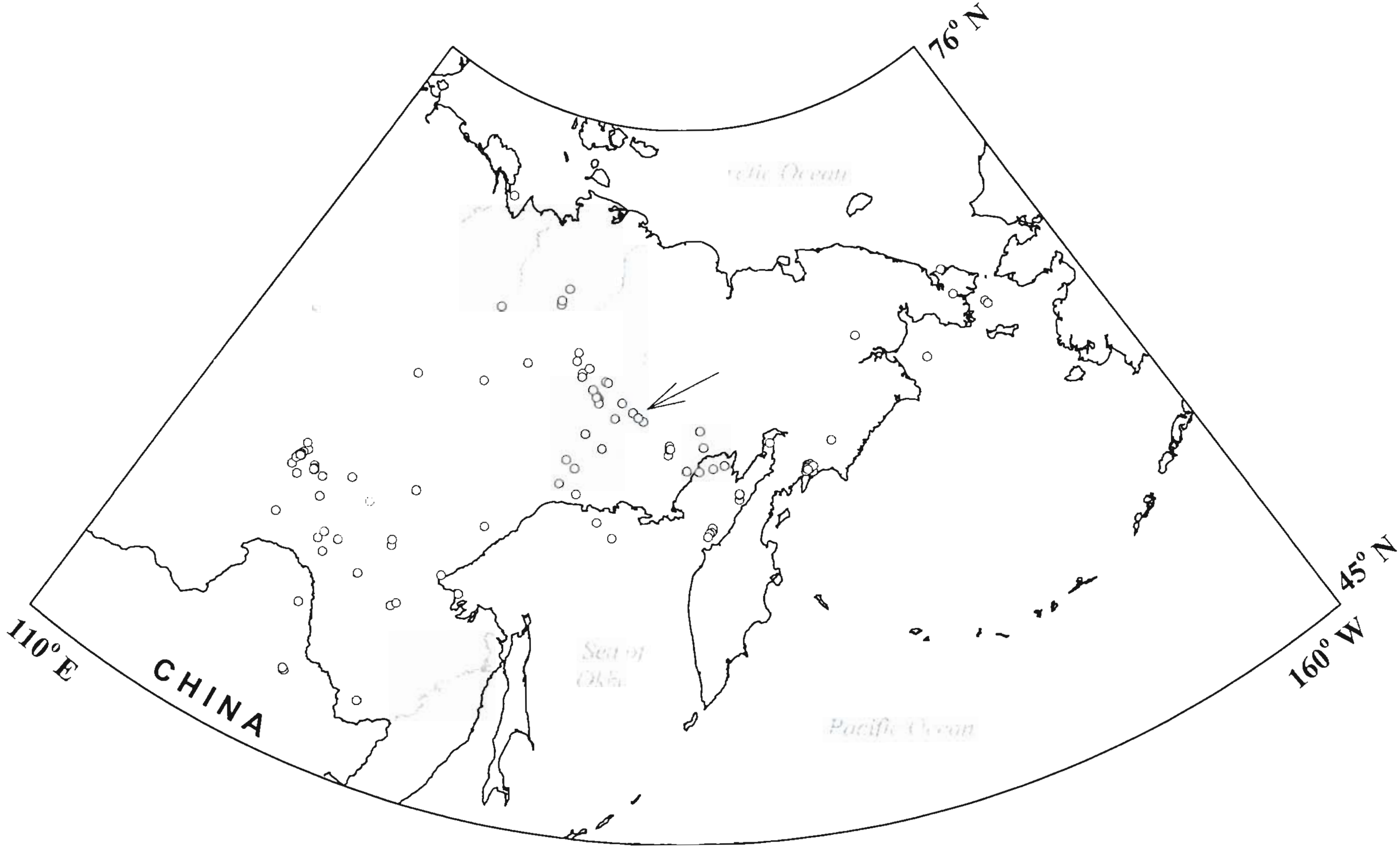

Figure 52. Relocations determined in this study using ISC data supplemented with local and regional time picks. Arrow indicates linear trend associated with the Ulakhan fault.

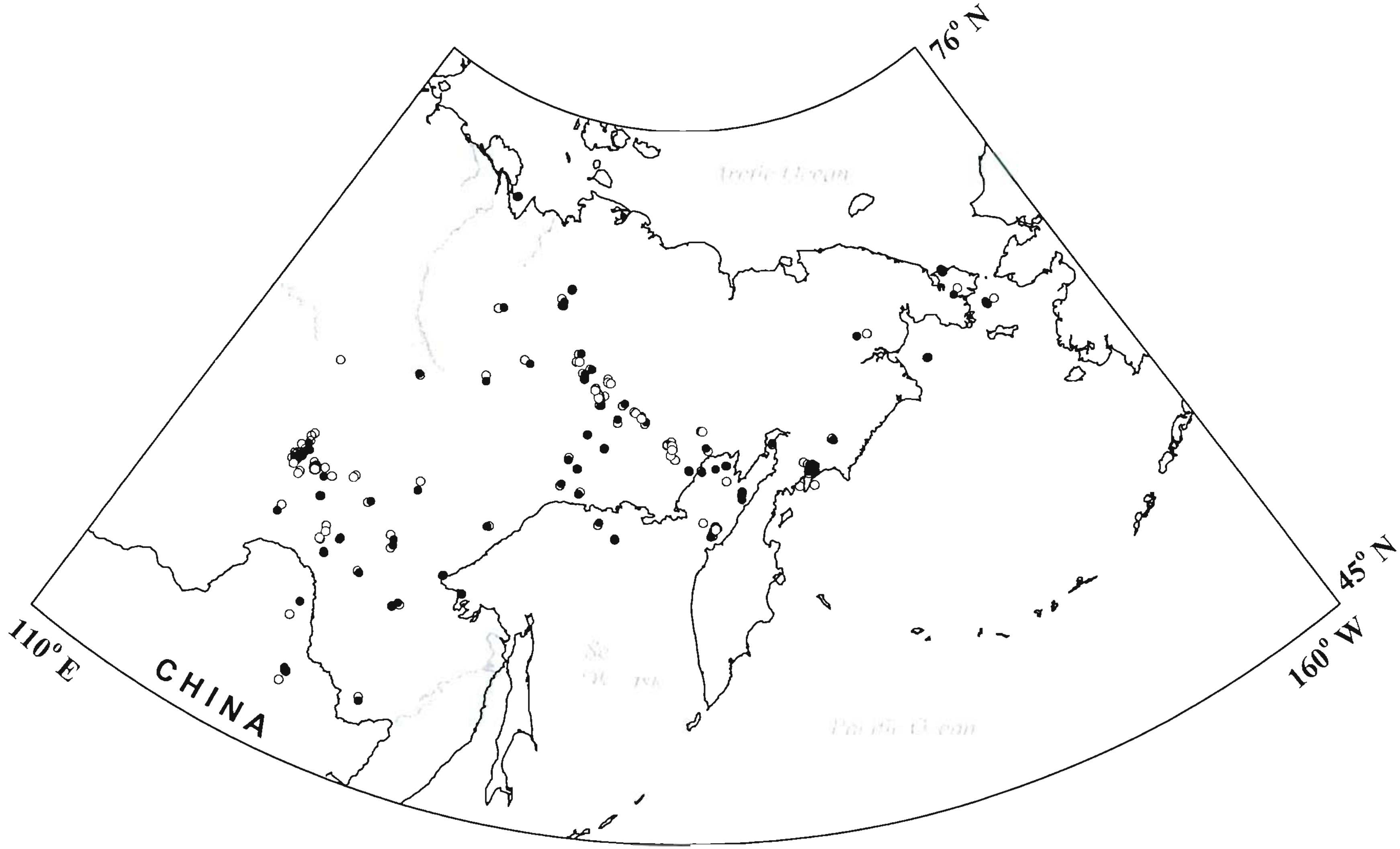

Figure 53. Comparison of ISC epicenters (open circles) and relocations (filled circles). Gray circles represent relocations that meet or exceed GT10 criteria. Note the relocations cluster tighter and form better lineaments near the center of the figure.

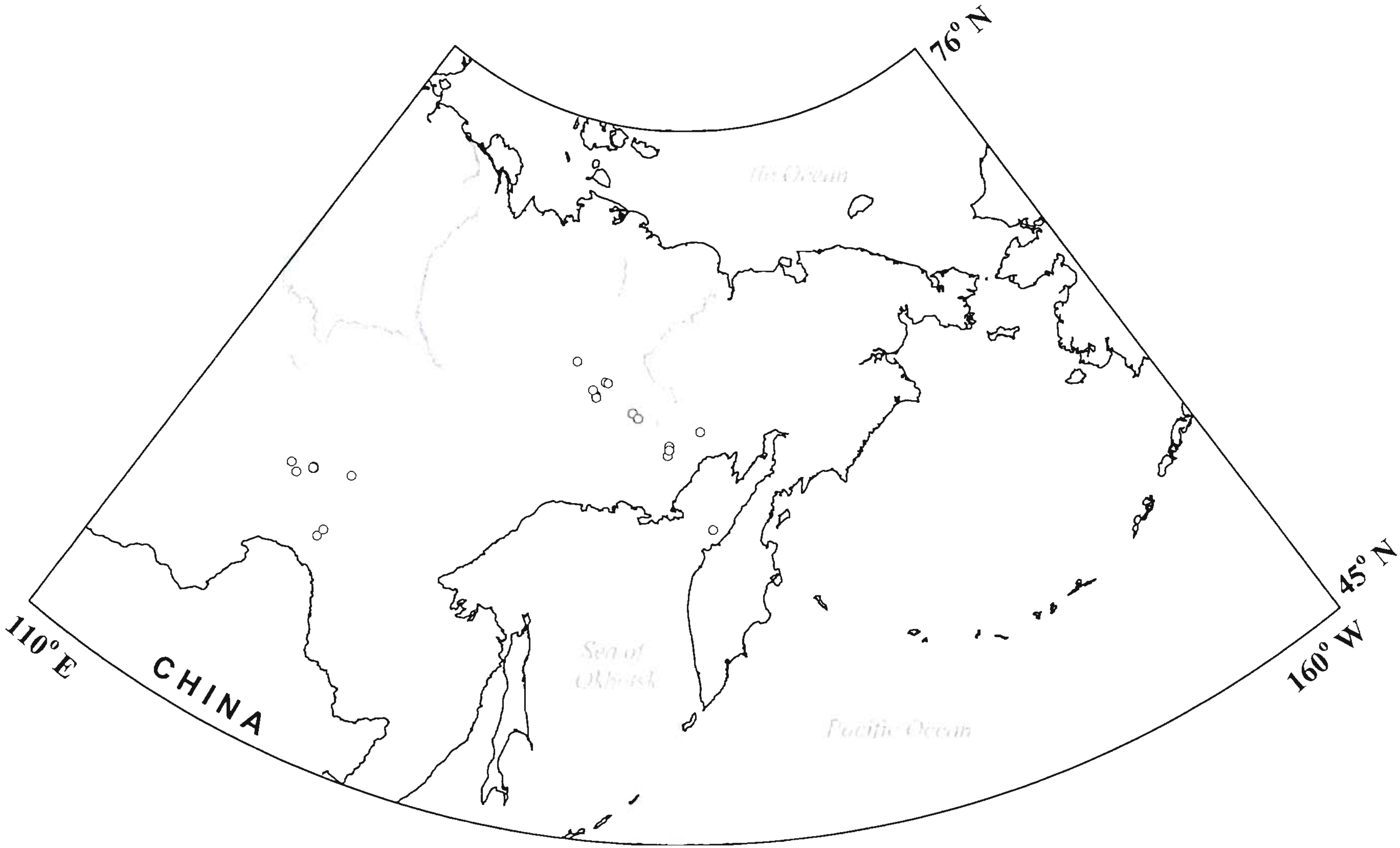

Figure 54. GT10 events.

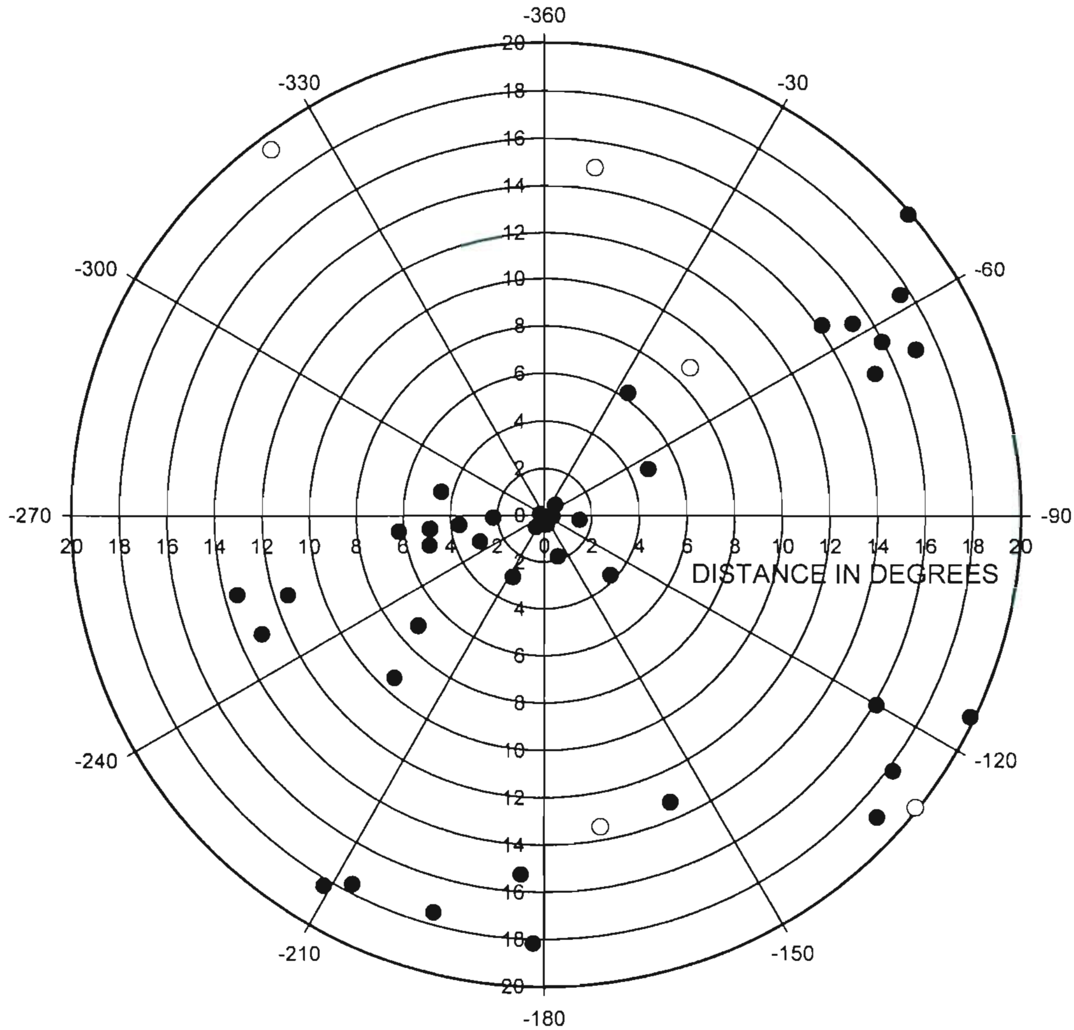

Origin time: 05 04 35.84 utc
Latitude: 57.057° N
Longitude: 122.237° E
Depth: 30.7 km
Magnitude: 5.6

Number of stations within 2°: 7
Number of stations within 3°: 10
Largest Azimuthal gap within 5°: 117.5°
Classification: GT-10

Figure 55. Distribution of stations used in the 20° distance relocation of the May 17, 1989 event. Stations shown in gray were omitted from the location computation due to high residuals (see Table 5).

Table 5. Relocation output of the May 17, 1989 (05:04 UTC) earthquake using only stations within 20 degrees distance. Arrivals in bold are those added in this study, supplementing ISC listings. See also Figure 55.

NUMBER OF ARRIVALS = 56

N	ORIGIN TIME	LAT. (DEG±KM)	LONG. (DEG±KM)	DEPTH. (KM)	RMS RESIDUAL
0	05 04 35.80	57.0500	122.2400	32.00	
1	05 04 35.84±.17	57.0560±1.62	122.2367±1.24	30.69 ±1.96	.84
2	05 04 35.84±.17	57.0562±1.62	122.2365±1.23	30.69 ±1.96	.84
3	05 04 35.84±.17	57.0562±1.60	122.2365±1.23	30.69 ±1.96	.84
4	05 04 35.84±.17	57.0562±1.60	122.2365±1.23	30.69 ±1.96	.84
5	05 04 35.84±.17	57.0562±1.60	122.2365±1.23	30.69 ±1.96	.84

STATION	PHASE	TIME	DISTANCE	AZIMUTH	RESIDUAL	WEIGHT
SYL	**PG**	**5 4 42.2**	**.20**	**288.35**	**.24**	**1.0**
ACH	**PG**	**5 4 44.4**	**.35**	**97.35**	**.57**	**1.0**
KBK	**PG**	**5 4 44.5**	**.40**	**165.34**	**.02**	**1.0**
YRG	**PG**	**5 4 49.0**	**.63**	**45.80**	**.94**	**1.0**
USZ	**PG**	**5 4 47.6**	**.61**	**215.82**	**-.22**	**1.0**
CLNS	**PG**	**5 5 3.2**	**1.48**	**97.33**	**.66**	**1.0**
CLNS	**SG**	**5 5 22.0**	**1.48**	**97.33**	**-.02**	**.5**
UUR	**P**	**5 5 6.0**	**1.84**	**162.30**	**.13**	**1.0**
CRS	P	5 5 12.1	2.18	267.54	1.45	1.0
SRK	**P**	**5 5 22.0**	**2.95**	**248.05**	**.32**	**1.0**
TUP	IP	5 5 21.5	2.94	207.24	-.04	1.0
TUP	**PG**	**5 5 27.5**	**2.94**	**207.24**	**-.71**	**1.0**
TUP	**SG**	**5 6 5.5**	**2.94**	**207.24**	**-.98**	**.5**
NLY	**IP**	**5 5 32.0**	**3.64**	**263.80**	**.54**	**1.0**
KIRS	**P**	**5 5 32.8**	**3.76**	**132.48**	**-.33**	**1.0**
BOD	P	5 5 44.0	4.50	283.06	.41	1.0
BOD	**PG**	**5 5 54.7**	**4.50**	**283.06**	**-1.06**	**1.0**
BOD	**SG**	**5 6 50.0**	**4.50**	**283.06**	**-3.98***	**.0**
CGD	**IP**	**5 5 48.5**	**4.78**	**65.70**	**.91**	**1.0**
SVK	**IP**	**5 5 50.0**	**4.89**	**263.34**	**.83**	**1.0**
SVK	**PG**	**5 6 6.0**	**4.89**	**263.34**	**3.35***	**.0**
UKT	**IP**	**5 5 51.7**	**5.04**	**255.40**	**.26**	**1.0**
UKT	**PG**	**5 6 5.5**	**5.04**	**255.40**	**.04**	**1.0**
YAK	P	5 6 6.7	6.25	34.16	-1.45	1.0
YAK	**PG**	**5 6 26.4**	**6.25**	**34.16**	**-.23**	**1.0**
YAK	**SG**	**5 7 46.0**	**6.25**	**34.16**	**-1.40**	**.5**
KMO	**P**	**5 6 8.1**	**6.23**	**263.75**	**.19**	**1.0**
CIT	P	5 6 18.3	7.13	228.76	-2.35	1.0
CIT	**PG**	**5 6 46.0**	**7.13**	**228.76**	**3.69***	**.0**
CIT	**SG**	**5 8 14.0**	**7.13**	**228.76**	**-.51**	**.5**
KHG	**P**	**5 6 20.5**	**8.73**	**44.52**	**-22.28***	**.0**
KPC	**P**	**5 6 51.0**	**9.42**	**222.73**	**-1.40**	**1.0**
IRK	P	5 7 20.0	11.42	252.78	.27	1.0
ZAK	P	5 7 42.5	13.03	247.20	1.06	1.0
MDJ	P	5 7 44.0	13.28	156.55	-.62	1.0
MOY	P	5 7 47.3	13.47	255.51	.07	1.0
CN2	P	5 7 43.0	13.43	169.94	-3.49*	.0
SUUS	**P**	**5 7 54.9**	**14.14**	**55.37**	**-.85**	**1.0**

Table 5 (Cont.)

TIK	P	5	8	1.0	14.90	8.19	-4.56*	.0
DBI	**P**	**5**	**8**	**10.3**	**15.25**	**57.89**	**.10**	**1.0**
SNY	IP	5	8	10.0	15.27	176.19	-.53	1.0
MGD	P	5	8	8.1	15.11	66.67	-.34	1.0
TL-S	**EP**	**5**	**8**	**18.3**	**15.94**	**62.62**	**-.79**	**1.0**
YSS	P	5	8	22.0	16.09	120.12	.91	1.0
TTY	**EP**	**5**	**8**	**33.8**	**17.08**	**65.82**	**.40**	**1.0**
BJI	EP	5	8	38.0	17.48	195.66	-.58	1.0
OMS	**EP**	**5**	**8**	**39.4**	**17.59**	**58.01**	**-.46**	**1.0**
HHC	P	5	8	40.5	17.63	207.64	-.13	1.0
DL2	IP	5	8	48.0	18.17	181.52	.90	1.0
BTO	P	5	8	50.0	18.28	210.92	1.34	1.0
ASAJ	EP	5	8	50.0	18.21	126.66	2.45	1.0
MRRJ	EP	5	8	56.4	18.94	132.58	-.21	1.0
NRI	P	5	8	55.3	19.38	323.22	-5.89*	.0
KUR	EP	5	9	5.0	19.83	115.67	-1.40	1.0
HOOJ	EP	5	9	4.6	19.90	128.56	-2.61*	.0
OMO	**EP**	**5**	**9**	**7.3**	**19.91**	**50.06**	**.11**	**1.0**

* Arrivals excluded from the location solution due to high residuals.

study area the aftershock relocations are better, with solutions falling in closer proximity to the mainshock, a result of a better data set using larger numbers of close-in stations. Because the magnitude of the largest event does not exceed 7.0, aftershock areas are not expected to be large.

The area where relocation solutions may have some problem is in northern Yakutia and the Laptev Sea. Here, if only local and regional arrivals are used, there are no stations to the north, resulting in poor azimuthal. Rapid variations in crustal seismic velocities in the Laptev Sea region are suspected of further degrading the quality of the relocations (see Section 3). Because of poor azimuth distributions and poorly resolved crustal velocities, teleseismic earthquakes occurring in the Laptev Sea are excluded from this study even though additional local and regional data are available.

4.3.2 South Yakutian Sequence.

Many of the best located events are from the aftershocks of the South Yakutian earthquake of 1989 (M_w 6.3-6.4) where five temporary stations were deployed by the Yakut regional network in the aftershock zone (Koz'min et al., 1993). Figure 56 shows relocations of the main shock and seven aftershocks based on local, regional, and all (including teleseismic) data. For these events, the regional (<20°) relocations are suspected to be best, with the exception of one aftershock, where the local (<10°) location is better. The relocated aftershocks cluster in a zone with dimensions of about 7 x 10 km, with the mainshock located approximately 12 km northwest of the aftershocks (Figure 56). Since all seven aftershocks meet GT10 criteria, based on the tight clustering of the aftershocks, it is likely that the accuracy of these solutions may be better. The data for one of the aftershocks is presented in Table 5 and the variation in solutions for that event is shown in Figure 57 (see Figure 55 also). In contrast, three of the original ISC epicenters are located 30, 90, and 500 km from the cluster (Figures 48 - 51) and the remaining four aftershock solutions from ISC are offset about 10-15 km to the northwest of the relocated cluster. In general, the ISC solutions that differ greatly from the relocations are probably the result of poor time picks or little data, while the four events showing the 10-15 km offset probably better represent a true location bias in the ISC solutions. The aftershock sequence from this event continued for many months and over three-thousand events were recorded.

The relocation of the mainshock was somewhat problematic. There was considerable variability between the solutions and all solutions tended to be 15 to 20 km to the north of the aftershock cluster and away from inferred faults in the area; this was most pronounced for the regional solution (Table 6). However, this may be due to the higher seismic velocities along ray-paths to stations on the northern edge of the Siberian platform (see discussion on travel-time variations, below). Exclusion of these stations yielded more reasonable solutions and the mainshock and three of the aftershocks align along a possible northwest-southeast striking fault (Figure 56). The remaining four aftershocks cluster about 5 km to the south.

4.3.3 Ulakhan Fault.

All of the relocated events in the Chersky Range relocate into essentially straight lines which parallel the Ulakhan and Chai-Yureya faults. These faults are among those thought to represent major breaks along which the strain between the Okhotsk and North American plates are partitioned (Imaev et al., 1990, 1994). The Ulakhan fault (Figure 58) is well defined in the topography between the Indigirka and Kolyma Rivers. It shows clear river offsets (Figure 59) at several levels, but with a probable maximum of 40 km of left-lateral movement since the establishment of the river network (inferred as mid-Pliocene based on Grossheim and Khain, 1967).

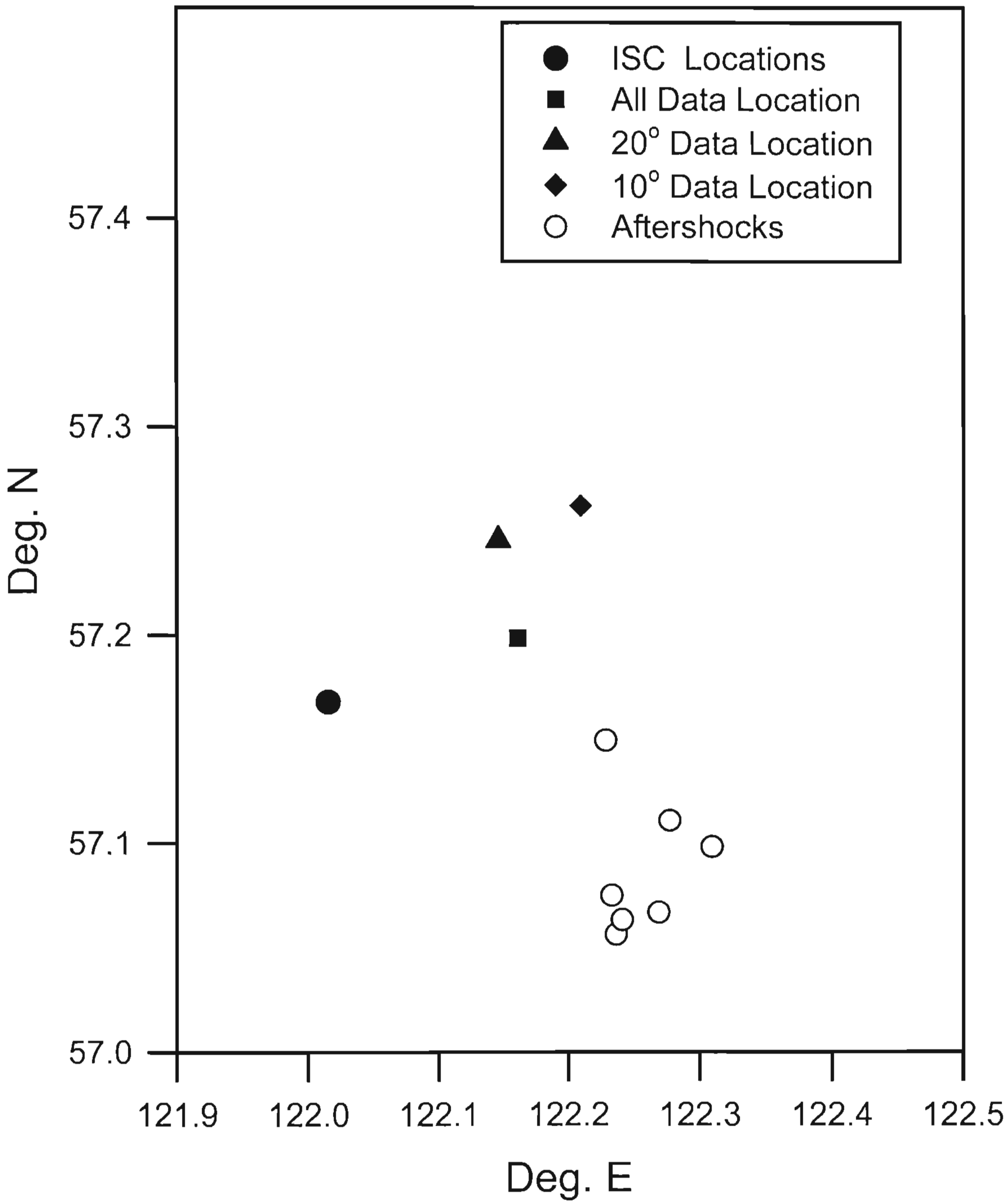

Figure 56. Parameters for the magnitude 6.6 south Yakutia earthquake comparing ISC parameters with relocation solutions calculated using different data sets.Preferred locations of aftershocks are shown in grey.

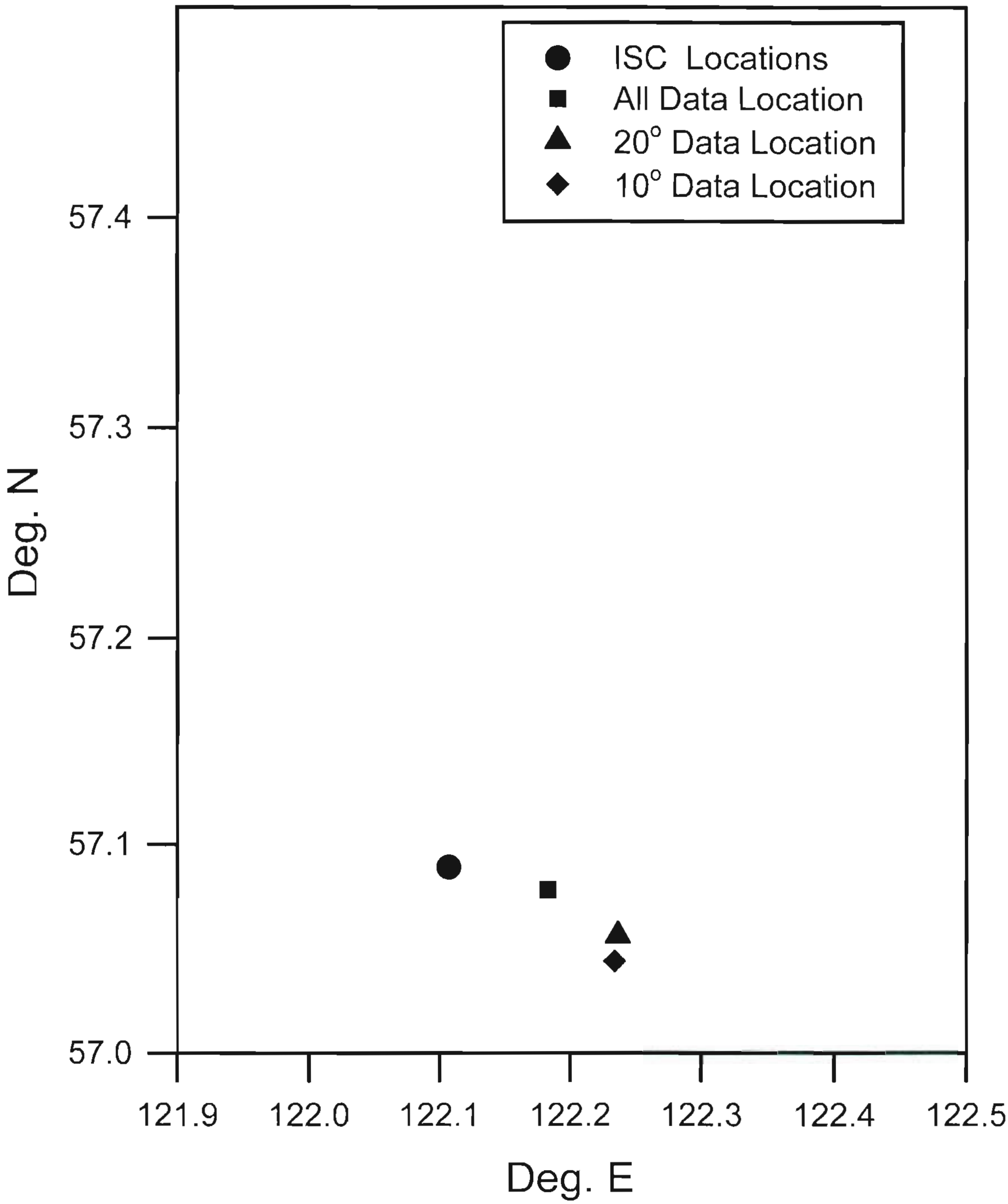

Figure 57. Epicenter calculations for the May 17 aftershock of the south Yakutia event comparing ISC parameters with relocation parameters using different data sets. The 20° solution is preferred. See also Table 5 and Figure 55.

Table 6. Comparison of 1989 South Yakutia Earthquake mainshock solutions. Bold entries in the table are relocations determined in this study.

Solution	Date	Time	Lat.	Long.	Depth
All Data	**1989 04 20**	**22 59 53.39**	**57.198**	**122.161**	**22.5 ± 2.5**
Regional	**1989 04 20**	**22 59 53.63**	**57.245**	**122.146**	**29.9 ± 4.1**
Local	**1989 04 20**	**22 59 53.52**	**57.262**	**122.209**	**32.1 ± 6.0**
ISC	1989 04 20	22 59 54.24	57.168	122.015	26.0, 32 ± 2.1 pP
Yakut Net	1989 04 20	22 59 54.8	57.17	122.31	27
NEIC	1989 04 20	22 59 54.0	57.17	121.98	26
Moscow	1989 04 20	22 59 54.8	57.19	122.08	32 sP, 35 pP
Doser (1991)	1989 04 20		57.08	122.12	24 ± 4 synth
Harvard CMT	1989 04 20	23 00 01.4	57.03	121.23	48 ± 1.8
Beijing	1989 04 20	22 59 53.6	57.15	122.44	35

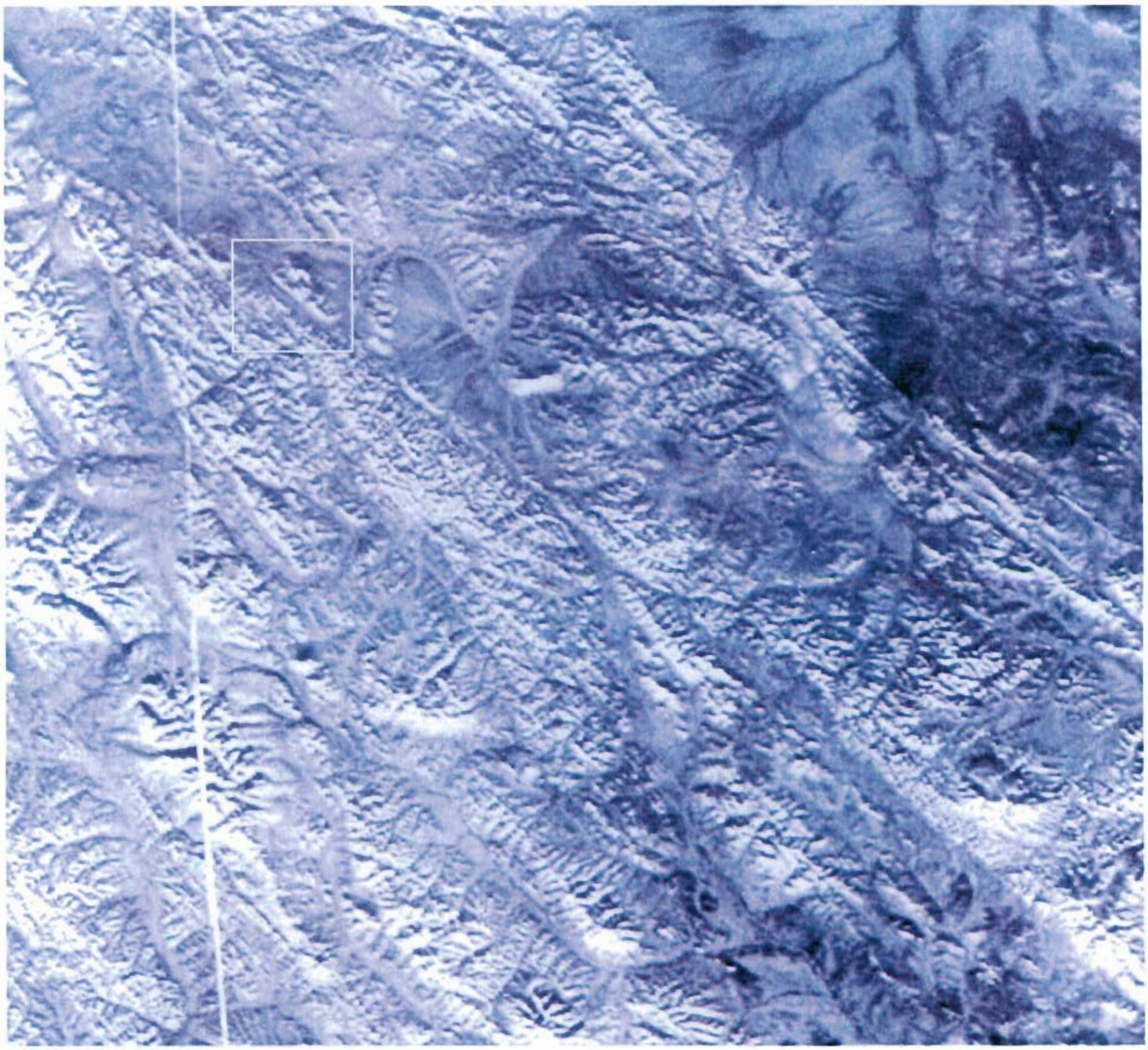

Figure 58. Meteor satellite image of the central portion of the Ulakhan fault, extending from the lower right corner to the upper left corner of the image. This image depicts a section of the fault several hundred kilometers in length. Box indicates location of map in Figure 59.

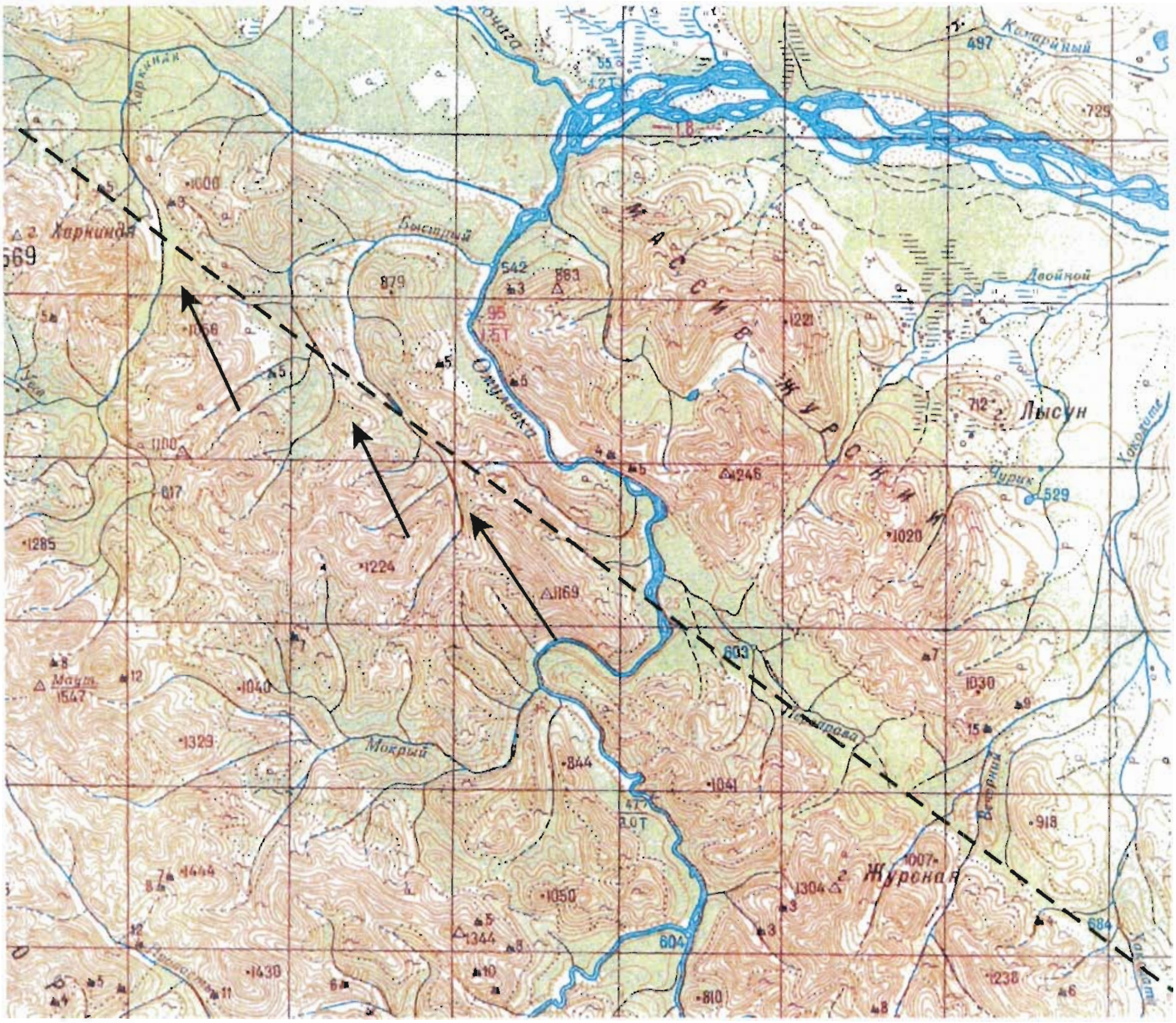

Figure 59. Topographic map of a portion of the Ulakhan fault, depicted by the dashed line. Note large river offsets showing a left lateral sense of motion along the fault (arrows). One square on this map represents approximately 4 km. The base map used here is a 1:200,000 Russian military topographic map.

This age and offset is consistent with current estimates of motion of about 0.8-1.0 cm/yr (Imaev et al., 1990; Seno et al., 1996).

The seismicity along the Ulakhan can be broken into two linear segments to the east and west of the Darpir-Yuryakh River, with a very slight change in strike. While these segments closely follow the surface trace of the Ulakhan fault, they remove the arcuate curve to the north that is observed in the surface topography. The seismicity is furthest offset from the surface expression of the Ulakhan to the east of the Darpir-Yuryakh River. This offset region is associated with the presence of Early Paleozoic rocks at the surface. To the west, Parfenov et al. (1989) have interpreted the Paleozoic rocks as being rootless and representing a large klippe. If this is also true in the Omulevka Mountains, it is possible that the main trace of the Ulakhan fault is in fact straight at depth below the Paleozoic and offset from the surface expression of the fault, which is located at the edge of the Paleozoic. This conjecture is supported by the fact that the microseismicity becomes more diffuse through the region of the Omulevka Mountains (McLean et al., 2000). In any case, except at the point of maximum deviation of the seismicity trend from the surface expression of the fault, all events are within 10 km of the mapped fault, and in several cases within 5 km. A second satellite image, slightly to the northwest of Figure 60 shows another section of the Ulakhan fault and the proximity of two relocations to the fault. A third event is further north on a parallel fault (Figure 60).

The Chai-Yureya fault is thought to represent a splay off the Ulakhan and strikes in a more southeasterly direction just east of the town of Artyk. Relocations of seven events that fall along the Chai-Yureya; a straight line can be fit with an error of less than two km through six of the events (the seventh is the most poorly located event of the set). Relocated epicenters also fall almost directly on the surface expression of the Chai-Yureya fault, with a maximum deviation among the GT10 and GT25 events of 6 km from the trace, suggesting that epicentral locations are accurate to 10 km or better (Figure 52). One of the events is a magnitude 7 earthquake, the largest in the Chersky Range, which occurred along this fault in 1971. This event, while nominally GT25, falls almost directly on the surface expression of the fault.

4.3.4 Travel-time variations in northeast Russia.

To investigate further improvement in hypocentral locations by determining Source Specific Station Corrections (SSSC's), travel-time residuals relative to JB for nine regional stations from events in northeast Russia were investigated. The stations have epicentral distances from the events of about 1 - 20°.

The results for Tiksi (TIK, TIXI; Figure 61), based on all the events studied, are characteristic. High negative residuals, indicating fast velocities, are observed from events in south Yakutia. These rays pass through sub-Siberian shield mantle, which is expected to have higher velocities. Slightly negative residuals are obtained from the Chersky Range, indicating some higher velocity upper mantle exists in the region of the Kolyma-Omolon superterrane. Events from the eastern Sea of Okhotsk and Koryakia have slightly positive residuals, and suggest there may be slower mantle due either to lithospheric rifting (Penzhina and Parapol basins; Worrall et al., 1996) or to effects of the supra-subduction mantle wedge. Similarly, a few events with slightly positive residuals in northeast Amur District may be related with extension along the western Sea of Okhotsk (Shantar-Liziansky basin) also proposed by Worrall et al. (1996). One event in the Yana River valley gives a high positive residual, which may be related to the present or recent extension of the Arctic Mid-Ocean ridge into the continent. The restricted number and distribution of GT10 events provides only information from southern Yakutia and the Chersky Range, but leave no doubt as to the faster velocities to Tiksi from those two regions. Travel paths under the Siberian platform to

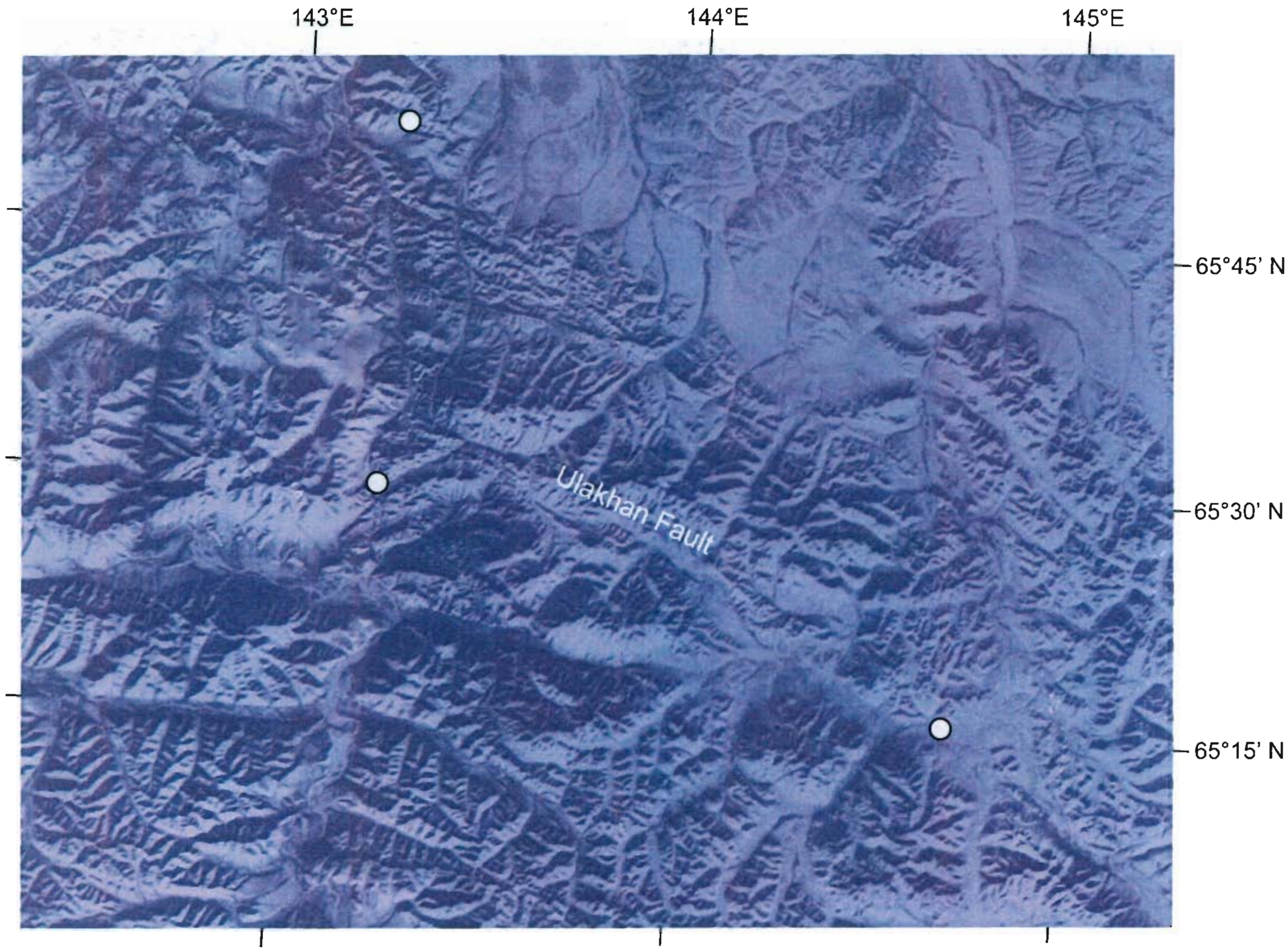

Figure 60. Relocated teleseismic epicenters near and along the western Ulakhan Fault superimposed on a Landsat image. Epicenters relocate to within five to ten km of the fault. The third epicenter epicenter locates along a parallel fault 30 km north of the Ulakhan.

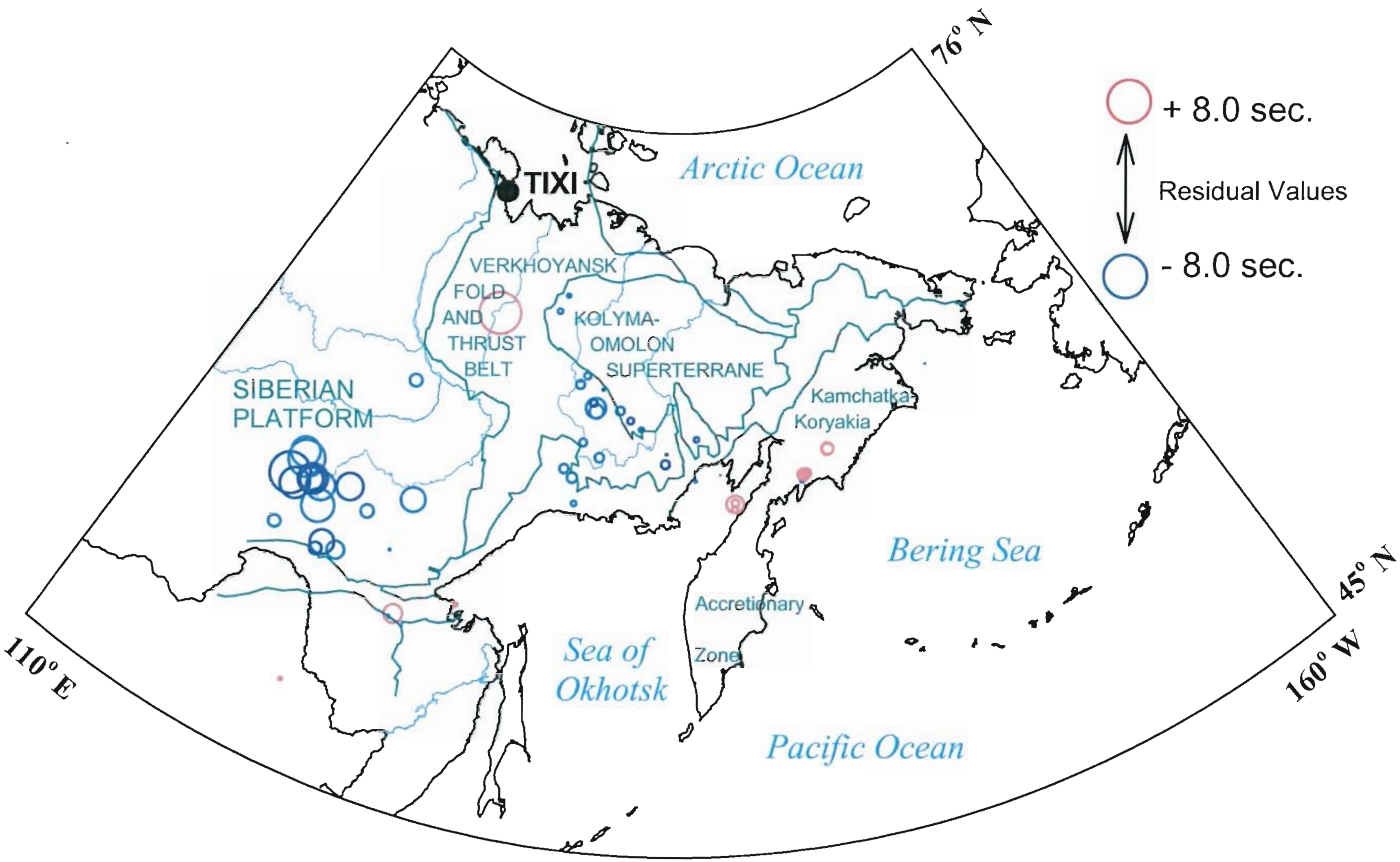

Figure 61. Tiksi (TIK, TIXI) residuals for all GT analyzed events. Solid colors are from GT10 events while the lighter shade represents GT25 or poorer classification. Note the consistently large negative residuals for paths associated with the Siberian platform, and lower residuals elsewhere. Residuals are especially consistent among the GT10 events and essentially represent Source Specific Station Corrections (SSSCs).

Norilsk also yield consistently negative residuals of a magnitude similar to those at Tiksi (Figure 62).

Arrivals at Yuzhno Sakhalinsk confirm that ray paths through the sub-northern Sea of Okhotsk mantle yield high positive residuals (Figure 63). Events from the Amur region with origins in the Siberian platform west of the proposed rift again yield slightly positive residuals, suggesting that their respective higher and lower velocities tend to cancel each other out. All arrivals at Petropavlovsk are late, indicative of passage through the supra-subduction zone upper mantle (Figure 64). Similar to Yuzhno Sakhalinsk, as events occur farther into the higher velocity Siberian platform relative to Petropavlovsk residuals become less negative.

Bilibino also yields slightly positive residuals from the northern Sea of Okhotsk and negative residuals for the Kolyma-Omolon superterrane and Koryakia, suggesting that upper mantle velocities in far northeast Russia are slightly fast (Figure 65). Peleduy, however, yields late arrivals from the Kolyma-Omolon superterrane. Arrivals from the northern Sea of Okhotsk are again late, and early arrivals are observed on Siberian platform crossing paths from the Verkhoyansk Range (Figure 66).

Residual patterns for Seymchan and Magadan are similar (Figures 67 and 68). The arrivals from Shelikhov Bay (northeast Sea of Okhotsk) and the Amur region are again all late, while a mix of residuals is observed from the Chersky seismic belt. From these stations, Chukotka paths are slightly slow. Finally, Yakutsk shows a wide mix of arrivals with generally early arrivals from the Aldan shield and the Verkhoyansk Range and very late arrivals from Shelikhov Bay and Chukotka (Figure 69). Surprisingly the arrivals from the south Yakutia events of 1989 show a mix of residuals for both GT25 and GT10 events.

4.4 CONCLUSIONS.

By determining locally calibrated travel time curves and relocating regional earthquakes recorded both teleseismically and by regional networks operating in northeast Russia, epicenters have been greatly improved relative to the ISC Bulletin. GT classifications have been assigned to 134 events, with 26 events meeting or exceeding GT10 criteria. Using the relocated events, travel time residuals for several internationally reported seismic stations located in northeast Russia were plotted. The resulting residual distributions are consistent with high velocities under the Siberian Platform, and low velocities under the Sea of Okhotsk. Taken as a whole, it is clear that ray paths traversing the upper mantle under the Siberia platform are fast, while those originating from, or traversing, the supra-subduction zone or rift regions of the Sea of Okhotsk are very slow. There is an indication of low velocities under the northern Amur district, although this is less distinct. Velocities under Chukotka are less certain. The situation in the Chersky Range is also less clear, although ray paths traveling greater distances may be marginally faster than those to nearby stations. These observations will help in constraining upper mantle velocities and developing better Source Specific Station Corrections (SSSCs) for the region.

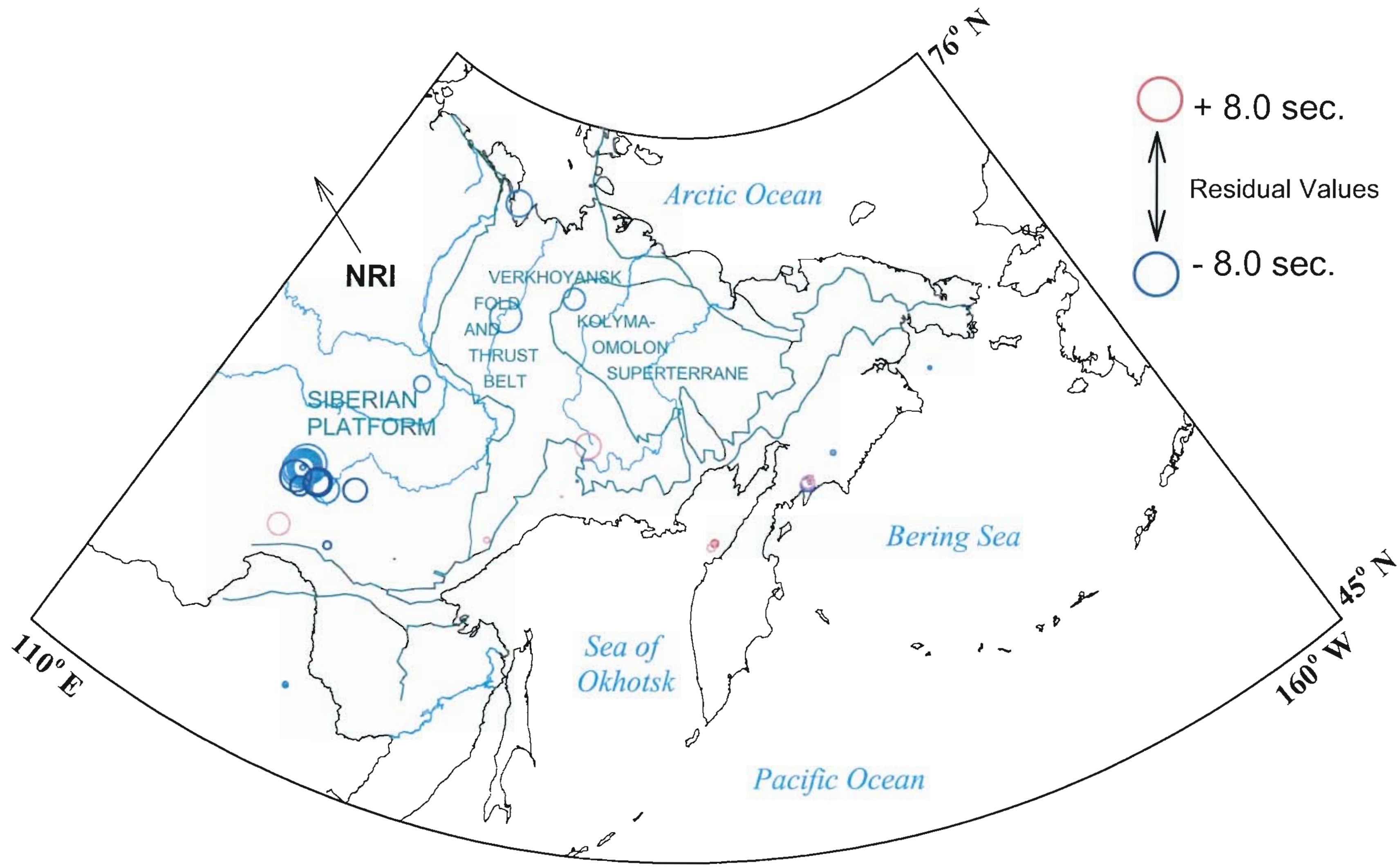

Figure 62. Norilsk (NRI) residuals for all GT analyzed events. Solid colors are from GT10 events while the lighter shade represents GT25 or poorer classification. Note the consistently large negative residuals for paths associatedentirely with the Siberian platform, and lower residuals elsewhere. Residuals are especially consistent among the GT10 events and essentially represent Source Specific Station Corrections (SSSCs).

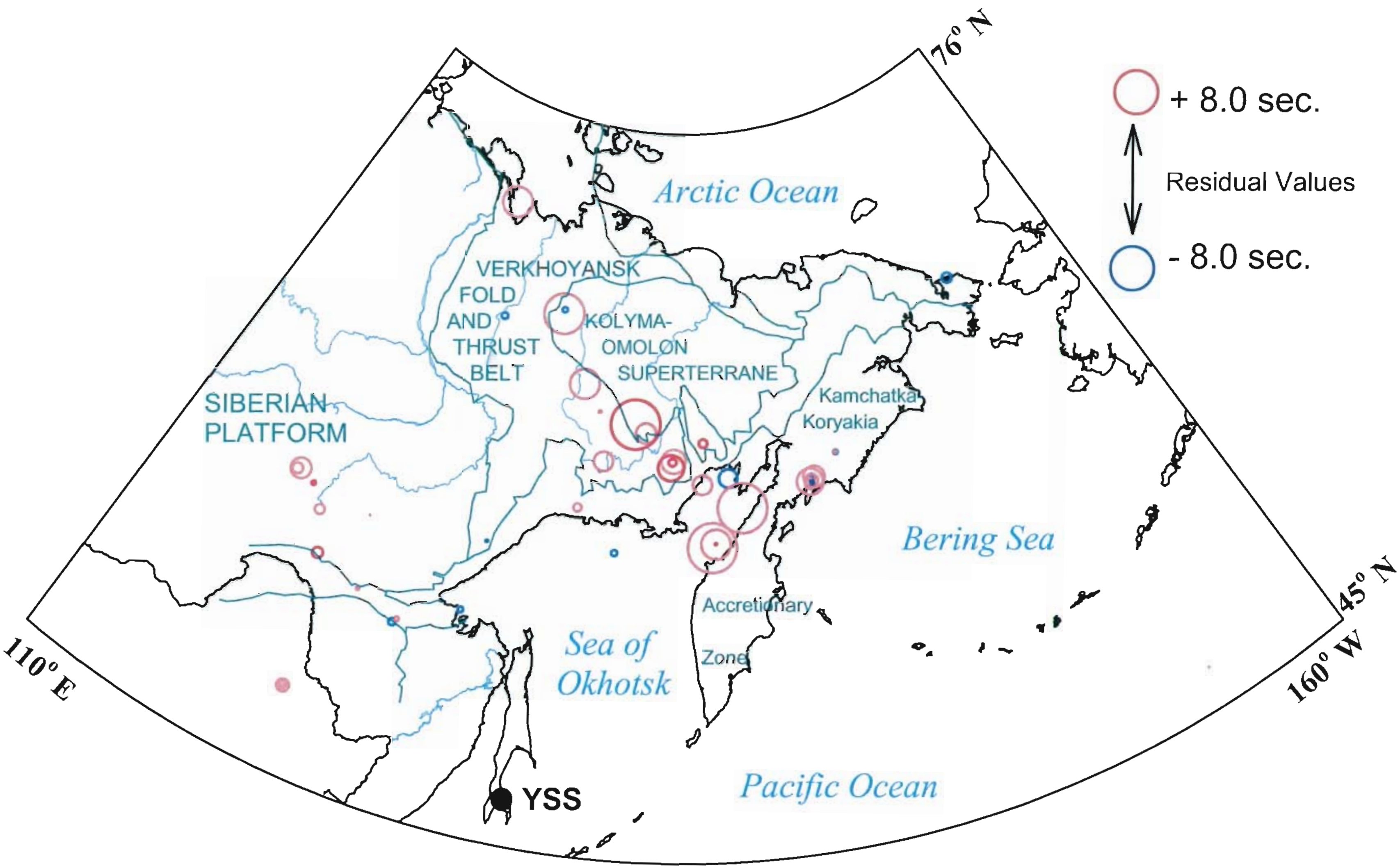

Figure 63. Yuzhno Sakhalinsk (YSS) residuals for all GT analyzed events. Solid colors are from GT10 events while the lighter shade represents GT25 or poorer classification. Note the generally large positive residuals for paths crossing the Sea of Okhotsk, while paths originating in the Siberian platform are smaller. Residuals are essentially representing Source Specific Station Corrections (SSSCs).

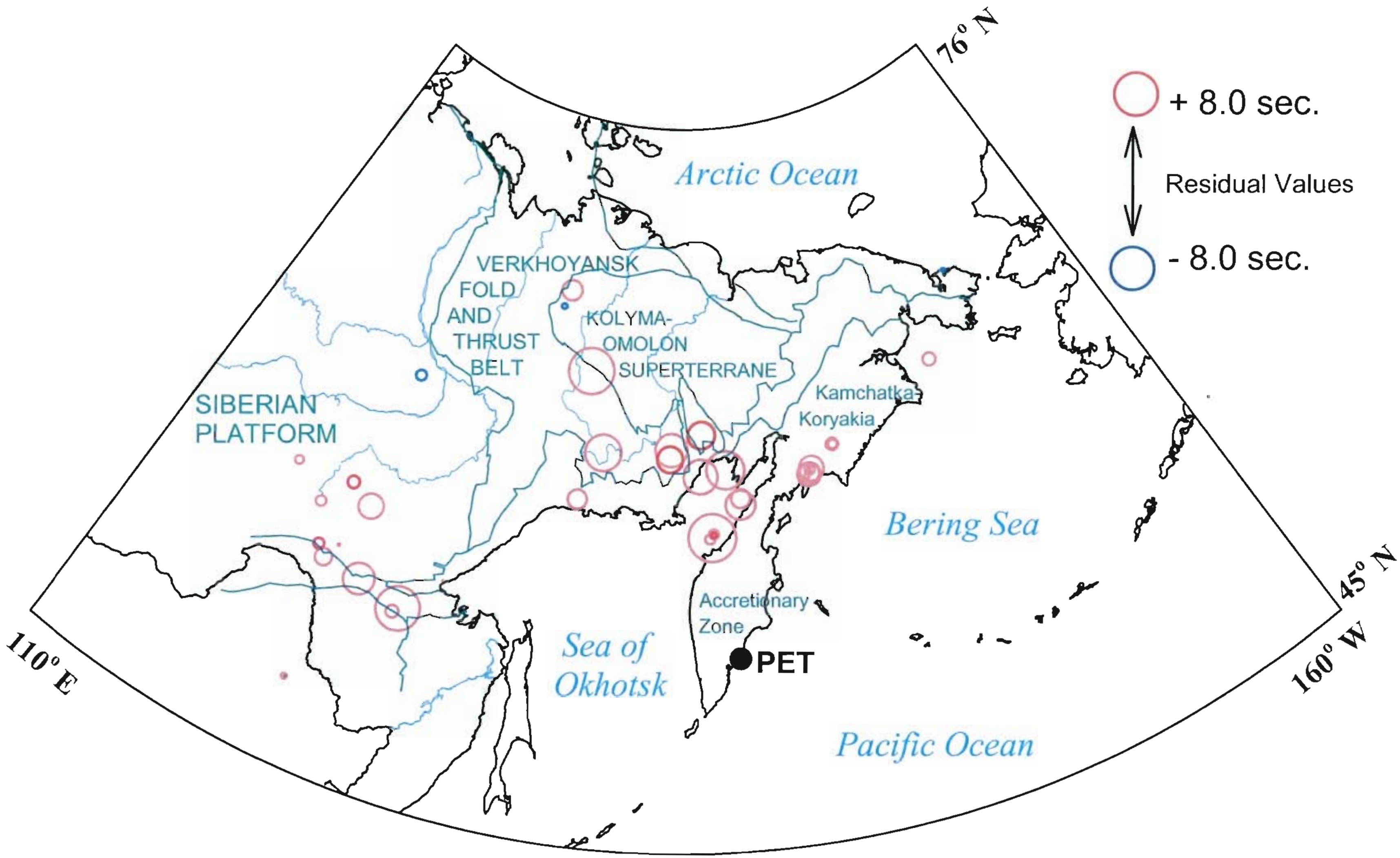

Figure 64. Petropavlovsk (PET) residuals for all GT analyzed events. Solid colors are from GT10 events while the lighter shade represents GT25 or poorer classifications. Note that most residuals are large and positive. For events progressively further into the Siberian platform, residuals decrease, possible a result of high platform velocities countering low velocities under the Sea of Okhotsk. Residuals essentially represent Source Specific Station Corrections (SSSCs).

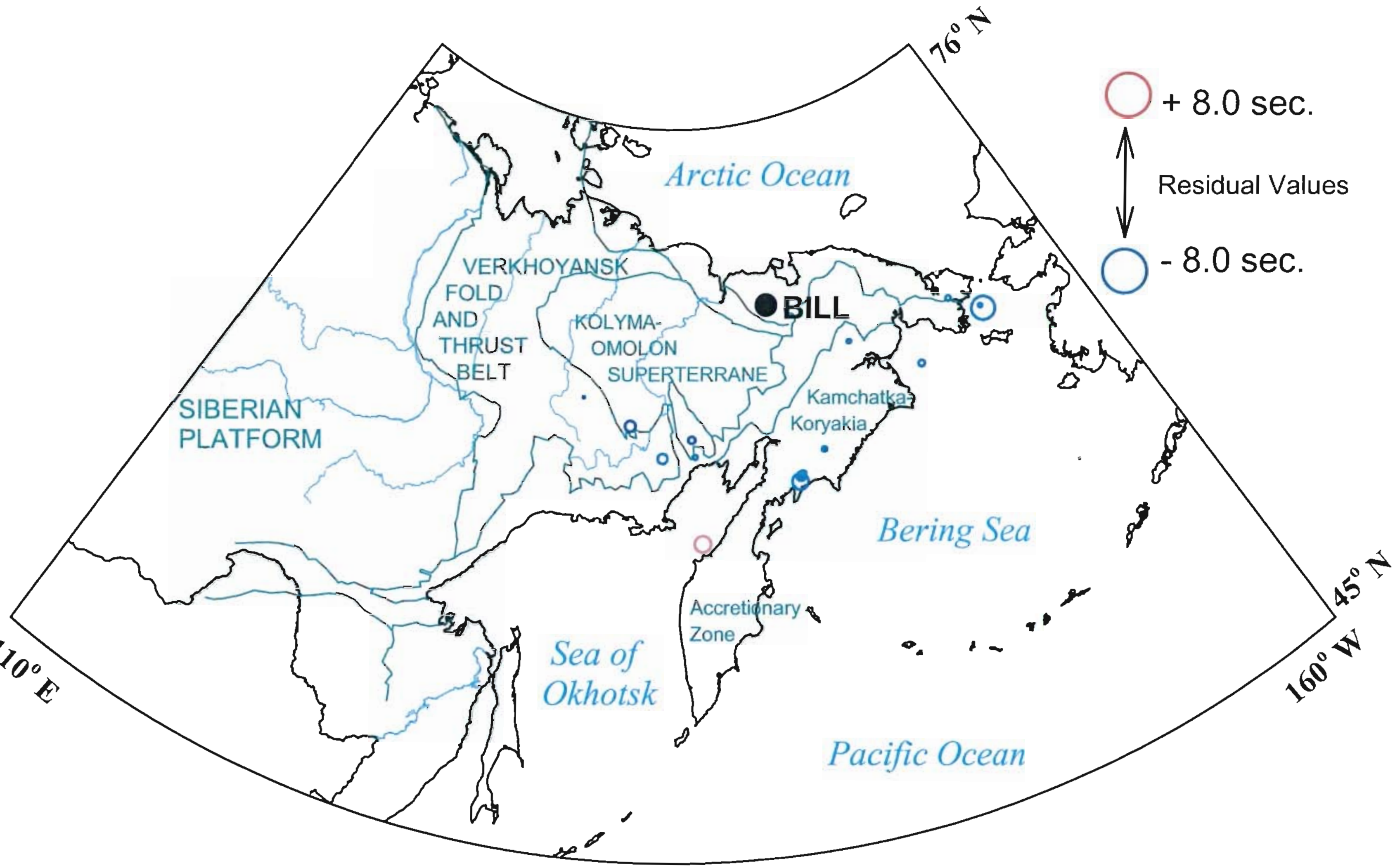

Figure 65. Bilibino (BILL) residuals for all GT analyzed events. Solid colors are from GT10 events while the lighter shade represents GT25 or poorer classifications. Residuals essentially represent Source Specific Station Corrections (SSSCs).

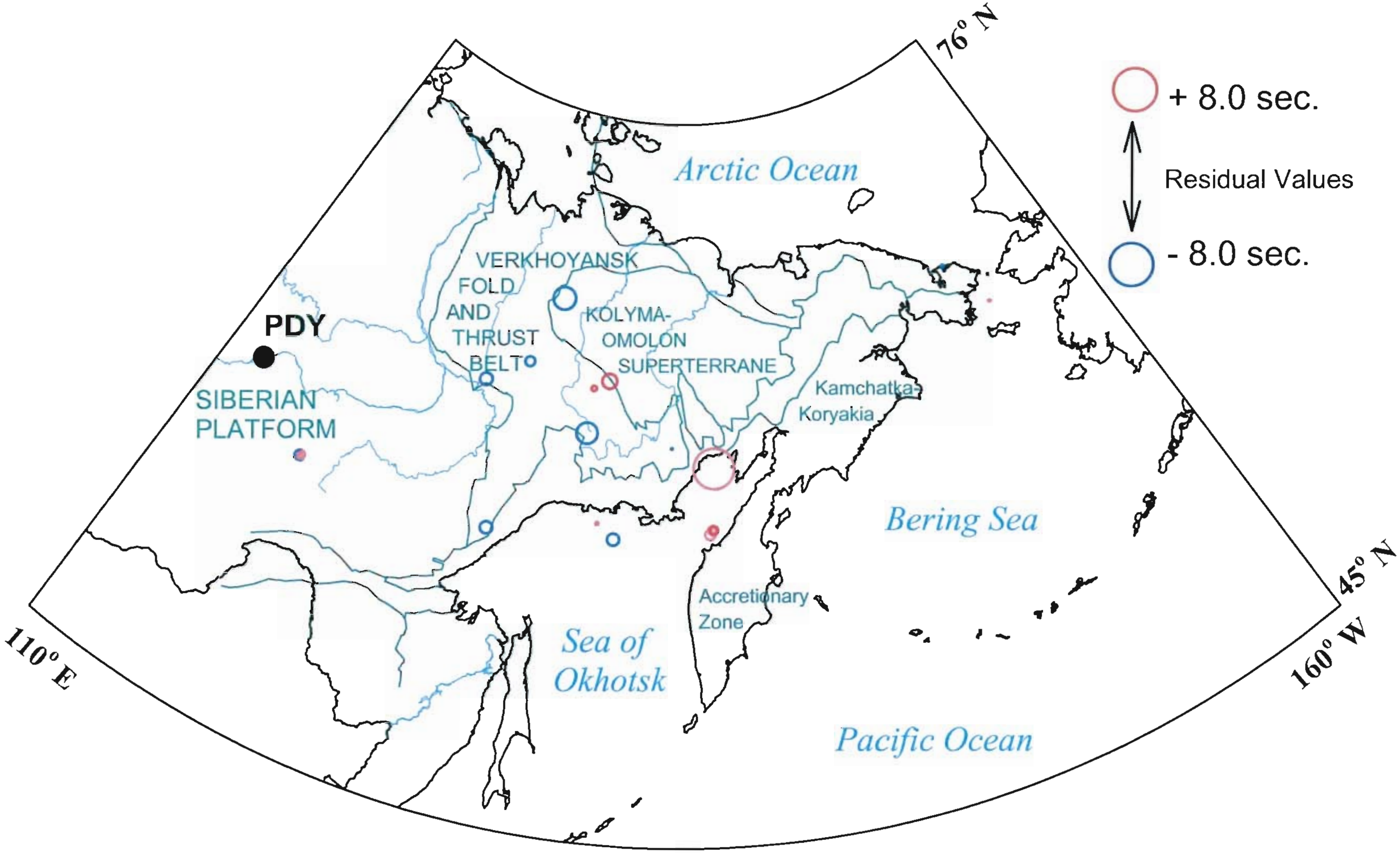

Figure 66. Peleduy (PDY) residuals for all GT analyzed events. Solid colors are from GT10 events while the lighter shade represents GT25 or poorer classifications. Residuals essentially represent Source Specific Station Corrections (SSSCs).

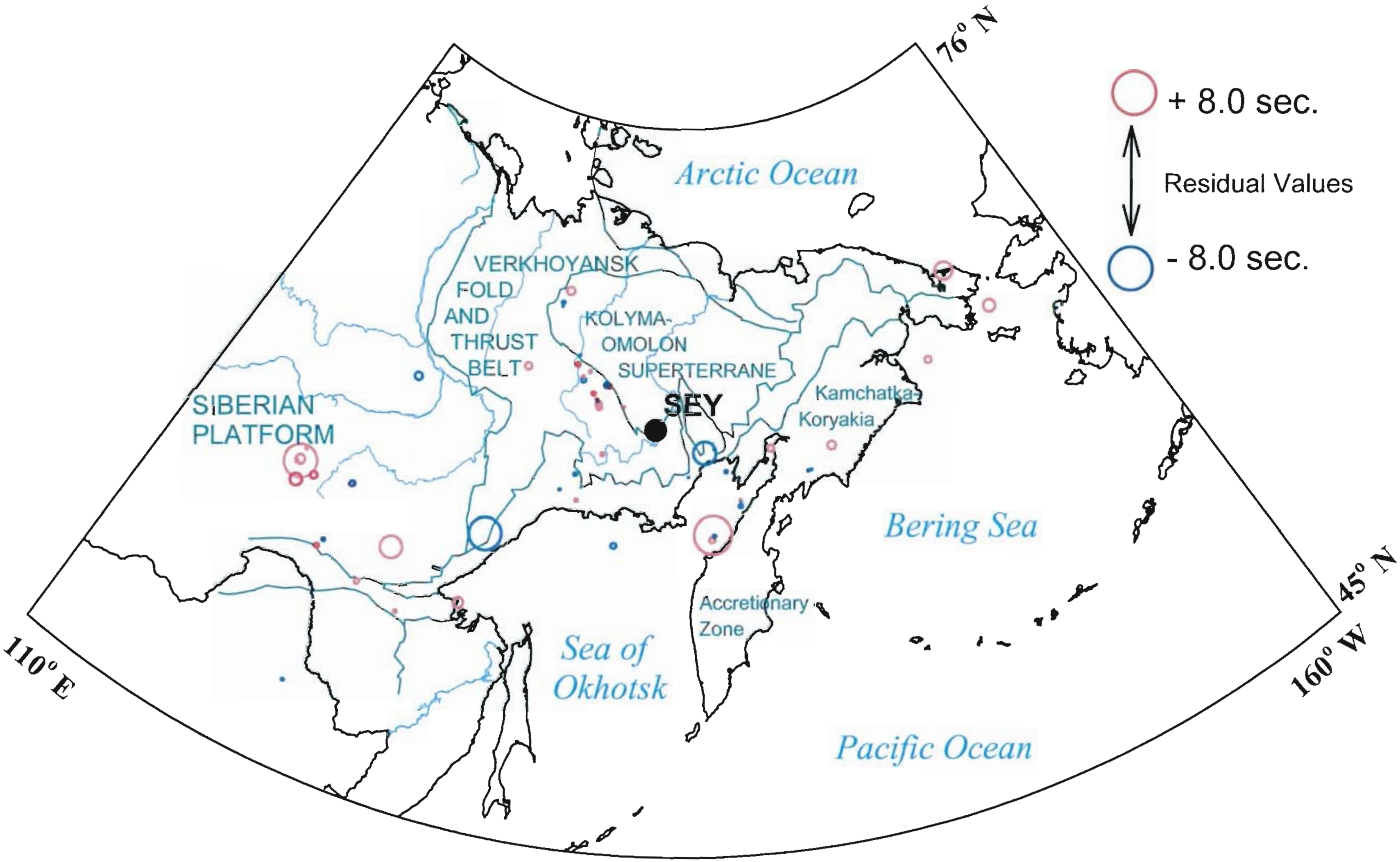

Figure 67. Seymchan (SEY) residuals for all GT analyzed events. Solid colors are from GT10 events while the lighter shade represents GT25 or poorer classifications. Residuals essentially represent Source Specific Station Corrections (SSSCs).

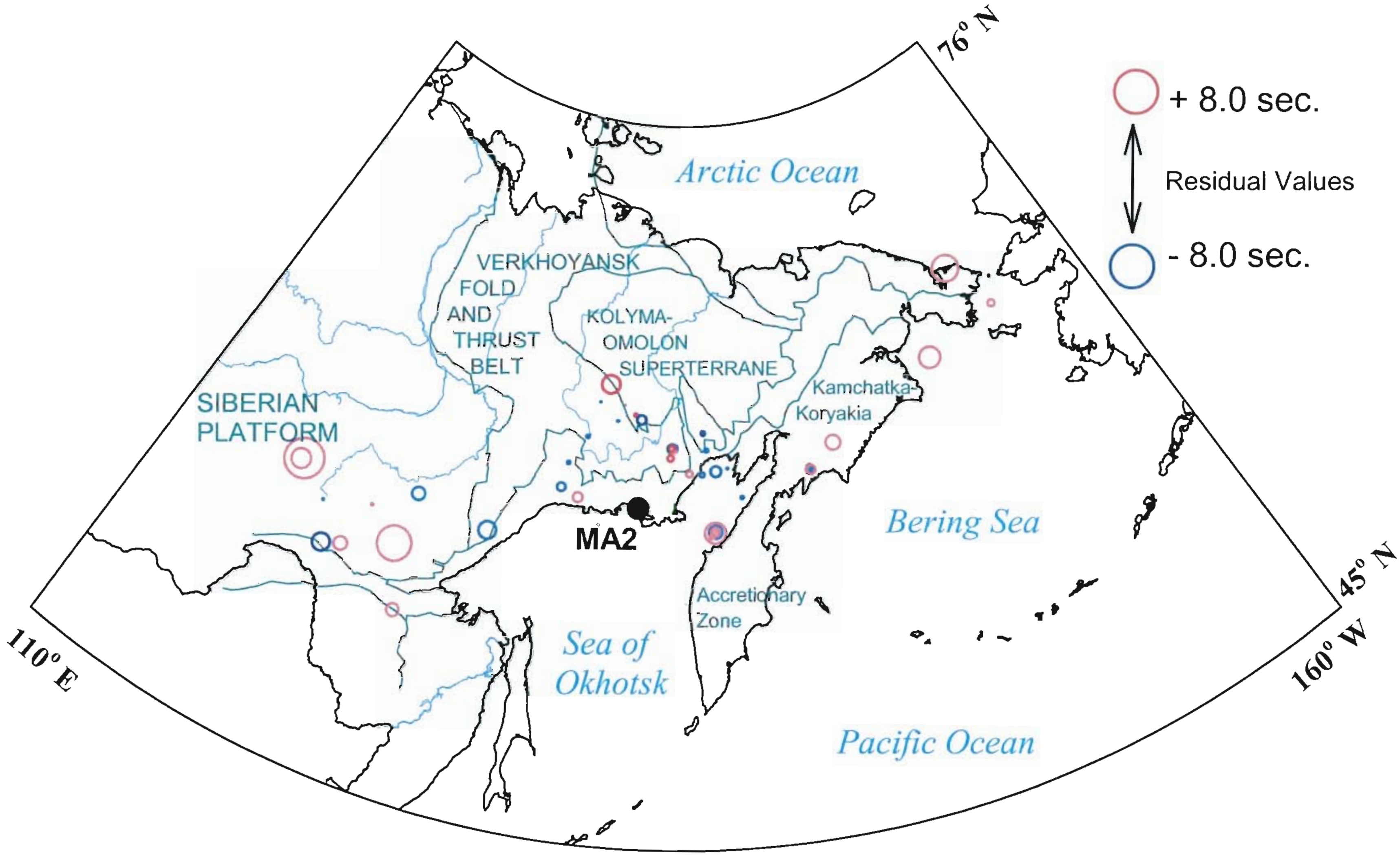

Figure 68. Magadan (MAG, MA2) residuals for all GT analyzed events. Solid colors are from GT10 events while the lighter shade represents GT25 or poorer classifications. Residuals essentially represent Source Specific Station Corrections (SSSCs).

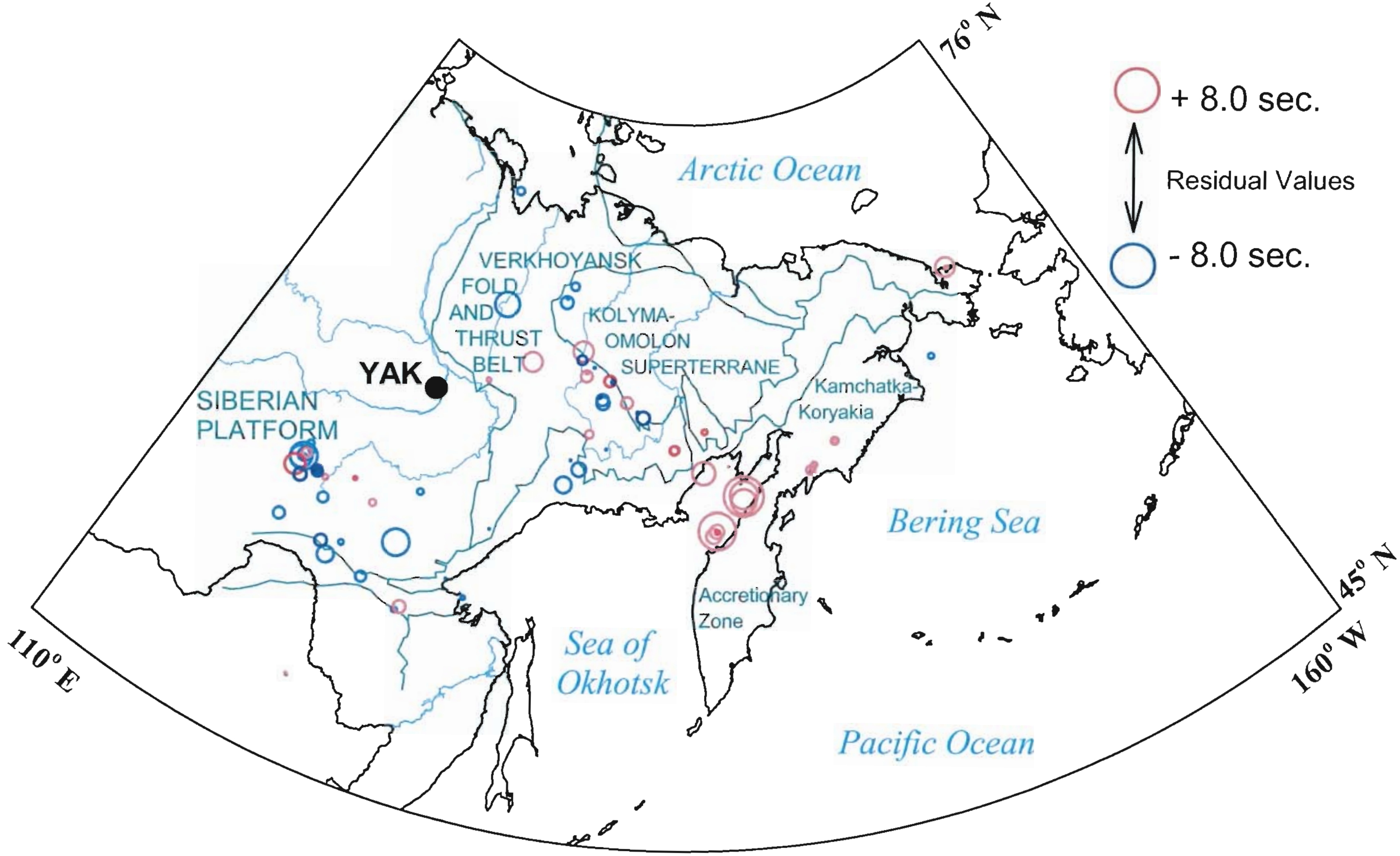

Figure 69. Yakutsk (YAK) residuals for all GT analyzed events. Solid colors are from GT10 events while the lighter shade represents GT25 or poorer classifications. Note that most residuals traveling through the Siberian platform have negative residuals while those from the Kamchatka-Koryakia accretionary zone show positive residuals. Residuals essentially represent Source Specific Station Corrections (SSSCs).

SECTION 5

DIGITAL STATION DEPLOYMENTS

5.1 INTRODUCTION.

In the summer of 1999, a program began to develop seismic discriminants for CTBT monitoring by digitally recording local explosions and earthquakes. To obtain better records for study, existing photopaper analog stations in the Magadan and Yakutsk networks were converted to digital data acquisition. At present, seven digital stations are deployed in northeast Russia, most in the Magadan region (Figure 70; Table 7). Since the initial deployment, a couple of stations have had to be moved due to logistical reasons. A few stations were also deployed in temporary locations for the purpose of recording known explosions or earthquake aftershocks. A description of each station location is given in Appendix D. All stations are 3 component, with three stations recording broadband instruments (Seymchan - STS-1, Okhotsk - Guralp CMG-40T, and Omsukchan - CMG-40T). The remaining stations use short-period Russian seismometers (SKM-3, SM3 or SM3-KV). All stations recording SM3 or SM3-KV seismometers are equipped with anti-aliasing filters to cut frequencies above 10 hz. All seismometer outputs are digitized at 30 samples per second with a 24-bit A/D converter and logged on a PC. Digital data acquired as a part of this study is supplemented with records from the IRIS stations at Magadan (MA2) and Bilibino (BILL), and other regional analog photopaper stations. Using waveforms of both tectonic events and mine blasts, explosion discrimination using amplitude ratios of various Lg frequencies has been addressed. Preliminary results indicate that the ratio Lg(4-8Hz)/Lg(0.75-1.5Hz) using peak amplitudes may not be sufficient to discriminate mining explosions from earthquakes in northeast Russia.

5.2 RESEARCH PERFORMED.

5.2.1 Earthquakes.

Approximately 250 local and near regional earthquakes have been located by the network from August, 1999 through August, 2001 (Figure 70). Arrival times for all local and near regional earthquakes are routinely picked from the digital waveform data and a complete catalog is maintained. Catalog development includes calculating hypocenters for all locatable earthquakes, as well as identification of signals from anthropogenic sources. The stations are located close to areas of both tectonic seismicity and active mining, thus record signals from both. Figure 71 depicts digital records from one local tectonic event. Many smaller events are also recorded, but are not locatable. The magnitude cutoff for locatable events for the central portion of the study is about $M_L = 2.5$, and about $M_L = 3.0$ outside the aperture of the deployed stations. Some variation exists depending on specific location relative to operating stations. The largest event from eastern Russia recorded by the network was the M_w 6.8 Uglegorsk earthquake from the southern part of Sakhalin Island, which occurred at 21 hours on August 4, 2000 (Figure 72). This event occurred approximately 1000 km south of the network, at the edge of the scope of this project. The stations have also recorded several hundred other regional and teleseismic earthquakes.

In a qualitative sense, both Pg and Lg phases appear to propagate well throughout the region enclosed within the network. Clean arrivals from both phases are often well recorded beyond 700 km, the aperture of the deployed digital network. With a few exceptions, P_n arrivals are generally much lower in amplitude, or not visible at these near regional distances. Almost no S_n arrivals are

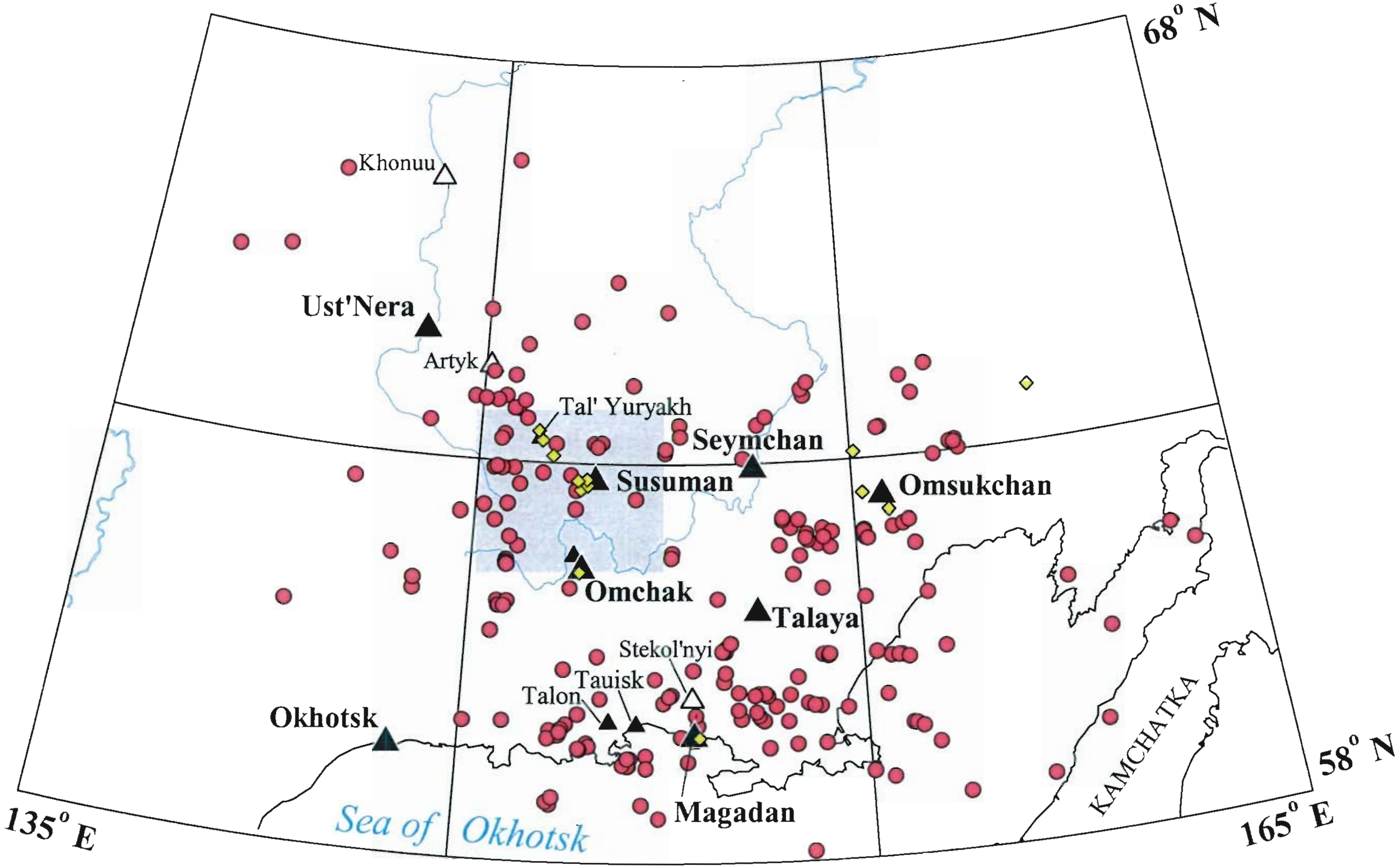

Figure 70. Digital seismic network deployed by MSU in eastern Russia (permanent stations - large triangles, temporary stations - small triangles, and supporting analog stations - open triangles). Also shown are earthquakes located from August 1999 through August 2001 (red circles) and explosion sources (diamonds). Shaded area shown in Figure 75.

Table 7. Digital seismic stations deployed or used in this study.

Station Name	Code	Lat.	Long	Instrument	Notes
Anadyr	ANYS	64.734°N	177.496°E	CMG-40T	3/00 - 4/01*
Bilibino	BILL	68.039°N	166.271°E	STS-1	IRIS
Magadan	MA2	59.5756°N	150.768°E	STS-1	IRIS
Matrosova	MATR	61.643°N	147.820°E	SM3-kv	7/99 - 7/99
Nel'koba	NKB	61.338°N	148.813°E	SM3-kv	7/99 - 9/99
Okhotsk	OHT	59.359°N	143.331°E	CMG-40T	7/00 - OPEN
Omchak	OCH	61.67°N	147.87°E	SM3-kv	9/99 - OPEN
Omsukchan	OMS	62.52°N	155.77°E	CMG-40T	7/01 - OPEN
Seymchan	SEY	62.933°N	152.368°E	STS-1**	9/99 - OPEN
Susuman	SUUS	62.780°N	148.163°E	SM3-kv	7/99 - OPEN
Stokolviya	STV	61.8475°N	147.6598°E	SM3-kv	7/99 - 7/99
Talaya	TL-S	61.129°N	152.392°E	SM3-kv	7/99 - OPEN
Talon	TON	59.757°N	148.661°E	SM3-kv	1/01 - 2/01
Tal-Yuryakh	TUR	63.307°N	146.634°E	SM3-kv	3/01 - 6/01
Tauisk	TAUS	59.729°N	149.335°E	SM3-kv	1/01 - 4/01
Ust'Nera	UNR	64.565°N	143.242°E	SKM	7/99 - OPEN

* Open and close dates of the digital station. Station did not acquire data for most of this time.
** Seismometers and support equipment left from non-operational Seymchan GEOSCOPE station

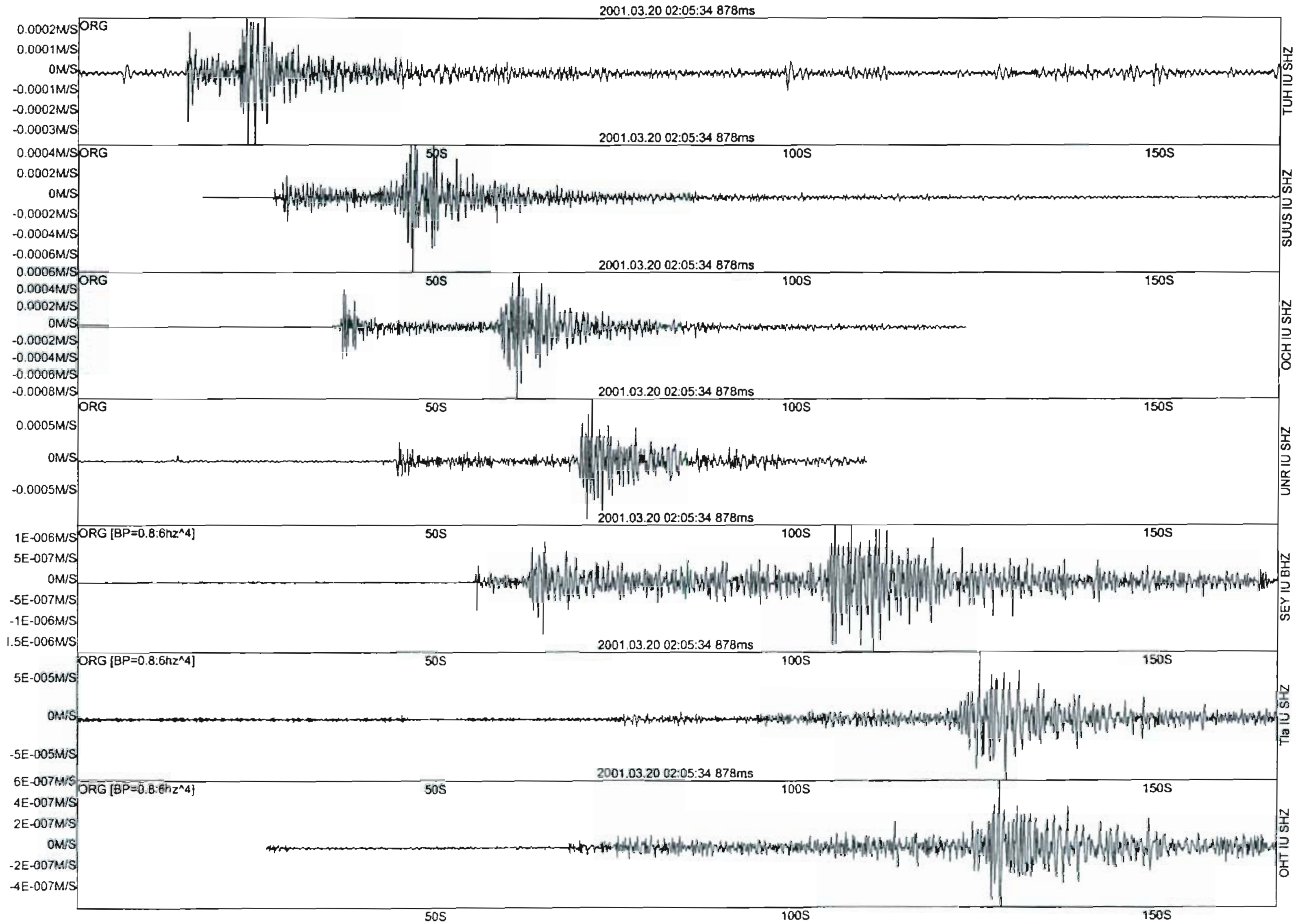

Figure 71. Seismograms of the 20 March, 2001, local earthquake that occurred northwest of Susuman. Stations are, from top to bottom, Tal-Yuryakh, Susuman, Omchak, Ust'Nera, Seymchan, Talaya, and Okhotsk. All stations depict the vertical component.

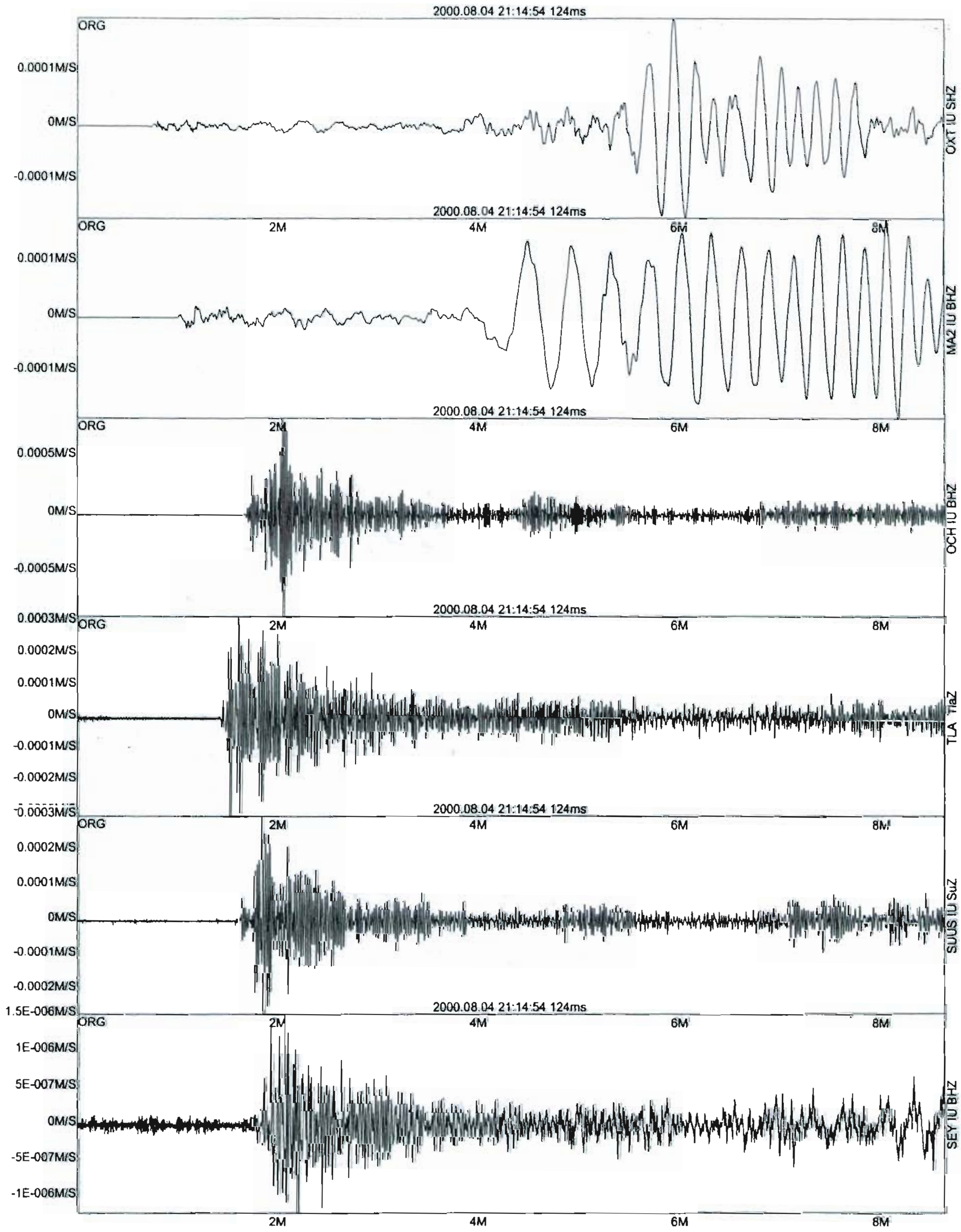

Figure 72. Seismograms of the August 4, 2000 Mw 6.8 Uglegorsk earthquake. Stations are, from top to bottom, Okhotsk, Magadan, Omchak (time out), Talaya, Susuman, and Seymchan. Instrument types are given in Table 7

visible in the digital records.

Initial analysis of waveforms indicates that the Lg arrival sometimes appears to have two distinct arrivals, Lg_1 and Lg_2. Lg_1 being a slightly faster phase penetrating deeper and having less high frequency attenuation, and Lg_2 being a slower, shallower phase with attenuation of high frequencies (Hartse, pers. comm.). This characteristic is most prominent at Susuman (Figure 73).

For some events at local distances, the mantle reflection phases PmP and SmP appear to be prominent, occasionally greatly exceeding the amplitudes of Pg and Sg (Figure 74). It should be noted that the moveout of these suspected mantle reflection phase arrival times has not been investigated to confirm positive identification.

An effort was undertaken to acquire improved ground truth data for earthquakes. In January, 2001, two moderate earthquakes occurred approximately 100 km west of Magadan. Two temporary stations (Talon and Tauisk) were deployed to investigate the aftershock sequences of both events. About 15 events were locatable, although several more were recorded.

5.2.2 Explosion ground truth and discrimination.

Identification of local and regional mine blasts has been an integral part of the data analysis of the digital network data. Three stations are located in active mining regions, which lends itself to acquisition of ground truth data directly useful for calibration of several IMS Alternate Stations in the region. To obtain ground truth information on explosions, mine locations were either visited or temporary stations deployed to obtain information on blast size, time and location. Blasting schedules for some other mines were also obtained, although mine sites have not yet been field checked for accurate locations. Specific mine locations and mine types in the Susuman region are plotted on Figure 75. Full data on explosions recorded between late 1999 and late 2001 can be found in the annual data compilation reports issued separately as a part of this study (Mackey and Fujita, 2001a,b,c).

Many mine blasts were recorded from many locations throughout the study region. The most active region is around Susuman where blasting originates in both gold and coal mines. Explosions in the placer gold deposits, used to break up frozen ground, have explosive yields ranging up to or exceeding 40 T. Figure 76 shows one 40 T mine blast which occurred at the Neksikan placer gold deposit, about 25 km from Susuman in April 2001. This seismogram also shows a clear acoustic arrival, which is visible on the Susuman seismograms for about 25 percent of large blasts from Neksikan. There were approximately 15 similar blasts detonated in April and May, 2001, to form the currently active placer mining pit in Neksikan (Figure 77).

Preliminary analysis of mine blasts show distinctive Rg arrivals at short distances of less than about 50 km (Figure 76). Lg arrivals from several of the 40 T Neksikan blasts were recorded at Magadan (MA2) and the farthest station, Okhotsk, over 400 km distant (Figure 78). Lg arrivals recorded at Magadan and Okhotsk are characterized by low frequency arrivals (0.7-1.5 Hz) with higher frequencies (4.0-8.0 Hz) being absent or completely obscured by background noise.

The largest explosion in the field area during the period of study is believed to have occurred 10 June, 2000, at one of two pits at the Kadakchan coal mine northwest of Susuman. This explosion was identified by location, time of day, similarity of waveforms to known blasts from Kadakchan, as well as a large acoustic arrival recorded at Omchak. The actual tonnage of the event is unknown, although it had a K-class of 9.5, which corresponds to a magnitude of about 3.3. This explosion was well recorded at the farthest stations in the network, including Magadan (MA2; Figure 79). Appendix E expands the discussion on this event with additional seismograms and maps.

A few temporary stations were deployed at or within a few kilometers of mine sites to obtain ground truth locations and origin times of explosions. The longest deployment was at the Tal-

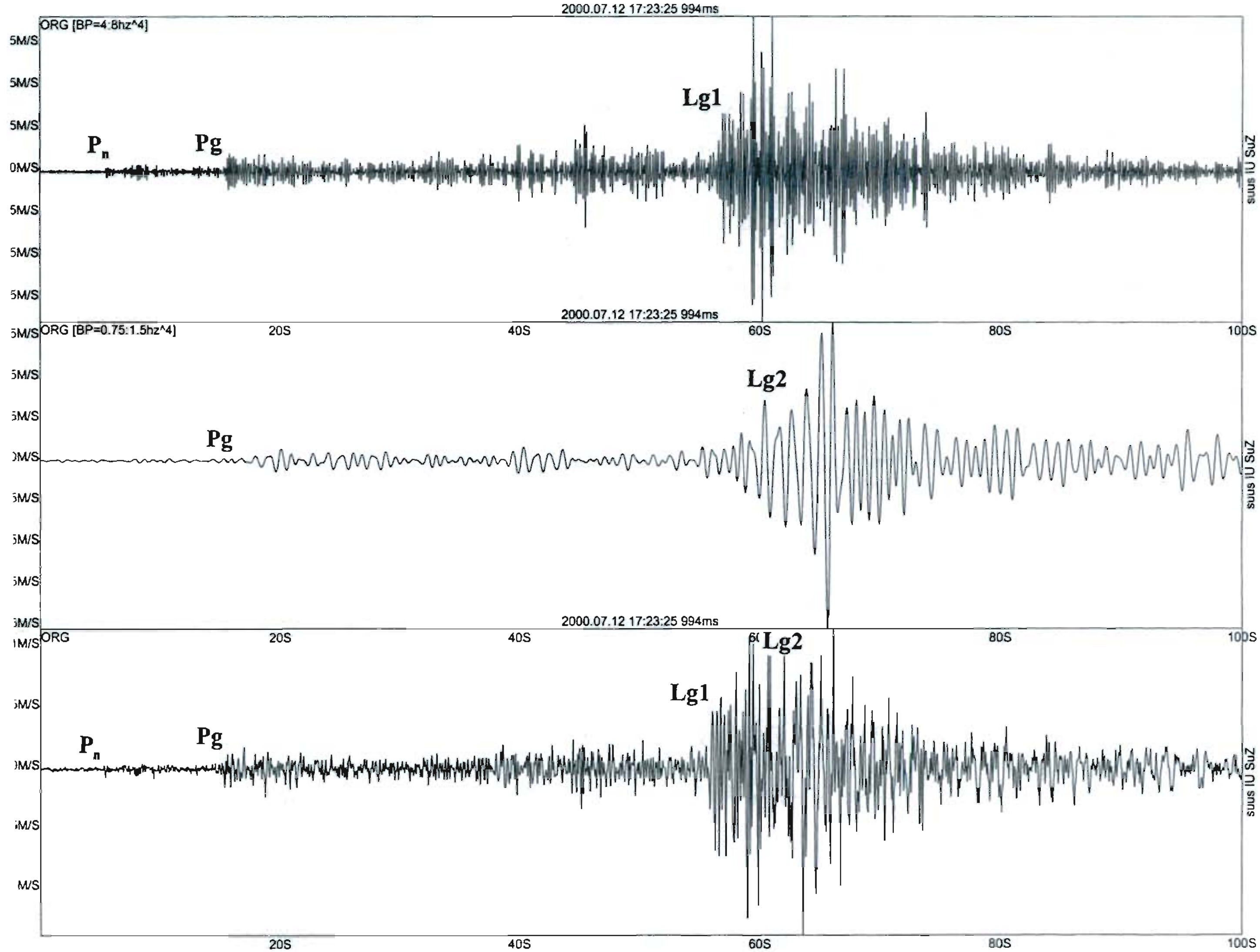

Figure 73. Susuman seismograms of a tectonic earthquake showing characteristic Lg1 and Lg2 arrivals. The upper trace is bandpass filtered 4-8 Hz, and shows an early high frequency maximum amplitude. The middle trace is bandpass filtered 0.75-1.5 Hz, and shows that the low frequency maximum amplitude is later. The lower trace shows the full waveform where the low frequency arrival is visible about seven seconds after the initial onset of Lg.

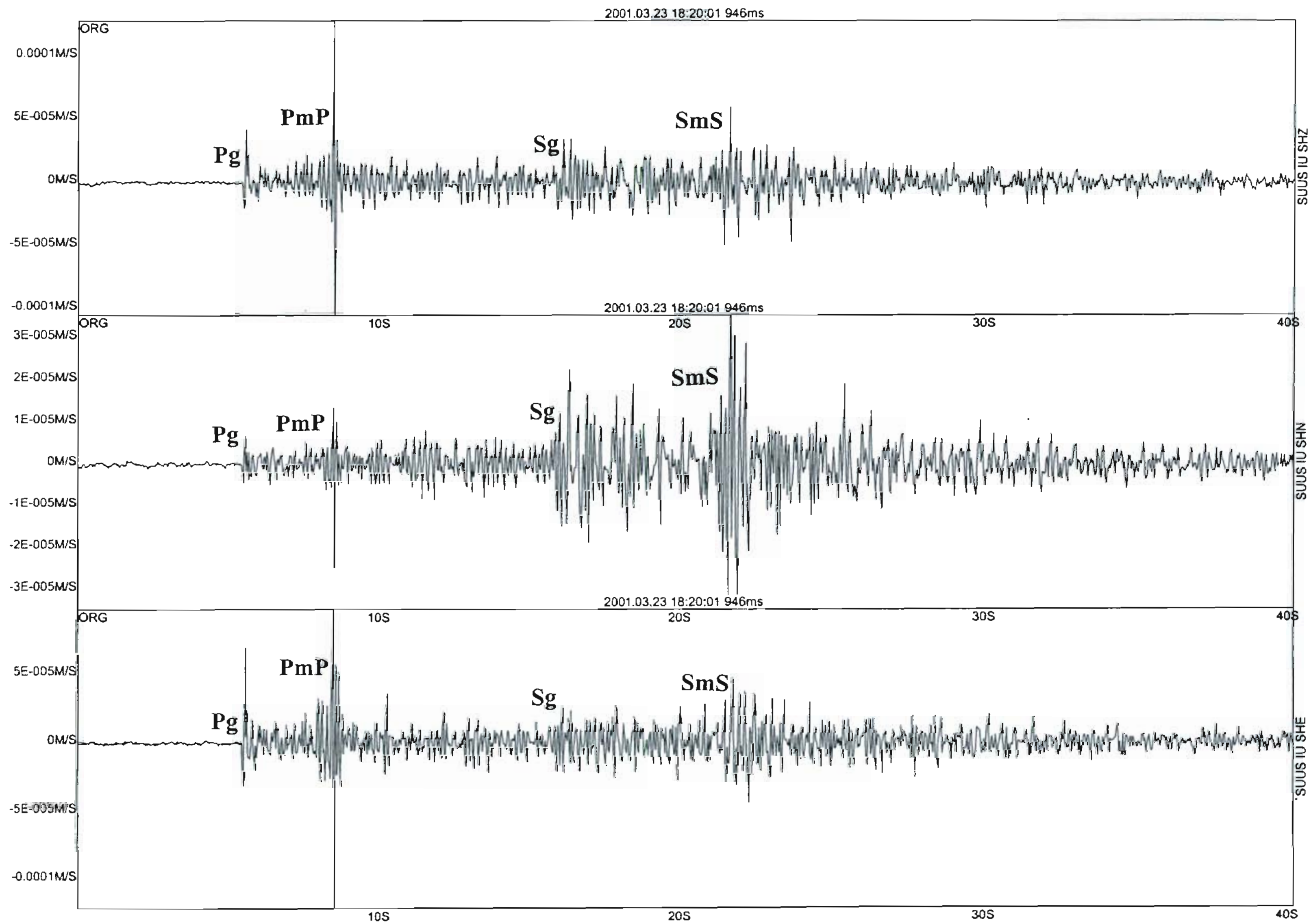

Figure 74. Susuman seismogram of a tectonic earthquake showing strong secondary arrivals, presumed to be PmP and SmS. The amplitudes of the secondary arrivals exceeds the first arriving Pg and Sg phases.

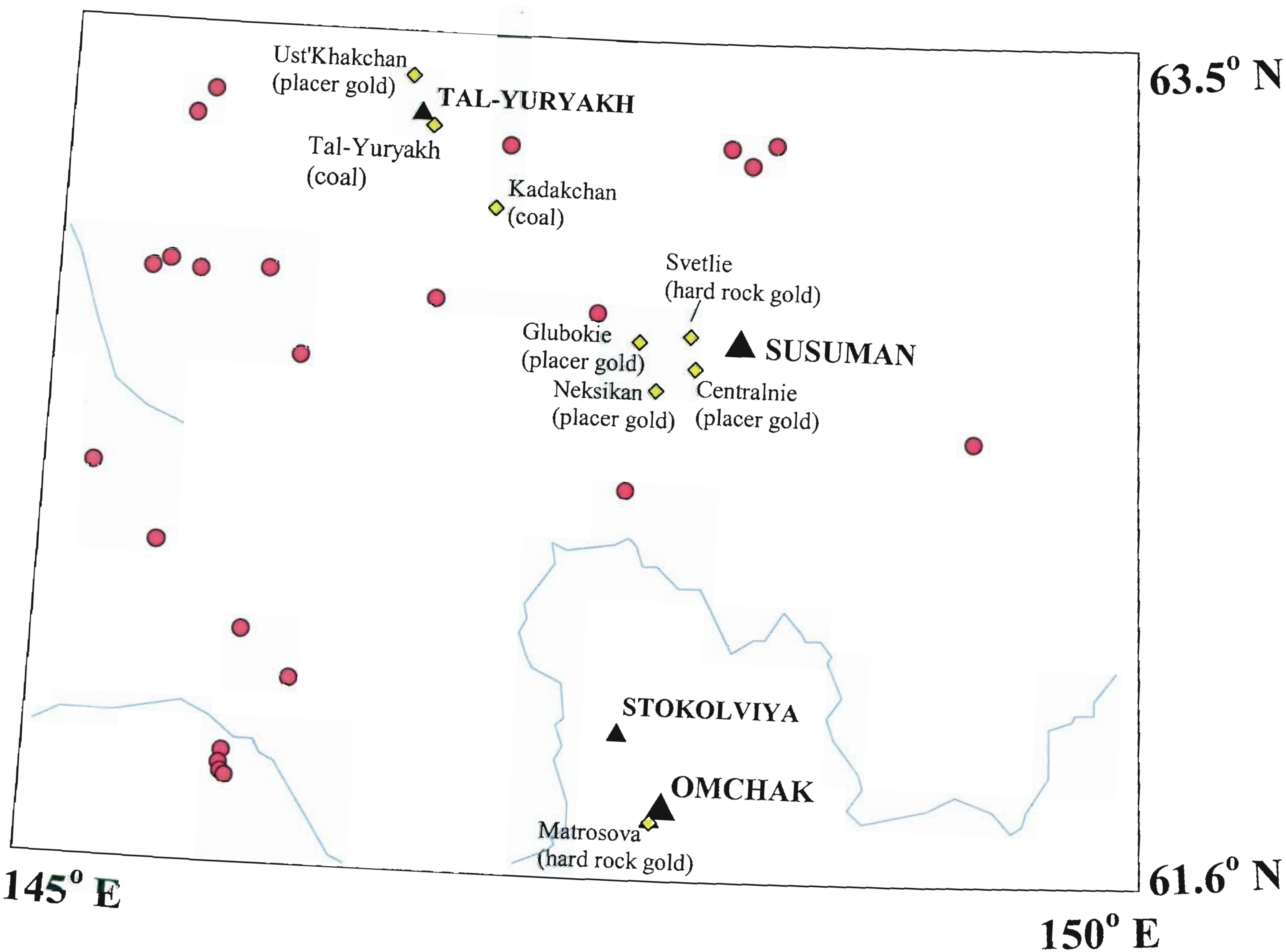

Figure 75. Susuman mining region depicting located tectonic events and specific known active mines. Symbols as in Figure 70.

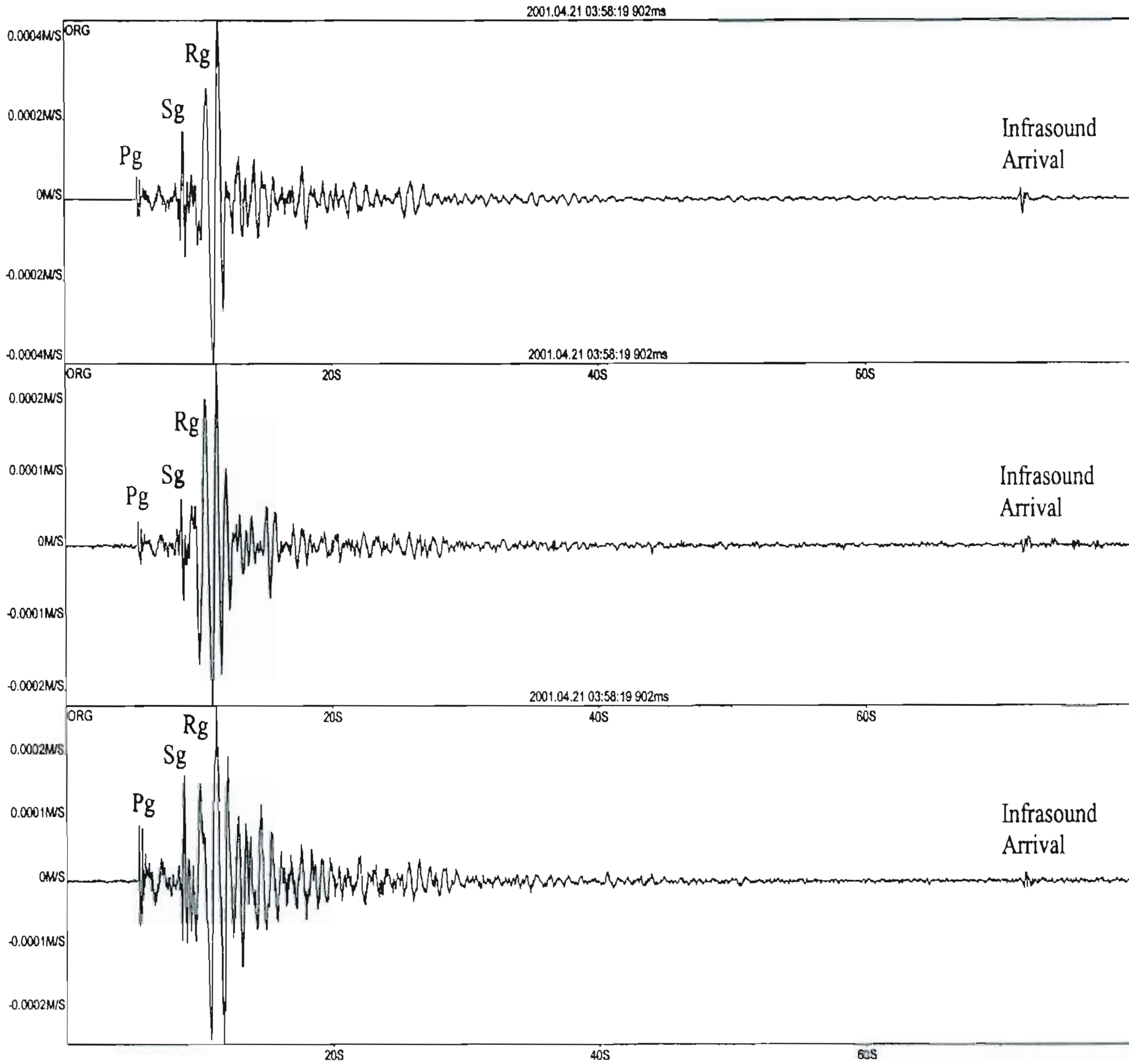

Figure 76. 3-component seismogram (top - Z, middle - N-S, bottom - E-W) of a 40,000 kg explosion recorded at Susuman. This explosion occurred April 21, 2001, in a placer gold mine near the town of Neksikan, about 21 km southwest of Susuman. Note the clearly developed Pg, Sg, and Rg arrivals, as well as a clear acoustic arrival recorded on all seismometer components about 70 seconds after Pg.

Figure 77. Placer gold mine at Neksikan. Approximately fifteen blasts in the 30,000 to 40,000 kg range were detonated in April, 2001, to prepare frozen sediments for the excavation of the pit seen here. Some of these blasts were recorded throughout the deployed digital network (see Figures 76 and 78).

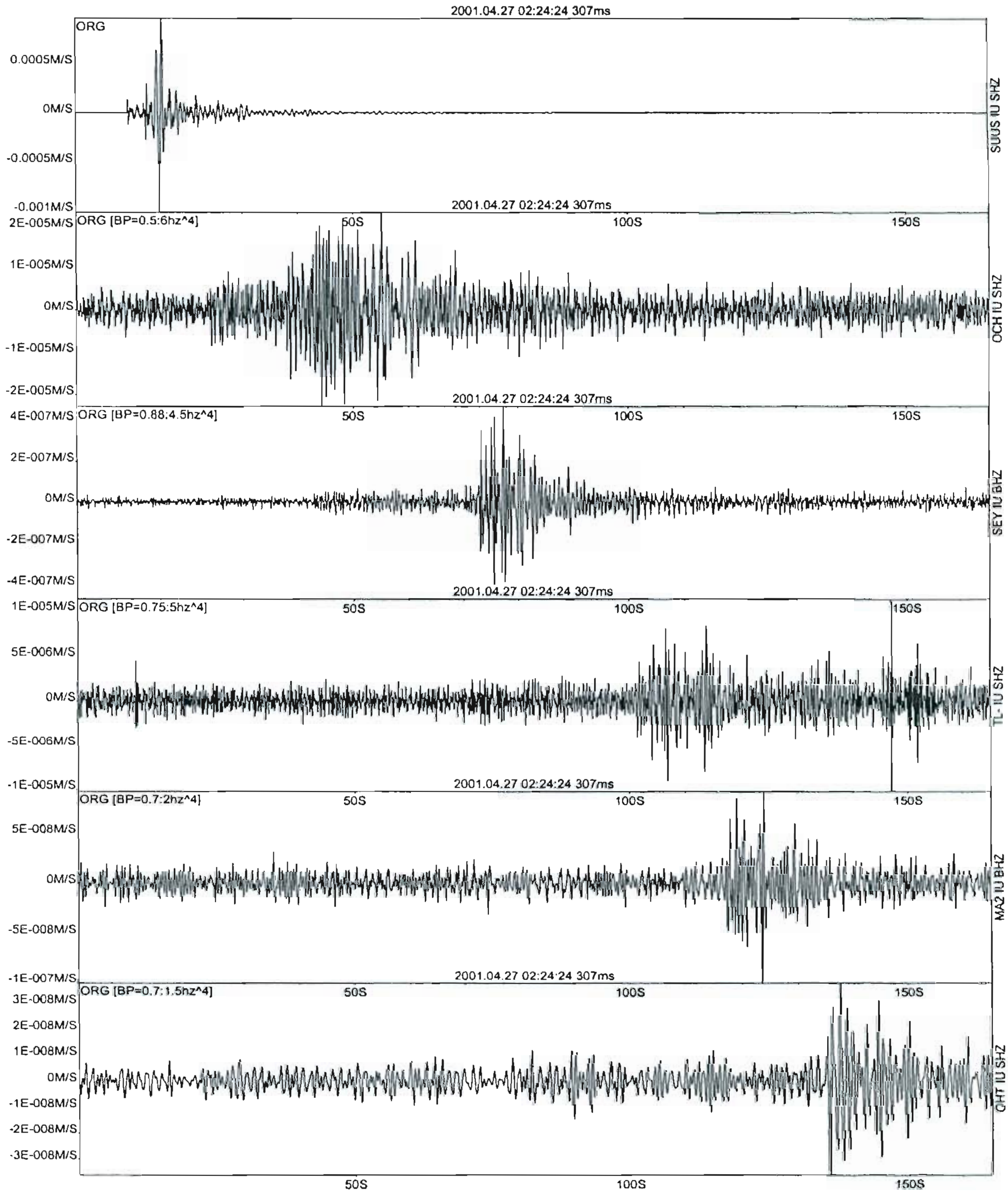

Figure 78. 40,000 kg blast of April 27, 2001 as recorded by several of our stations (top to bottom: Susuman (22 km), Omchak (111km), Seymchan (236 km), Talaya (297 km), Magadan (MA2; 381 km), and Okhotsk (441 km). Note the well developed low frequency Lg arrival at Okhotsk. All records except Susuman are bandpass filtered.

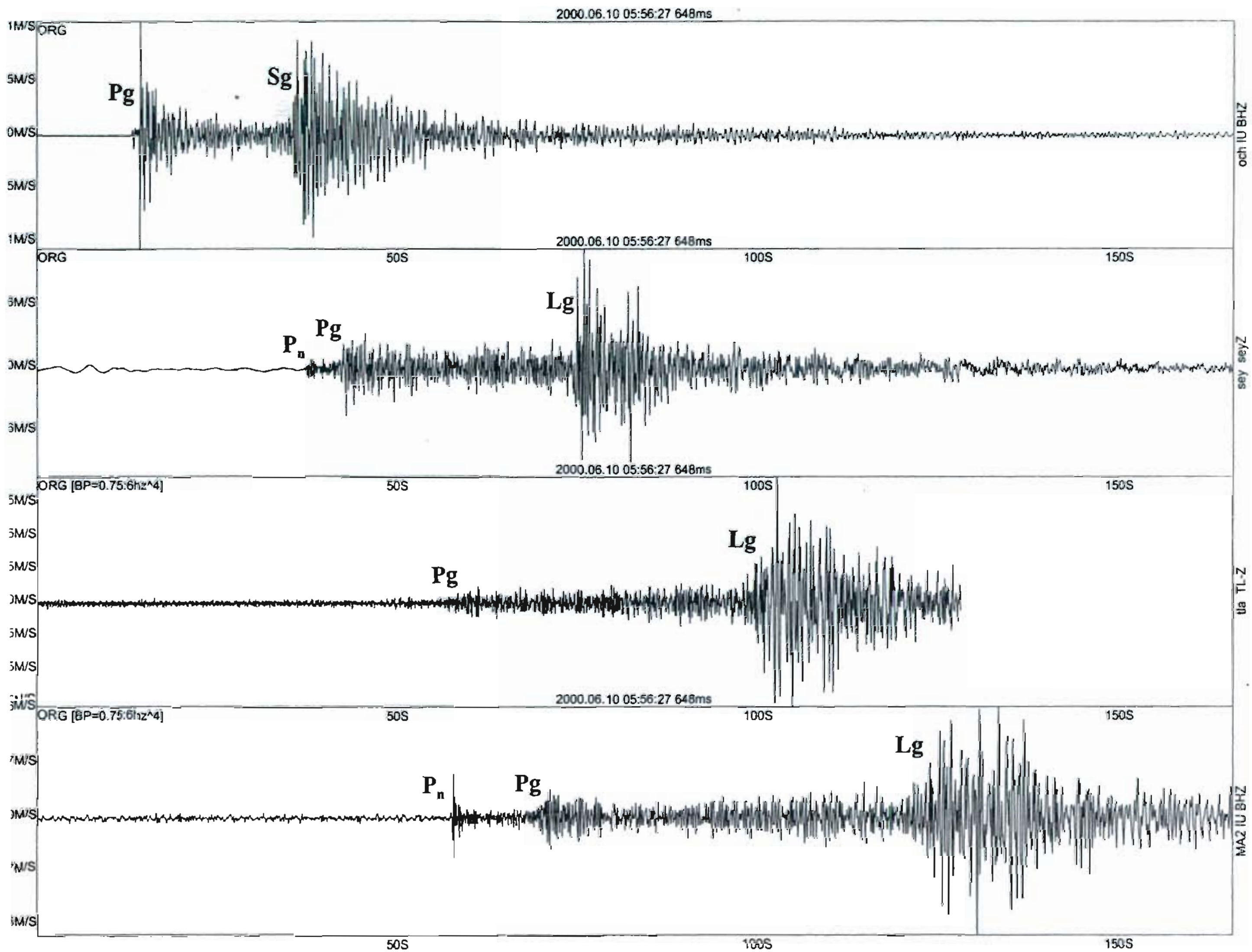

Figure 79. Seismograms from what is suspected to be the largest explosion recorded during the study. Stations are, top to bottom, Omchak, Seymchan, Talaya, and Magadan. The explosion was identified by location, acoustic arrivals, and characteristic waveform to have occurred at the Kadakchan coal mine (see Figure 70). This explosion is discussed in detail in Appendix E.

Yuryakh coal mine, northwest of Susuman (Figure 75). This temporary station operated from March through May, 2001, and recorded several explosions from coal mines at both Tal-Yuryakh and Kadakchan. The largest explosion recorded from this deployment was about 24 T. A sample seismogram from Tal-Yuryakh is shown in Figure 80. Temporary stations were also deployed at the Matrosova mine and near the Magadan granite quarry.

Careful examination of explosions originating at several mines and recorded at several stations indicates that the correlation of waveforms is very high when viewing the waveforms from the same explosion source/station pair. In many cases, waveforms can be matched swing for swing, including relative amplitudes of individual peaks. Work is currently underway to construct a catalog of characteristic waveforms for all explosion source/station pairs.

As a large number of earthquakes and explosions from throughout the study region have been recorded, it is possible to attempt to discriminate between explosions and earthquakes using various Lg amplitude ratios. Preliminary results indicate that the ratio Lg(4-8Hz)/Lg(0.75-1.5Hz) using peak amplitudes is not sufficient to discriminate mining explosions from earthquakes at local and near regional distances (<500km) in northeast Russia (Figure 81). In general, the overall relationship (slope and intercept) between earthquake Lg ratios vs. distance is nearly identical to that of HIA where the ratio has been used to effectively discriminate between nuclear explosions and tectonic earthquakes (Hartse, 2000). It should be noted that this represents only the most simple approach to an Lg discriminant for northeast Russia. Additional more comprehensive research is underway to look at the RMS amplitudes of the full Lg wave packet (Hartse, 2000) as opposed to peak amplitudes. Additional phase amplitude ratios (Pg/Lg, P_n/Lg, etc.) are also planned to be investigated.

5.3 CONCLUSION.

In order to obtain ground truth seismic events, a small network of digital seismic stations was deployed in the Magadan district, including at or near active mines. The network has recorded and located a large number of both earthquakes and explosions. Several temporary stations were also deployed to record mine blasts of aftershocks from larger earthquakes. Preliminary analysis of Lg amplitude ratios indicate that the ratio Lg(4-8Hz)/Lg(0.75-1.5Hz) using peak amplitudes is not sufficient to discriminate mining explosions from earthquakes at local and near regional distances (<500km) in northeast Russia.

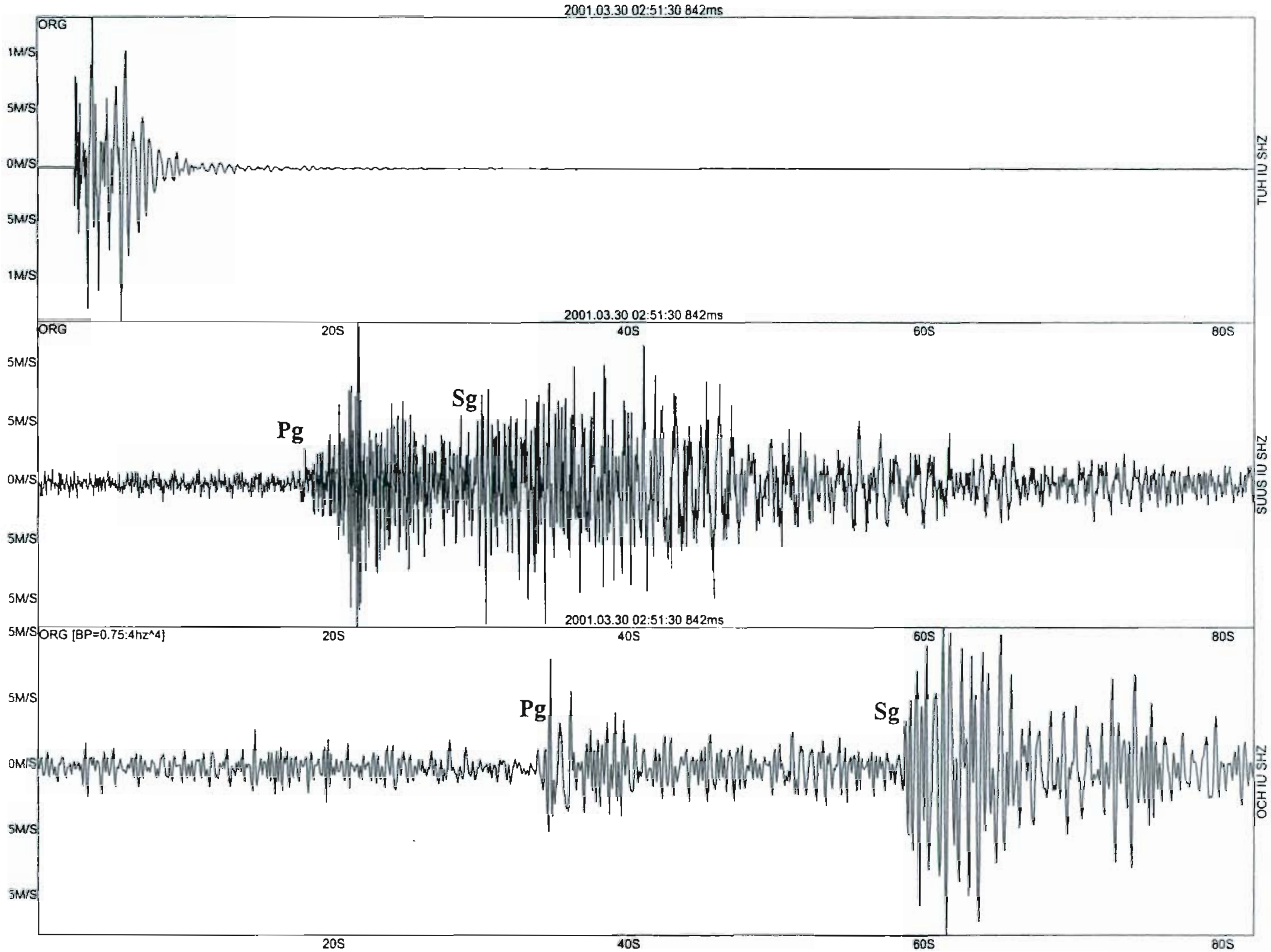

Figure 80. Explosion from the Tal-Yuryakh coal mine recorded by the temporary seismic station deployed at the mine, as well as Susuman (center) and Omchak (bottom). The yield of this blast was 4590 kg. The complex waveform recorded at Susuman is characteristic of Tal-Yuryakh explosions and can be used as a discriminant for this mine. The complexity of the waveform is much reduced in the filtered seismogram from Omchak.

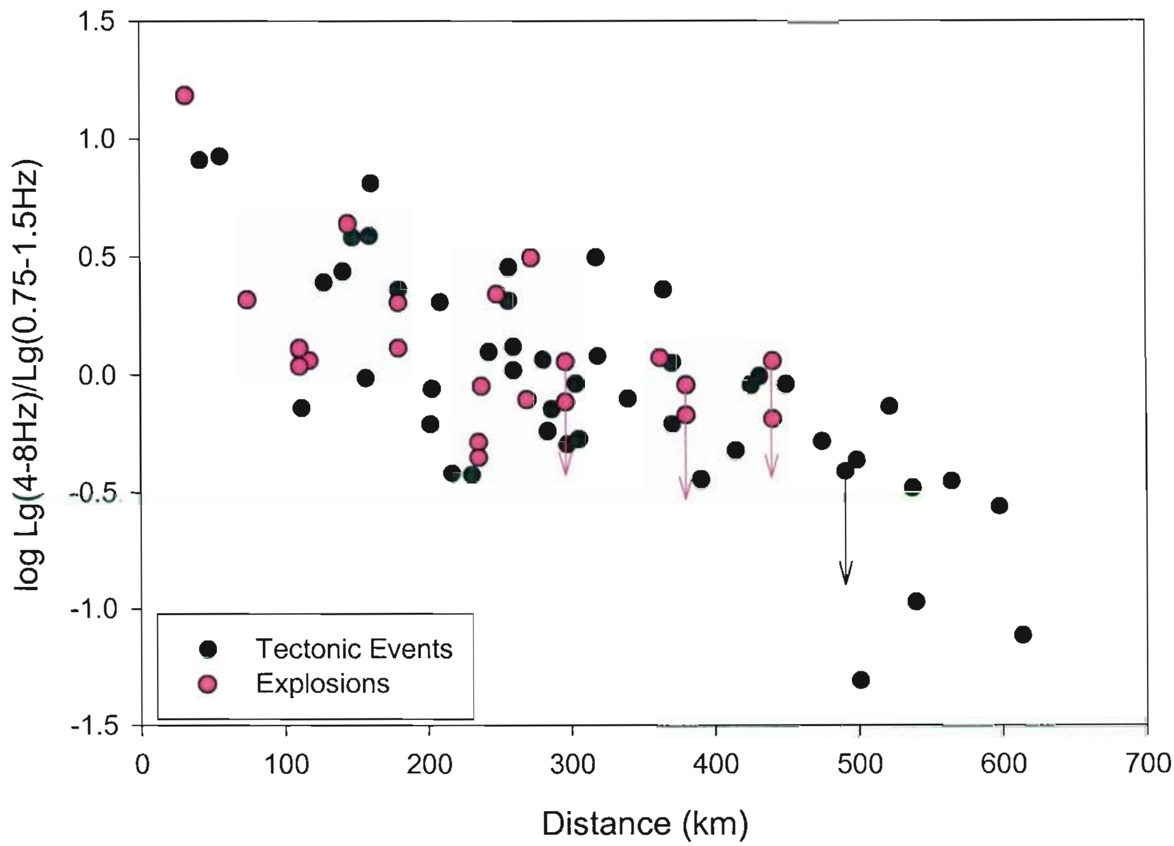

Figure 81. Composite plot of Lg spectral ratio vs. distance for tectonic events and explosions using all stations except Omsukchan. Lg amplitudes used were maximum peak to peak. There is no apparent difference in the plotting of earthquakes and explosion, thus discrimination is difficult here using this method at these distances. Points with arrows represent maximum possible ratio for arrivals with a clear low frequency Lg arrival (see Okhotsk, Figure 78) but no apparent high frequency arrival. In these cases, the high frequency Lg is substituted with the high frequency background.

SECTION 6

CONCLUSIONS

A catalog covering historic seismicity and associated phases and arrival times compiled for northeast Russia has proven useful for seismic characterization of the region. The resultant catalog was found to be contaminated by industrial explosions, particularly in the Amur and central Magadan districts where dramatic differences between daytime and nighttime seismicity were found. In the process of developing the seismicity catalog, operational procedures, network histories and seismic station parameters were researched.

Phase arrivals were used to develop a crustal velocity model by obtaining best fit travel-time curves over 3 x 5 degree regions. The velocities obtained are generally in agreement with inferred tectonic regimes. These travel-time curves were then used to relocate larger regional events, improving relative locations as aftershock clusters are tighter and earthquakes better align along faults..

Using the developed crustal velocities, 134 seismic events reported in the International Seismological Centre (ISC) were relocated. All events were assigned GT levels, with 26 events classified as GT10. From relocated events, consistent patterns of residuals, essentially representing path corrections, show upper mantle velocities are elevated under the Siberian platform and slower below the Sea of Okhotsk..

To further improve calibration capabilities in northeast Russia, a small network of digital seismic stations was deployed in the in the Magadan region, recording both earthquakes and ground truth mine blasts. Preliminary analysis of Lg amplitude ratios indicate that the ratio Lg(4-8Hz)/Lg(0.75-1.5Hz) using peak amplitudes is not sufficient to discriminate mining explosions from earthquakes at local and near regional distances (<500km) in northeast Russia.

SECTION 7

REFERENCES

Agnew, D. C., 1990. The use of time-of-day seismicity maps for earthquake/explosion discrimination by local networks, with an application to the seismicity of San Diego county, *Bulletin of the Seismological Society of America,* v. 80, p. 747-750. (UNCLASSIFIED)

Andreev, T. A., Kravets, I. F., and Mishin, S. V.,1967. On the seismic activity of the Northeast: *Trudy SVKNII* (Magadan), v. 30, p. 159-166 (in Russian). (UNCLASSIFIED)

Ansimov, E. M., Sedov, B. M., and Shvarts, D. B., 1967. Seismic exploration in the northeast USSR, *in* Fotiadi, E.E., ed., *Geological results of Geophysical Investigations in Siberia and the Far East*: Nauka, Novosibirsk, p. 438-442 (in Russian). (UNCLASSIFIED)

Avetisov, G. P., 1996. *Seismoactive Zones of the Arctic*: VNIIOkeanologiya, St. Petersburg, 185 pp. (in Russian). (UNCLASSIFIED)

Belyaevsky, N. A., 1974. *The Earth's Crust Within the Territory of the USSR*: Moscow, Nedra, 278 pp. (in Russian). (UNCLASSIFIED)

Belyaevsky, N. A., and Borisov, A. A., 1974. Structure and thickness of the earth's crust in the USSR, *in* Nalivkin, D. V., ed., *Structural Basement of Platformal Regions of the USSR*: Leningrad, Nauka, p. 381-393 (in Russian). (UNCLASSIFIED)

Bobrobnikov, V. A., and Izmailov, L. I., 1989. Present day structure and geodynamics of the earth's crust in the southeastern portion of the Yana-Kolyma system, *in* Lin'kova, T. I., and Krasnyi, L. L., eds., *Geophysical Investigations for the Solution of Geologic Problems*: SVKNII DVNTs AN SSSR, Magadan, p. 5-23 (in Russian). (UNCLASSIFIED)

Bulin, N. K., 1989. Deep structure of the Verkhoyana-Chukotka folded region according to seismic data: *Tikhookeanskaya Geologiya*, v. 8(1), p. 77-85 (in Russian). (UNCLASSIFIED)

Cook, D. B., Fujita, K., and McMullen, C. A., 1986. Present-day plate interactions in northeast Asia: North American, Eurasian and Okhotsk plates: *Journal of Geodynamics*, v. 6, p. 33-51. (UNCLASSIFIED)

Chapman, M. E., and Solomon, S. C., 1976. North American - Eurasian plate boundary in Northeast Asia: *Journal of Geophysical Research*, v. 81, p. 921-930. (UNCLASSIFIED)

Davydova, N.I., Shvarts, Ya. B., and Yaroshevskaya, G.A., 1968. Wave patterns in deep seismic sounding along Magadan-Kolyma profile, *in* Deep Seismic Soundings of the Earth's Crust in the USSR: *International Geology Review - Book Section*, v. 10, p. 93-102. (UNCLASSIFIED)

Doser, D. I., 1991. Faulting within the eastern Baikal rift as characterized by earthquake studies: *Tectonophysics*, v.196, p. 109-139. (UNCLASSIFIED)

Drachev, S. S., 1998. Laptev Sea rifted continental margin: Modern knowledge and unsolved questions: *Polarforschung* v.68, p. 41-50. (UNCLASSIFIED)

England, P., and Jackson, J., 1989. Active deformation of the continents: *Annual Reviews of Earth and Planetary Science Letters*, v. 17, p. 197-226. (UNCLASSIFIED)

Fujita, K., Cambray, F. W., and Velbel, M. A., 1990a. Tectonics of the Laptev Sea and Moma rift systems, northeastern USSR: *Marine Geology*, v. 98, p. 95-118. (UNCLASSIFIED)

Fujita, K., Cook, D. B., Hasegawa, H., Forsyth, D., and Wetmiller, R., 1990b. Seismicity and focal mechanisms of the Arctic region and the North American plate boundary in Asia, *in* Grantz, A., Johnson, L., and Sweeney, J. F., eds., *The Arctic Ocean Region; The Geology of North America* v. L: The Geological Society of America, Boulder, p. 79-100. (UNCLASSIFIED)

Fujita, K., Stone, D. B., Layer, P. W., Parfenov, L. M., and Koz'min, B. M., 1997. Cooperative program helps decipher tectonics of northeastern Russia: *Eos (Transactions of the American Geophysical Union)*, v. 78, p. 245, 252-253. (UNCLASSIFIED)

Fujita, K., Mackey, K. G., McCaleb, R. C., Gunbina, L. V., Kovalev, V. N., Imaev, V. S., and Smirnov, V. N., in press. The seismicity of Chukotka, northeast Russia, *in Geological Society of America, Special Paper* 360. (UNCLASSIFIED)

Godzikovskaya, A. A., 1995. *Local Explosions and Earthquakes*: Rossiskoe Aksionernoe Obshchestvo Energy and Electrification "EES Rossii", Moscow, p. 55-66 (In Russian). (UNCLASSIFIED)

Grachev, A. F., 1973. Moma continental rift (Northeast USSR): *Geofizicheskie Metody Razvedki v Arktike*, v. 8, p. 56-75 (in Russian). (UNCLASSIFIED)

Grossheim, V. A., and Khain, V. E., eds., 1967. *Atlas of the Lithological-Paleogeographical Maps of the USSR, v. IV, Paleogene, Neogene and Quaternary*: Ministry of Geology of the USSR, Moscow, 55 sheets. (UNCLASSIFIED)

Hartse, H. E., 2000. Regional Seismic Event Discrimination: in *22nd Annual DoD/DOE Seismic Research Symposium Proceedings, "Planning for Verification of and Compliance with the Comprehensive Nuclear-Test-Ban Treaty (CTBT),"* Volume II, p. 137-146. (UNCLASSIFIED)

Hearn, T.M., 1984. P_n travel times in southern California: *Journal of Geopyhsical Research*, v. 89, p. 1843-1855. (UNCLASSIFIED)

Hearn, T.M., Beghoul, N., and Barazangi, M., 1991. Tomography of the western United States from regional arrival times: *Journal of Geopyhsical Research*, v. 96, p. 16,369-16,381. (UNCLASSIFIED)

Imaev, V. S., Imaeva, L. P., and Koz'min, B. M., 1990. *Active Faults and Seismotectonics of Northeast Yakutia*: Yakut Science Center, Yakutsk, 138 pp. (in Russian). (UNCLASSIFIED)

Imaev, V. S., Imaeva, L. P., Koz'min, B. M., and Fujita, K, 1994. Active faults and modern geodynamics of the Yakutia seismic belts: *Geotectonics*, v. 28, p. 146-158, and v. 28(3), cover. (UNCLASSIFIED)

Imaev, V. S., Imaeva, L. P., and Koz'min, B. M., 2000. *Seismotectonics of Yakutia*: GEOS, Moscow, 226 pp. (in Russian). (UNCLASSIFIED)

Jeffreys, H., and Bullen, K. E., 1970. *Seismological Tables*: Office of the British Association, London, 50 pp. (UNCLASSIFIED)

Kennett, B. N. L., 1991. *IASPEI 1991 Seismological Tables*: Research School of Earth Sciences, Australian National University, Canberra, 167 pp. (UNCLASSIFIED)

Kim, B. I., 1986. Structural continuation of the rift valley of Gakkel' ridge on the Laptev shelf, *in* Egiazarov, B. K., and Kazmin, Y. B., eds., *Structure and History of Development of the Arctic Ocean*: Sevmorgeologiya, Leningrad, p. 133-139 (in Russian). (UNCLASSIFIED)

Kondorskaya, N. V., and Shebalin, N. V., eds., 1982. *New Catalog of Strong Earthquakes in the U.S.S.R. From Ancient Times Through 1977*: World Data Center A for Solid Earth Geophysics, Report SE-31, xi+608 pp. (UNCLASSIFIED)

Koz'min, B. M., 1984. *Seismic Belts of Yakutia and the Focal Mechanisms of Their Earthquakes*: Nauka, Moscow, 125 p. (in Russian). (UNCLASSIFIED)

Koz'min, B. M., Golenetsky, S.I., Nikolaev, V. V.,Avdeed, V. A.,Borob'eva, E. A., Borotyntsev, V. G.,Golenetskaya, I. G., Zelenkov, P. Y., Imaev, V. S., Kleshchenko, S. V., Kovalenko, N. S., Kornilova, Z. A., Larionov, A. G., Semenov, R. A., Serebrennikov, S. P., Skrypnyuk, A.M., Khudaeva, I. Y., Chepkunas, L. S., Chipizubov, A. V., and Sholokhova, A. A., 1993, South Yakutian earthquake of 20(21).04.1989 and its aftershocks: in Kondorskaya, N. V., ed., *Earthquakes of the USSR in 1989*: Nauka, Moscow, p. 172-193 (In Russian). (UNCLASSIFIED)

Lay, T., and Wallace, T., 1995. *Modern Global Seismology*: Academic Press, San Diego, xii + 521 pp. (UNCLASSIFIED)

Layer, P. W., Newberry, R., Fujita, K., Parfenov, L., Trunilina, V., and Bakharev, A., 2001. Tectonic setting of the plutonic belts of Yakutia, northeast Russia, based on $^{40}Ar/^{39}Ar$ geochronology and trace element geochemistry: *Geology*, v. 29, p. 167-170. (UNCLASSIFIED)

Leith, W., 1994. *Final report, AC94-1A-3003*: U. S. Geological Survey, Reston, 106 pp. (UNCLASSIFIED)

Mackey, K. G., 1996. *Crustal Thickness of Northeast Russia*: M.S. Thesis, Michigan State University, ix + 102 pp. (UNCLASSIFIED)

Mackey, K. G., 1999. *Seismological Studies in Northeast Russia*: Ph.D. Dissertation, Michigan State University, East Lansing, xxiii + 346 pp. (UNCLASSIFIED)

Mackey, K. G., and Fujita, K., 1999. The northeast Russia seismicity database and explosion contamination of the Russian earthquake catalog, *in* Proceedings of the 21st Seismic Research Symposium: Technologies for Monitoring The Comprehensive Nuclear-Test-Ban Treaty, v.1, p.151-161. (UNCLASSIFIED)

Mackey, K. G., and Fujita, K., 2001a. Seismicity Characterization and Velocity Structure of Northeast Russia - Analysis of Events and Digital Data, January 1999 - December 1999, *NERSP Report* #6: Michigan State University, Department of Geological Sciences, East Lansing, 56 pp. (UNCLASSIFIED)

Mackey, K. G., and Fujita, K., 2001b. Seismicity Characterization and Velocity Structure of Northeast Russia - Analysis of Events and Digital Data, January 2000 - December 2000, *NERSP Report* #7: Michigan State University, Department of Geological Sciences, East Lansing, 103 pp. (UNCLASSIFIED)

Mackey, K. G., and Fujita, K., 2001c. Seismicity Characterization and Velocity Structure of Northeast Russia - Analysis of Events and Digital Data, January 2001 - September 2001, *NERSP Report* #9: Michigan State University, Department of Geological Sciences, East Lansing. (UNCLASSIFIED)

Mackey, K. G., Fujita, K., Gunbina, L. V., Kovalev, V. N., Imaev, V. S., Koz'min, B. M., and Imaeva, L. P., 1997. Seismicity of the Bering Strait region: evidence for a Bering block: *Geology*, v. 25, p. 979-982. (UNCLASSIFIED)

Mackey, K. G., Fujita, K., and Ruff, L. J., 1998. Crustal thickness of northeast Russia: *Tectonophysics*, v. 284, p. 283-297. (UNCLASSIFIED)

Materialy po Seismichnost' Sibiri, 1970-1992: Academy of Sciences of the USSR, Siberian Branch, Irkutsk (bi-monthly, in Russian). (UNCLASSIFIED)

McLean, M. S., Fujita, K., and Mackey, K. G., 2000. Neotectonics of the central Chersky seismic belt, northeastern Russia: *Eos (Transactions of the American Geophysical Union)*, v. 81(19), Supplement, p. S414. (UNCLASSIFIED)

McNamara, D.E., 1995. *Lithospheric structure of the Tibetan Plateau*: PhD. Dissertation, University of South Carolina, x + 259 pp. (UNCLASSIFIED)

McNamara, D.E., Walter, W.R., Owens, T.J., and Ammon, C.J., 1997. Upper mantle velocity beneath the Tibetan Plateau from P_n travel time tomography: *Journal of Geopyhsical Research*, v. 102, p. 493-505. (UNCLASSIFIED)

Mishin, S. V., 1967. *Experimental Instrumental Seismological Investigations in the Northeast USSR*: Laboratory of Regional Geodynamics, NEISRI, Magadan, 165 pp. (In Russian). (UNCLASSIFIED)

Mishin, S. V., and Dareshkina, N. M., 1966. Isolation of converted waves on records of distant earthquakes: *Izvestia, Physics of the Solid Earth*, v. 2, p. 598-601. (UNCLASSIFIED)

Neustroev, A. P., and Parfenov, L. M., 1985. Thickness of the earth's crust in the eastern part of the Siberian platform: *Soviet Geology and Geophysics*, v. 26(2), p. 126-129. (UNCLASSIFIED)

Nokleberg, W. J., Parfenov, L. M., Monger, J. W. H., Baranov, B. V., Byalobzhesky, S. G., Bunbtzen, T. K., Feeney, T. D., Fujita, K., Gordey, S. P., Grantz, A., Khanchuk, A. I., Natal'in, B. A., Natapov, L. M., Norton, I. O., Patton, W. W., Jr., Plafker, G., Scholl, D. W., Sokolov, S. D., Sosunov, G. M., Stone, D. B., Tabor, R. W., Tsukanov, N. V., Vallier, T. L., Wakita, K., 1994. Circum-North Pacific tectonostratigraphic terrane map: *U. S. Geological Survey Open-File Report* 94-714, 221 pp., 5 plates. (UNCLASSIFIED)

Nokleberg, W. J., Parfenov, L. M., Monger, J. W. H., Norton, I. O., Khanchuk, A. I., Scotese, C. R., Stone, D. B., Scholl, D. W., and Fujita, K., 2000. Phanerozoic tectonic evolution of the circum-north Pacific: *U. S. Geological Survey Professional Paper* 1626, 122 pp. + VII. (UNCLASSIFIED)

Odinyets, M. G., 1996. The problem of polluting the earthquake catalog with industrial blasts in northeastern Russia, *in* Lin'kova, T. I., and Bobrobnikov, V. A., eds., *Geophysical Models of Geologic Processes in Northeast Russia*: NEISRI, Magadan, p. 90-99 (in Russian). (UNCLASSIFIED)

Parfenov, L. M., 1991. Tectonics of the Verkhoyansk-Kolyma Mesozoides in the context of plate tectonics: *Tectonophysics*, v. 199, p. 319-342. (UNCLASSIFIED)

Parfenov, L. M., Oksman, V. S., and Sashkin, M. M., 1989. Mid-Late Jurassic tectonic sheets in the Tas-Khayakhtakh zone (Chersky mountain system): *Geologiya i Geofizika*, v. 30(1), p. 130-134 (in Russian). (UNCLASSIFIED)

Peltzer, G., and Tapponnier, P., 1988. Formation and Evolution of Strike-Slip Faults, Rifts, and Basins During the India-Asia Collision: An Experimental Approach: *Journal of Geophysical Research*, v. 93, p. 15,085-15,117. (UNCLASSIFIED)

Pilyasov, A. N., 1993. Regularities in the mining-industrial mastery of northeast Russia: *Kolyma*, 1993(8), p. 5-12 (in Russian). (UNCLASSIFIED)

Pustovitenko, B.G., and Kul'chitskii, B. E., 1974. About energy extimates of earthquakes in the Crimea-Black Sea region, *in* Kondorskaya, N. V., Nersesov, I. L., Gorbunova, I. L., Rautian, T. G., and Korchagina, T. G., eds., *Magnitude and Energy Classification of Earthquakes*, v. 2,: IPE AS USSR, Moscow, p. 113-124 (in Russian). (UNCLASSIFIED)

Riegel, S. A., 1994. *Seismotectonics of northeast Russia and the Okhotsk plate*: M.S. Thesis, Michigan State University, East Lansing, ix + 70 pp. (UNCLASSIFIED)

Riegel, S. A., Fujita, K., Koz'min, B. M., Imaev, V. S., and Cook, D. B., 1993. Extrusion tectonics of the Okhotsk plate, northeast Asia: *Geophysical Research Letters*, v. 20, p. 607-610. (UNCLASSIFIED)

Ruff, L. J., LaForge, R., Thorson, R., Wagner, T., and Goudaen, F., 1994. Geophysical Investigation of the Western Ohio-Indiana Region, Final Report 1986-1992: *U.S. Nuclear Regulatory Commission* NUREG/CR-3145, v. 10, 73 p. (UNCLASSIFIED)

Seismologicheskii Byulleten' - Dal'nego Vostoka, 1972-1990: Academy of Sciences of the USSR, Far Eastern Branch, Yuzhno Sakhalinsk (in Russian). (UNCLASSIFIED)

Sekretov, S. B., 1998. Petroleum potential of Laptev Sea basins: geological, tectonic and geodynamic factors: *Polarforschung* v.68, p. 179 - 186. (UNCLASSIFIED)

Seno, T., Sakurai, T., and Stein, S., 1996. Can the Okhotsk plate be discriminated from the North American plate?: *Journal of Geophysical Research*, v. 101, p. 11305-11315. (UNCLASSIFIED)

Shabad, T., 1969. *Basic Industrial Resources of the USSR*: Columbia University Press, New York, 393 pp. (UNCLASSIFIED)

Solonenko, 1974. Energy classification of earthquakes of Prebaikalia,. *in* Kondorskaya, N.V., Nersesov, I.L., Gorbunova, I.V., Rautian, T.G., and Korchagina, T.G., eds., *Magnitude and Energy Classification of Earthquakes*, v. 2,: IPE AS USSR, Moscow, p. 174-179 (In Russian). (UNCLASSIFIED)

Starovoit, O. E., Gabsatarova, I. P., Kolomiets, M. V., and Chepkunas, L. S., 1995. Operational determination of focal parameters of the Neftegorsk earthquake of 27(28) May, 1995: *Federal System of Seismological Observations and Earthquake Prediction Informational Analytical Bulletin, Special Issue*, p. 27-35 (in Russian). (UNCLASSIFIED)

Stavsky, A. P., Chekhovitch, V. D., Kononov, M. V., and Zonenshain, L. P., 1990. Plate tectonics and palinspatic reconstructions of the Anadyr-Koryak region, northeast USSR: *Tectonics*, v.9, p.81-101. (UNCLASSIFIED)

Suvorov, V. D., and Kornilova, Z.A., 1986. Thickness of the earth's crust in the southeastern Verkhoyana-Kolyma fold system (according to near earthquakes): *Tikhookeanskaya Geologiya*, v. 5(4), p. 32-36 (in Russian). (UNCLASSIFIED)

Tapponnier, P., Peltzer, G., Le Dain, A. Y., Armijo, R., and Cobbold, P., 1982. Propagating extrusion tectonics is Asia: new insights from simple experiments with plasticine: *Geology*, v. 10, p. 611-616. (UNCLASSIFIED)

Vashchilov, Y.Y., 1979. Seismicity and questions regarding the deep structure of the northeast USSR, *in* Shilo, N. A., Izmailov, L. I., Linkova, T. I., Akhlamova, I. I., eds., *Geophysical Investigations on the Structure and Geodynamics of the Earth's Crust and Upper Mantle in the Northeast USSR*: SVKNII DVNTs AN SSSR, Magadan, p. 138-157 (in Russian). (UNCLASSIFIED)

Vazhenin, B. P., Mishin, S. V.,and Sharafudinova, L. V., 1997. *Earthquakes in the Magadan Region*, SVKNII, Magadan, 44 pp (in Russian). (UNCLASSIFIED)

Wallace, T.C., and Tinker, M.A., 1998. Seismic characterization of Siberia: in *Proceedings of 20th Annual Symposium on Monitoring a Comprehensive Test Ban Treaty (CTBT)*, p. 536-541. (UNCLASSIFIED)

Worrall, D. M., Kruglyak, V., Kunst, F., and Kuznetsov, V., 1996. Tertiary tectonics of the Sea of Okhotsk, Russia: Far-field effects of the India-Eurasia collision: *Tectonics*, v. 15, p. 813-826. (UNCLASSIFIED)

Yang, X, and Romney, C., 1999. PIDC ground truth event (GT) database: *CMR Technical Report* CMR-99/15, 25 pp. (UNCLASSIFIED)

Zemletryaseniya v SSSR, 1963-1989: Moscow, USSR, Nauka (annual, in Russian). (UNCLASSIFIED)

Zemletryaseniya v SSSR, 1990-1991: Moscow, Russian Academy of Science (annual, in Russian). (UNCLASSIFIED)

Zemletryaseniya Severnoi Evrazii, 1992-1994: Moscow, Russian Academy of Science (annual, in Russian). (UNCLASSIFIED)

APPENDIX A

Alphabetized list of northeastern Russia seismic stations.

Station Name	Engl. Code	Russian Code	Lat. (°N)	Long. (°E)	Elev. (m)	Date Open	Date Close	Qual.
Aku			56.46	120.91	700	--/68	--/68	1
Aldan	ALDR		58.67	125.40		–/99	OPEN	1
Alla	ALL	АЛ	54.688	110.82	550	10/63	5/70	1
Alygdzher	ALY		53.633	98.218	920	1/66	1/67	1
Amedichi	ACHS	АМД	57.03	122.85	930	05/89	08/89	1
Amguema	AMG	АМГ	67.05	178.88W	150	11/65	4/66	2
Ammonl'naya	MMS		64.55	143.18	540	--/61	--/62	1
Anadyr	ANYS	АНД	64.734	177.496	55	4/89	7/93	1
						9/96	OPEN	
Anadyr-1	ANSS	АНД	64.77	177.57	40	11/80	1/89	3
Angarakan	AGK		56.348	113.67	1430	11/76	8/81	1
Anyuisk	ANC	АНС	68.34	161.56	10	6/64	3/65	1
Apacha	APC		52.925	157.131		2/90	OPEN	1
Apakhonchich	APN	АПХ	56.00	160.84	700	–/64	–/80	1
Arshan	ARS	АРШ	51.908	102.433	840	–/58		1
Artyk	AYKS	АР	64.18	145.13	700	06/71	--/71	1
			64.1831	145.1347	700	—/88	OPEN	G
Avacha - old	AVH	АВЧ	53.07	158.5	---	–/63	10/76	-
Avacha - new	AVH	АВЧ	53.265	158.738	900	7.76	OPEN	1
Babushkin	BAU		51.717	105.867	470	6/66	9/66	1
Baikal'sk	BKK		51.522	104.133	460	1/64	2/66	1
Balygychan	BLG	БЛГ	63.91	154.09	139	7/63	6/64	1
Barluk	BRUS		54.533	101.717	525	11.60		1
Batagai	BTGS	БТГ	67.653	134.630	127	--/75	OPEN	1
Bazovskii			56.53	123.42	1080	--/70	--/70	1
Berezovaya	BER	БРЗ	52.27	158.433		–/81	–/94	1
Bering (Nikol'skoe)	BKI	БРН БРГ	55.195	165.99	400	–/62	OPEN	-
Bilibino GSN	BILL	BILL	68.065	166.452	299	8/95	OPEN	1
Bilibino	BILS	БЛБ БЛН	68.059	166.449	283	8/81	4/92	1
Bilibino-1	BL1	БЛБ	68.04	166.44	260	8/64	1/65	1
Bodaibo	BOD	БДБ	57.807	114.03	245	11/60	---	1
Bodon	BDN	БОД БДН	53.713	110.1	540	11/69	--/83	1
Bogachevka	BGC		54.850	160.900		–/64	–/65	1
Bomnak	BMKS	БМН	54.705	128.847	325	3/74	---	1
Bykov			47.317	142.567	40	6/68	10/68	-

Chagda	CGD	ЧГД	58.75	130.60	185	--/68	---	1
Chara	CRS	ЧР	56.9	118.267	710	11/61	---	1
Cherskii	CES	ЧРС	68.75	161.33	10	--/79	--/88	1
Chil'chi			56.06	122.33	500	--/70	--/70	1
Chita	CIT	ЧТ	52.033	113.55	790	6/70		1
Chochurdakh			72.83	116.25		08/13/75	09/26/75	-
Chokchoi	CKHS	ЧКЧ	57.65	121.72	240	--/89	--/89	1
Chul'man-1	CL1S	ЧЛМ	56.85	124.90	650	--/62	--/86	1
Chul'man-2	CLNS	ЧЛМ	56.84	124.90	760	--/86	---	1
Davsha	DAS		54.538	109.503	460	1/64	6/65	1
Debin	DBI	ДБН	62.339	150.751	332	–/74	6/86	G
			62.3433	150.7594	332	6/86	--/92	G
Dimnoe			73.233	142.400		3/74	4/74	-
Dovochan	DOV		56.462	117.533	1094	7/62	9/63	1
Dunai	DUYS	ДН	73.92	124.49	5	11/89	---	1
Dyrynmakit			56.60	121.13	460	--/67	--/67	1
Egvekinot	EGVS	ЭГВ	66.323	179.127W	18	–/90	–/94	1
Ekimchan	EKI	ЕКМ	53.067	132.945	485	11/79	---	1
Emegachi	EMG		56.567	118.158	960	9/62	4/63	1
Esso	ESO	ЭСС	55.925	158.700	490	–/65	OPEN	1
Esutoru (Uglegorsk)	ESU		49.083	142.033	100	12/39	--/45	-
Evensk	EVES	ЭВН	61.92	159.23	22	–/80	7/93	1
Firsovo			47.65	142.567	20	8/79	11/79	-
Ganali	GNL	ГНЛ	53.942	157.620	1200	1/88	OPEN	1
Garmanda	GRM	ГРМ	62.18	159.08	140	12/66	5/67	1
Gorely	GRL	ГРЛ	52.552	158.080	1250	7/80	OPEN	1
Gornotaezhnoe	GRZ GRT	ГРТ	43.70	132.15	220	7/90	---	3
Gornovodnoe	GRD GRV	ГРВ	43.70	134.733	270	7/88	---	1
Gornozavodsk			46.567	141.85	50	12/71	6/72	-
Gornyi	GNY	ГРН	50.762	136.455	500	12/78	---	2
Gusinoozersk	GOO	ГСН	51.283	106,517	600	11/71	2/72	1
Ilirnei	ILR	ИЛР	67.26	167.96	350	10/64	10/65	1
Imangra-1			56.75	121.24	395	07/67	08/67	1
Imangra-2	IMNS	ИМГ	56.62	120.71	540	--/75	--/79	1
Institut Vulkanologii	INS		53.066	158.605	175	11/81	OPEN	1
Irkana	IKN		55.867	111.253	480	1/64	3/66	1
Irkutsk	IRK	ИРК	52.272	104.31	467	12/01	OPEN	1
Iul'tin	ILT	ИЛТ	67.87	178.74W	235	3/66	7/93	1
Kabaktan	KBKS	КБК КБТ	56.68	122.42	1010	05/89	08/89	1
Kabansk	KAB	КБ	52.05	106.658	465	1/51		1
Kalgannakh			71.83	114.33		07/21/75	08/10/75	-
Kamenistyi	UL2S	КМН	65.41	144.83	670	--/88	--/88	1

Kamenistaya	KMN		55.76	160.240	1100	10/90	OPEN	1
Kamenskoe	KAM		62.456	166.210		–/94	OPEN	1
Karam	KRMS		55.133	107.583	600	1/66	3/66	1
Karymski - old	KII	КРМ?	54.030	159.480	790	7/74	–/86	1
		КАР?						
Karymski - new	KRY		54.036	159.449	900	9/89	OPEN	1
Khaim	KAIS	ХМ	52.602	108.085	480	10/69	5/70	1
Khandyga	KHG	ХНД	62.65	135.56	125	--/69	--/94	1
Khani	KHNS	ХН	57.04	121.01	390	--/67	--/67	1
						--/75?	--/76?	
Khapcheranga	KPC	ХПЧ	49.707	112.392	950	12/68		1
Khatystyr	KHY	ХТС	55.71	121.57	475	--/68	--/68	1
						--/75	--/82?	
Khingansk	KNN	ХНГ	49.122	131.192	520	7/80	4/84	1
	KNG							
Kigilyakh			73.367	139.867		6/73	9/73	-
Kirovskii	KIRS	КРС	54.428	126.983	440	4/74	---	1
Klyuchi	KLY	КЛЧ	56.313	160.852	80	–/48	---	1
						2/89	OPEN	
Kobdi	AY1S		64.20	145.51	800	06/71	--/71	1
Kolokol'chik						–/67	–/67	
Korito	KRT		55.966	160.222	1000	10/97	OPEN	1
Korsakov						--/51	1/52	-
Koryak	KRK	КРК	53.292	158.636	1050	7.75	OPEN	1
Kotelnyi			75.767	137.60		8/72	9/72	-
Kotikovo			49.133	144.25	10	7/69	9/70	-
Kovokta	KVO	КВК	56.133	113.05	1180	--/81	---	1
Kozelskaya	KZL	КЗЛ	53.201	158.894	950	–/76	–/84	1
Kozyrevsk	KOZ	КЗР	56.05	159.87	40	–/62	–/89	1
Kozyr	KZY		56.070	159.900	450	11/89	OPEN	1
Krestovaya	KTB		52.665	106.395	560	7/71	9/71	1
Krestovskii	KRS		56.214	160.558	1200	7/87	OPEN	1
Kronoki	KRI	КРН	54.596	161.134	5	8/66	OPEN	1
Krutoberegovo	KBG	КБГ	56.255	162.705	10	–/68	OPEN	1
		КБ						
		КРБ						
Kul'dur	KLDS	КЛД	49.205	131.642	425	---	---	1
Kulu	KU-S	КЛ	61.889	147.431	655	1/80	10/92	G
		КЛУ						
Kumora	KMO	КМР	55.883	111.208	475	9/66	---	1
Kurbulik	KBK		53.708	109.038	460	1/64	9/65	1
Kurul'ta			56.90	121.11	495	--/68	--/68	1
Kyakhta	KYA	КХТ	50.35	106.45	760	3.52	5/70	1
Kyubyme			63.38	140.95	950	--/74	--/74	2
Kyusyur	KYUS	КСР	70.68	127.37	20	--/85	08/89	1
Lamutskoe	LMT	ЛМТ	65.54	168.85	178	4/65	10/65	1
Lapri			55.69	124.91	640	--/72	--/73	1

Lazarev	LZR	ЛЗР	52.2	141.493	120	12/80	---	2
Lesogorsk			49.442	142.2	40	7/69	10/69	-
Lopatino			46.6	141.825	40	4/69	10/69	-
Lurbun	LRB		56.63	117.883	780	8/62	9/63	1
						5/67	9.68	1
Magadan	MAG	МГД	59.560	150.805	78	1/52	1/92	1
Magadan-GSN	MA2	MA2	59.575	150.768	339	9/93	OPEN	1
Maiskii	MKI	МАЙ	68.97	173.71	261	8/82	6/94	1
Mal. Ipelka	MIP		52.276	156.758	370	8/97	OPEN	1
Maritui	MRU		51.783	104.217	520	–/08	–/18	1
Markovo	MKV	МРК	64.68	170.41	25	10/86	4/92	1
	MKN							
Matrosova	MATR		61.643	147.82		7/99 - 7/99		G
Mednyi	MED	МДН	54.786	167.556		–/73	–/75	1
Milkovo	MLK	МЛК	54.70	158.63	155	–/62	–/63	1
						10/89	–.93	
Moma-Khonuu	MKUS	MOMA	66.47	143.22	192	--/83	---	1
Moneron			46.258	141.25	40	9/71	5/72	-
Mondy	MOY	МНД	51.673	100.993	1300	–/58		1
Murino	MUO		51.475	104.408	470	8/66	9/66	1
Myakit	MYA	МКТ	61.407	152.093	670	--/83	--/88	G
Mys Kozlova	MKZ		54.556	161.730				1
Mys Khvoinova			74.267	140.883		4/76	6/76	-
Mys Nerpichii			75.833	143.333		4/76	6/76	-
Mys Diring-Ayan			75.950	139.917		5/76	6/76	-
Mys Shmidta	SMT	ШМТ	68.88	179.38W	5	4/65	1/66	1
Nagornyi Sta		НГР	55.92	124.97	920	--/77	--/77	1
Nagornyi			55.95	124.92	840	--/69	--/69	1
Naiba	NAYS	НБ	70.85	130.73	5	--/85	---	1
Nalychevo	NLC	НЛЧ	53.171	159.345	5	–/67	–/67	-
						3/69	12/69	-
						3/84	—	1
Naminga	NMG		56.60	118.517	1380	5/67	4/69	1
Naminga-1	NMG1		56.70	118.583	1160	--/63	--/63	1
Nel'koba	NKBS	НЛБ	61.34	148.81	531	9/83	6/97	1
			61.338	148.813	531	6/97	9/99	G
Nel'koba	NK1	НЛБ	61.34	148.81	531	6/63	1/64	1
Nelyaty	NLY	НЛТ	56.492	115.7	470	1/61	---	1
Nesterikha	NSR	НСТ	53.647	109.708	480	7/70	9/70	1
Neryungri	NYGS	НРГ	56.68	124.66	760	--/77	--/78	1
						--/80	--/82	
			56.657	124.723	840	11.01	OPEN	
Nezhdaninsk	NZDS	НЖД	62.50	139.06	603	--/80	---	1
Nikola	NKO		51.893	104.827	460	7.71	9.71	1
Nikolaevsk-Amur	NKL	НКЛ	53.142	140.783	25	9/70	---	1
Nizhnii Angarsk	NIZ	Н-А	55.766	109.55	487	10/61		1
Nizhnii Armudan			50.817	142.533	150	9/66	4/69	-

Nogliki			51.817	143.15	25	10/64	12/64	-
						--/88	---	-
Novaya Sibir			75.050	147.000		4/75	6/75	-
Nyvrovo	NVV	НВР	54.317	142.617	5	11/81	---	-
O. Vrangelya	VRN	ВРН	70.94	179.62W	10	2/66	4/66	3
Obo	OBO		61.80	149.77	440	--/77	—/77	1
Ogon'ki			46.775	142.383	70	6/68	9/68	-
Oimur	OIM		53.333	106.833	460	10/59	–/60	1
Okha (New)						--/65	---	-
Okha	OKH	ОХА	53.55	142.933	24	12/58	--/65	-
Ol'khon	OLK		53.20	107.342	490	7/69	9.69	1
Okhotsk	OHT	ОХТ	59.3587143.3308			7/2000	OPEN	G
Omchak	OCH	ОМЧ	61.67	147.87	820	9/99	OPEN	1
Omolon	OMO	ОМЛ	65.23	160.54	260	6/82	7/93	1
Omolon-1	OL1	ОМЛ	65.25	160.52	260	12/63	1/65	1
Omsukchan	OS1	ОМС	62.52	155.77	527	1/63	1/64	1
Omsukchan	OMS	ОМС	62.52	155.77	527	12/67	OPEN	1
Onguren	ONR	ОНГ	53.233	107.592	500	–/88		2
Ootomari (Korsakov)	OOT		46.65	142.767	36	--/09	--/45	-
Oran	ORA	ОРН	55.933	113.667	705	9/79	---	1
Orlik	ORA	ОРЛ	56.295	113.983	620	9/78		1
Orotukan	ORT		62.26	151.34	470	--/77	--/77	1
Ossora	OSS	ОСС	59.25	163.065	10	–/73	OPEN	1
Ostrov Mednyi	MED	МДН	54.786	167.566	---	–/73	–/75	-
Otiai (Bykov?)	OTI		47.325	142.783	20	2/34	--/45	-
Ozernaya	OZE	ОЗН	56.295	113.983	620	9/78	---	1
Ozernaya	AY2S	ОЗР	63.75	146.11	875	06/71	--/71	2
Ozero	OZR	ОЗР	54.692	160.392	---	10/66	–/77	1
Ozhidaevo			47.033	142.392	220	--/76	--/77	-
Pakhach	PCH		60.558	169.125		–/92	–/94	1
Palana	PAL		59.093	159.963		–/94	–/96	1
Pauzhetka	PAU	ПЖТ	51.467	156.810	110	11/61	OPEN	1
Petropavlovsk	PET	ПТР	53.024	158.650	150	–/51	OPEN	1
Pevek	PVK	ПВК	69.70	170.27	20	5/65	11/65	1
Podkova	PDK	ПДК	56.140	160.780	800	–/83?	OPEN	1
Polovinka	PLK		51.798	104.35	470	8/66	9/66	1
Pravda			46.942	142.008	40	9/71	11/71	-
Provideniya	PVD	ПРВ	64.424	173.226W	25	9/80	12/93	1
Provideniya-1	PV1	ПРВ	64.45	173.18W	20	1/65	6/66	2
Romny	RMNS	РМН	50.855	129.4	210	10/78	–/87	2
Russkaya	RUS	РУС	52.432	158.507	75	12/87	OPEN	1
Saidy	SAYS	СД	68.70	134.45	88	--/80	---	1
Sasyr	SSYS	ССР	65.16	147.08	580	--/86	---	1
Savino	SOV		52.543	102.15	720	9/68	8/69	1
Sedlovina	SDL		53.278	158.884	1235	9/91	---	1
Semlyachik	SEL	СМЛ	54.12	159.98	---	11/61	7/74	1

Severo Baikalsk	SVBS	С-Б	55.64	109.35	505	–/78	–/89	1
Severo Muisk	SVK	С-М	56.183	113.533	850	11/76	---	2
Seymchan	SEY	СМЧ	62.9339	152.3844	211	4/69	OPEN	G
Shamanka	SHMS		53.125	105.6	700	8/59	2/63	1
Shara-Tagot	SRTS		53.005	106.717	500	10/59	–/60	1
Shebunino			46.433	141.858	40	9/71	11/71	-
Shikka	SKK		49.233	143.117	2	--/28	--/45	-
(Shikuka; Poronaisk)								
Shimki	SMKS		51.675	102.012	765	11/66	11/67	1
Shipunski	SPN	ШПН	53.107	160.011	170	–/62	OPEN	1
Sinegor'e	SNES	СНГ	62.09	150.52	400	--/76	--/88	1
Slyuda			56.33	124.12	1080	--/73	--/73	2
Solontsovaya	SOL	СЛЦ	54.17	108.35	458	–/79	–/87	1
Sovetskaya Gavan			48.967	140.283	50	6/69	11/70	-
Srednekolymsk	S-K	С-К	67.46	158.71	30	4/64	12/64	1
Srednii Kalar	SRK	КЛР	55.86	117.38	716	–/61	---	1
Srednii Sakutan	SDK		56.898	118.095	750	2/63	10/63	1
Stekol'nyi	STK	СТК	60.046	150.730	221	7/64	5/66	1
Stekol'nyi	MGD	МА1	60.046	150.730	221	3/71	–/94	1
		МГД-1	(60.046)	(150.730)		–/94	OPEN	1
		СТК						
Stokolviya	STV		61.8475	147.6598		7/99 - 7/99		G
Stolb	SOTS	СТБ	72.40	126.82	10	--/85	---	1
Susuman	SUUS	СМН	62.7786	148.1503	640	8/69	--/95	G
		ССМ	62.7786	148.1481	640	--/95	--/98	G
			62.779	148.163	640	--/98	OPEN	G
Sutam			55.96	127.59	700	--/69	--/69	1
Suvo	SUVS	СУВ	63.655	110.008	1000	–/84	---	1
Syllakh	SYLS	СЛХ	57.12	121.86	600	--/89	--/89	1
Syul'ban	SYB		56.065	117.222	1000	6/62	9/63	1
Tabalakh	TBKS	ТБЛ	67.54	136.52	200	--/80	---	1
		ТБ						
Taimylyr	TMLS	ТМЛ	72.61	121.92	60	--/86	---	1
		ТМР						
Takhtoyamsk	TTY	ТХТ	60.20	154.68	11	9/87	---	1
Talaya 1and 2	TL-	ТЛА	61.1325	152.3952	730	1/89	OPEN	G
	TLAR	ТЛ						
Talaya	TAL	ТАЛ	51.681	103.644	579	11/82	OPEN	1
Tal-Yuryakh	TUR	TUR	63.307	146.634	900	3/01	6/01	G
Talon	TON	TON	59.757	148.661	20	1/01	2/01	G
TasYuryakh-1			56.64	121.33	395	02/67	03/67	1
TasYuryakh-2			56.62	121.41	415	07/67	08/67	1
Tauisk	TAUS	TAUS	59.729	149.335	5	1/01	4/01	G
Tenkeli	TLIS	ТНК	70.18	140.78	110	--/84	--/93	1
Ternei	TEI	ТРН	45.067	136.6	30	7/82	---	2
Tilichiki	TIL		60.433	166.075		–/94	–/96	1
Tikhmenevo			49.2	142.9	150	6/69	10/69	-

Tiksi	TIK	ТКС	71.632	128.863	38	3/56	--/93	1
TIXI	Tiksi-GSN		71.64	128.87	30	--/95	OPEN	1
Tokarikan			56.10	126.42	800	--/72	--/73	3
Tokhoi	TKH	ТХ	51.361	106.608	640	11/71	4/73	1
Tonnel'nyi	TNL	ТНЛ	56.283	113.35	820	11/76	---	1
Topolovo	TOP	ТОП ТПЛ	53.230	158.041	155	11/61	–/93	1
Toyohara (Yuzhno)						--/43	--/45	-
Tsipikan	ZIP	ЦРК	54.917	113.35	1110	–/75	2/86	1
Tsiveluch	SVL	ШВЛ	56.583	161.225	900	10/80	OPEN	1
Tungurcha-1	TUG1		57.33	121.48	440	--/70	--/70	1
Tungurcha-2	TUG	ТНГ	57.27	121.48	315	--/78	---	1
Tungusskii	AY3S		64.20	146.38	1080	--/71	--/71	1
Tupik	TUP	ТПК	54.425	119.933	630	11/61	---	1
Turan	TRNS		51.633	101.666	870	12/66	11/68	1
Turikan	TRKS	ТРК	56.383	113.108	695	8/81	---	1
Tymovskoe	TYV TMSS	ТМС	50.85	142.65	100	4/69	---	-
Tynda	TYD	ТНД	55.133	123.717	610	7/70	1/72	2
Tyrgan	TRG	ТРГ	52.758	106.342	600	1/60		1
Tyubelyakh	UL1S	ТЕБ	65.37	143.15	380	--/88	--/88	3
Uakit	UKT	УКТ	55.495	113.62	1140	12/62	–/75	2
Udokan	UDK		56.75	118.305	810	4/67	4/69	1
Udzha			71.25	117.17		08/27/75	09/19/75	-
Uelen			66.16	169.84W	5	--/81	–/82	1
Uglegorsk	UGL	УГЛ	49.083	142.083	20	-/51	---	-
Ulyukchikan	UCK	УЛК	53.87	109.598	490	7/70	9/70	1
Ulyunkhan	ULNS	УЛХ	54.867	111.07	560	7/89	OPEN	2
Uoyan	YOA	УН	56.13	111.77	520	–/79	---	1
Ust' Nera-1	UNR1	У-НР	64.566	143.230	485	--/62	--/92	1
Ust' Nera-2	UNR	У-Н	64.565	143.242	485	--/92	OPEN	G
Ust' Nyukzha	USZ	У-Н	56.56	121.59	415	--/64	---	1
Ust' Urkima	UURS	УРК	56.31	123.16	540	8/81	3/99	1
Ust' Bolsheretsk	UBL		52.842	156.308	20	11/61	–/64	1
Ust' Belaya	U-B	У-Б	65.51	173.28	20	11/66	5/67	1
Ust' Srednikan SRD		СРД	62.44	152.32	580	12/62	11/63	1
Ust' Omchug	USO	У-ОМ	61.13	149.63	580	--/68	--/83	1
Utesnoe			46.6	143.075	20	7/73	9/79	-
Vankarem	VNK	ВНК	67.84	175.85W	10	3/66	6/66	1
Verkhene Kamchatsk	VKM		54.627	158.473	170	10/66	–/75?	1
Vladivostok	VLA	ВЛД	43.12	131.893	75	–/29	–/31	-
Vodopadnii	VDP	ВДР	55.770	160.220	1060	–/77	–/91	1
Vzmor'e			48.85	142.517	20	7/82	12/82	-
Yablochnyi			47.167	142.067	20	6/68	9/68	-
Yagodnoe	YAG		62.53	149.62	480	--/77	--/77	1
Yakutsk-1	YAK1		62.015	129.722	90	10/57	--/62	1
Yakutsk-2	YAK	ЯК	62.030	129.677	91	--/62	OPEN	1

Yaruga	YRGS	ЯРГ	57.49	123.07	780	--/89	--/89	2
Yasnyi	YASS	ЯСН	53.29	127.983	310	1/75	--	1
Yubileniya	YUBS	ЮБЛ ЮБТ	70.74	136.10	10	--/86	--/93	1
Yuzhno Sakhalinsk	YSS	ЮСХ	46.958	142.762	100	--/57	OPEN	1
Yuzhno Sakhalinsk (Novo Aleks-androvsk)	YSS1		47.02	142.717	40	10/47	--/57	-
Zakamensk	ZAK	ЗКМ	50.383	103.292	1125	12/60	---	1
Zapadnyi	ZAP		56.613	118.433	1600	4/67	8/67	1
Zarech'e	ZARS		52.550	107.15	460	7/59 7/69	–/60 9/69	1
Zarya	ZRY		57.24	118.917	655	10/59	9/68	2
Zemlya Bunge			74.833	142.583		4/75	6/75	-
Zeya	ZEA	ЗЕЯ	53.755	127.293	270	6.76	--	1
Zhigalovo	ZGL		54.808	105.15	625	12/67	2/67	1
Zhuravlikha	ZRV	ЖРВ	53.517	109.375	475	7/70	9/70	1
Zimniki	ZMN	ЗМН	45.475	134.258	150	7/88	--	2
Zyryanka	ZYRS	ЗРН	65.72	149.82	120	--/82	--/90	1
Zyryanka-1	ZY1	ЗРН	65.74	150.89	37	1/64	10/64	1

APPENDIX B

Relocations of events used to determine crustal velocities

DATE	TIME h	m	s	LAT.	LONG	DEP. km	MAG.
700321	11	21	10.84	56.92N	133.18E	6.8	.
700919	08	53	32.16	57.38N	127.50E	10.3	.
701014	23	57	13.00	56.61N	124.78E	33.0	.
710126	09	08	35.28	58.00N	126.75E	9.1	.
710202	12	11	40.74	63.49N	146.12E	8.4	.
710220	14	05	13.95	56.41N	127.41E	0.	.
710318	20	08	41.2	55.77N	133.48E	3.4	.
710414	11	18	03.2	56.54N	121.07E	7.1	.
710518	22	44	41.90	64.05N	145.76E	33.1	7.1
710518	23	09	08.04	64.14N	146.05E	1.2	.
710519	00	33	04.31	64.07N	145.79E	4.2	.
710519	02	53	46.48	63.99N	145.84E	11.9	.
710519	16	35	16.69	64.08N	145.83E	0.	.
710529	09	19	15.99	64.12N	145.68E	1.2	.
710607	12	09	46.79	64.02N	145.61E	4.7	.
710614	13	48	52.9	56.25N	123.70E	18.3	.
710614	14	25	54.0	56.20N	123.67E	12.7	.
710707	21	50	43.65	64.02N	146.13E	1.4	.
710801	18	50	05.62	56.90N	127.63E	19.7	.
710809	11	51	53.7	56.22N	123.59E	18.8	.
710812	09	54	22.2	56.18N	123.85E	3.0	.
710812	11	44	06.66	66.05N	142.20E	14.1	.
710912	13	32	57.46	65.89N	142.34E	33.1	.
711001	15	13	13.56	63.35N	150.37E	5.9	.
711004	12	59	08.33	66.12N	142.11E	0.0	.
711008	03	27	30.6	56.26N	123.60E	16.5	.
720113	17	24	17.07	61.63N	147.11E	0.9	.
720113	22	20	12.45	61.86N	147.11E	9.0	.
720115	18	08	00.1	57.69N	121.10E	4.5	.
720117	09	22	49.64	61.91N	147.12E	7.9	.
720117	10	38	29.25	61.87N	147.17E	11.4	.
720120	15	38	38.88	54.25N	127.24E	17.9	.
720120	19	48	46.28	62.51N	145.01E	16.3	.
720214	22	35	35.9	57.28N	122.14E	16.9	.
720330	20	20	52.40	64.01N	145.97E	6.1	.
720401	10	00	26.5	56.52N	121.08E	14.1	.
720404	11	32	18.77	54.54N	134.83E	1.8	.
720421	10	41	42.75	63.69N	151.47E	13.8	.
720428	02	57	24.6	56.63N	121.18E	13.2	.
720504	14	20	02.20	61.84N	147.11E	4.7	.
720509	21	32	25.47	67.39N	139.31E	33.0	.
720513	16	17	50.5	55.42N	124.13E	10.4	.
720519	08	42	44.17	54.01N	128.64E	21.6	.
720602	08	32	52.28	64.02N	146.10E	11.2	.
720613	10	45	03.55	54.88N	126.46E	19.7	.
720620	09	18	25.57	57.34N	127.66E	9.7	.
720717	03	05	10.56	64.10N	145.79E	14.9	.
720809	20	51	46.90	56.88N	127.80E	12.2	.
720811	12	45	21.1	53.95N	128.19E	7.1	.
720831	13	43	17.2	56.07N	124.56E	7.2	.
720908	19	48	53.4	56.00N	130.60E	0.0	.
721221	02	12	57.58	62.82N	140.45E	4.0	.
730130	22	53	22.38	56.69N	128.83E	0.	.
730222	05	44	15.1	54.07N	123.91E	30.1	.
730429	06	18	50.6	54.58N	124.72E	9.5	.
730519	02	24	24.80	59.98N	152.87E	0.	.
730527	05	49	09.67	62.23N	161.72E	2.5	.
730608	11	43	47.07	63.82N	146.17E	26.1	.
730616	02	12	18.31	59.99N	152.63E	11.1	.
730618	13	59	47.7	56.84N	121.05E	9.2	.
730727	15	09	19.99	60.19N	153.55E	0.	.
730813	06	50	19.74	62.68N	145.62E	4.6	.
730820	21	03	41.27	60.92N	148.05E	12.9	.
730821	01	26	53.05	67.09N	139.59E	0.8	.
730915	07	15	05.94	63.24N	154.41E	13.7	.
731012	03	08	38.48	61.40N	142.99E	0.	.
731022	05	12	56.0	57.54N	121.05E	30.9	.
731026	11	26	57.1	56.23N	123.55E	13.3	.
731028	17	45	51.02	64.07N	145.76E	7.2	.
731102	07	31	28.68	54.10N	125.71E	0.	.
731102	12	14	45.89	54.26N	125.80E	12.8	.
731114	17	12	35.60	62.27N	143.25E	0.	.
740111	23	10	18.93	60.51N	153.11E	0.	.
740406	19	00	50.33	62.19N	153.23E	5.8	.
740411	20	32	36.14	61.71N	156.78E	10.0	.
740426	03	33	13.06	57.29N	127.79E	8.7	.
740516	09	05	19.6	56.16N	123.74E	7.2	.
740518	06	45	06.25	59.26N	148.66E	30.0	.
740619	03	09	36.78	63.26N	151.10E	30.0	.
740629	14	33	23.9	56.55N	121.05E	7.5	.
740702	09	19	19.70	66.85N	139.51E	20.0	.
740702	17	04	03.15	66.53N	138.27E	12.2	.
740727	12	19	51.68	54.52N	127.23E	25.4	.
740829	06	18	51.37	59.89N	152.49E	33.0	.
740829	13	54	21.96	57.25N	127.24E	0.	.
740928	15	01	25.31	67.00N	139.41E	33.0	.
741206	12	43	09.95	67.92N	140.21E	33.0	.
741217	07	11	03.74	66.15N	125.79E	0.	.
741217	16	40	13.77	60.23N	153.15E	15.6	.
741220	22	58	13.94	64.12N	145.89E	16.5	.
741223	04	20	10.71	59.09N	150.41E	5.4	.
750119	16	22	33.76	59.82N	161.23E	16.5	.
750227	02	09	11.90	66.86N	129.02E	1.0	.
750315	07	36	42.3	56.27N	122.96E	10.9	.
750317	12	14	12.62	63.31N	146.09E	18.2	.
750629	12	24	39.6	53.11N	132.13E	4.7	.
750812	15	00	00.6	70.76N	126.95E	0.5	5.1
750921	09	30	37.5	54.13N	122.26E	31.7	.
750921	10	03	29.3	54.20N	122.33E	24.6	.
750924	20	12	54.91	66.13N	143.43E	3.8	.
751103	12	06	58.01	57.70N	126.24E	0.	.
751104	12	41	06.83	59.81N	160.17E	10.3	.
751224	01	29	02.01	61.85N	144.28E	0.	.
751227	03	54	20.52	62.06N	154.92E	10.9	.

760121	06	01	48.46	67.69N	140.27E	22.7	5.3
760216	22	06	23.82	58.17N	131.02E	4.4	4.6
760226	17	23	03.3	56.53N	121.10E	12.8	.
760408	04	20	58.28	67.03N	139.69E	10.0	.
760426	20	12	21.41	61.77N	155.97E	13.5	.
760508	11	39	25.77	60.09N	152.72E	2.3	.
760520	16	53	29.2	56.36N	132.48E	0.0	.
760614	11	58	01.9	55.57N	130.72E	5.9	.
760624	17	58	01.07	59.94N	157.70E	33.2	.
760627	16	03	23.8	55.39N	131.22E	1.8	.
760704	23	23	31.80	65.60N	134.98E	25.7	.
760730	21	53	19.7	55.61N	132.87E	0.0	.
760803	16	21	29.55	60.26N	146.99E	19.7	.
760907	20	04	29.02	61.19N	156.07E	15.2	.
760930	21	05	38.48	57.96N	147.55E	26.2	.
761120	08	02	54.3	54.02N	122.20E	12.0	.
761121	15	51	55.5	54.15N	121.98E	22.9	.
761124	18	33	34.1	54.12N	122.25E	31.8	.
761203	01	50	34.7	54.13N	122.17E	25.6	.
761203	03	55	56.5	54.14N	122.01E	17.9	5.
770116	00	09	28.9	55.66N	130.54E	5.1	.
770124	15	19	56.83	58.99N	149.38E	28.6	.
770203	11	13	24.99	61.40N	156.81E	7.7	.
770215	06	58	07.97	62.47N	147.00E	7.8	.
770410	15	48	43.99	65.99N	142.04E	0.	.
770422	18	29	12.41	54.48N	125.35E	13.9	.
770502	06	50	14.1	56.64N	121.19E	8.5	.
770503	11	40	26.00	60.70N	161.31E	33.1	.
770504	03	18	29.9	57.68N	121.11E	17.2	.
770514	21	18	57.11	58.96N	150.66E	18.5	.
770611	19	28	33.3	52.75N	123.49E	33.0	.
770627	17	47	15.58	62.80N	146.19E	6.4	.
770720	00	31	40.58	54.72N	126.43E	6.7	.
770720	02	03	37.90	54.73N	126.40E	7.1	.
770816	13	56	54.40	53.84N	128.86E	0.	.
771101	03	54	22.5	55.56N	130.64E	3.8	.
771106	04	31	20.26	59.20N	146.48E	24.5	.
771118	21	55	36.23	60.14N	143.42E	9.1	4.7
771210	11	42	23.79	54.11N	125.89E	3.8	.
780103	03	17	39.05	67.81N	139.38E	0.	.
780201	01	08	38.6	54.20N	123.00E	33.0	.
780207	04	55	21.69	63.27N	146.33E	6.1	.
780213	05	27	00.9	54.26N	122.97E	33.0	.
780222	23	41	46.48	63.08N	146.13E	12.0	.
780328	18	57	20.05	58.79N	151.04E	8.9	.
780401	16	56	35.7	56.86N	120.75E	19.7	.
780428	14	56	23.9	53.74N	124.99E	12.0	.
780505	16	06	58.25	67.61N	139.25E	23.7	.
780601	07	40	14.5	56.52N	121.20E	9.5	.
780605	07	05	56.92	60.12N	160.06E	31.8	.
780605	21	01	40.67	60.11N	159.72E	33.1	.
780622	06	12	35.73	62.94N	145.34E	5.8	.
780626	02	51	20.89	55.82N	126.31E	10.0	.
780630	11	57	01.5	53.92N	125.71E	11.9	.
780805	23	12	20.27	58.39N	134.48E	5.8	.
780821	10	15	53.4	55.21N	124.81E	15.2	.
780822	17	41	38.55	61.23N	144.48E	3.1	.
780822	18	26	27.02	61.27N	159.97E	19.0	.
781027	06	34	39.54	64.63N	145.36E	9.8	.
781201	13	25	59.4	55.17N	124.03E	5.9	.
781206	08	20	46.30	63.61N	144.27E	6.6	.
781211	14	05	58.9	53.82N	125.65E	12.7	.
790103	03	20	27.4	52.61N	127.48E	12.2	.
790104	21	50	16.7	54.18N	122.96E	29.2	.
790221	15	03	27.35	63.37N	146.28E	6.6	.
790427	19	38	13.8	55.76N	130.47E	12.7	.
790428	09	34	06.23	57.45N	126.92E	10.7	.
790502	22	10	28.88	64.19N	149.21E	2.5	.
790517	06	39	09.4	53.70N	126.09E	8.3	.
790523	17	37	33.9	53.61N	126.09E	21.2	.
790531	10	49	26.2	55.68N	130.26E	14.5	.
790531	11	52	35.3	56.51N	124.88E	13.8	.
790616	20	41	48.41	64.89N	143.67E	26.7	.
790618	22	09	57.41	57.50N	126.06E	5.3	.
790623	08	22	37.82	58.14N	133.73E	4.9	.
790627	17	45	11.6	53.18N	135.16E	0.0	.
790713	15	12	46.9	62.29N	130.29E	18.1	.
790727	04	28	47.64	63.08N	172.66E	11.3	4.4
790818	19	31	47.9	60.60N	131.82E	29.3	.
790819	07	10	00.09	61.28N	159.81E	7.0	.
790827	02	55	01.00	62.97N	145.53E	11.0	.
791007	01	29	26.10	64.99N	144.03E	13.0	.
791026	00	26	26.24	62.19N	153.87E	13.4	.
791111	19	27	35.91	62.27N	153.75E	12.2	.
791116	07	24	05.1	56.45N	124.26E	11.0	.
791118	08	59	15.84	62.24N	153.80E	11.9	.
791229	04	22	16.69	61.45N	142.68E	9.5	.
800102	00	42	39.20	59.68N	156.07E	9.1	.
800110	20	57	35.50	64.14N	148.58E	10.9	.
800125	18	45	46.77	64.07N	146.00E	18.2	.
800127	18	55	40.06	63.36N	150.50E	5.1	.
800128	05	11	57.58	63.42N	150.57E	12.1	.
800129	08	55	17.59	64.07N	149.02E	11.0	.
800129	17	35	52.83	61.01N	155.80E	5.4	.
800201	17	30	17.83	73.27N	119.98E	15.4	5.7
800205	11	10	32.8	66.79N	146.58E	0.0	.
800205	13	14	04.8	55.95N	122.59E	28.1	.
800214	04	09	46.0	52.24N	126.67E	23.4	.
800225	23	50	02.67	54.91N	125.21E	31.5	.
800307	03	15	14.22	62.01N	150.50E	15.0	.
800311	18	11	21.46	56.99N	127.72E	2.6	.
800321	15	03	55.7	51.46N	133.19E	22.6	.
800321	17	26	51.0	51.32N	133.26E	20.6	.
800404	23	10	18.84	63.23N	148.07E	5.2	.
800406	02	28	55.0	54.00N	127.93E	24.8	.
800422	19	07	44.66	65.55N	136.65E	1.0	.
800507	05	04	35.	60.25N	152.03E	23.	.
800508	10	28	11.16	62.65N	155.32E	7.2	.
800512	09	06	56.82	63.24N	147.70E	0.	.
800512	09	09	13.57	63.15N	147.67E	4.0	.
800512	19	30	13.46	63.14N	147.64E	5.2	.
800514	08	24	07.0	49.66N	130.13E	22.8	.
800514	19	20	30.8	49.66N	130.15E	24.6	.
800516	20	53	46.73	57.58N	128.06E	11.0	.
800519	17	29	47.00	59.92N	144.24E	28.1	.
800602	13	15	06.91	62.85N	145.86E	8.2	.
800607	02	04	51.54	64.30N	145.41E	3.2	.
800616	01	52	29.36	58.85N	150.11E	7.4	.
800622	00	07	48.34	59.76N	146.14E	1.8	.
800701	03	57	15.52	56.32N	125.67E	19.3	.
800706	22	02	07.74	56.77N	127.66E	5.5	.
800714	10	20	17.22	64.16N	154.68E	11.7	.
800719	17	21	11.52	56.99N	127.71E	13.2	.
800720	03	19	07.92	59.47N	144.63E	10.3	.
800723	11	51	13.23	62.57N	155.34E	12.2	.
800808	16	36	33.95	59.43N	147.91E	7.8	.

800829	16	31	55.01	56.14N	129.59E	19.4	.
800916	11	17	51.81	61.52N	143.29E	14.4	.
800919	18	28	49.57	63.23N	148.22E	10.4	.
801015	02	52	49.8	54.73N	133.90E	12.6	.
801021	18	06	19.7	58.56N	121.81E	29.0	.
801103	06	31	10.23	63.35N	146.25E	7.8	.
801127	14	26	00.38	57.51N	125.66E	11.0	.
801203	17	58	15.05	63.65N	152.22E	8.7	.
801208	05	27	22.59	58.79N	149.86E	14.4	.
801217	08	59	42.56	67.11N	129.08E	11.3	.
801223	01	38	02.8	53.47N	132.31E	16.2	.
801229	20	19	07.83	69.73N	139.11E	4.0	.
801231	05	00	17.98	63.92N	140.69E	23.9	.
810202	19	15	15.92	62.36N	144.44E	14.4	.
810217	12	15	13.34	64.12N	145.91E	11.5	.
810222	23	06	20.73	63.15N	150.98E	3.9	.
810301	18	39	33.88	62.14N	143.25E	7.3	.
810304	10	43	02.8	57.78N	120.68E	10.6	.
810313	12	49	58.16	63.79N	149.07E	12.0	.
810315	03	50	34.85	69.63N	137.59E	24.7	.
810324	17	06	38.46	64.75N	149.55E	2.7	.
810404	11	49	19.38	62.41N	144.65E	21.4	.
810406	08	34	37.05	63.38N	146.70E	4.2	.
810429	02	35	28.81	59.62N	144.09E	0.	.
810505	02	08	19.66	56.25N	125.86E	20.0	.
810509	07	48	28.43	56.67N	127.48E	2.6	.
810510	18	08	26.38	61.54N	157.26E	10.1	.
810522	04	59	20.88	61.12N	156.72E	9.4	.
810527	02	57	00.51	54.40N	125.55E	24.8	.
810527	08	45	21.41	54.36N	125.52E	17.6	.
810528	12	17	09.2	48.50N	130.71E	13.6	.
810718	19	53	51.16	59.79N	153.93E	9.5	.
810718	20	08	30.13	59.91N	153.89E	5.5	.
810803	08	16	38.50	70.43N	130.49E	25.9	.
810809	19	13	39.23	63.36N	146.36E	6.9	.
810809	19	17	02.62	63.27N	146.12E	30.0	.
810817	06	58	08.16	63.11N	147.99E	1.3	.
810819	19	17	29.66	67.56N	140.25E	9.1	.
810820	14	14	38.3	57.66N	121.08E	13.1	.
810826	10	45	04.91	58.46N	140.97E	7.2	.
810905	01	52	59.2	51.17N	132.33E	12.4	.
810905	13	01	33.50	59.75N	146.71E	1.5	.
811006	23	32	06.91	63.17N	150.96E	9.1	.
811021	05	16	42.79	63.40N	146.21E	6.2	.
811022	12	45	40.9	53.13N	134.55E	21.9	.
811028	11	38	05.58	60.81N	142.80E	15.0	.
811103	03	43	01.29	70.28N	141.03E	7.9	.
811105	06	15	33.38	62.06N	150.39E	15.0	.
811108	21	56	09.35	61.82N	153.64E	21.9	.
811109	00	33	20.34	61.83N	153.67E	12.1	.
811109	05	23	40.20	61.80N	153.71E	13.0	.
811110	10	07	51.78	63.97N	148.67E	5.2	.
811110	10	54	15.80	63.92N	148.71E	10.7	.
811111	14	22	18.67	61.85N	153.62E	14.9	.
811111	15	29	48.07	61.79N	153.68E	5.1	.
811120	18	06	37.5	56.68N	122.59E	12.5	.
811122	21	44	48.9	51.85N	122.59E	14.8	.
811203	14	41	25.70	63.93N	148.55E	13.4	.
811205	01	49	09.0	57.00N	123.15E	18.0	.
811208	02	17	05.93	59.88N	153.82E	7.8	.
811208	10	57	21.18	61.83N	153.67E	15.8	.
811212	01	05	58.29	59.60N	148.10E	33.0	.
811215	19	19	13.75	61.82N	153.63E	5.6	.
811221	04	58	05.42	62.43N	150.13E	16.6	.
811229	05	10	34.93	61.99N	149.83E	8.8	.
820120	03	12	45.08	61.20N	156.99E	2.4	.
820123	04	15	49.58	62.73N	179.68E	11.6	.
820123	16	19	36.27	64.00N	154.30E	6.4	.
820123	19	55	36.54	63.03N	144.75E	11.3	.
820123	21	38	24.81	63.00N	144.79E	5.6	.
820124	17	02	37.01	62.66N	179.81E	31.7	.
820214	10	12	52.59	58.87N	155.13E	8.6	.
820223	17	29	56.14	63.26N	146.14E	13.3	.
820307	01	21	31.56	63.88N	148.62E	9.9	.
820316	19	23	28.2	53.02N	134.86E	14.0	.
820325	10	52	35.4	51.43N	131.94E	9.5	.
820404	11	45	28.18	66.04N	143.11E	33.	.
820406	14	41	13.75	61.79N	153.61E	3.2	.
820407	07	22	01.3	55.58N	130.50E	2.0	.
820416	08	11	13.9	51.12N	132.39E	7.4	.
820427	19	40	54.4	51.33N	136.85E	33.0	.
820502	03	28	35.6	52.59N	136.21E	10.9	.
820504	23	35	10.82	66.01N	172.91E	23.2	.
820623	08	04	28.92	60.50N	137.85E	0.	.
820626	18	47	11.32	63.33N	178.55E	14.1	.
820706	06	16	39.01	65.43N	136.47E	4.0	.
820707	01	40	12.00	55.78N	125.57E	18.6	.
820724	08	39	02.38	63.58N	146.24E	3.8	.
820725	14	29	38.52	59.85N	145.78E	12.5	.
820730	01	51	46.2	56.60N	121.07E	13.9	.
820803	05	41	52.19	64.17N	148.95E	14.2	.
820804	20	17	03.66	62.39N	146.95E	5.9	.
820806	19	06	42.31	54.00N	139.66E	22.0	.
820903	07	29	26.80	66.99N	133.53E	26.1	.
821005	01	52	27.36	54.37N	126.08E	23.6	.
821011	02	10	28.85	54.57N	126.27E	10.5	.
821217	16	42	35.96	59.64N	144.15E	20.2	.
821221	16	01	47.80	54.37N	126.08E	21.8	.
821222	12	10	02.78	64.04N	156.70E	12.4	.
821222	15	47	03.61	59.18N	152.70E	7.6	.
830104	07	17	14.13	62.14N	143.68E	4.2	.
830114	01	57	13.11	67.29N	172.44W	5.4	.
830122	05	20	29.4	53.66N	135.97E	14.8	.
830123	23	24	25.79	65.99N	172.89W	6.3	.
830130	08	44	30.40	65.98N	172.90W	8.5	.
830205	09	21	42.2	53.05N	127.18E	20.3	.
830207	15	34	27.0	53.53N	128.51E	31.8	.
830214	15	21	05.47	62.46N	145.83E	3.7	.
830307	18	42	19.9	56.73N	134.47E	7.0	.
830312	11	55	12.43	64.23N	140.96E	14.1	.
830315	22	10	24.4	51.50N	134.89E	0.0	.
830323	14	45	06.73	62.96N	155.66E	10.7	.
830325	10	36	56.02	63.54N	149.93E	8.1	.
830404	14	37	35.26	66.97N	140.09E	13.6	.
830409	19	57	18.73	69.26N	178.36E	16.5	.
830427	00	30	36.7	50.49N	132.23E	11.2	.
830504	06	52	56.55	57.54N	125.38E	17.1	.
830509	16	48	05.84	63.27N	146.26E	8.9	.
830510	05	27	24.32	64.21N	150.95E	5.0	.
830514	08	09	13.46	65.85N	174.82E	0.	.
830515	04	53	38.49	65.90N	173.19W	11.5	.
830515	04	57	19.77	65.96N	173.03W	0.9	.
830515	05	05	43.42	65.96N	173.07W	4.8	.
830515	06	00	36.69	65.86N	173.24W	2.9	.
830515	06	22	47.62	65.96N	173.04W	8.1	.
830515	06	37	06.34	65.89N	173.09W	6.0	.

830516	03	28	29.67	65.93N	173.13W	6.8	.
830516	06	33	56.24	65.92N	173.13W	11.2	.
830516	18	41	00.86	65.94N	173.02W	15.6	.
830517	04	14	02.01	65.95N	173.03W	0.	.
830518	12	07	58.96	65.94N	173.12W	6.9	.
830528	02	57	57.57	61.98N	150.43E	6.0	.
830530	07	04	18.66	65.94N	173.05W	5.0	.
830608	18	29	43.26	59.40N	148.07E	7.9	.
830626	05	43	56.98	71.26N	129.65E	28.0	.
830629	13	42	55.77	61.98N	152.56E	10.5	.
830706	18	49	44.70	58.61N	147.65E	12.9	.
830710	14	40	45.9	48.51N	134.03E	12.5	.
830730	15	42	09.4	53.30N	132.48E	13.2	4.8
831012	16	07	25.11	60.04N	149.98E	8.0	.
831025	19	44	59.98	60.03N	153.04E	9.9	.
831107	14	20	58.82	65.43N	136.53E	17.7	.
831112	01	17	41.12	57.64N	125.43E	2.3	.
831125	11	22	43.6	51.05N	132.87E	10.0	.
831201	15	48	43.45	63.62N	142.82E	8.8	.
831211	11	01	15.96	59.60N	147.18E	5.8	.
831224	15	17	31.39	62.91N	145.46E	2.1	.
840108	23	18	37.35	54.47N	125.09E	24.2	.
840203	18	35	55.8	49.38N	128.26E	26.4	.
840217	20	34	18.89	59.76N	152.45E	10.3	.
840307	12	24	10.23	54.45N	136.98E	11.9	.
840324	01	03	19.16	54.50N	136.96E	12.9	.
840324	02	23	40.11	54.57N	137.04E	8.4	.
840401	22	43	47.84	59.42N	146.56E	5.4	.
840403	02	53	24.94	57.54N	125.53E	0.	.
840405	10	35	22.25	58.66N	148.70E	2.9	.
840411	20	50	38.97	59.29N	147.99E	6.0	.
840524	20	55	36.98	63.69N	145.58E	0.2	.
840529	06	20	22.54	63.29N	146.60E	0.	.
840625	08	13	17.87	62.10N	157.05E	2.2	.
840707	08	06	53.55	59.81N	152.62E	0.	.
840716	18	26	43.59	66.58N	170.47E	0.	.
840802	21	25	39.50	60.89N	144.59E	23.3	.
840808	22	33	46.33	63.29N	152.78E	15.9	.
840812	14	45	31.8	49.05N	131.42E	17.4	.
840821	17	41	02.66	60.92N	153.85E	06.7	.
840912	20	10	41.05	59.37N	138.57E	8.8	.
840915	13	52	08.39	54.30N	126.37E	23.6	.
840919	11	36	33.01	63.44N	145.63E	17.9	.
840926	19	01	08.5	57.60N	120.91E	7.2	.
841003	13	11	04.74	63.22N	176.81E	9.2	.
841019	20	26	26.4	57.04N	120.68E	13.0	.
841020	08	41	36.21	54.23N	126.24E	22.2	.
841029	14	06	14.17	62.13N	163.77E	19.9	.
841101	21	49	03.4	52.86N	138.86E	11.4	.
841103	18	48	55.0	49.19N	139.91E	8.2	.
841117	22	40	15.8	52.71N	135.62E	11.0	.
841121	07	31	36.2	56.84N	121.09E	18.1	.
841122	13	52	57.27	68.47N	140.84E	21.8	.
841129	21	03	33.2	50.66N	132.60E	21.2	.
841202	08	35	44.98	63.39N	150.50E	20.6	.
841202	12	32	02.58	63.38N	150.50E	0.	.
850103	12	47	13.82	55.81N	129.36E	18.1	.
850104	09	08	57.02	65.87N	173.16W	14.4	.
850105	12	58	48.0	50.30N	139.40E	11.2	.
850108	09	20	16.14	67.02N	169.39W	0.0	.
850117	01	05	26.5	52.53N	133.05E	11.0	.
850121	18	03	51.11	60.81N	155.28E	7.7	.
850121	23	53	55.5	51.40N	130.09E	11.2	.
850124	20	26	34.02	66.92N	132.96E	16.7	.
850129	00	36	06.03	64.17N	145.84E	6.0	4.6
850129	09	45	51.84	64.15N	145.75E	8.4	.
850130	05	12	49.8	51.18N	133.14E	9.1	.
850131	20	02	05.2	53.65N	124.86E	11.4	.
850201	08	31	45.9	62.91N	127.20E	20.5	4.9
850201	10	20	50.6	62.72N	127.55E	17.7	.
850201	21	53	18.04	64.17N	145.77E	3.4	.
850202	11	28	41.67	65.86N	137.04E	33.3	.
850205	08	07	04.9	53.58N	124.68E	8.7	.
850205	15	30	22.9	53.16N	134.44E	0.0	.
850213	06	05	22.3	51.16N	133.03E	10.3	.
850218	12	51	31.60	65.58N	136.40E	4.5	.
850218	14	22	33.0	55.35N	123.34E	24.7	.
850222	07	06	21.86	63.24N	146.00E	10.2	.
850224	19	59	23.3	55.63N	130.55E	0.0	.
850301	09	19	18.60	57.55N	125.49E	8.6	4.5
850306	10	06	57.70	54.34N	135.09E	6.9	.
850308	22	24	38.14	59.35N	152.10E	19.4	.
850311	21	12	07.08	53.92N	128.47E	27.3	.
850318	23	09	15.4	53.72N	125.51E	24.7	.
850321	19	26	55.49	63.59N	148.48E	9.7	.
850330	04	51	39.5	51.18N	133.04E	33.0	.
850331	06	13	01.6	53.40N	132.91E	12.6	.
850402	15	50	16.7	50.98N	132.08E	12.1	.
850406	22	01	56.0	53.62N	125.50E	24.0	.
850410	11	27	44.55	70.43N	141.27E	20.1	.
850410	13	50	51.70	54.48N	125.58E	15.6	.
850417	01	27	19.16	54.51N	135.37E	5.9	.
850417	20	37	20.14	65.37N	142.78E	16.0	.
850420	09	22	31.6	50.86N	131.56E	33.0	.
850420	22	29	16.83	59.22N	141.85E	10.9	.
850424	06	11	40.9	53.62N	124.71E	16.1	.
850426	03	19	53.82	59.79N	152.40E	0.	.
850429	20	36	31.09	62.81N	146.19E	15.9	.
850502	04	41	22.96	64.38N	175.65W	33.0	.
850506	06	02	57.4	52.04N	122.37E	21.3	.
850506	12	17	30.34	65.51N	171.16W	29.7	.
850506	12	48	42.16	65.52N	171.66W	33.0	.
850506	15	20	35.70	54.86N	126.11E	13.4	.
850507	19	47	09.88	60.20N	143.22E	33.1	.
850508	12	57	00.8	54.33N	122.90E	20.6	.
850516	02	52	04.88	60.03N	151.71E	10.8	.
850524	06	22	43.67	54.19N	125.90E	12.9	.
850525	21	32	05.7	54.42N	123.23E	10.4	.
850527	19	54	59.0	55.09N	131.46E	0.0	.
850529	19	04	60.0	55.58N	133.00E	12.0	.
850602	04	08	09.40	64.85N	144.06E	7.0	.
850609	15	16	15.6	55.14N	123.97E	22.4	.
850611	10	15	24.52	65.23N	144.70E	8.7	.
850612	04	04	33.7	52.50N	132.82E	11.1	5.2
850620	12	10	07.5	53.62N	135.19E	4.2	.
850622	15	38	04.24	64.85N	144.06E	12.0	.
850624	03	54	34.50	65.25N	144.63E	14.9	.
850627	00	37	55.0	54.04N	127.86E	10.6	.
850630	13	30	05.86	54.19N	125.91E	14.6	.
850701	11	07	44.91	67.41N	171.10W	27.7	.
850701	18	35	16.51	69.80N	133.63E	10.7	.
850704	05	12	40.1	53.68N	125.49E	14.2	.
850704	09	42	08.33	69.84N	176.30E	32.5	.
850707	12	15	49.76	55.91N	126.87E	20.9	.
850708	16	27	39.95	54.85N	126.10E	14.4	.
850712	16	03	53.8	55.61N	130.89E	0.0	.

850721	22	34	18.2	48.97N	126.48E	20.8	5.5
850812	15	19	56.8	49.80N	131.96E	10.2	.
850820	03	41	38.80	62.23N	145.58E	5.5	.
850901	19	03	47.38	58.92N	149.02E	16.8	.
850904	21	03	05.7	53.71N	135.99E	4.0	.
850910	10	52	56.34	62.22N	143.37E	27.1	.
850915	03	44	10.2	53.43N	125.01E	0.0	.
850921	19	28	20.2	55.95N	130.53E	0.0	.
850922	01	09	29.8	54.25N	123.64E	27.4	.
850928	05	12	59.0	49.71N	127.55E	22.4	.
851001	18	59	11.8	53.75N	125.54E	15.7	.
851005	22	32	35.95	59.43N	150.25E	17.5	.
851022	02	26	11.6	54.11N	128.94E	0.0	.
851025	07	06	08.3	53.58N	125.46E	1.5	.
851029	10	54	06.3	55.41N	132.19E	0.0	.
851030	03	34	09.9	54.74N	134.06E	0.0	.
851106	07	17	51.08	63.28N	146.65E	4.9	.
851108	03	53	47.27	65.67N	172.20W	5.6	.
851109	04	09	19.0	53.98N	136.80E	29.6	.
851110	16	47	51.8	50.30N	122.95E	8.1	.
851122	00	53	39.7	53.73N	125.52E	16.4	.
851122	02	37	32.10	60.63N	149.71E	0.	.
851123	23	00	00.45	64.30N	175.42E	29.5	.
851128	08	38	22.15	64.89N	144.25E	16.6	.
851128	20	13	49.02	57.29N	127.52E	18.5	.
851129	16	57	09.6	53.62N	125.47E	21.9	.
851204	05	42	03.86	55.86N	125.87E	16.2	.
851208	08	28	32.69	54.35N	135.38E	1.9	.
851210	12	27	14.34	55.16N	128.47E	15.1	.
851217	16	43	11.3	52.91N	128.94E	11.2	.
851221	05	42	49.0	51.26N	133.07E	22.4	.
860105	00	35	22.80	70.20N	128.53E	2.6	.
860106	05	27	24.5	53.08N	134.52E	28.8	5.4
860108	07	25	18.8	52.35N	132.69E	0.0	.
860110	02	30	38.70	64.70N	142.05E	6.8	.
860118	13	13	22.73	60.21N	153.71E	4.3	.
860124	13	25	22.91	60.56N	138.72E	0.	.
860201	02	29	57.33	54.78N	139.27E	22.8	.
860206	04	36	10.52	63.56N	179.79E	0.	.
860209	12	42	53.5	48.69N	126.41E	26.1	5.1
860211	18	44	57.0	54.72N	131.67E	17.3	.
860212	03	46	43.88	68.86N	128.23E	9.2	.
860215	20	30	26.41	63.98N	153.10E	3.5	.
860216	06	21	49.7	48.31N	126.25E	33.0	.
860228	17	07	24.6	48.61N	126.39E	19.1	.
860304	08	15	21.73	64.81N	144.02E	16.2	.
860307	23	28	08.21	64.11N	153.46E	15.4	.
860311	12	33	14.38	64.47N	172.58W	5.7	.
860313	11	17	58.5	54.00N	136.79E	19.1	.
860314	03	09	56.31	60.26N	161.04E	10.5	.
860315	04	01	54.67	59.82N	144.98E	17.9	.
860318	19	36	33.41	63.66N	152.66E	11.1	.
860327	09	44	44.3	49.87N	131.67E	16.1	.
860330	11	46	32.5	52.86N	134.74E	17.1	.
860402	20	06	19.3	53.96N	128.26E	15.8	.
860403	15	38	15.94	59.12N	154.48E	15.4	.
860406	01	27	20.73	70.72N	130.29E	10.5	.
860407	09	08	07.71	64.07N	145.25E	6.5	.
860407	12	19	30.1	49.40N	131.77E	6.0	.
860413	21	47	48.87	59.75N	145.79E	14.1	.
860428	09	39	02.3	54.97N	135.38E	5.2	.
860504	03	13	22.19	57.40N	126.38E	30.3	.
860508	18	21	03.4	55.30N	123.55E	30.9	.
860515	21	22	49.8	51.81N	131.93E	5.2	.
860601	15	34	00.31	64.86N	144.05E	16.0	.
860602	07	43	26.3	55.45N	124.44E	23.8	.
860603	12	49	40.8	55.89N	124.30E	24.1	.
860605	06	00	25.9	53.55N	124.74E	4.6	.
860605	09	46	52.00	64.08N	145.25E	9.8	.
860606	19	42	13.34	66.96N	130.34E	23.4	.
860615	06	55	38.09	72.81N	126.31E	25.3	.
860615	11	46	38.3	51.56N	138.09E	5.3	.
860616	19	40	25.45	59.89N	156.86E	7.9	.
860701	20	04	16.9	54.80N	131.08E	14.7	.
860703	22	41	06.3	49.03N	131.63E	24.0	5.2
860704	15	01	55.7	50.08N	132.36E	15.7	.
860707	16	26	06.41	72.87N	121.69E	16.8	.
860709	22	14	58.30	54.71N	126.49E	11.2	.
860712	09	52	09.1	49.58N	123.45E	33.0	.
860714	14	39	09.98	65.11N	176.28W	2.7	.
860716	14	04	59.0	52.15N	126.32E	20.0	.
860720	21	38	07.9	53.61N	125.47E	6.7	.
860726	20	58	04.5	56.50N	121.03E	9.0	.
860727	11	25	40.82	64.60N	147.10E	17.0	.
860730	20	41	18.1	53.91N	123.51E	33.0	.
860809	02	24	44.7	55.07N	123.42E	33.0	.
860810	11	11	59.55	63.55N	147.80E	5.6	.
860814	22	36	00.84	63.40N	143.98E	22.8	.
860815	17	53	09.3	48.70N	126.61E	29.3	.
860815	20	20	34.0	48.75N	126.36E	15.9	6.5
860825	17	00	44.0	52.98N	132.58E	17.9	.
860826	04	45	21.73	56.01N	125.99E	20.1	.
860826	13	09	14.6	52.34N	138.55E	13.9	.
860909	12	15	52.21	69.75N	140.40E	5.2	.
860909	22	21	39.8	52.41N	131.71E	17.8	.
860915	16	23	09.01	57.63N	125.52E	12.4	.
860916	14	30	32.4	51.96N	122.37E	5.5	.
860918	08	40	47.1	55.60N	120.76E	25.8	.
860919	05	45	32.5	52.17N	136.17E	4.6	.
860919	07	47	43.7	53.60N	132.07E	13.4	5.0
860925	21	52	07.0	54.01N	134.37E	8.5	.
861003	18	14	46.39	65.47N	173.10W	7.3	.
861007	01	01	15.90	55.65N	126.50E	21.7	.
861007	01	15	05.48	55.65N	126.49E	11.1	.
861010	20	52	31.9	53.69N	125.51E	11.4	.
861013	20	01	59.41	65.29N	170.33W	33.0	.
861019	18	30	58.46	63.88N	178.48W	16.6	5.1
861023	10	50	02.6	51.62N	130.11E	12.5	.
861030	10	15	06.28	65.37N	173.06W	24.3	.
861102	08	50	08.6	53.73N	125.53E	13.8	.
861103	09	16	26.1	55.77N	130.58E	5.7	.
861103	21	54	38.20	54.21N	126.06E	19.5	.
861111	17	58	06.89	63.78N	145.72E	12.2	.
861129	20	04	59.9	54.26N	131.37E	21.8	.
861130	03	17	12.70	64.94N	154.54E	13.9	.
861202	11	06	20.00	54.32N	126.12E	17.4	.
861203	19	32	37.5	53.66N	125.50E	19.9	.
861209	22	54	21.44	64.13N	148.42E	12.9	.
861218	09	26	40.43	67.49N	171.24W	10.8	.
861218	12	11	14.4	51.85N	133.69E	19.9	.
861218	18	04	12.03	61.20N	143.73E	22.7	.
861221	04	28	23.9	49.19N	130.83E	18.2	.
861225	19	12	29.45	62.36N	156.41E	5.7	.
861226	03	21	04.97	61.37N	149.44E	14.6	.
861229	17	16	49.6	55.04N	122.76E	33.0	.
861231	07	21	58.3	56.59N	121.11E	14.4	.

870109	04	29	45.00	60.04N	153.01E	2.4	.
870109	13	14	17.46	67.18N	140.08E	10.5	.
870110	19	33	25.18	65.44N	172.92W	32.3	.
870110	19	34	39.53	65.35N	173.38W	33.0	.
870116	23	53	18.12	58.57N	125.11E	10.3	.
870120	07	42	18.1	50.28N	134.78E	15.6	.
870122	19	01	23.4	55.71N	130.74E	3.0	.
870131	03	55	08.0	56.67N	124.78E	20.9	.
870203	17	16	45.7	55.54N	130.63E	9.0	.
870204	01	43	46.3	52.90N	132.72E	17.7	.
870204	05	58	31.62	64.53N	144.63E	17.0	.
870205	09	30	41.1	57.52N	120.85E	24.6	.
870208	19	57	21.8	49.15N	131.48E	14.1	.
870209	23	00	01.30	65.44N	172.78W	14.4	.
870210	12	34	42.73	65.47N	172.65W	22.8	.
870211	00	58	20.93	62.87N	156.84E	5.6	4.8
870211	01	03	09.55	62.77N	156.88E	14.8	.
870211	01	09	51.56	62.84N	156.78E	9.0	.
870211	01	22	23.15	62.89N	156.87E	5.1	.
870211	05	52	49.59	62.88N	156.78E	10.0	.
870211	06	19	16.38	62.85N	156.77E	8.1	.
870211	07	28	18.00	62.84N	156.91E	11.6	.
870211	07	28	59.72	62.89N	156.85E	5.6	.
870211	07	47	11.44	62.87N	156.86E	2.6	.
870211	08	42	45.18	62.86N	156.86E	8.3	.
870211	11	36	16.41	62.86N	156.86E	6.0	.
870211	17	32	23.70	62.88N	156.85E	10.7	.
870212	02	10	47.0	49.62N	134.74E	2.2	.
870212	02	12	21.01	62.81N	156.80E	8.9	.
870214	07	16	29.76	59.44N	148.03E	0.	.
870218	21	53	15.3	50.35N	132.28E	6.1	.
870222	16	12	04.33	62.90N	156.83E	7.2	.
870225	03	03	38.29	63.02N	179.04E	17.7	.
870303	04	52	02.51	65.40N	136.29E	12.1	.
870304	00	09	28.42	61.15N	148.42E	10.5	.
870308	06	47	26.71	62.06N	143.57E	11.7	.
870308	13	52	12.05	59.77N	145.49E	5.2	.
870310	06	00	02.0	50.41N	143.54E	2.1	.
870316	20	58	53.45	64.08N	167.31E	0.	.
870322	00	19	50.43	65.40N	172.98W	17.4	.
870324	02	39	54.16	65.41N	173.05W	13.2	.
870326	00	45	57.33	65.43N	173.00W	14.5	.
870329	20	16	36.8	52.46N	142.08E	12.6	3.4
870403	13	06	12.1	52.88N	134.63E	9.1	.
870405	10	00	15.49	63.11N	174.89E	12.1	.
870405	11	36	36.46	63.18N	174.81E	9.0	.
870412	02	31	18.5	53.61N	125.69E	11.3	.
870415	23	09	21.1	58.56N	121.59E	33.0	.
870421	12	39	48.43	64.92N	170.43W	12.6	.
870421	13	21	00.30	64.82N	170.86W	30.1	.
870421	18	20	46.72	64.90N	170.47W	18.9	.
870422	03	38	20.69	72.18N	129.73E	11.9	.
870430	03	57	45.88	69.34N	178.23E	14.2	.
870430	05	41	35.5	54.74N	123.28E	23.3	.
870430	20	04	20.34	62.87N	156.86E	1.5	.
870505	22	29	03.2	56.80N	122.95E	22.3	.
870510	12	11	04.73	64.46N	172.64W	9.3	.
870512	09	41	25.8	51.85N	132.60E	12.5	.
870516	09	29	41.1	48.44N	130.95E	27.1	.
870524	16	15	47.7	54.38N	121.75E	33.0	.
870525	00	58	03.0	53.26N	133.05E	13.2	.
870526	13	59	12.68	65.38N	173.27W	33.0	.
870528	14	46	55.68	66.96N	172.17W	27.4	.
870602	16	40	20.06	62.74N	156.73E	6.6	.
870603	11	36	36.4	52.57N	135.99E	8.2	.
870606	14	14	49.6	50.92N	135.51E	4.3	.
870610	02	12	14.0	53.71N	124.81E	10.2	.
870623	23	07	24.83	53.99N	127.92E	9.9	.
870701	11	52	32.3	52.03N	132.91E	13.7	.
870703	13	23	08.19	59.31N	148.65E	4.1	.
870704	18	30	29.2	54.31N	134.62E	11.4	.
870705	00	08	55.24	61.26N	144.60E	6.6	.
870711	03	15	14.3	49.11N	135.59E	0.8	.
870721	05	02	28.63	58.64N	149.64E	5.9	.
870725	15	49	25.25	62.86N	156.78E	7.2	.
870731	06	40	41.0	53.15N	127.76E	12.1	.
870731	12	55	25.4	48.73N	131.97E	23.7	.
870804	21	31	53.0	48.74N	132.02E	19.1	.
870806	14	50	07.50	56.16N	125.07E	22.4	.
870808	00	09	56.4	51.07N	131.87E	28.6	5.4
870808	03	37	36.6	51.09N	131.89E	25.7	.
870815	18	16	00.50	63.16N	175.90E	12.8	.
870821	07	07	07.9	53.39N	132.07E	16.8	4.4
870821	17	58	50.6	53.40N	132.05E	11.9	.
870821	19	33	14.6	53.49N	132.13E	26.7	4.8
870825	11	31	22.6	55.43N	131.20E	5.6	.
870909	04	43	22.95	60.15N	150.41E	7.6	.
870909	19	10	41.9	51.81N	123.58E	20.9	.
870922	23	20	52.4	54.40N	132.19E	10.7	.
870923	17	43	01.0	53.01N	138.76E	14.6	.
870927	13	16	35.82	61.16N	160.97E	4.5	.
871007	16	21	48.8	52.82N	138.64E	7.7	.
871015	03	09	50.85	57.61N	125.45E	4.2	.
871030	21	42	48.1	48.89N	130.00E	33.0	.
871102	03	20	42.69	57.54N	128.20E	5.3	.
871102	23	21	05.41	55.05N	136.60E	2.9	.
871108	06	44	07.2	52.33N	132.66E	15.1	.
871115	07	07	47.87	63.18N	177.27E	15.2	.
871115	19	51	21.9	51.54N	138.19E	21.3	.
871116	07	41	47.06	57.61N	125.35E	13.5	.
871121	18	15	18.79	62.22N	170.88E	7.5	.
871125	00	43	07.41	62.91N	144.94E	12.6	.
871203	07	34	51.17	59.32N	147.87E	10.6	.
871205	21	16	21.07	71.18N	141.69E	20.8	.
871206	10	54	26.59	63.32N	144.60E	1.6	.
871207	10	50	58.61	63.68N	145.56E	10.3	.
871212	07	51	06.44	57.37N	127.40E	12.7	.
871215	06	56	02.0	56.73N	123.01E	9.6	.
871222	22	04	33.79	62.95N	145.04E	4.0	.
871226	18	02	32.62	58.94N	147.76E	0.	.
880101	14	36	12.94	74.59N	130.81E	33.0	.
880114	14	35	33.3	52.60N	132.43E	22.8	.
880119	10	35	32.19	63.71N	145.68E	7.4	.
880122	12	51	56.52	62.20N	146.03E	6.2	.
880208	20	47	57.88	64.01N	146.03E	9.5	.
880212	09	19	25.2	56.61N	121.08E	9.9	.
880217	23	00	43.88	64.10N	145.62E	3.6	.
880219	00	04	04.40	64.33N	148.58E	9.7	.
880219	20	41	05.2	53.04N	138.61E	9.3	.
880219	23	50	25.40	64.19N	145.81E	12.3	.
880221	23	10	04.9	56.58N	121.11E	12.2	.
880227	02	07	29.6	54.36N	124.27E	24.5	.
880309	20	18	01.55	68.04N	130.71E	14.9	.
880314	18	33	53.91	61.37N	154.22E	1.5	.
880315	19	10	31.9	52.72N	134.66E	28.8	.
880321	11	29	06.6	51.29N	131.43E	0.0	.

880325	06	30	09.24	64.51N	144.68E	9.7	.
880403	02	01	29.00	69.46N	138.77E	22.1	.
880503	00	39	00.74	65.38N	173.40W	5.8	.
880519	11	53	20.52	55.91N	128.82E	20.3	.
880525	16	55	43.86	64.21N	150.95E	9.0	.
880605	14	51	43.41	56.23N	128.67E	2.4	.
880609	13	37	33.18	63.27N	157.59E	8.1	.
880609	20	12	08.25	63.13N	173.04E	9.6	.
880614	14	44	44.27	63.37N	149.50E	10.3	.
880619	11	53	19.99	55.92N	128.87E	14.6	.
880620	18	30	53.9	65.49N	131.08E	11.1	.
880621	18	33	34.90	54.73N	135.58E	5.7	.
880621	22	50	18.1	57.86N	124.86E	14.1	.
880623	17	59	05.91	63.79N	169.87E	8.8	.
880701	21	37	33.73	64.72N	145.93E	19.1	.
880707	17	43	35.54	63.08N	144.69E	0.7	.
880717	23	08	00.41	63.43N	145.47E	2.8	.
880728	15	30	47.34	57.12N	129.47E	13.7	.
880804	06	07	15.39	56.01N	129.85E	1.4	.
880818	08	00	43.08	59.69N	145.67E	0.	.
880825	05	03	27.58	56.87N	127.15E	5.6	.
880825	07	17	24.40	56.86N	127.17E	7.8	.
880830	12	58	55.7	54.00N	137.68E	18.6	.
880902	09	35	32.4	54.16N	122.71E	33.0	.
880922	11	25	41.9	57.41N	122.68E	19.2	.
880922	23	58	11.30	61.89N	160.48E	17.6	.
880923	08	32	14.25	55.45N	137.21E	33.0	.
880926	08	59	49.57	67.53N	143.86E	5.8	.
880930	03	09	09.3	54.15N	137.75E	10.4	.
881007	00	56	29.24	57.57N	125.12E	17.6	.
881013	00	32	09.10	61.71N	169.78E	8.7	5.9
881013	00	49	26.91	61.81N	169.63E	33.0	.
881013	03	24	33.51	61.95N	169.62E	24.0	.
881015	07	05	37.98	61.89N	169.57E	25.4	.
881017	00	27	59.09	62.85N	148.80E	6.7	.
881020	04	17	55.42	56.77N	127.11E	6.1	.
881024	07	15	32.1	54.80N	133.02E	17.2	.
881025	10	12	52.89	62.87N	148.85E	8.5	.
881101	21	37	31.2	56.85N	123.93E	14.0	.
881102	23	32	55.4	53.86N	126.39E	6.0	.
881109	13	07	58.6	57.90N	120.57E	22.5	.
881112	10	27	10.91	57.77N	126.45E	15.2	.
881118	11	29	32.4	57.86N	121.19E	26.0	.
881118	22	22	05.1	56.67N	121.68E	7.6	.
881203	15	29	49.50	56.06N	126.35E	11.5	.
881207	16	50	30.55	65.23N	144.66E	0.	.
881207	18	23	22.27	65.29N	144.71E	0.4	.
881222	20	10	11.1	52.46N	134.43E	28.5	.
881224	02	43	21.51	64.10N	148.74E	8.9	.
881226	13	29	00.65	61.63N	168.93E	10.9	.
881230	07	16	43.30	61.12N	153.70E	1.7	.
890113	12	52	11.1	49.01N	131.59E	22.1	.
890113	16	21	59.87	64.59N	147.17E	10.4	.
890114	04	53	36.49	61.89N	143.74E	9.5	.
890115	17	17	30.78	58.69N	151.20E	6.1	.
890115	22	13	26.8	57.08N	121.61E	32.5	.
890124	16	50	14.54	65.41N	144.43E	19.0	.
890129	23	23	01.67	62.86N	144.88E	12.7	.
890202	07	18	12.67	57.59N	128.30E	13.1	.
890205	16	26	59.20	54.21N	126.66E	25.7	.
890212	03	54	21.16	59.20N	147.66E	5.7	.
890213	09	35	29.09	66.17N	172.58E	11.8	.
890215	18	46	19.32	58.07N	129.42E	17.3	.
890217	02	57	48.16	63.37N	146.19E	6.9	.
890217	19	10	15.20	69.80N	129.14E	20.4	.
890218	05	47	41.5	48.52N	131.47E	2.5	.
890219	18	00	30.11	65.18N	146.22E	5.7	.
890224	11	44	19.57	61.25N	162.91E	9.8	.
890225	04	56	17.06	61.73N	157.71E	8.6	.
890321	10	53	05.21	64.91N	145.19E	9.3	.
890329	01	10	46.0	56.79N	123.52E	15.5	.
890331	12	47	12.06	69.73N	128.96E	17.0	.
890404	07	30	24.43	62.09N	157.49E	20.3	.
890409	04	16	24.70	59.80N	145.14E	33.0	5.0
890410	09	12	58.94	66.75N	174.60W	33.0	.
890412	00	45	33.7	56.72N	120.37E	22.2	.
890420	22	56	00.2	57.13N	122.23E	31.8	.
890420	22	59	52.3	57.34N	122.11E	16.3	6.6
890421	00	04	44.9	57.04N	122.18E	23.4	.
890421	00	16	00.7	57.08N	122.20E	18.8	.
890421	00	52	30.7	57.04N	122.18E	22.3	.
890421	00	57	54.6	57.01N	122.17E	19.2	.
890421	01	04	20.1	57.10N	122.06E	31.5	.
890421	01	44	00.1	57.01N	122.19E	17.7	.
890421	03	12	05.8	57.07N	122.14E	23.9	.
890421	08	10	05.7	57.05N	122.20E	22.7	.
890421	08	29	29.5	57.06N	122.16E	27.7	.
890421	08	30	08.2	57.10N	122.16E	25.7	.
890421	08	51	39.0	57.04N	122.18E	28.6	.
890421	15	22	01.0	57.04N	122.22E	27.6	.
890421	15	49	35.7	57.05N	122.21E	25.7	.
890421	19	08	37.4	57.07N	122.27E	33.0	4.9
890421	19	29	28.5	57.06N	122.25E	30.8	.
890421	20	09	42.2	57.07N	122.22E	30.8	.
890421	22	30	36.0	57.05N	122.18E	25.6	.
890423	02	45	40.1	57.08N	122.17E	24.1	.
890423	03	44	27.9	57.06N	122.18E	25.1	.
890423	17	58	28.7	57.09N	122.22E	29.3	.
890424	01	33	59.8	57.11N	122.27E	24.4	5.0
890424	04	45	38.19	58.95N	151.87E	10.0	.
890424	08	18	37.1	57.09N	122.18E	26.7	.
890428	15	20	53.0	57.07N	122.21E	33.0	.
890429	00	05	07.9	57.18N	122.20E	33.0	.
890429	01	27	13.8	57.09N	122.22E	30.6	.
890429	06	25	38.9	57.15N	122.24E	33.0	5.6
890429	07	05	24.2	57.14N	122.25E	28.2	.
890429	08	40	01.6	57.08N	122.30E	0.0	.
890429	10	33	56.1	57.05N	122.29E	0.0	.
890429	17	35	30.1	57.05N	122.25E	0.3	.
890429	21	00	46.4	57.08N	122.25E	24.4	.
890503	23	53	38.4	57.03N	122.17E	23.2	.
890504	14	10	28.4	56.57N	121.15E	14.8	.
890504	14	10	28.4	56.57N	121.15E	14.8	.
890506	06	54	38.5	57.13N	122.02E	26.8	.
890507	16	28	05.9	57.08N	122.22E	33.0	5.1
890508	11	49	47.0	57.05N	122.21E	27.8	.
890511	14	37	43.2	57.07N	122.20E	29.4	.
890514	16	21	51.7	57.14N	122.19E	27.0	.
890517	05	04	35.8	57.05N	122.24E	32.0	5.8
890517	07	25	49.0	57.05N	122.25E	30.7	.
890517	07	40	39.1	57.00N	122.13E	23.5	.
890517	10	21	02.1	57.06N	122.14E	19.9	.
890517	15	55	22.9	57.06N	122.24E	32.1	.
890518	10	06	01.1	57.02N	122.21E	29.8	.
890519	15	39	08.1	57.06N	122.22E	26.3	.
890519	19	29	23.96	62.42N	155.21E	3.3	.

890519	22	06	27.6	57.07N	122.20E	27.9	.
890523	08	12	12.2	57.00N	122.18E	29.2	.
890524	09	38	02.21	61.31N	144.72E	11.2	.
890524	19	42	32.5	57.07N	122.23E	30.5	.
890525	11	48	06.2	57.06N	122.23E	33.0	.
890601	08	17	10.5	57.07N	122.20E	29.9	.
890601	16	41	42.51	63.47N	139.82E	0.	.
890601	16	41	42.51	63.47N	139.82E	0.	.
890601	19	25	46.7	57.07N	122.29E	28.4	.
890601	22	38	53.0	56.99N	122.16E	28.5	.
890603	08	57	17.1	54.51N	123.23E	23.5	.
890604	04	17	01.52	68.12N	132.54E	30.9	.
890604	21	49	34.7	57.08N	122.14E	27.6	.
890605	00	13	20.7	57.02N	122.22E	30.3	.
890608	22	41	20.2	57.10N	122.25E	24.4	.
890610	05	09	43.96	71.31N	129.13E	2.9	.
890615	16	24	12.2	57.03N	122.23E	30.2	.
890616	07	36	08.68	63.57N	142.74E	9.0	.
890616	19	40	45.76	61.02N	145.44E	14.6	.
890617	13	37	27.02	67.24N	143.75E	8.5	.
890619	15	48	34.3	57.13N	122.27E	30.3	.
890622	20	52	20.7	57.10N	122.28E	23.5	.
890627	10	38	36.3	57.15N	122.30E	27.3	.
890628	20	16	28.1	57.05N	122.14E	26.5	.
890630	20	00	00.25	59.25N	152.73E	2.2	.
890701	14	14	40.42	57.21N	137.80E	33.	.
890702	23	58	49.62	59.61N	150.01E	4.2	.
890706	04	08	09.4	57.09N	122.22E	33.0	.
890707	10	51	43.57	64.99N	141.66E	14.4	.
890709	18	11	49.32	59.91N	152.71E	8.8	.
890709	20	07	46.3	57.09N	122.32E	33.0	4.2
890709	21	04	27.2	57.06N	122.24E	33.0	.
890710	07	19	33.9	57.05N	122.20E	33.0	.
890713	19	13	54.00	62.57N	143.88E	0.	.
890716	16	32	31.2	57.07N	122.21E	30.4	.
890718	03	02	54.7	57.07N	122.22E	33.0	.
890719	00	24	03.7	57.08N	122.17E	26.8	.
890720	02	53	38.2	57.05N	122.17E	30.1	.
890720	03	16	21.8	57.05N	122.18E	31.5	.
890720	23	26	43.7	57.09N	122.15E	9.7	.
890721	01	40	08.2	57.10N	122.16E	10.3	.
890721	01	46	35.0	57.04N	122.16E	26.6	.
890721	07	43	50.5	57.08N	122.20E	10.5	.
890722	02	36	12.6	57.09N	122.15E	7.5	.
890722	10	01	40.8	57.07N	122.22E	27.7	.
890723	12	01	31.2	54.54N	124.92E	27.0	.
890723	14	33	00.4	54.55N	124.97E	18.8	.
890723	14	33	01.4	54.61N	124.94E	21.2	.
890723	22	35	55.3	57.12N	122.24E	31.4	.
890724	01	35	24.2	54.54N	124.93E	18.4	.
890725	00	58	37.6	51.53N	132.00E	8.2	.
890731	00	27	03.6	54.47N	122.99E	.	.
890801	00	03	03.4	57.09N	122.17E	14.7	.
890801	17	05	23.61	59.89N	151.65E	20.3	.
890803	21	46	19.90	54.14N	136.77E	25.8	.
890804	11	35	25.1	57.08N	122.16E	10.8	.
890804	11	48	30.8	57.10N	122.11E	13.0	.
890804	13	47	50.1	57.08N	122.13E	4.8	.
890804	21	39	26.0	57.11N	122.12E	8.7	.
890806	00	59	48.3	56.99N	122.22E	2.9	.
890906	15	20	32.20	61.73N	144.18E	6.9	.
890910	05	16	37.9	57.06N	122.20E	27.0	.
890918	11	47	43.84	72.18N	128.86E	0.2	.
890919	22	44	26.29	54.43N	129.57E	23.1	.
890924	10	18	10.38	65.47N	169.97E	21.5	.
890924	16	35	43.98	63.97N	169.72E	1.6	.
890926	06	41	32.9	57.06N	122.10E	13.7	.
890927	15	42	43.4	57.11N	122.08E	14.1	.
891004	20	56	47.62	64.70N	146.83E	11.0	.
891017	03	47	41.7	57.08N	122.18E	26.6	.
891018	18	49	22.58	68.76N	133.09E	19.7	.
891027	01	18	42.1	55.36N	120.45E	23.8	.
891028	16	41	50.18	57.57N	125.38E	10.0	.
891030	01	03	39.4	48.48N	129.62E	33.0	.
891030	03	38	25.9	57.09N	122.14E	33.0	.
891106	10	01	11.57	54.40N	129.58E	12.6	.
891109	09	57	37.20	68.46N	132.58E	33.0	.
891109	20	57	54.53	66.16N	165.74E	11.1	.
891110	08	55	55.7	48.88N	131.55E	17.1	.
891113	18	15	40.26	62.28N	143.54E	15.1	.
891118	05	22	38.1	57.01N	122.20E	18.0	.
891202	16	21	59.0	57.15N	122.25E	29.7	.
891207	21	33	54.5	57.00N	122.18E	21.3	.
891208	01	36	10.07	64.93N	145.90E	10.7	.
891208	09	57	25.9	54.95N	134.96E	3.1	.
891212	15	19	04.4	57.06N	122.13E	25.0	.
891213	21	39	09.3	57.03N	122.21E	31.7	.
891222	12	46	34.70	65.48N	136.71E	10.8	.
891223	01	24	26.1	54.12N	122.00E	24.9	.
900108	06	18	52.0	57.64N	121.13E	17.4	.
900109	01	44	43.62	57.57N	125.39E	3.1	.
900110	16	29	04.0	57.02N	122.22E	26.5	.
900114	16	07	31.1	50.20N	125.48E	23.8	.
900121	14	37	11.80	63.10N	151.95E	6.4	.
900202	06	02	55.8	56.94N	132.17E	8.9	.
900206	03	40	46.6	57.06N	122.06E	9.2	.
900208	09	19	35.9	57.15N	122.08E	33.0	.
900208	20	22	30.5	57.12N	122.15E	16.9	.
900216	12	59	41.3	57.10N	122.16E	32.4	.
900224	16	29	24.42	57.08N	125.75E	9.6	.
900225	21	17	23.1	54.35N	122.85E	28.6	.
900227	13	04	13.5	57.06N	122.25E	26.3	.
900303	22	24	15.91	57.01N	125.66E	19.2	.
900305	15	40	16.20	54.60N	125.00E	18.8	.
900306	07	18	08.99	67.05N	125.24E	26.7	.
900312	03	26	58.1	52.75N	138.63E	19.2	.
900313	00	33	01.59	73.30N	134.76E	32.8	.
900314	01	12	22.02	73.32N	134.34E	11.6	.
900318	02	22	49.1	57.03N	122.31E	20.6	.
900319	14	34	18.4	53.14N	131.66E	16.6	.
900321	04	31	25.21	73.30N	133.99E	33.0	.
900329	20	47	29.87	64.02N	145.04E	6.8	.
900330	10	16	45.2	54.96N	123.89E	26.8	.
900330	15	15	38.63	64.04N	145.07E	7.2	.
900330	22	46	11.4	57.02N	122.18E	27.3	.
900402	15	32	46.87	62.12N	138.02E	15.4	.
900408	10	58	40.6	57.03N	122.19E	20.7	.
900411	16	09	43.42	61.96N	154.26E	6.4	.
900412	19	10	48.37	62.40N	138.12E	0.	.
900419	09	00	39.81	72.95N	123.81E	0.	.
900421	02	15	30.68	65.48N	170.68E	17.2	.
900424	08	24	09.6	57.95N	120.95E	16.7	.
900426	23	19	05.09	70.57N	137.26E	25.2	.
900427	10	12	27.0	50.66N	132.62E	0.0	.
900501	13	27	29.40	56.86N	132.09E	13.6	.
900502	10	12	58.04	57.77N	128.21E	3.3	.

900504	18	13	17.11	66.28N	172.56W	13.8	.
900505	03	28	08.24	59.34N	149.48E	0.	.
900517	18	37	36.4	56.52N	121.19E	18.4	.
900524	02	44	24.0	57.10N	122.22E	31.6	.
900528	23	47	38.3	57.11N	122.99E	20.4	.
900530	11	56	45.68	62.91N	144.88E	6.0	.
900530	14	06	04.06	62.90N	144.92E	9.2	.
900602	17	11	19.7	55.65N	130.66E	10.9	.
900614	19	39	35.66	64.08N	156.62E	5.3	.
900618	13	22	59.88	64.03N	175.02E	5.1	.
900624	10	15	33.2	53.99N	122.29E	17.3	.
900625	07	33	54.07	66.81N	130.68E	18.8	.
900625	13	12	48.23	66.88N	130.45E	8.1	.
900629	12	30	10.1	56.72N	124.04E	22.9	.
900701	17	03	53.76	61.94N	154.22E	7.9	.
900704	12	11	28.25	59.31N	126.38E	0.	.
900705	15	32	55.46	62.88N	153.26E	0.	.
900706	03	16	04.3	56.82N	124.39E	33.0	.
900706	16	09	08.59	67.17N	144.67E	0.0	.
900712	02	22	50.75	62.07N	153.82E	7.5	.
900717	03	37	25.0	48.70N	132.00E	19.2	.
900717	04	01	11.3	48.71N	132.05E	17.3	.
900717	05	15	32.2	57.01N	124.63E	25.5	.
900724	15	17	19.86	60.25N	142.65E	0.	.
900726	17	34	20.1	57.10N	122.25E	20.5	.
900729	13	17	25.96	63.55N	174.40E	15.1	.
900731	05	50	45.1	53.67N	124.78E	15.2	.
900802	03	22	15.90	54.27N	126.45E	19.5	.
900803	05	06	52.46	65.49N	136.68E	17.5	.
900803	14	02	08.49	57.54N	127.81E	19.0	.
900812	20	51	01.20	65.28N	173.49W	9.8	.
900816	19	52	33.63	69.92N	139.29E	18.6	.
900819	19	45	35.00	72.98N	122.75E	16.4	.
900820	23	48	16.3	54.34N	123.57E	6.1	.
900824	01	04	44.73	63.04N	151.18E	9.6	.
900825	03	17	34.67	60.12N	165.48E	33.0	.
900827	01	31	06.1	56.55N	121.08E	12.0	.
900901	21	56	05.51	54.23N	125.97E	20.2	.
900906	17	41	18.23	63.05N	172.92E	14.2	.
900907	07	15	16.50	65.19N	148.22E	12.6	.
900928	11	47	56.7	57.02N	122.16E	30.8	.
901006	00	17	17.2	55.31N	121.84E	26.6	.
901008	22	58	13.28	57.02N	129.48E	33.0	.
901015	15	27	17.61	65.36N	173.01W	26.6	.
901016	10	03	30.31	65.35N	173.16W	1.1	.
901016	12	04	26.5	49.84N	129.54E	18.8	.
901018	23	27	40.84	55.26N	139.01E	7.9	.
901025	15	36	41.1	56.82N	121.07E	18.6	.
901029	10	21	07.95	54.70N	136.54E	11.6	.
901031	21	04	25.9	57.05N	122.20E	22.3	.
901101	04	58	32.57	57.59N	125.47E	13.1	.
901101	13	42	05.88	61.29N	156.90E	6.6	.
901102	21	54	02.28	64.81N	146.61E	3.9	4.2
901109	17	16	48.69	68.84N	131.89E	11.1	.
901111	17	47	35.51	59.33N	152.22E	3.4	.
901116	13	39	26.03	69.44N	129.71E	10.1	.
901117	11	11	09.4	57.71N	121.50E	18.4	.
901117	14	14	26.82	57.25N	125.46E	20.5	.
901121	01	12	19.11	59.84N	153.46E	2.9	.
901121	04	04	03.61	61.73N	142.87E	11.4	.
901122	19	36	25.37	62.78N	156.82E	7.0	.
901203	04	33	44.7	57.15N	122.23E	23.1	.
901204	08	46	20.24	61.78N	169.79E	18.0	.
901208	08	23	30.66	59.42N	152.52E	4.9	.
901213	21	34	39.60	64.46N	140.51E	11.2	.
910102	04	19	22.94	61.77N	145.69E	0.	.
910109	08	15	37.4	56.88N	120.39E	20.0	.
910201	08	09	25.81	65.68N	145.97E	0.	.
910210	18	16	31.98	62.94N	145.58E	12.5	.
910211	10	58	26.96	72.60N	125.08E	16.3	.
910213	09	46	15.45	62.21N	160.73E	10.0	.
910217	20	15	00.74	60.68N	167.35E	0.	.
910217	20	47	09.33	60.81N	167.04E	1.1	.
910217	23	41	23.6	56.80N	132.02E	1.2	.
910218	11	13	49.00	60.88N	167.01E	15.8	.
910220	04	46	32.45	60.84N	167.09E	0.	.
910301	18	14	14.03	60.02N	152.79E	3.9	.
910301	01	57	04.56	72.17N	126.74E	26.5	5.0
910307	16	20	43.04	61.28N	157.00E	5.8	.
910308	09	02	21.93	60.86N	167.03E	33.0	.
910309	01	49	34.4	57.39N	120.87E	33.0	.
910314	02	20	42.8	54.76N	120.88E	19.6	.
910316	11	02	10.12	62.39N	153.10E	13.3	.
910322	16	00	22.89	62.35N	148.41E	8.4	.
910330	01	52	52.22	57.12N	132.96E	8.5	.
910330	17	06	23.65	66.64N	126.07E	14.0	.
910331	15	39	45.44	58.93N	149.12E	0.	.
910401	07	21	57.27	71.36N	130.02E	8.4	.
910420	11	48	29.64	56.90N	127.14E	7.9	.
910505	16	17	47.70	54.68N	125.40E	11.4	.
910518	08	49	28.0	57.44N	120.92E	33.0	.
910527	08	55	35.2	57.07N	122.20E	30.7	.
910621	11	04	24.3	55.85N	124.50E	25.4	.
910701	20	41	59.50	63.82N	156.12E	11.5	.
910711	23	23	07.30	62.73N	175.42E	0.	.
910722	12	05	27.3	55.79N	131.11E	32.3	.
910723	10	28	19.41	59.74N	156.45E	11.9	.
910724	02	26	03.08	62.25N	143.64E	3.7	.
910728	01	37	01.15	59.88N	153.36E	0.6	.
910731	01	44	03.82	72.08N	127.59E	11.5	.
910804	19	08	06.08	65.49N	143.24E	25.1	.
910804	19	14	40.50	65.48N	143.25E	10.5	.
910811	18	50	48.20	59.97N	150.19E	5.0	.
910825	13	51	02.79	70.64N	140.99E	11.8	.
910826	09	35	49.41	63.33N	146.31E	1.0	.
910915	10	56	22.12	63.82N	151.66E	6.7	.
911013	00	36	28.86	60.87N	144.94E	13.7	3.5
911016	05	04	25.7	54.58N	120.80E	27.6	.
911105	10	16	38.60	59.01N	150.60E	6.0	.
911106	19	14	17.47	63.66N	155.03E	3.6	.
911114	01	01	50.65	62.38N	153.14E	6.0	.
911201	17	13	50.30	59.41N	147.66E	0.	.
911216	07	34	56.14	62.76N	146.03E	7.9	.
911223	06	04	15.31	62.45N	140.86E	33.0	.
920112	11	21	48.48	64.51N	174.36W	11.8	.
920121	18	07	36.05	61.79N	169.77E	14.6	4.6
920122	06	29	16.56	65.86N	143.27E	11.2	.
920128	00	07	26.80	68.17N	133.13E	19.5	.
920212	17	14	52.51	64.89N	153.01E	7.3	.
920222	17	55	21.52	70.09N	139.44E	7.0	.
920223	08	21	41.66	70.05N	139.45E	9.9	.
920301	18	04	13.7	57.01N	120.79E	26.9	.
920307	06	07	14.46	66.85N	177.89E	7.1	.
920322	12	35	00.41	60.84N	166.87E	33.0	.
920323	15	37	22.29	60.54N	167.14E	7.1	.
920324	03	58	42.27	62.07N	169.60E	12.7	.

920405	17	55	25.64	59.33N	152.39E	0.	.
920413	22	47	21.2	56.59N	121.13E	15.1	.
920507	23	22	54.7	63.65N	133.51E	33.0	.
920628	23	53	17.73	63.74N	145.70E	5.6	.
920709	09	57	15.79	63.14N	156.74E	11.9	.
920826	11	02	16.12	71.60N	133.23E	1.7	.
920828	14	27	05.12	58.94N	149.22E	22.4	3.8
920909	00	14	31.84	71.42N	132.83E	9.9	.
920913	21	42	56.22	62.07N	153.79E	9.7	4.9
920913	22	05	31.34	62.04N	153.78E	4.3	.
920928	08	05	55.06	64.66N	173.41W	10.7	.
921009	21	43	39.25	68.57N	140.84E	4.9	.
921010	17	47	51.42	62.49N	154.05E	7.0	.
921011	21	40	09.21	62.05N	153.61E	11.1	.
921030	14	20	30.07	72.75N	123.74E	27.1	.
921114	20	43	15.37	73.01N	123.21E	21.7	.
921117	07	55	14.2	67.20N	128.59E	24.2	.
921121	06	09	38.38	65.60N	170.41W	33.0	.
921206	08	39	43.42	62.06N	157.13E	4.0	.
921214	16	46	32.61	65.28N	171.31W	4.3	.
921218	13	28	08.81	63.39N	156.39E	13.5	.
921220	10	20	23.65	62.06N	157.00E	7.2	.
921221	07	40	14.63	64.37N	173.30W	15.6	.
921222	08	54	39.43	63.26N	152.37E	8.2	.
921223	12	48	25.10	62.04N	157.01E	10.2	.
930121	05	08	56.12	63.13N	146.43E	17.4	.
930124	20	10	28.6	56.78N	131.52E	7.9	.
930124	20	45	17.2	57.23N	123.29E	22.8	.
930206	22	05	37.23	62.22N	156.78E	2.4	.
930210	14	09	48.95	59.42N	147.42E	10.4	.
930221	09	37	53.1	57.96N	120.71E	28.1	.
930224	17	45	25.24	69.59N	128.82E	0.	.
930305	01	43	43.31	62.95N	145.59E	7.9	.
930305	04	21	03.78	63.73N	145.65E	8.1	.
930313	03	26	28.31	63.77N	142.40E	22.2	.
930322	18	14	04.48	62.91N	145.56E	7.4	.
930324	16	19	06.11	65.38N	142.64E	11.9	.
930324	22	43	29.02	71.68N	130.34E	12.8	4.5
930413	02	36	25.63	62.52N	155.34E	10.7	.
930429	12	21	31.23	69.21N	139.91E	25.8	.
930519	08	32	06.79	57.97N	140.63E	0.	.
930615	11	51	14.06	62.33N	141.50E	1.9	.
930618	19	16	14.33	62.05N	146.22E	12.0	.
930701	03	52	03.21	63.26N	146.72E	11.1	.
930705	05	44	53.91	63.28N	179.51E	13.7	.
930820	21	26	20.20	57.52N	126.62E	9.4	.
930825	11	50	10.7	56.86N	124.64E	10.8	.
930830	07	56	35.44	64.07N	145.84E	5.5	.
930926	10	58	20.86	59.66N	145.14E	29.7	.
931019	07	02	40.2	56.69N	124.60E	23.9	.
931028	09	40	51.87	59.28N	148.04E	25.6	.
931220	03	42	07.66	63.48N	150.51E	6.5	.
940104	20	00	24.5	53.53N	132.24E	22.6	.
940105	12	29	31.7	57.45N	122.49E	17.5	.
940116	14	51	07.5	57.42N	122.50E	23.5	.
940128	01	05	12.10	55.06N	135.29E	6.6	5.0
940130	08	18	38.9	57.53N	122.37E	33.0	.
940204	17	10	10.46	59.66N	143.93E	10.1	.
940215	17	40	57.09	57.86N	128.57E	8.2	.
940216	12	43	17.5	56.96N	123.51E	23.8	.
940223	17	56	12.2	57.30N	123.25E	17.4	.
940301	17	48	03.00	55.13N	138.47E	0.	.
940317	13	55	31.6	57.06N	121.57E	26.5	.
940328	00	57	32.40	62.49N	147.57E	8.9	3.6
940331	15	14	18.06	72.07N	127.78E	2.4	.
940331	22	28	42.96	71.77N	128.31E	33.0	.
940402	11	30	00.2	66.70N	148.33E	14.0	.
940409	08	36	19.6	56.15N	124.06E	16.1	.
940419	21	16	54.9	54.88N	124.10E	33.0	.
940421	15	15	47.75	56.52N	127.71E	7.6	.
940426	09	55	39.00	57.02N	127.82E	4.1	.
940426	14	58	45.4	54.75N	122.02E	13.1	.
940504	00	36	22.57	58.83N	146.40E	14.7	.
940510	13	39	10.4	54.27N	122.96E	25.2	.
940522	11	35	12.6	54.63N	123.39E	33.0	.
940523	07	22	47.8	57.04N	122.20E	33.0	.
940609	02	27	17.94	62.51N	147.59E	8 4	.
940616	17	53	18.18	62.46N	147.58E	12.8	3.8
940619	19	03	27.16	62.43N	147.50E	5.6	.
940621	14	52	00.5	57.08N	122.22E	20.9	.
940703	08	41	29.3	56.70N	122.48E	19.6	.
940705	13	32	04.0	54.27N	122.86E	26.1	.
940708	13	40	29.5	56.66N	132.92E	6.2	.
940710	22	30	06.1	55.75N	122.92E	25.6	.
940711	02	39	36.48	62.49N	147.59E	10.9	3.5
940711	11	33	04.04	62.13N	143.57E	6.2	.
940711	16	48	02.43	62.53N	147.59E	7.4	.
940715	00	20	42.86	66.90N	130.08E	31.9	.
940718	15	43	04.16	62.02N	153.64E	13.8	.
940722	18	39	09.0	54.73N	131.83E	0.0	.
940727	00	17	04.9	57.00N	122.36E	28.6	.
940731	04	45	38.32	73.03N	123.50E	7.1	.
940802	02	30	44.77	57.28N	125.54E	8.8	.
940803	18	51	44.0	57.38N	122.17E	15.7	.
940811	22	44	12.8	57.09N	122.19E	21.5	.
940828	10	11	28.2	55.45N	122.50E	20.3	.
940918	16	17	49.07	62.42N	147.64E	18.2	.
940928	10	38	08.4	52.73N	122.26E	29.2	.
941001	08	52	54.27	72.26N	127.24E	11.9	.
941003	23	12	59.06	72.41N	127.50E	4.4	.
941007	12	58	52.2	54.31N	124.57E	18.1	.
941026	07	53	18.76	57.22N	125.81E	13.9	.
941105	06	42	09.12	71.79N	130.98E	14.3	.
941207	19	52	17.4	56.12N	124.15E	11.4	.
941228	06	23	27.98	57.55N	132.08E	33.0	.
950106	13	05	14.96	58.59N	148.46E	5.8	2.6
950115	00	54	27.77	60.77N	148.39E	5.7	.
950131	12	43	43.36	72.73N	131.66E	33.0	.
950201	07	57	35.2	56.64N	121.86E	14.4	.
950209	16	53	19.1	63.64N	133.92E	26.5	.
950301	17	29	29.7	51.83N	125.51E	33.0	.
950327	21	20	00.18	54.22N	126.78E	29.5	.
950504	13	53	37.0	57.24N	122.22E	16.6	.
950527	13	03	52.7	52.63N	142.83E	.	.
950616	11	34	53.4	57.11N	124.90E	14.5	.
950806	08	30	43.7	56.99N	122.00E	14.0	.
950815	01	53	25.23	58.12N	148.90E	14.1	.
960128	01	10	18.76	59.30N	147.66E	9.5	.
960212	18	56	59.9	57.53N	120.77E	26.2	.
960220	23	32	54.09	61.23N	158.42E	25.4	.
960303	10	53	57.77	58.26N	158.17E	4.4	.
960303	11	54	41.62	58.26N	158.04E	33.0	.
960318	20	15	14.89	58.35N	143.97E	30.6	.
960403	23	39	29.97	62.85N	147.32E	6.1	.
960406	00	20	39.37	62.83N	147.63E	11.6	.
960606	21	53	42.36	63.02N	144.73E	6.0	.

960612	17	08	01.2	56.84N	121.24E	24.9	.
960707	10	50	00.61	58.58N	157.54E	12.2	5.8
960707	14	19	52.14	58.63N	157.34E	6.3	.
960707	14	29	03.55	58.56N	157.50E	12.0	.
960707	15	39	03.11	58.28N	157.42E	31.6	.
960707	17	58	34.14	58.53N	157.49E	3.9	.
960707	23	23	49.02	58.50N	157.32E	16.8	.
960708	01	06	25.24	58.47N	157.28E	0.	.
960708	13	29	51.71	58.59N	157.38E	15.1	.
960709	04	07	41.83	58.43N	157.17E	8.4	.
960709	10	07	05.5	56.61N	120.95E	7.4	.
960709	11	52	51.98	58.33N	157.19E	0.	.
960710	05	20	11.74	58.45N	157.70E	0.8	.
960710	06	22	05.38	58.52N	157.34E	18.2	.
960710	07	15	54.93	58.67N	157.45E	15.2	.
960710	14	09	33.80	58.57N	157.64E	3.9	.
960710	18	36	37.17	58.46N	157.30E	28.1	.
960727	07	28	34.95	60.49N	148.66E	7.4	3.6
960803	12	32	49.64	58.65N	157.21E	29.4	.
960803	13	09	13.64	58.68N	157.08E	0.	.
960807	18	51	14.48	58.58N	157.21E	7.6	.
960808	17	09	40.38	58.75N	157.20E	22.2	.
960824	07	29	41.80	60.05N	153.05E	17.7	.
960902	23	37	54.6	56.60N	123.88E	19.4	.
960904	12	56	31.38	57.55N	128.03E	15.1	.
960913	15	45	07.54	58.70N	157.64E	6.5	.
960914	05	29	59.84	58.65N	157.41E	9.8	.
960914	05	41	45.02	58.73N	157.48E	8.3	.
960914	09	57	57.82	58.74N	157.14E	0.	.
960916	03	05	07.56	58.56N	157.35E	14.6	.
960925	01	48	26.12	63.38N	150.43E	9.9	.
961024	19	31	50.91	67.04N	173.08W	0.	6.0
961024	21	57	36.71	67.08N	173.20W	14.1	.
961126	20	18	18.31	58.66N	157.54E	5.8	.
961207	10	38	20.98	62.12N	153.75E	10.6	.
970129	15	51	38.11	58.81N	149.65E	5.4	.
970304	21	49	26.30	62.07N	155.92E	10.0	.
970607	11	59	41.19	64.19N	148.32E	0.	.
970614	13	31	08.39	63.87N	148.57E	2.9	.
970616	09	54	07.72	64.07N	148.43E	9.0	.
970629	21	37	46.82	59.78N	152.40E	4.6	.
970721	12	37	49.52	60.08N	144.68E	10.2	.
970825	06	00	43.24	63.54N	144.91E	8.2	.
970910	18	42	42.47	61.77N	156.15E	1.5	.
970914	14	07	54.73	61.10N	145.23E	0.	.
970915	05	48	00.77	59.95N	151.96E	0.	.
971122	11	41	15.58	61.14N	155.44E	7.7	.
971206	16	06	07.04	59.40N	147.91E	10.9	.
980103	03	15	51.98	59.81N	152.50E	0.	.
980130	23	11	39.97	63.48N	150.29E	20.1	.
980201	02	33	13.50	63.24N	150.00E	2.4	.
980215	04	35	42.38	61.49N	147.43E	0.	.
980221	22	22	47.82	60.33N	152.86E	5.4	.
980304	04	57	18.17	62.08N	156.99E	6.3	.
980309	10	38	11.91	63.87N	156.95E	0.	.
980311	23	46	07.01	58.46N	157.22E	0.	.
980312	03	15	54.71	62.10N	157.03E	1.5	.
980314	17	03	29.87	58.40N	157.41E	3.5	.
980316	05	33	08.13	58.42N	157.30E	13.7	.
980318	21	30	34.19	58.39N	156.98E	8.3	.
980320	16	50	52.81	62.06N	157.06E	7.9	.
980325	23	52	55.66	62.11N	156.94E	5.0	.
980326	02	17	29.32	62.09N	157.05E	3.4	.
980326	02	24	00.38	62.08N	156.93E	3.2	.
980326	06	41	33.48	62.09N	156.73E	8.7	.
980327	09	29	59.56	62.07N	156.87E	5.6	.
980327	09	42	36.02	62.09N	156.95E	7.2	.
980404	14	02	34.13	62.05N	156.76E	7.6	.
980505	21	31	57.75	59.05N	147.14E	5.1	.
980508	22	32	49.88	62.02N	157.03E	4.9	.
980531	08	02	51.19	62.04N	156.54E	11.7	.
980604	12	03	23.75	62.06N	157.18E	2.3	.
980901	10	26	39.52	63.06N	147.28E	8.4	.
980917	22	50	11.78	64.95N	149.24E	0.	.
981106	03	48	20.34	63.40N	158.75E	12.6	.
981218	14	03	48.02	63.23N	159.45E	4.2	.

APPENDIX C

Relocations and GT classifications of Teleseismically recorded earthquakes from eastern Russia. Each location was relocated using the crustal models calculated in Section 3. Each event listed had a significant amount of local/regional data added, supplementing that reported in the ISC. ISC calculated parameters are given for reference. Location types indicate which data set was considered best for calculating relocations: T - teleseismic, R - regional, L - local. See text in Section 4 for additional discussion on selection of the best data set.

DATE	MSU RELOCATIONS				ISC SOLUTION				MAG	LOC	GT
	ORIGIN TIME h. m. s.	LAT.	LONG	DEPTH	ORIGIN TIME h. m. s.	LAT.	LONG.	DEPTH			
710518	22 44 42.23	63.960	146.064	20.85	22 44 39.25	63.921	146.101	0.0	7.1	T	25
710518	23 09 09.20	64.029	146.100	2.62	23 09 09.46	64.181	146.450	0.0	.	T	--
710614	13 48 52.96	56.200	123.636	11.91	13 48 53.66	56.183	123.594	15.0	5.4	T	25
710614	14 25 54.16	56.187	123.654	12.56	14 25 56.90	56.171	123.562	33.0	4.4	T	--
720113	17 24 19.62	61.902	147.034	9.74	17 24 23.17	61.940	147.038	33.0	5.3	T	25
720115	18 08 00.31	57.718	121.062	8.83	18 08 00.79	58.073	120.748	0.0	4.6	R	--
720330	20 20 52.45	64.004	145.969	4.98	20 20 50.17	63.769	145.994	0.0	.	T	25
720613	10 45 03.27	54.849	126.435	18.75	10 45 03.19	54.911	126.460	0.0	4.9	T	25
720809	20 51 47.59	56.945	127.625	19.38	20 51 51.76	56.838	127.410	36.0	4.7	R	25
730608	11 43 47.07	63.822	146.173	26.07	11 43 48.25	63.776	146.200	33.0	.	T	--
731102	07 31 28.80	54.094	125.697	1.63	07 31 32.86	54.042	125.746	0.0	4.9	T	--
740619	03 09 37.00	63.236	151.037	30.64	03 09 36.12	63.140	150.921	14.7	4.9	R	25
750629	12 24 39.55	53.110	132.134	4.74	12 24 43.28	53.074	132.111	33.0	4.8	T	25
751104	12 41 05.39	59.827	160.326	5.08	12 41 12.39	60.020	160.317	52.3	4.7	T	--
760121	06 01 48.56	67.731	140.194	18.98	06 01 48.51	67.734	140.034	0.0	5.0	T	25
760216	22 06 24.32	58.170	131.044	0.00	22 06 32.07	58.573	131.012	33.0	4.5	T	--
770816	13 56 54.67	53.878	128.875	0.00	13 56 59.80	53.926	128.715	33.0	4.2	T	--
771101	03 54 22.45	55.556	130.641	3.84	03 54 26.14	55.411	130.522	31.7	4.5	T	--
771118	21 55 36.34	60.142	143.423	9.54	21 55 39.45	60.052	143.321	33.0	4.5	T	25
780605	07 05 52.16	60.042	160.361	3.78	07 05 59.37	60.131	160.406	55.8	5.1	R	25
780605	21 01 34.09	60.089	160.385	8.06	21 01 37.40	60.163	160.390	28.2	4.5	R	25
790427	19 38 13.16	55.797	130.528	15.46	19 38 18.41	55.935	130.166	32.8	4.6	R	25
790819	07 10 06.14	61.326	159.131	29.50	07 10 06.67	61.329	159.041	30.7	5.1	T	25
791007	01 29 26.09	65.003	144.016	12.29	01 29 26.26	65.019	143.774	6.1	4.8	R	25
791026	00 26 26.18	62.238	153.783	19.01	00 26 28.60	62.258	153.319	27.9	4.5	T	10
791118	08 59 15.88	62.213	153.801	2.02	08 59 19.08	62.302	153.318	20.6	.	T	--
800225	23 50 02.71	54.892	125.191	30.98	23 50 00.58	55.143	125.047	3.0	4.0	R	10
810522	04 59 21.03	61.098	156.699	9.22	04 59 25.89	61.148	156.624	50.6	5.1	R	--
811108	21 56 09.29	61.821	153.675	20.81	21 56 11.50	61.834	153.686	37.4	5.6	R	10
811110	10 07 52.32	63.954	148.697	24.38	10 07 52.73	63.862	148.484	33.0	4.7	R	25
811205	01 49 08.92	56.996	123.143	18.0	01 49 10.84	57.356	122.930	36.9	.	R	25
820903	07 29 26.40	66.933	133.319	29.76	07 29 22.17	66.823	132.776	0.0	4.5	T	25
830325	10 36 55.41	63.580	149.908	5.40	10 36 56.85	63.632	149.740	15.7	4.7	R	10
830514	08 09 13.46	65.852	174.822	0.00	08 09 22.26	65.811	175.975	33.0	4.5	T	25
830515	06 00 36.88	65.861	-173.216	2.58	06 00 43.30	66.031	-172.540	33.0	4.2	T	25
830730	15 42 09.76	53.303	132.479	22.24	15 42 12.20	53.242	132.642	26.0	4.4	R	25
840324	01 03 19.24	54.517	136.970	23.26	01 03 17.81	54.512	137.036	3.0	5.0	R	25
840802	21 25 39.14	60.897	144.640	8.02	21 25 37.78	60.887	144.683	0.0	4.9	R	25
841029	14 06 14.27	62.113	163.756	26.73	14 06 14.59	62.049	163.736	33.0	4.6	T	--
841122	13 52 57.11	68.473	140.821	18.71	13 52 57.17	68.521	140.815	19.1	5.3	R	25
841202	08 35 45.04	63.383	150.502	22.06	08 35 47.94	63.461	150.525	43.9	5.2	R	10
850129	00 36 05.81	64.159	145.778	10.17	00 36 09.38	64.286	145.672	33.0	4.5	L	10
850201	08 31 45.86	62.892	127.241	12.63	08 31 45.85	62.843	127.381	3.0	4.6	T	--
850301	09 19 18.42	57.556	125.461	10.60	09 19 21.89	57.667	125.573	33.0	4.6	R	10

850602	04	08	09.37	64.846	144.052	8.26	04	08	12.81	64.788	144.045	33.0	.	R	25
850624	03	54	34.78	65.257	144.698	17.58	03	54	32.38	65.252	144.489	0.0	4.6	R	25
860209	12	42	53.73	48.770	126.467	13.77	12	42	51.24	48.685	126.625	0.0	4.8	T	25
860228	17	07	24.63	48.699	126.543	0.00	17	07	24.42	48.645	126.656	0.0	4.8	T	25
860815	17	53	08.20	48.691	126.621	19.22	17	53	14.51	48.181	126.434	33.0	4.3	T	25
860815	20	20	33.58	48.755	126.492	3.70	20	20	37.80	48.676	126.559	33.0	5.1	T	25
861019	18	30	58.82	63.894	-178.546	19.79	18	30	56.86	63.897	-178.693	6.4	5.3	T	25
861218	18	04	12.17	61.216	143.719	25.85	18	04	10.22	61.312	143.729	0.0	4.6	R	25
870211	00	58	20.89	62.849	156.863	5.68	00	58	23.59	62.877	156.699	22.8	4.4	R	10
870421	12	39	48.43	64.922	-170.428	12.58	12	39	56.90	64.829	-169.398	33.0	.	T	25
881013	00	32	10.79	61.769	169.699	21.07	00	32	12.87	61.853	169.651	33.2	5.4	T	25
890409	04	16	22.76	59.828	145.125	14.64	04	16	27.35	59.916	145.230	0.0	4.8	R	25
890420	22	59	53.63	57.245	122.146	29.30	22	59	54.24	57.168	122.015	26.0	5.9	R	25
890421	19	08	37.29	57.067	122.269	33.00	19	08	41.00	57.168	123.768	33.0	4.8	L	10
890424	01	33	59.74	57.111	122.277	24.88	01	34	01.57	57.278	122.155	39.6	4.8	R	10
890429	06	25	39.17	57.149	122.229	33.00	06	25	38.78	57.175	122.159	26.1	5.3	R	10
890507	16	28	05.70	57.075	122.233	33.00	16	28	05.22	57.123	122.162	27.0	5.0	R	10
890517	05	04	35.84	57.056	122.237	30.69	05	00	35.56	57.089	122.107	26.9	5.6	R	10
890517	15	55	22.85	57.063	122.241	32.05	15	55	56.12	61.804	119.599	33.0	4.5	R	10
890709	20	07	46.33	57.098	122.309	33.00	20	07	49.17	57.348	121.903	52.1	4.8	R	10
890723	12	01	31.20	54.532	124.934	25.26	12	01	29.97	54.498	125.054	10.0	4.6	R	10
900717	03	37	25.23	48.707	132.023	18.95	03	37	26.30	48.857	131.928	15.0	4.5	R	25
901102	21	54	02.63	64.785	146.640	6.97	21	54	03.19	64.931	146.604	10.0	4.6	R	10
910109	08	15	37.55	56.844	120.386	21.56	08	15	35.50	56.998	120.405	5.2	4.6	R	10
910217	20	47	08.66	60.644	166.940	0.0	20	47	13.91	60.970	166.830	33.0	4.1	T	--
910218	11	13	48.52	60.861	167.026	12.39	11	13	43.75	60.089	165.784	33.0	4.8	T	--
910220	04	46	32.49	60.841	167.086	0.0	04	46	37.17	60.711	167.125	33.0	4.5	T	25
910304	18	12	28.02	54.705	121.041	33.00	18	12	29.75	55.015	121.116	33.0	.	T	25
910308	09	02	19.61	60.934	167.009	15.26	09	02	20.45	60.815	167.087	23.1	5.2	T	25
910308	11	36	30.89	60.928	166.988	33.00	11	36	28.39	60.856	167.016	13.0	6.7	T	25
910308	11	54	58.49	60.769	167.063	16.68	11	54	57.86	60.810	167.058	10.0	6.1	T	25
910310	12	26	44.68	60.948	167.289	6.10	12	26	46.07	60.914	167.261	14.2	5.1	T	25
910311	15	33	46.34	60.762	166.857	33.00	15	33	46.27	60.763	166.897	33.0	4.7	T	25
910311	19	46	50.60	60.663	166.770	33.00	19	46	46.2	60.557	166.818	5.4	4.8	T	25
910312	19	43	25.03	60.889	167.110	23.93	19	43	25.86	60.825	167.116	29.5	5.2	T	25
910313	06	58	43.34	60.781	166.863	33.00	06	58	43.2	60.651	167.241	33.0	4.2	T	--
910317	06	26	52.06	60.809	167.007	33.00	06	26	52.16	60.814	167.003	33.0	5.2	T	25
910321	14	28	33.45	60.619	167.438	28.14	14	28	35.27	60.890	167.022	33.0	4.5	T	--
910322	07	55	16.90	60.728	167.166	7.31	07	55	20.83	61.078	166.481	33.0	4.7	T	--
910322	17	18	22.79	60.836	167.543	5.84	17	18	26.50	60.027	167.136	33.0	4.4	T	--
910329	13	27	50.44	60.723	166.993	21.40	13	27	52.05	60.709	166.921	32.5	5.0	T	25
910527	08	55	35.05	57.088	122.209	31.16	08	55	33.55	57.060	122.129	33.0	4.2	R	10
910804	19	08	06.24	65.477	143.229	21.87	19	08	07.24	65.467	142.905	33.0	4.3	R	10
920121	18	07	35.63	61.764	169.741	11.19	18	07	39.36	61.832	169.574	33.0	4.6	T	25
920122	06	29	16.67	65.855	143.255	20.06	06	29	17.10	65.806	142.990	33.0	4.6	R	25
920413	22	47	21.21	56.569	121.112	14.35	22	47	22.76	56.693	121.157	33.0	4.1	R	10
920913	21	42	56.24	62.065	153.795	10.20	21	42	57.64	61.634	154.105	21.3	4.7	R	10
930221	09	37	53.24	57.954	120.714	24.42	09	37	54.70	58.289	120.613	33.0	4.2	R	25
930324	22	43	29.89	71.659	130.225	19.09	22	43	29.78	71.686	130.405	20.3	4.8	T	25
930830	07	56	35.56	64.068	145.825	6.37	07	56	34.88	64.162	145.941	10.0	4.2	R	10
940128	01	05	13.17	55.077	135.226	12.46	01	05	13.78	55.054	135.175	15.3	4.9	T	25
950209	16	53	19.00	63.653	133.925	23.53	16	53	17.56	63.882	133.722	10.0	4.5	T	25
950301	17	29	26.41	51.673	125.602	27.51	17	29	38.30	50.960	125.290	6.0	3.5	T	--
950815	01	53	23.06	58.122	148.817	0.00	01	53	25.85	58.069	148.844	16.2	4.6	T	25
960212	18	56	59.87	57.527	120.771	26.12	18	57	01.18	57.656	120.677	33.0	4.3	T	25
960220	23	32	57.92	61.215	158.014	15.99	23	33	01.86	60.650	159.011	33.0	3.6	T	--
960707	10	49	59.79	58.611	157.794	13.00	10	49	59.59	58.585	157.697	10.0	5.6	T	10
960707	23	23	47.20	58.591	157.812	8.20	23	23	53.59	58.689	157.838	59.0	4.1	T	25
960708	13	29	49.65	58.641	157.798	7.29	13	29	59.58	58.730	157.738	87.7	4.0	T	25
960710	05	20	14.54	58.614	157.660	8.03	05	20	15.66	58.649	157.942	11.0	3.6	T	--
960710	07	15	52.00	58.637	157.780	5.86	07	15	56.25	58.685	157.718	35.3	4.5	T	25
960918	09	51	41.77	67.906	140.171	0.0	09	51	46.82	68.013	139.821	33.0	4.6	T	25
961003	16	09	18.79	62.092	153.901	6.29	16	09	20.4	62.410	153.709	10.0	4.5	R	25

961024	19	31	50.64	67.026	-173.119	0.00	19	31	54.1	66.96	-173.24	20.0	6.1	T	25
961024	21	57	37.27	67.068	-173.257	12.77	21	57	37.5	67.08	-173.28	18.0	4.9	T	25
961103	23	24	33.77	64.754	-170.281	33.00	23	24	30.7	64.84	-170.41	10.0	4.9	T	25
961126	20	18	17.03	58.681	157.725	11.10	20	18	17.6	58.743	157.773	15.4	4.0	T	--
961129	04	38	50.56	64.376	145.366	10.43	04	38	53.82	64.464	145.389	33.0	3.4	T	10
970618	06	13	43.11	64.934	137.934	11.53	06	13	46.85	65.033	137.258	38.6	4.0	T	25
970620	04	57	02.43	64.759	146.963	18.24	04	57	04.32	64.759	146.887	33.0	3.6	T	10
970902	22	30	10.65	57.629	137.669	29.28	22	30	07.71	57.658	137.823	10.0	3.9	T	--
971019	16	58	18.17	57.321	120.600	9.79	16	58	26.43	57.759	120.216	51.1	3.8	T	--
971021	00	18	08.71	57.303	120.706	22.09	00	18	12.22	57.026	120.055	46.1	3.8	R	--
971024	11	50	13.43	57.341	120.743	24.51	11	50	17.52	57.232	120.174	47.4	4.3	R	25
971024	11	58	11.55	57.316	120.680	33.00	11	58	12.78	57.117	120.226	22.3	3.6	L	--
971024	12	05	46.25	57.337	120.749	12.53	12	05	46.32	57.131	120.291	10.0	4.0	R	--
971024	12	19	03.53	57.356	120.560	14.07	12	19	04.73	57.338	120.590	25.0	4.1	T	--
971024	12	52	50.76	57.267	120.492	18.60	12	52	53.84	57.290	120.035	42.2	4.4	R	25
971024	13	14	04.54	57.157	120.441	33.00	13	14	03.77	57.096	120.483	31.9	3.4	T	--
971106	19	50	29.56	57.407	120.662	0.99	19	50	35.72	57.421	120.436	54.4	4.1	R	25
971106	20	24	39.83	57.342	120.656	12.61	20	24	45.03	57.348	120.229	33.0	3.5	R	--
971108	15	07	08.12	57.336	120.667	9.93	15	07	12.86	58.461	120.766	0.0	3.6	T	--
971122	11	41	15.21	61.137	155.498	8.68	11	41	18.81	61.177	155.442	36.8	3.7	T	25
980314	17	03	29.69	58.491	157.636	9.45	17	03	32.33	58.555	157.581	28.4	4.2	T	25
980316	05	33	07.58	58.442	157.461	10.04	05	33	11.69	58.352	157.513	44.	4.2	T	25
980318	21	30	31.19	58.310	157.307	2.67	21	30	20.2	58.910	156.670	0.0	4.1	T	--
980326	06	41	29.94	62.131	157.150	0.0	06	41	31.76	62.001	157.352	10.0	4.3	T	--
990827	20	14	40.16	58.724	147.292	3.6	20	14	44.32	58.61	147.21	33.0	4.1	T	--
991002	07	01	23.32	63.254	148.095	5.1	07	01	27.73	63.089	148.113	43.8	4.0	T	--
000927	13	26	59.59	62.443	145.227	7.6	13	26	59.6	62.433	145.193	10.0	.	T	--

APPENDIX D

Digital station deployment sites and observations

OVERVIEW

In the summers of 1999 and 2000, as well as winter and summer 2001, the senior author traveled to Magadan to upgrade existing photo paper seismic stations to digital acquisition. This work was performed in conjunction with the Magadan Experimental Methodological Seismological Division (MEMSD), from Magadan, Russia.

A total of nine digital acquisition systems have been purchased and imported into Russia for deployment. The digital acquisition systems were manufactured by PC System Design, Palo Alto, California, and use 8 channel, 24 bit A/D cards with GPS timing. Data are recorded on PC computers, which were purchased in Russia. Except as noted, the seismometers recorded are three-component Russian (Soviet) SM3-KV short period instruments, with the free period set at 1.5 seconds. Seismometer output is amplified 1000 times, and a 10 Hz cutoff low pass filter is used. The amplifier/filter was designed and manufactured by MEMSD. Digitization of time and all seismometer components is 30 s.p.s. A description of each station follows.

PERMANENT STATIONS

ANADYR. Anadyr is located several thousand kilometers east and a bit north of the other deployed stations. The station recorded a Guralp CMG 40T broadband seismometer, upgrading an existing analog photopaper station. The station vault consists of a concrete pad set into permafrost underneath the station building. The recording computer failed shortly after installation in March, 2000, and was logistically problematic to repair. The station was removed in May, 2001.

MAGADAN. Although not installed as a part of this study, data from data from the IRIS GSN station Magadan (MA2), has actively been used. There are two station sites in Magadan. The original Magadan station (MAG), and headquarters of the Magadan network, is located in a residential part of the city about 1 km south and a little west from the center of town. The station consists of a single story, moderately sized, wooden, office building. The seismic vault is located under the station in a cellar about 5 m below the ground surface. The vault contains a large concrete pad measuring about 2 m per side mounted in a rocky soil. This old station site in Magadan had considerable noise due to vault conditions and cultural noise. The vault is no longer used except for instrument testing purposes.

The new GSN station Magadan (MA2) is recorded at the old Magadan station site. The vault of the new Magadan GSN station is located on top of a mountain about 2.5 km to the northwest of the old station. The vault consists of a bunker set into bedrock of granitic composition. Seismometers used at MA2 are Streckeisen STS-1.

NEL'KOBA. Nel'koba is a small town whose primary function was a regional supply and repair center for support of the gold mining industry in the region. The seismic vault in Nelkoba consists of a concrete pad measuring approximately 1 m x 1 m set into permafrost. The concrete pad is housed in a small wooden shed on the grounds of the Nelkoba kindergarten, on the west side of town. The current station site was constructed in the summer of 1997 and is approximately 200 m north of a previous site. At some time in the past, SKM instruments were operated at the old station site. The town of Nelkoba was permanently abandoned in late September, 1999. Our equipment was moved to establish the station in Omchak, near the Matrosova temporary station deployment site (see below).

OKHOTSK. Okhotsk is located on the north coast of the Sea of Okhotsk. The seismic station is located in the town's telecommunication center and operated under contract from the Magadan EMSD. The Guralp CMG 40T broadband sensor is deployed in a small shelter and set on a 1 meter square concrete pad set 1.5 meters into rocky ground on a terrace above the coast of the Sea of Okhotsk. The station at Okhotsk is a new site, opened in early July, 2000.

OMCHAK. Omchak is a mining town with a large refinery operation that supports the Matrosova gold mine a few kilometers away. The station at Omchak is a new station site using equipment moved from the station in Nel'koba after the town was abandoned. Seismometers at Omchak sit on a concrete pad directly on bedrock in an abandoned mine adit. Background noise levels at Omchak are the lowest of all stations deployed in this study. The Omchak station frequently records mine blasts from the Matrosova gold mine a few kilometers distant.

OMSUKCHAN. Omsukchan is a local administrative center in the eastern part of the Magadan region. The digital station was deployed in mid July 2001, using the Guralp CMG-40T removed from Anadyr. The station is situated on a 1.5 meter square concrete pad at the bottom of a blind stairwell adjacent to a large apartment building near the center of town. The seismometer is approximately 2 meters below ground level. Omsukchan frequently records blasts from nearby coal, gold and silver mines

SEYMCHAN. Seymchan is one of the longest running seismic station sites in the Magadan district, opening in 1969. A GEOSCOPE station was installed here in the early 1990's, which broke after about 4 years of operation due to a failed tape drive to record data. The station was not repaired, but all equipment, including the STS-1 seismometers, remains in place. The station deployed here as a part of this study digitizes an analog output from the GEOSCOPE station and logs the data on a computer. At Seymchan, the seismometers are located in an underground permafrost vault, set on a concrete pier that extends several meters into permafrost. Temperatures remain constant in the vault at around minus 1° C. The station at Seymchan is situated within the town not far from the power plant. Considerable noise is recorded by the Seymchan station when the power plant grinds coal.

SUSUMAN. Susuman is a town of approximately 5,000 people and is the center of placer gold production in the Magadan region. The seismic station is operated by MEMSD and is located at the meteorological station just west of the main town. The station is sufficiently far from the town that cultural noise is minimal. The seismic vault in Susuman consists of a large concrete block set approximately 1.5 m into a permafrost foundation. The vault is inside a small building adjacent to the meteorological station building.

TALAYA Talaya is a resort town of approximately 500 people; the main attraction is the natural hot springs. Two digital seismic stations have operated here, both by MEMSD. The seismic vault at the old Talaya site consisted of a 1 m square concrete pad set into volcanic bedrock on the side of a hill. The seismic station was located on the east side of town next to the now abandoned cinema theater. This Talaya site was abandoned in September, 2000 as electricity and heat were cut off from the abandoned portion of the town where the station was located.

The new Talaya site was established approximately 300m ESE from the old Talaya site, also in September, 2000. The site is located in the town's new administrative/hospital building that is housed in the old school. The seismic vault consists of a 2 m square concrete pad set into the ground below the building, which consists of sand and rocky material. Distance to bedrock is uncertain. Background noise levels are similar to the old Talaya site.

UST' NERA. The seismic station in Ust' Nera is operated by the Yakutsk seismic network. The station in Ust' Nera has occupied its present site since 1992. The seismic vault consists of a large concrete block set into a permafrost foundation. The vault is located between two large apartment buildings, thus cultural noise can be high at times due to passing cars and children playing on top of the vault. Seismometers recorded here are Russian (Soviet) SKM short-period instruments. Seismometer output is amplified 60 db and a 30hz cutoff low pass filter is applied. The amplifier used in Ust' Nera is a USGS Prototype Series Seismic Amplifier. The amplifier was originally part of an IASPEI system installed in Ust' Nera in 1997.

TEMPORARY STATIONS

MATROSOVA (61.6432° N, 147.8205° E). Matrosova is a small town with an operating gold mine. Seismometers were located on the concrete foundation of a building used for ore transfer. The foundation of the building was set into bedrock consisting of black shale. In Matrosova, digitization of time and all seismometer components was 120 s.p.s. The station was operated for only a few hours, to record blasting from the mine. Two large blasts of 1,300 and 1,500 kg of Ammonite were recorded, among several much smaller explosions. Several abandoned mine adits are also in and near Matrosova, which may be good sites for future permanent stations.

STOKOLVIYA (61.8475° N, 147.6598° E). Stokolviya is a hydrological research station in a remote, unpopulated region. The seismic vault consisted of a one meter pit dug into the side of a hill. Ground material consisted primarily of angular cobble sized rocks of volcanic origin. The material was consistent with the bedrock surface being close. When installing the station, it was intended that Stokolviya would be a permanent site. All permissions were obtained, and the hydrologic research station agreed to operate it prior to installation. However, the individual workers at the station were unfamiliar with computers and refused to consider operating the station. This was unfortunate, as the site is quiet. Also at Stokolviya are several boreholes, some of which exceed 200 m depth. These boreholes are not is use, thus may be ideal for future borehole instrument installation. The temporary station deployed at Stokolviya recorded two explosions from the Matrosova gold mine.

TAUISK (59.729°N, 149.335°E). Tauisk is a coastal village west of Magadan whose primary function is a small army frontier border patrol post. The station at Tauisk was deployed from January 18 - April 18, 2001 to record aftershocks of the January 07, 2001 Mb 5.3 earthquake that occurred about 80 km west of Magadan. The station was situated on the concrete slab in the basement rifle firing range of the school, which is located in the center of the village. Many earthquake aftershocks were recorded in Tauisk.

TALON (59.757°N, 148.661°E). The seismic station deployed at Talon was installed in the dirt basement of a house in the south edge of the village to record aftershocks of the January 07, 2001 Mb earthquake that occurred about 80 km west of Magadan. The station operated from January 26 - February 16, 2001. The station was quite noisy and only a few events were recorded.

TAL'YURYAKH (63.307°N,146.634°E). Tal'Yuryakh was deployed a few kilometers northwest of the active pit at the Tal'Yuryakh coal mine to obtain blasting information. The station operated from March 16 - June 16, 2001. The station did not operate properly after mid May 2001 due to a power failure in the amplifier. Seismometers deployed were three component SM3 instruments located in a small pit adjacent to a mine outbuilding. Several blasts and tectonic events were recorded.

APPENDIX E

The 10 June, 2000, Kadakchan explosion.

The largest explosion to have occurred during the period of the study is believed to have occurred at the Kadakchan coal mine northwest of Susuman on 10 June, 2000. This appendix outlines the evidence used to determine its nature as an anthropogenic event.

This event was well recorded by four of the digital seismic stations deployed as a part of this study, as well as two additional operating analog photopaper stations in the Magadan region (Table E-1). The K-class of the event was 9.5, which corresponds to a local magnitude of 3.3. Given the size of the event, it was routinely located and cataloged as a tectonic earthquake. The event was located using the calibrated crustal velocity model discussed in Section 3 above. Results of the location, including arrival residuals are shown in Table E-2.

The closest operating recording station to the event was Omchak (Susuman was down). Unfortunately, timing at Omchak was not working. In the process of locating the event, data from Omchak was used with a manual time correction applied. The time correction was determined by minimizing the sum of residuals for all Omchak arrivals, which is essentially using Sg-Pg-Pn time differences to fit the data. It should be noted that as the event was originally considered tectonic, there was no attempt to 'force' the event to any particular location, mine or otherwise.

The tectonic nature of the event was not questioned until September, 2001, when it was found that the calculated epicenter of the event falls very close to the Kadakhan mine (Figure E-1). The proximity to the Kadakchan mine, and distance to other tectonic events, flagged this event for a closer look.

Upon closer inspection of the seismogram from Omchak, a large acoustic arrival was noted about seven minutes after the P arrival (Figures E-2 and E-3). Using the calculated origin time of the event, the velocity of the acoustic arrival over the 163 km between the epicenter and the station in Omchak was 328 m/s. The existence of the acoustic arrival is most consistent with an explosion and not a tectonic earthquake.

During the 2001 field season, work was undertaken to acquire better information and waveforms from mines in northeastern Russia. Three confirmed blasts from Kadakchan were recorded at a nearby temporary station, as well as the station in Omchak. Yields of the blasts were provided by the mining company. Figure E-4 compares the Omchak waveforms of the 10 June, 2000, event with a 10,140 kg Kadakchan explosion from 23 March, 2001. The character of the waveform and relative amplitudes correlate quite well for the Pg arrival, especially accounting for the noise on the 2001 trace and the width of one sample. The Pn arrivals are also not inconsistent with each other. For both records, the Sg-Pg time differences are also the same. The correlated waveforms between the two records is consistent with the 10 June, 2000, event being a large mine blast.

Considering the $M_L = 3.3$ size of the 10 June, 2000, event, any explosion source would have to be quite large. Leith (1994) tabulated large explosions in the Magadan region covering the time period 1989 - 1992. The largest explosion to occur took place at the Kadakchan coal mine, and had a yield of 256 tons. Given the history of large blasts at Kadakchan, an explosion source for the 10 June, 2000, event can not be ruled out. The origin time of the 10 June, 2000 event is 05 hours, 54 minutes UTC, which is the middle of local day and consistent with historic blasting in the region. Therefore, origin time can not rule out a large mine blast source.

All available lines of evidence either directly support a Kadakchan mine explosion origin

Table E-1. Original data from the 10 June, 2000, event.

STATION	PHASE TYPE	ARRIVAL TIME H. M. S.	PERIOD S	AMPLITUDE IN MICRONS N-S	E-W	VERT	K CLASS	NOTES
OCH	P	05 56 49.9						INFRASONIC ARRIVAL AT:
	Pg	56 50.9						06 04 40.5
	Sg	57 11.7						All OCH TIMES REFLECT
								MANUAL CORRECTION OF + 9.3s
SEY	eP	05 57 05.0						
	ePg	57 09.8						
	Pgm	57 11.3	0.2	0.07		0.16		
	eS	57 33.5						
	eSg	57 42.3						
	Sgm	57 46.0	0.2	0.13	0.09		K= 9.4	
TL-	eP	05 57 15.0						
	ePg	57 23.8						
	eSg	58 05.9						
	Sgm	58 10.0	0.7	0.37	0.30		K=10.3	
MGD	eP	05 57 18.5						
	ePg	57 28.5						
	iSg	58 17.0						
	Sgm	58 27.0	0.9	0.21	0.24		K=10.1	
MA2	eP	05 57 25.2						
	ePg	57 38.1						
	Pgm	57 38.7	0.3			0.01		
	eSg	58 30.2						
	Sgm	58 38.5	0.4	0.04	0.07		K= 9.7	
OMS	ePg	05 57 39.4						
	eSg	58 32.0						
	Sgm	58 42.6	0.9	0.13	0.11		K= 9.9	

Table E-2. Location parameters from the 10 June, 2000, event. Low residuals indicate a stable location.

Origin Time: 05 56 23.8 UTC
Latitude: 63.082°N
Longitude: 146.976°E
Depth: 14 km
Infrasonic velocity to Omchak: 328 m/s

STATION	PHAS.	ARR. TIME	DIST. (DEG.)	AZIMUTH	RESIDUAL	WEIGHT
OCH	P	5 56 49.9	1.48	163.23	.13	1.0
	PG	5 56 50.9	1.48	163.23	-.39	1.0
	SG	5 57 11.7	1.48	163.23	.69	.5
SEY	P	5 57 4.7	2.47	91.06	.54	1.0
	PG	5 57 9.8	2.47	91.06	.34	1.0
	SG	5 57 42.0	2.47	91.06	-.28	.5
TL-S	P	5 57 15.0	3.21	125.17	.25	1.0
	PG	5 57 23.8	3.21	125.17	.57	1.0
	SG	5 58 5.9	3.21	125.17	.12	.5
MGD	P	5 57 18.5	3.54	147.81	-.78	1.0
	PG	5 57 28.5	3.54	147.81	-.65	1.0
	SG	5 58 17.0	3.54	147.81	1.04	.5
OMS	PG	5 57 39.4	4.08	94.09	.22	1.0
	SG	5 58 32.0	4.08	94.09	-1.29	.5
MA2	P	5 57 25.2	3.97	150.87	-.18	1.0
	PG	5 57 37.1	3.97	150.87	.05	1.0
	SG	5 58 29.1	3.97	150.87	-.52	.5

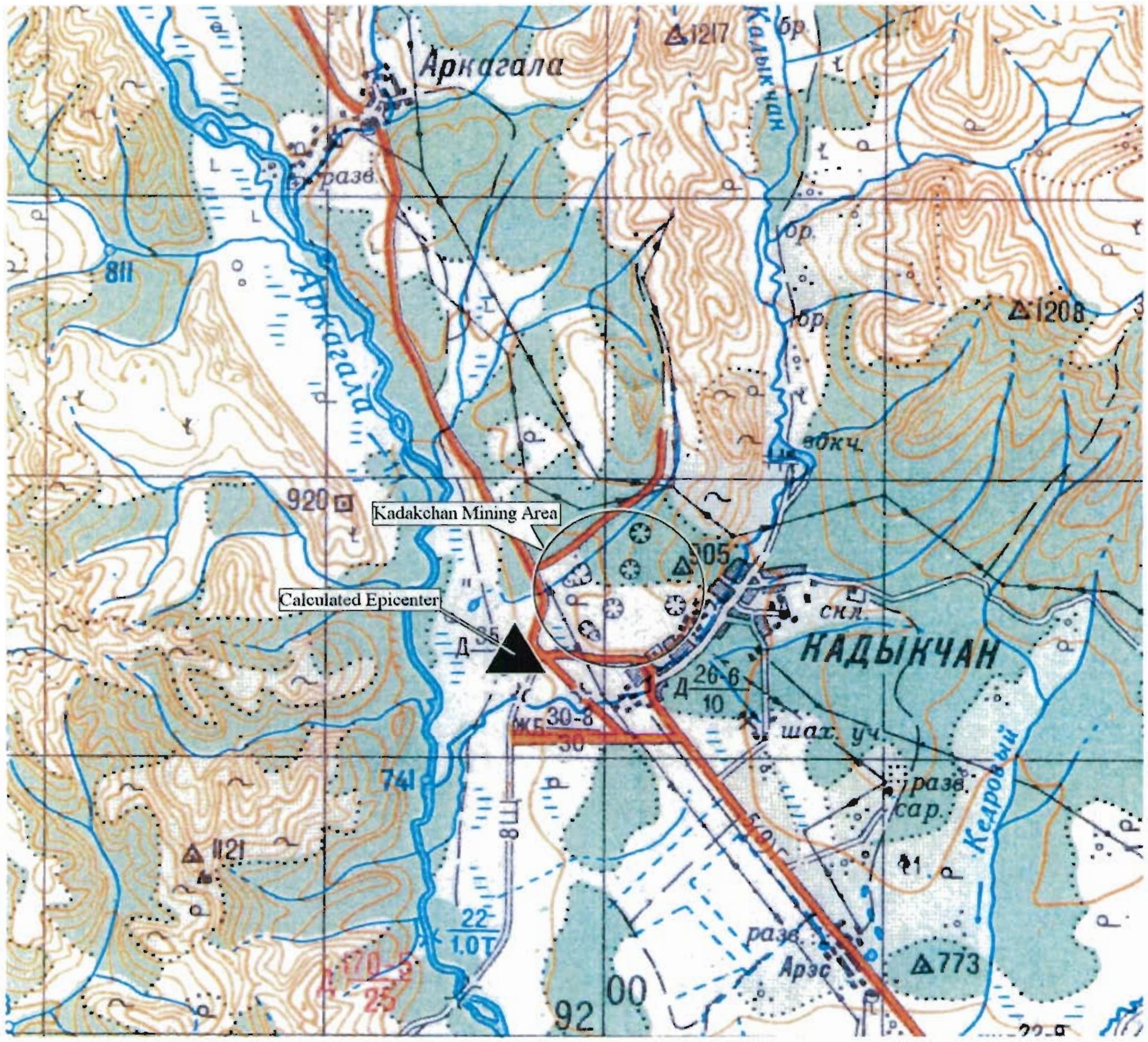

Figure E-1. Kadakchan mining region. The calculated epicenter is shown as the triangle. Note the close proximity of the calculated epicenter to the mapped mine pits enclosed by the circle. It is unknown exactly where the currently active pit is in Kadakchan, as the mine has not been field checked. One square on this map represents approximately 4 km. The base map used here is a 1:200,000 Russian military topographic map.

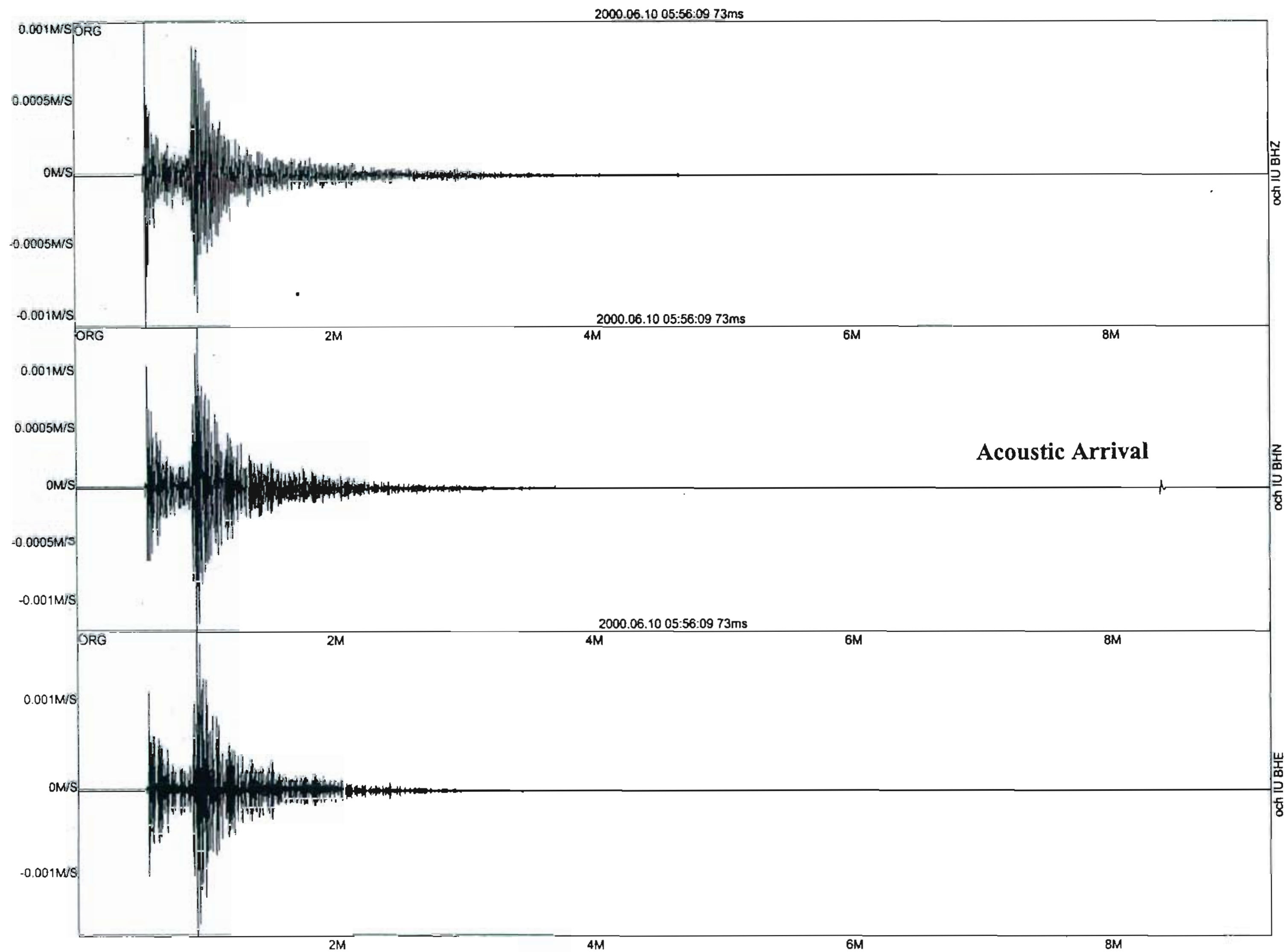

Figure E-2. Omchak short period seismograms of the 10 June, 2000 event showing a clear acoustic arrival about eight minutes after the P arrival. The acoustic arrival is only visible on the N-S component at this scale. Figure E-3 enlarges the acoustic arrival. Seismogram components are, top to bottom, Z, N-S, and E-W.

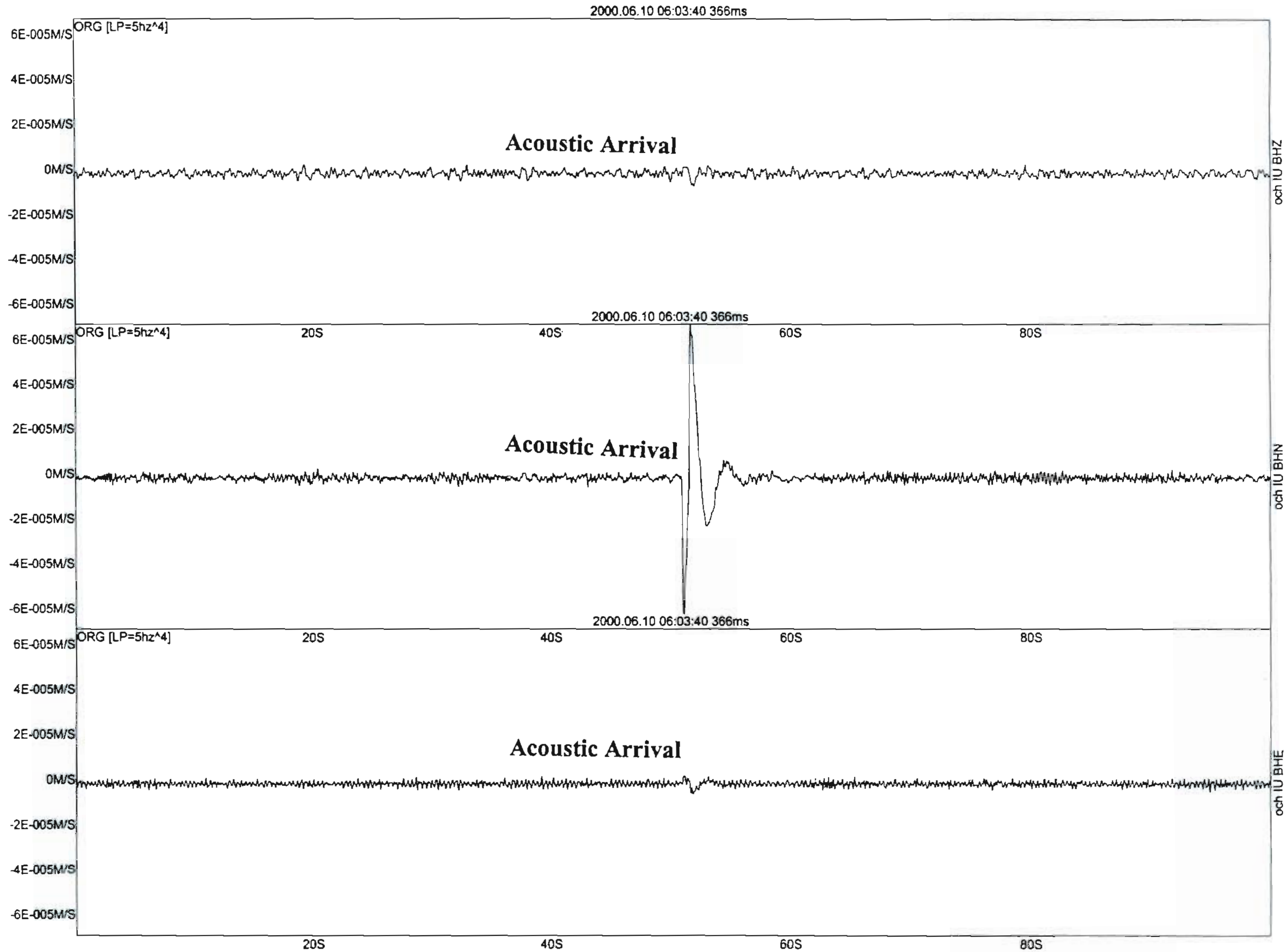

Figure E-3. Enlargement of the acoustic arrival recorded at Omchak from the 10 June, 2000 event. The acoustic arrival is strongest on the N-S component, consistent with Omchak being due south of the explosion source at Kadakchan. Seismogram components are, top to bottom, Z, N-S, and E-W.

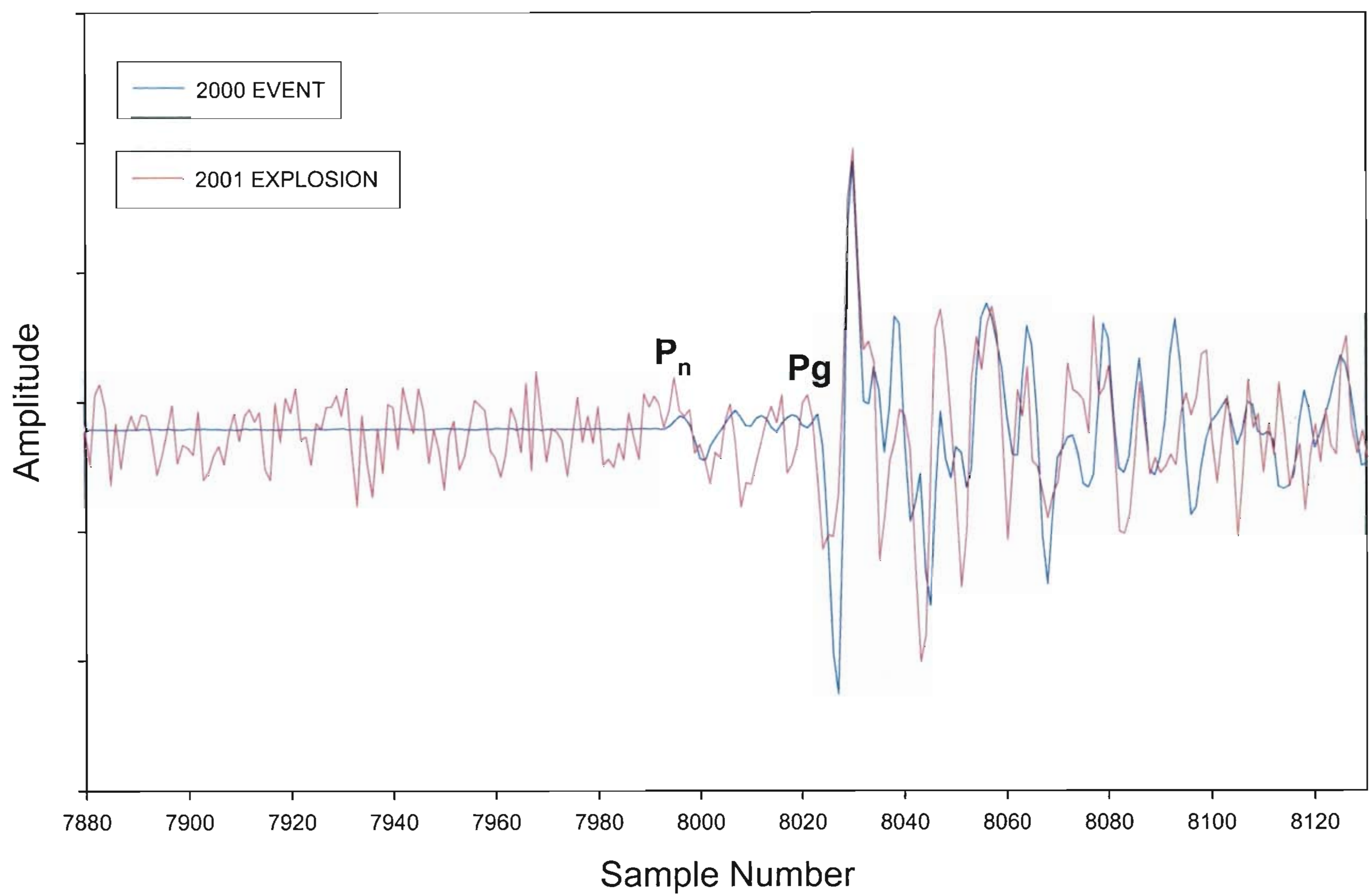

Figure E-4. Comparison between waveforms of the 10 June, 2000, event and a known Kadakchan explosion from 24 March, 2001. Note that the waveforms correlate well, especially accounting for the noise superimposed on the 2001 (red) trace. The correlation here suggests that the 2000 event is also an explosion from the Kadakchan coal mine. The yield of the 2001 explosion was 10,140 kg of explosives. Amplitude of the 2001 explosion is increased for clarity of correlation.

for the 10 June, 2000, event, or can not rule it out. The size of this explosion and quality of recording at Magadan (MA2) make this event a good candidate for a ground truth event worthy of additional research. Given the limited knowledge of the exact layout of the Kadakchan mine, this event should currently be classified as GT-5. However, a future field check of the Kadakchan mine should improve this to a GT-1. In addition to MA2, this explosion may have been recorded at other globally reported regional stations, such as Yakutsk (YAK).

Figures E-5 through E-8 provide additional digital seismograms from the Magadan region stations Omchak, Seymchan, Talaya, and Magadan.

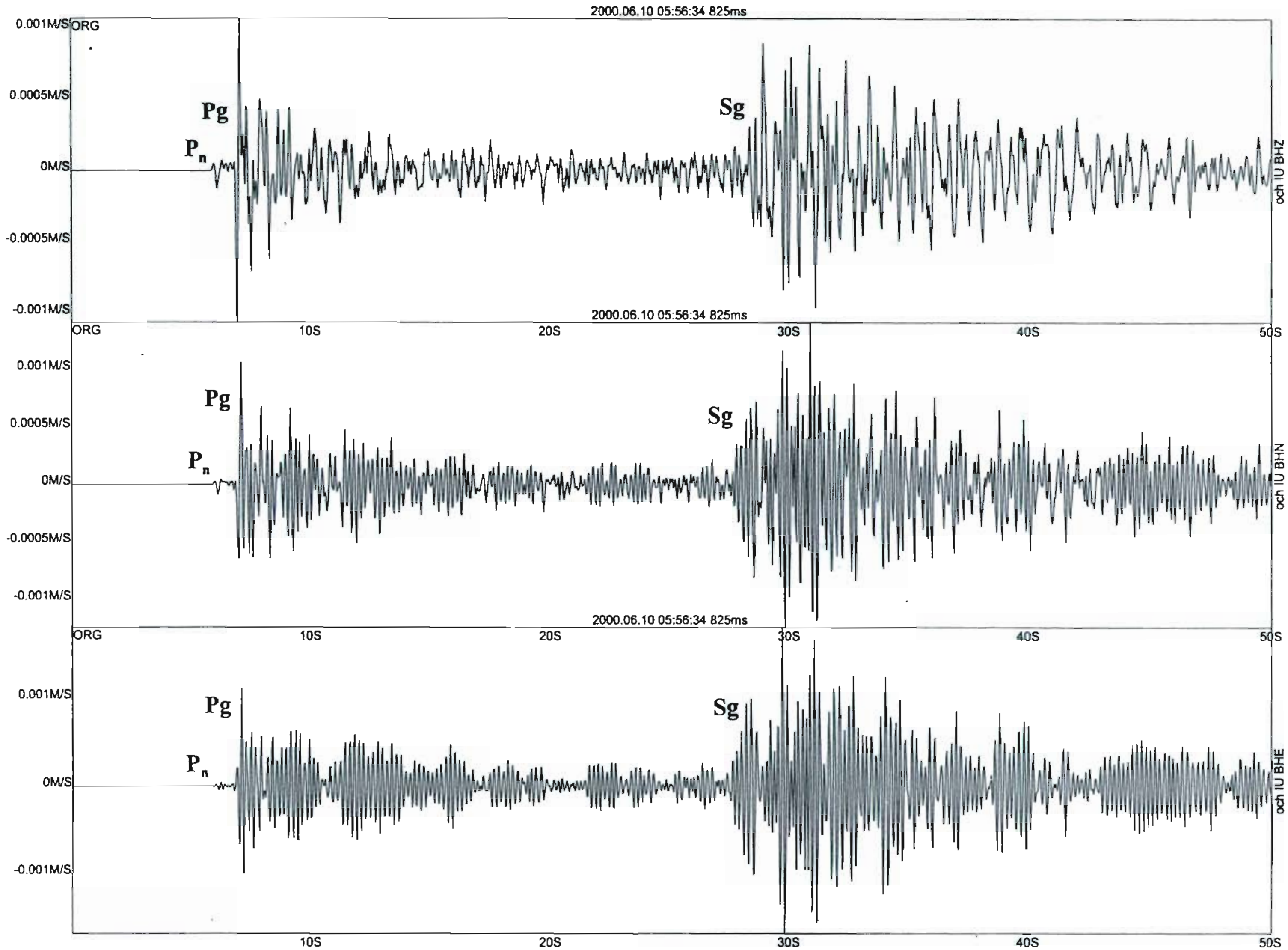

Figure E-5. Omchak short period seismograms of the 10 June, 2000 event. Seismogram components are, top to bottom, Z, N-S, and E-W.

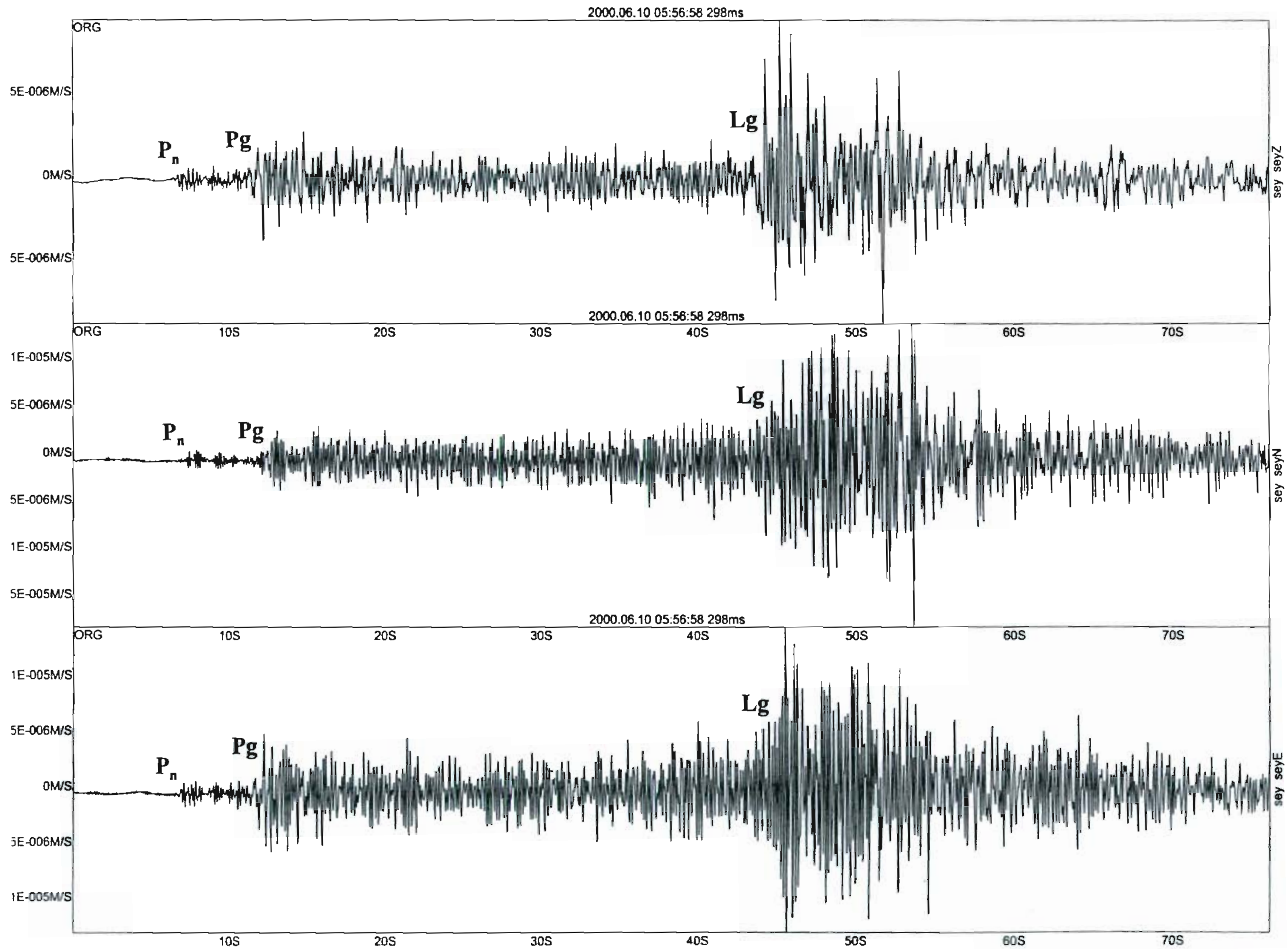

Figure E-6. Seymchan short period seismograms of the 10 June, 2000 event. Seismogram components are, top to bottom, Z, N-S, and E-W.

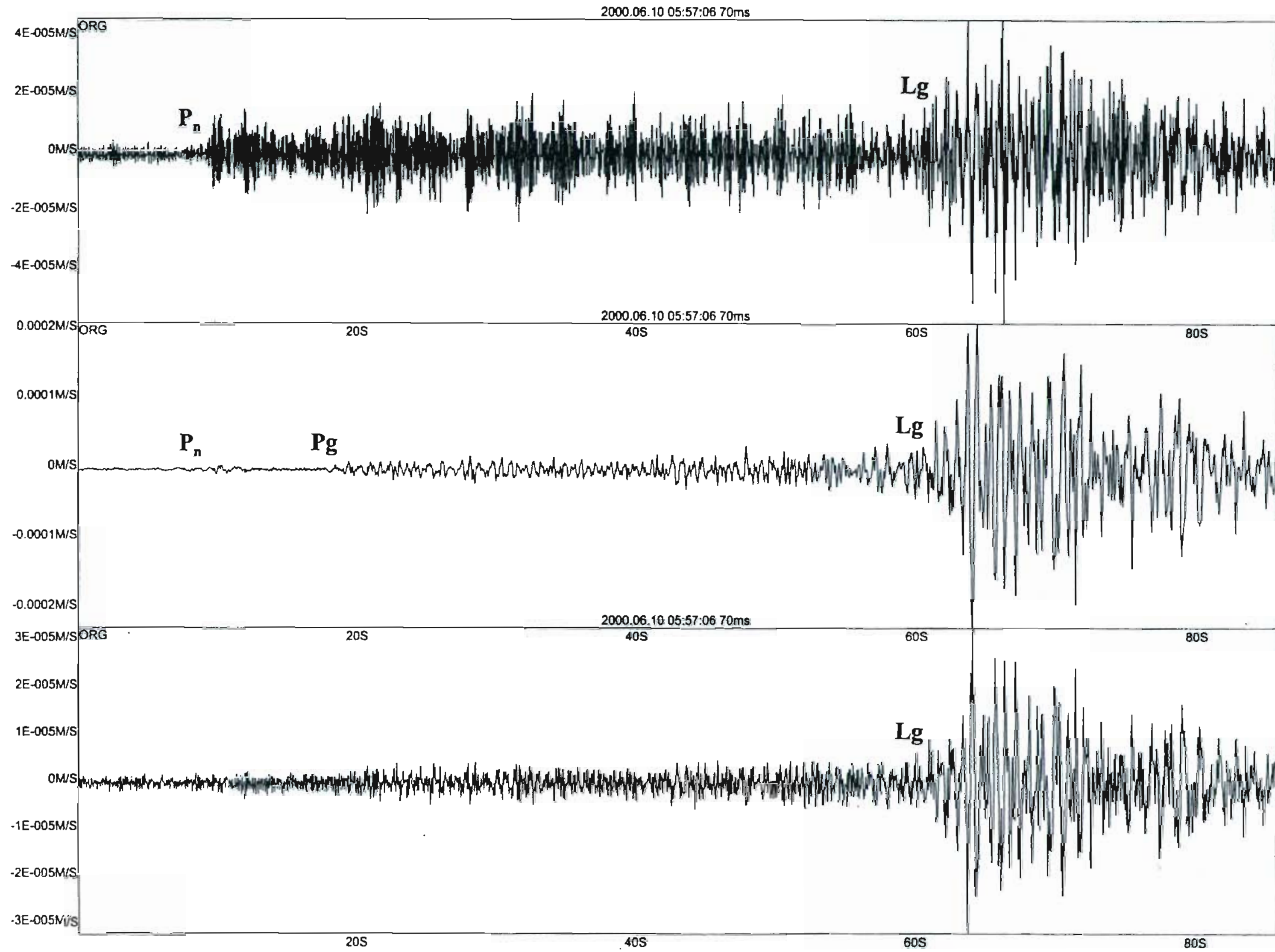

Figure E-7. Talaya short period seismograms of the 10 June, 2000 event. Seismogram components are, top to bottom, Z, N-S, and E-W.

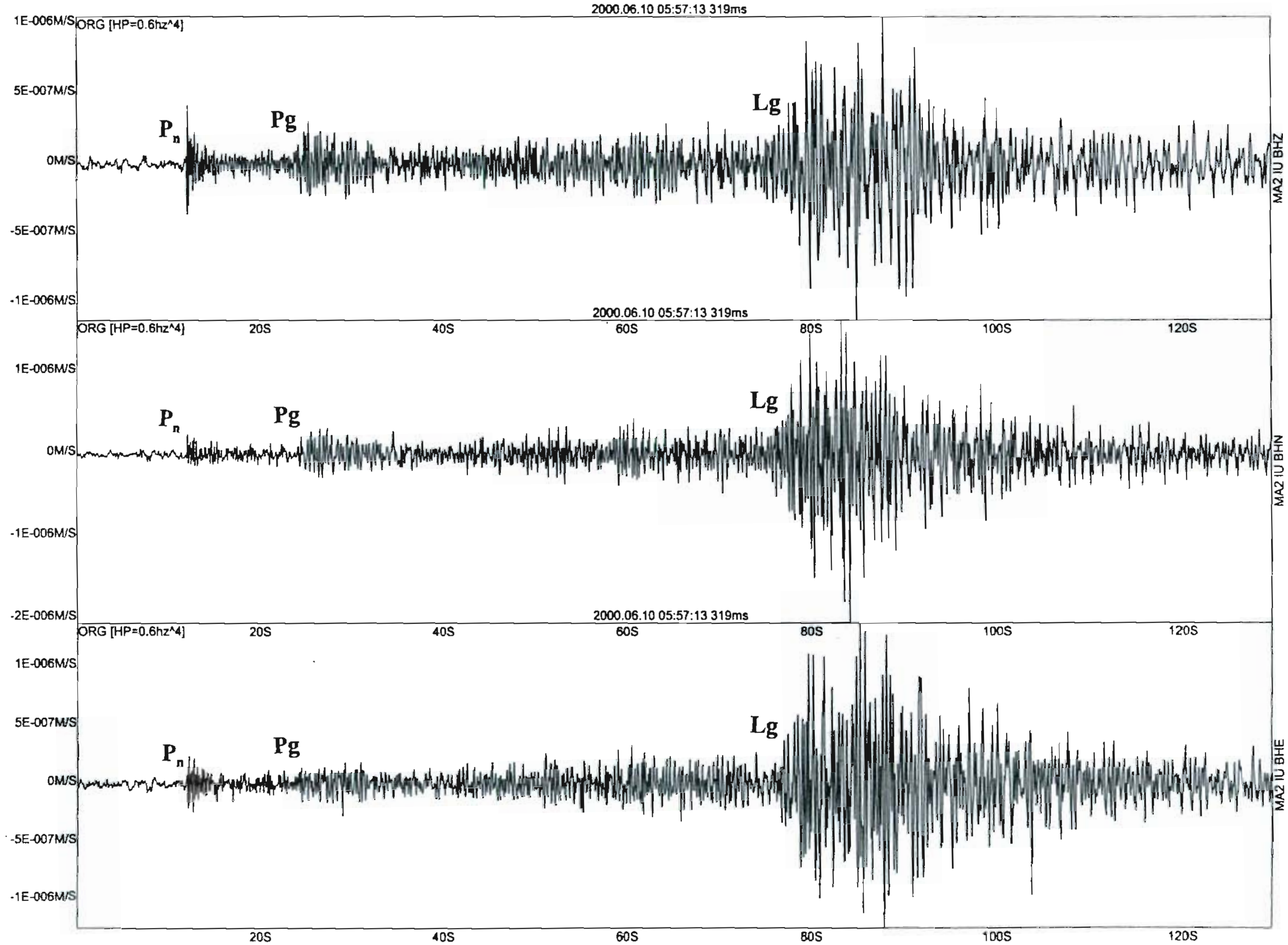

Figure E-8. Magadan broadband seismograms of the 10 June, 2000 event. Seismogram components are, top to bottom, Z, N-S, and E-W. A 0.6 Hz high pass filter was applied to these records.

DEPARTMENT OF DEFENSE

DIRECTOR
DEFENSE INTELLIGENCE AGENCY
BUILDING 6000
WASHINGTON, DC 20340-5100
ATTN: DTIB

DIRECTOR
DEFENSE RESEARCH AND ENGINEERING
3030 DEFENSE PENTAGON
WASHINGTON, D.C. 20301-3030
ATTN: DDR&E, ROOM 3E808

DEFENSE TECHNICAL INFORMATION CENTER
8725 JOHN J. KINGMAN ROAD, SUITE 0944
FT. BELVOIR, VA 22060-6218
2 CYS ATTN: DTIC/OCA

DEFENSE THREAT REDUCTION AGENCY
8725 JOHN J. KINGMAN ROAD MS 6201
FT. BELVOIR, VA 22060-6201
ATTN: TDND, CPT. BARBER

OFFICE OF THE SECRETARY OF DEFENSE
CHEMICAL DEMILITARIZATION AND THREAT
REDUCTION OFFICE
1515 WILSON BOULEVARD, SUITE 720
ARLINGTON, VA 22209-2402
ATTN: P. WAKEFIELD
ATTN: DR. S. MANGINO

DEPARTMENT OF THE ARMY

US ARMY SMDC
SMDC-TC-YD
P.O. BOX 1500
HUNTSVILLE, AL 35807 3801
ATTN: B. ANDRE

DEPARTMENT OF THE AIR FORCE

AIR FORCE RESEARCH LABORATORY
29 RANDOLPH ROAD
HANSCOM AFB, MA 01731
ATTN: RESEARCH LIBRARY
ATTN: VSBL, R. RAISTRICK

USAF AT USGS
2201 SUNRISE VALLEY DRIVE MS 951
RESTON, VA 20192
ATTN: R. BLANDFORD
ATTN: R. JIH

AIR FORCE TECHNICAL APPLICATIONS CTR
1030 S. HIGHWAY AIA
PATRICK AFB, FL 32925 3002
ATTN: CA/STINFO
ATTN: TTR, D. CLAUTER
ATTN: CTI, DR. B. KEMERAIT
ATTN: TT, DR. D. RUSSELL
ATTN: TTR, F. SCHULTZ
ATTN: TTR, G. ROTHE
ATTN: TTR, V. HSU
ATTN: DR. B. NGUYEN
ATTN: DR. E. SMART
ATTN: DR. G. WAGNER
ATTN: DR. M. WOODS

DEPARTMENT OF THE NAVY

NAVAL RESEARCH LABORATORY
4555 OVERLOOK AVE, SW, CODE 7643
WASHINGTON, DC 20375 0001
ATTN: DR. D. DROB

DEPARTMENT OF ENERGY

NATIONAL NUCLEAR SECURITY
ADMINISTRATION
1000 INDEPENDENCE AVE SW
WASHINGTON, DC 20585 0420
ATTN: L. CASEY
ATTN: G. KIERNAN

UNIVERSITY OF CALIFORNIA
LAWRENCE LIVERMORE NATIONAL LAB
P.O. BOX 808
LIVERMORE, CA 94551 9900
ATTN: MS L205, DR. D. HARRIS
ATTN: MS 205, TECHNICAL STAFF

LOS ALAMOS NATIONAL LABORATORY
P.O. BOX 1663
LOS ALAMOS, NM 87545
ATTN: MS C335, DR. S. R. TAYLOR

PACIFIC NORTHWEST NATIONAL LABORATORY
P.O. BOX 999
1 BATTELEE BOULEVARD
RICHLAND, WA 99352
ATTN: MS P8-20, T. HEIMBIGNER
ATTN: MS K8-29, DR. N. WOGMAN

SANDIA NATIONAL LABORATAORIES
MAIL SERVICES
P.O. BOX 5800
ALBUQUERQUE, NM 87185 1164
ATTN: WILLIAM GUYTON

OTHER GOVERNMENT

DEPARTMENT OF STATE
2201 C STREET NW
WASHINGTON, DC 20520
ATTN: R. MORROW, ROOM 5741

US GEOLOGICAL SURVEY
905 NATION CENTER
12201 SUNRISE VALLEY DR
RESTON, VA 20192
ATTN: W. LEITH

US GEOLOGICAL SURVEY
345 MIDDLEFIELD RD MS 977
MENLO PARK, CA 94025
ATTN: S. DETWEILER
ATTN: DR. W. MOONEY

DEPARTMENT OF DEFENSE CONTRACTORS

BATTELLE
MANAGER, ENERGETIC SYSTEMS & SECURITY TECHNOLOGIES
505 KING AVE
COLUMBUS, OH 43201-2693
ATTN: NEAL OWENS (7-2-081)

BBN CORPORATION
1300 N 17TH STREET, SUITE 400
ARLINGTON, VA 22209
ATTN: DR. D. NORRIS
ATTN: R. GIBSON
ATTN: J. PULLI

CENTER FOR MONITORING RESEARCH
1953 GALLOWS ROAD, SUITE 260
VIENNA, VA 22182 3997
ATTN: DR. K. L. MCLAUGLHLIN
ATTN: DR. R. WOODWARD
ATTN: DR. R. NORTH
ATTN: DR. X. YANG
ATTN: LIBRARIAN

ENSCO, INC.
5400 PORT ROYAL ROAD
SPRINGFIELD, VA 22151 2312
ATTN: D. BAUMGARDT
ATTN: Z. DER

WESTON GEOPHYSICAL CORPORATION
27 BEDFORD ST, SUITE 102
LEXINGTON, MA 02420
ATTN: DR. D. REITER
ATTN: J. LEWKOWICZ
ATTN: DR. A. ROSCA
ATTN: DR. I. TIBULEAC
ATTN: M. JOHNSON

ITT INDUSTRIES
ITT SYSTEMS CORPORATION
1680 TEXAS STREET SE

KIRTLAND AFB, NM 87117 5669
2 CYS ATTN: DTRIAC
ATTN: DARE

TITAN
1900 CAMPUS COMMONS DR SUITE 600
RESTON, VA 20191-1535
ATTN: DR. C. P. KNOWLES

MISSION RESEARCH CORPORATION
8560 CINDERBED ROAD, SUITE 700
NEWINGTON, VA 22122
ATTN: DR. M. FISK

MULTIMAX, INC
1441 MC CORMICK DRIVE
LANDOVER, MD 20785
ATTN: DR. I. N. GUPTA
ATTN: W. RIVERS

MULTIMAX, INC
1090 N HIGHWAY A1A SUITE D
INDIANLATIC, FL 32903
ATTN: DR. H. GHALIB

SCIENCE APPLICATIONS INTERNATIONAL CORP
10260 CAMPUS POINT DRIVE
SAN DIEGO, CA 92121 1578
ATTN: DR.M. ENEVA
ATTN: DR. G. E. BAKER
ATTN: DR. J. STEVENS
ATTN: DR. D. ADAMS

SCIENCE APPLICATIONS INT'L CORP
1227 S. PATRICK DR SUITE 110
SATELLITE BEACH, FL 32937
ATTN: DR. M. FELIX
ATTN: DR. H. GIVEN

URS CORPORATION
566 EL DORADO STREET
PASADENA, CA 91109 3245
ATTN: DR. N.B. WOODS
ATTN: DR. C. SAIKIA
ATTN: DR. G. ICHINOSE

DIRECTORY OF OTHER (LIBRARIES AND UNIVERSITIES)

BOSTON COLLEGE
INSTITUTE FOR SPACE RESEARCH
140 COMMONWEALTH AVENUE
CHESTNUT HILL, MA 02167
ATTN: DR. D. HARKRIDER
ATTN: B. SULLIVAN

BROWN UNIVERSITY
DEPARTMENT OF GEOLOGICAL SCIENCES
75 WATERMAN STREET
PROVIDENCE, RI 02912 1846
ATTN: PROF. D. FORSYTH

CALIFORNIA INSTITUTE OF TECHNOLOGY
DIVISION OF GEOLOGY & PLANETARY SCIENCES
PASADENA, CA 91125
ATTN: PROF. DONALD V. HELMBERGER
ATTN: PROF. THOMAS AHRENS

UNIVERSITY OF CALIFORNIA BERKELEY
281 MCCONE HALL
BERKELEY, CA 94720 2599
ATTN: PROF. B. ROMANOWICZ
ATTN: DR. D. DREGER

UNIVERSITY OF CALIFORNIA-DAVIS
DEPT OF STATISTICS
DAVIS, CA 95616
ATTN:. R H SHUMWAY, DIV STATS

UNIVERSITY OF CALIFORNIA SAN DIEGO
SCRIPPS INSTITUTION OF TECHNOLOGY
9500 GILMAN DRIVE
LA JOLLA, CA 92093 0225
ATTN: DR. L. DEGROOT - HEDLIN
ATTN: DR. M. HEDLIN
ATTN: PROF. F. VERNON
ATTN: PROF. J. BERGER
ATTN: J. ORCUTT

UNIVERSITY OF CALIFORNIA SANTA CRUZ
INSTITUTE OF TECTONICS
SANTA CRUZ, CA 95064
ATTN: DR. R. S. WU
ATTN: PROF. T. LAY

UNIVERSITY OF COLORADO BOULDER
DEPT OF PHYSICS, CAMPUS BOX 390
BOULDER, CO 80309
ATTN: DR.R. ENGDAHL
ATTN: M. RITZWOLLER
ATTN: PROF. C. ARCHAMBEAU

COLUMBIA UNIVERSITY
LAMONT DOHERTY EARTH OBSERVATORY
PALISADES, NY 10964
ATTN: DR. J. XIE
ATTN: DR. W. Y. KIM
ATTN: PROF. P.G. RICHARDS
ATTN: DR. M. TOLSTOY

UNIVERSITY OF CONNECTICUT
DEPARTMENT OF GEOLOGY & GEOPHYSICS
STOORS, CT 06269 2045
ATTN: PROF. V.F. CORMIER, U-45,
ROOM 207

CORNELL UNIVERSITY
DEPARTMENT OF GEOLOGICAL SCIENCES
3126 SNEE HALL
ITHACA, NY 14853
ATTN: PROF. M.A. BARAZANGI

HARVARD UNIVERSITY
HOFFMAN LABORATORY
20 OXFORD STREET
CAMBRIDGE, MA 02138
ATTN: PROF. A. DZIEWONSKI
ATTN: PROF. G. EKSTROM

INDIANA UNIVERSITY
DEPARTMENT OF GEOLOGICAL SCIENCES
1005 10TH STREET
BLOOMINGTON, IN 47405
ATTN: PROF. G. PAVLIS

IRIS
1200 NEW YORK AVENUE, NW SUITE 800
WASHINGTON, DC 20005
ATTN: DR. D. SIMPSON

IRIS
1408 NE 45TH ST #201
SEATTLE, WA 98105
ATTN: DR. T. AHERN

MASSACHUSETTS INSTITUTE OF TECHNOLOGY
EARTH RESOURCES LABORATORY
42 CARLETON STREET
CAMBRIDGE, MA 02142
ATTN: DR. W. RODI
ATTN: PROF. M.N. TOKSOZ

MICHIGAN STATE UNIVERSITY LIBRARY
450 ADMINISTRATION BUILDING
EAST LANSING, MI 48824
ATTN: K. FUJITA

NEW MEXICO STATE UNIVERSITY
DEPARTMENT OF PHYSICS
LAS CRUCES, NM 88003
ATTN: PROF. J. NI
ATTN: PROF. T. HEARN

NORTHWESTERN UNIVERSITY
DEPARTMENT OF GEOLOGICAL SCIENCES
1847 SHERIDAN RD
EVANSTON, IL 60208
ATTN: PROF. E. OKAL

PENNSYLVANIA STATE UNIVERSITY
GEOSCIENCES DEPARTMENT
403 DEIKE BUILDING
UNIVERSITY PARK, PA 16802
ATTN: PROF. C. AMMON
ATTN: PROF. S. ALEXANDER
ATTN: DR. A. NYBLADE

SAN DIEGO STATE UNIVERSITY
DEPARTMENT OF GEOLOGICAL SCIENCES
SAN DIEGO, CA 92182
ATTN: PROF. S. M. DAY

SOUTHERN METHODIST UNIVERSITY
DEPARTMENT OF GEOLOGICAL SCIENCES
P.O. BOX 750395
DALLAS, TX 75275
ATTN: B. STUMP
ATTN: E. HERRIN
ATTN: P. GOLDEN

UNIVERSITY OF HAWAII- MANOA
P.O. BOX 1599
KAILUA-KONA, HI 96745 1599
ATTN: DR. M. A. GARCES

UNIVERSITY OF MISSISSIPPI
1 COLISEUM DRIVE
UNIVERSITY, MS 38677
ATTN: PROF. H. BASS

UNIVERSITY OF SOUTHERN CALIFORNIA
520 SEAVER SCIENCE CENTER
UNIVERSITY PARK
LOS ANGELES, CA 90089 0483
ATTN: PROF. C. G. SAMMIS
ATTN: PROF. T. JORDAN

UNIVERSITY OF WISCONSIN MADISON
1215 W DAYTON ST
MADSION, WI 53706 1600
ATTN: DR. C. THURBER

ST LOUIS UNIVERSITY
EARTH & ATMOSPHERIC SCIENCES
STATION 3507 LACLEDE AVE
ST LOUIS, MO 63103
ATTN: PROF. B. J. MITCHELL
ATTN: PROF. R. HERRMAN

UNIVERSITY OF MEMPHIS
3890 CENTRAL AVE
MEMPHIS, TN 38152
ATTN: DR. J. PUJOL

UNIVERSITY OF MEMPHIS
3876 CENTRAL AVE
MEMPHIS, TN 38152
ATTN: DR. C. LANGSTON

UNIVERSITY OF TEXAS AUSTIN
IGS 130
AUSTIN, TX 78712
ATTN: DR. J. PULLIAM

UNIVERSITY OF TEXAS AUSTIN
IGS 131
AUSTIN, TX 78712
ATTN: DR. M. SEN

UNIVERSITY OF TEXAS EL PASO
DEPT OF GEOLOGICAL SCIENCES
EL PASO, TX 79901
ATTN: PROF. G. KELLER
ATTN: DR. D. DOSER
ATTN: DR. A. VELASCO

FOREIGN

AUSTRALIAN GEOLOGICAL SURVEY
ORGANIZATION
CORNER OF JERRAGOMRRRA &
NINDMARSH DRIVE
CANBERRA, ACT 2609
AUSTRALIA
ATTN: D. JEPSON

GEOPHYSICAL INSTITUTE OF ISRAEL
POB 182
LOD, 7100 ISRAEL
ATTN: DR. Y. GITTERMAN
ATTN: DR. A. SHAPIRA

GEOLOGICAL SURVEY OF CANADA
7 OBSERVATORY CRESCENT
OTTAWA K1A 0Y3 ONT
CANADA
ATTN: C. WOODGOLD

I.R.I.G.M. B.P. 68
38402 ST. MARTIN D'HERES
CEDEX, FRANCE
ATTN: DR. M. BOUCHON

MINISTRY OF DEFENSE
PROCUREMENT EXEUTIVE
BLACKNESS, BRIMPTON
READING FG7-4RS ENGLAND
ATTN: DR. D. BOWERS

NTNF/NORSAR
P.O. BOX 51
N-2007 KJELLER, NORWAY
ATTN: DR. F. RINGDAL
ATTN: T. KVAERNA
ATTN: S. MYKKELTVEIT